Exploring the role of endoplasmic reticulum stress in skeletal dysplasia

A thesis submitted to Newcastle University for the degree of Doctor of Philosophy in the Biosciences Institute, Faculty of Medical Sciences

March 2022

Helen Friederike Dietmar

Abstract

The term skeletal dysplasia comprises a range of diseases that lead to varying degrees of skeletal deformities, causing pain and reduction in quality of life. Whilst each disease is typically rare, together they are estimated to occur in up to 1 of 5000 people. The intracellular retention of secreted proteins has been identified as one common disease mechanism in several skeletal dysplasias, including pseudoachondroplasia (PSACH) and multiple epiphyseal dysplasia (MED). Yet, the specific pathways that are involved may be mutation-, gene- or disease-specific, or subject to disease modifiers and thus require specific treatments.

Several approaches to study skeletal dysplasia and the resulting endoplasmic reticulum stress *in vitro,* including the use of human induced pluripotent stem cells (hiPSCs), were evaluated. HT1080 fibrosarcoma cells overexpressing wild type and mutant p.D469del COMP were validated as an *in vitro* model system for PSACH before performing RNA sequencing and DNA methylation analysis. Additionally, several mutant COMP constructs were overexpressed in HT1080 cells to study a potential common mechanism of *COMP*-MED and PSACH.

Whilst hiPSCs offer exciting opportunities for the *in vitro* study of skeletal diseases, high variation during differentiation protocols rendered them unsuitable for this study. DNA methylation analysis revealed an unexpectedly large number of differentially methylated CpG sites, whilst RNA sequencing of D469del COMP cells revealed an increase in inflammatory signalling, and a marked upregulation of *MMP9* and *GALNT18*. Elevated *MMP9* expression correlated with increased extracellular MMP9 activity. This was also found in cell lines overexpressing other disease-causing COMP proteins, but not in a cell model of *MATN3*-MED.

The data presented in this thesis indicates that COMP mutations act via a common mechanism that is distinct from MED-causing mutations in *MATN3*. It also provides evidence that MMP9 could be a marker for COMP-caused stress *in vitro* and thus facilitate future drug screenings.

Meiner Familie

Acknowledgements

I would like to begin by thanking my supervisors Prof Michael Briggs, Prof David Young, and Dr Louise Reynard for their patience, encouragement and advice during the last three and half years. Thank you for all your support and guidance, comments and feedback, all while you were also living through a pandemic.

I would like to thank Prof John Bateman and Dr Shireen Lamandé and their groups, who have welcomed, supported and taught me so much during my stay in Melbourne and have provided the hiPSC lines used to perform osteogenesis experiments. Special thanks to Prof John Bateman for providing the cartilage-like pellets of control and MCDS-patient derived hiPSCs.

Thanks to Lee Murphy and Nicola Wrobel from the Edinburgh Clinical Research Facility, Wellcome Trust CRF, Western General Hospital, Edinburgh, and the Genomics Core Facility at Newcastle University for their help with the Illumina Infinium MethylationEPIC array and RNA sequencing, respectively.
I would like to thank the FGU staff – especially Steve, Michael and Kim - for their advice, help and technical expertise. Thank you also to Lisa Hodgson for her technical assistance with microscopy.
I would also like to thank Dr Beth Gibson for generating the COMP cell lines and Dr Ella Dennis for providing the pcDNA3.1-*MATN3* constructs.

Thank you also to Fran, Rachel, Marc and especially Ella and Adam for being lovely colleagues (and always bringing cake)! Special thanks to David, Louise, Dan, Jamie and Fran for patiently helping me with various questions about DNA methylation analysis, R studio, and RNA sequencing.

Financial support from the MCDS therapy project and RUBICON network (both EU Horizon 2020 funded) is gratefully acknowledged.

Ein besonderer Dank gilt meiner Familie und meinem Partner für ihre Unterstützung und Liebe.

Table of Contents

List of Figures

List of Tables

Abbreviations

AD	Alzheimer's disease
ADP	Adenosine diphosphate
ALS	Amyotrophic lateral sclerosis
AMP	Adenosine monophosphate
ANOVA	Analysis of variance
APS	Ammonium persulfate
ATF4	Activating transcription factor 4
ATF6	Activating transcription factor 6
ATP	Adenosine triphosphate
BCA	Bicinchoninic acid
BiP	Binding immunoglobulin protein
BMP	Bone morphogenetic protein
BMPR	Bone morphogenetic protein receptor
BrdU	Bromodeoxyuridine
BSA	Bovine serum albumin
CATSHL	Campodactylyl, tall stature and hearing loss
CBZ	Carbamazepine
cDNA	Complementary DNA
CHOP	C/EBP homologous protein
CNP	C-natriuretic peptide
Cog	Congenital goitre (resulting from a mutation in thyroglobulin)
COMP	Cartilage oligomeric matrix protein
CS	Chondroitin sulphate
CSCD	Congenital stromal corneal dystrophy
CTD	C-terminal domain
(k)Da	(kilo) Dalton
DAPI	4',6-diamidino-2-phenylindole
DEG	Differentially expressed gene
DMEM/F12	Dulbecco's modified eagle medium/nutrient mixture F12
DMP	Differentially methylated probe
DMR	Differentially methylated region
DMSO	Dimethyl sulfoxide
DNMT	DNA-methyltransferases

dNTP	Deoxynucleotide triphosphate
DTD	Diastrophic dysplasia
DTT	Dithiothreitol
ECL	Enhanced chemiluminescence
ECM	Extracellular matrix
EDS	Ehlers-Danlos syndrome
EDTA	Ethylenediaminetetraacetic acid
EGF	Epidermal growth factor
eiF2α	Eukaryotic translation initiation factor 2A
ER	Endoplasmic reticulum
ERAD	ER-associated degradation
ERSE	ER-stress response element
FACIT	Fibril-associated with interrupted triple helices
FBS	Foetal bovine serum
FGF	Fibroblast growth factor
FGFR	Fibroblast growth factor receptor
GAG	Glycosaminoglycan
GALNT18	Polypeptide N-Acetylgalactosaminyltransferase 18
GAPDH	Glyceraldyhyde 3-phosphate dehydrogenase
GDF	Growth differentiation factor
GFP	Green fluorescent protein
GRP	Glucose-regulated protein
HD	Huntington's disease
HIF	Hypoxia-inducible factor
hiPSC(s)	Human induced pluripotent stem cell(s)
HRP	Horseradish peroxidase
HS	Heparan sulphate
IHC	Immunohistochemistry
IHH	Indian hedgehog
IRE1	Inositol-requiring enzyme 1
ISR	Integrated stress response
ISRIB	Integrated stress response inhibitor
JNK	c-Jun N-terminal kinases
KEGG	Kyoto Encyclopaedia of Genes and Genomes
KS	Keratan sulphate

LADD	Lacrimoauriculodentodigital
LAP	Latency-associated peptide
LB	Lysogeny broth
LC3B	Microtubule-associated proteins 1A/1B light chain 3B
LTBP	Latent TGFβ binding protein
MAPK	Mitogen-activated protein kinase
MCDS	Metaphyseal chondrodysplasia Schmid type
MED (EDM)	Multiple epiphyseal dysplasia
MES	2-(*N*-morpholino)ethanesulfonic acid
MMP	Matrix-metalloproteinase
MSC(s)	Mesenchymal stem cell(s)
mTORC	Mammalian target of rapamycin complex
NBT	Nitroblue tetrazolium chloride
NC	Non-collagenous
NFκB	Nuclear factor κB
NICD	Notch intracellular domain
NMD	Nonsense-mediated RNA decay
OCD	Osteochondritis dissecans
OI	Osteogenesis imperfecta
PBS	Phosphate-buffer saline
PD	Parkinson's disease
PDI	Protein disulphide isomerase
PERK	PKR-like endoplasmic reticulum kinase
PGs	Proteoglycan
pMEFs	Primary mouse embryonic fibroblasts
PSACH	Pseudoachondroplasia
PTH	Parathyroid hormone
PTHrP	Parathyroid hormone related peptide
qRT-PCR	Quantitative reverse transcription polymerase chain reaction
RDW	Recessive congenital dwarfism (resulting from a mutation in thyroglobulin)
RIDD	Regulated IRE1-dependent decay
RNAi	RNA interference
ROS	Reactive oxygen species
RUNX2	Runt-related transcription factor 2

S1P	Site-1-protease
S2P	Site-2-protease
SDS	Sodium dodecyl sulphate
SED	Spondyloepiphyseal dysplasia
SEMD	Spondyloepimetaphyseal dysplasia
SLRRP	Small leucine rich repeat proteoglycan
SMAD	Mothers against decapentaplegic homolog
SOC	Super optimal broth with catabolite repression
SOX9	SRY-box transcription factor 9
TBS	Tris-buffered saline
TEMED	Tetramethylethylenediamine
TET	Ten-Eleven-Translocation
TGFβ	Transforming growth factor beta
TGFBR	Transforming growth factor beta receptor
TNF	Tumor Necrosis Factor
TSP	Thrombospondin
TUDCA	Tauroursodeoxycholic acid
TUNEL	Terminal deoxynucleotide transferase dUTP nick end labelling
UCMD	Ulrich congenital muscular dystrophy
UPR	Unfolded protein response
UPRE	Unfolded protein response element
VEGF	Vascular-endothelial growth factor
VWFA	Von Willebrand Factor A
XBP1	X-box binding protein 1
4-PBA	4-phenylbutyric acid, sodium salt

Chapter 1. Introduction

1.1 Endochondral ossification

The mammalian skeleton consists of two major tissue types: cartilage and bone. They are supported by ligaments, tendons and muscles and together, they protect inner organs and enable movement.

In mammals, bones are formed by two distinct mechanisms; intramembranous ossification forms the craniofacial bones, whilst most other bones are formed via a process termed endochondral ossification. During intramembranous ossification, mesenchymal stem cells (MSCs) differentiate directly into bone-depositing cells called osteoblasts (Reviewed in detail by (Percival and Richtsmeier, 2013)). In contrast, endochondral ossification is dependent on the formation of a cartilage template (extensively reviewed, for example (Long and Ornitz, 2013; Mackie et al., 2011, 2008)). During embryonic development, MSCs condensate and differentiate into cartilage-forming cells called chondrocytes, which form a cartilaginous extracellular matrix-rich template of the bone. The outer cell layer of this condensation forms a dense connective tissue called perichondrium. The major components of the cartilage specific extracellular matrix (ECM) are proteoglycans, especially aggrecan, collagens, mainly type II collagen, and glycoproteins. As chondrocytes proliferate, they promote longitudinal growth before they differentiate into hypertrophic chondrocytes. The increase in cell volume during hypertrophy further contributes to the growing process, whilst the associated changes in gene expression allow the surrounding ECM to become calcified (Ortega et al., 2004). Instead of aggrecan and type II collagen, hypertrophic chondrocytes express mainly type X collagen. Cells of the perichondrium adjacent to hypertrophic chondrocytes differentiate into osteoblasts, beginning to form the bone collar. Terminal hypertrophic chondrocytes secrete factors such as vascular-endothelial growth factor (VEGF) that attract blood vessels, bone-degrading cells called osteoclasts, and osteoblast precursors that invade the mid-shaft of the future bone to form the primary ossification centre (Mackie et al., 2008; Xie et al., 2014). More recently, it has been revealed that some hypertrophic chondrocytes may transition into osteoblasts in a process also known as trans-differentiation (G. Yang et al., 2014; L. Yang et al., 2014; Zhou et al., 2014). Eventually, the calcified cartilage matrix is degraded by proteases, such as matrix-metalloproteinases (MMPs). Osteoblasts then replace the degraded cartilage matrix with a bone specific ECM rich in type I collagen (Ortega et al., 2004).

At the time of birth (in humans) a secondary ossification centre in the epiphysis develops resulting in the formation of the growth plate. In the growth plate, chondrocytes form distinct zones (Long and Ornitz, 2013): At the top of the growth plate, resting chondrocytes with a characteristic round shape function as a cell reservoir for the growth plate. In the proliferative zone, chondrocytes typically exhibit a flattened shape and are arranged in columnar structures. Finally, chondrocytes become hypertrophic, which is marked by an increase in cell volume and type X collagen expression (Long and Ornitz, 2013; Noonan et al., 1998).

In late puberty, the primary and secondary ossification centres fuse (epiphyseal closure) thereby preventing further growth at skeletal maturity (Mackie et al., 2008). In the adult skeleton most cartilage is replaced by bone except for articular cartilage, which remains to cover the joint surface. Articular cartilage fulfils important roles in the distribution of joint load and reduction of friction between the joint surfaces (Decker, 2017).

1.2 Skeletal dysplasia

The processes of endochondral ossification and intramembranous ossification are tightly regulated and disturbances frequently result in skeletal dysplasia. To date, more than 400 different types of skeletal dysplasia have been described (Zankl et al., 2018). Chondro- and osteodysplasia differ in their involvement in the development of cartilage and bone respectively (Krakow and Rimoin, 2010). Symptoms include short stature and a varying range of skeletal deformities, such as *coxa vara*/*valga* (deformities of the hip) and *genu varus*/*valgus* (deformities of the knee) accompanied by joint pain and restricted movement. Severe cases of skeletal dysplasia, such as some types of osteogenesis imperfecta (OI), also called brittle bone disease, may be diagnosed *in utero*, whilst most of the milder skeletal dysplasias are diagnosed in early childhood and typically when a child begins to walk (Panda et al., 2014). Disease-causing mutations have been identified in several structural proteins of the extracellular matrix as well as in growth factors, their receptors and proteins involved in protein trafficking, all ultimately resulting in impaired endochondral ossification, intramembranous ossification or both.

In addition to *in vitro* studies, the generation of mouse models for various skeletal dysplasia types facilitated the characterisation of common and distinct disease mechanisms as well as uncovering the role of several proteins in skeletal development (Briggs et al., 2015).

1.3 Signalling pathways of the developing skeleton

A large number of molecules that participate in the regulation of chondrocyte proliferation, differentiation and thus endochondral ossification, are secreted signalling factors, their receptors and their target transcription factors (Karsenty et al., 2009; Xie et al., 2014). Both gain-of-function as well as loss-of-function mutations in some components of these signalling pathways have been described to cause skeletal disorders in humans.

During endochondral ossification, chondrocyte proliferation and differentiation are controlled by the parathyroid hormone related peptide (PTHrP) – Indian hedgehog (IHH) signalling loop (Lanske et al., 1996; St-Jacques et al., 1999). Early proliferating chondrocytes secrete PTHrP, which diffuses throughout the growth plate and induces cell proliferation in the surrounding chondrocytes. As the PTHrP concentration decreases towards the end of the proliferative zone, hypertrophy is induced as well as IHH expression. Secreted IHH in turn stimulates PTHrP production and chondrocyte proliferation (Kronenberg and Chung, 2001), effectively controlling the rate of chondrocyte differentiation. The loss of *PTHrP* in a mouse model as well as in Blomstrand chondrodysplasia (caused by mutation of the gene encoding the PTH/PTHrP receptor) causes a premature end of chondrocyte proliferation, resulting in a shortened proliferative zone (Jobert et al., 1998; Karaplis et al., 1994; Zhang et al., 1998). Conversely, enhanced PTHrP signalling increased the length of proliferative columns and thus delayed endochondral ossification (Schipani et al., 1997; Weir et al., 1996). The deletion of *Ihh* in turn led to a reduction in chondrocyte proliferation and simultaneous uncontrolled differentiation (St-Jacques et al., 1999) whilst the induction of IHH signalling inhibited chondrocyte hypertrophy (Vortkamp et al., 1996). These findings demonstrate the importance of the PTHrP/IHH feedback loop for skeletal development, and of controlled cell proliferation and differentiation for endochondral ossification.

Another important regulatory element of endochondral ossification is the fibroblast growth factor (FGF) family which consists of at least 18 growth factors (FGFs) that interact with four receptor tyrosine kinases (FGFR). Their expression during skeletal development is highly dependent on location and developmental stage, and the numerous aspects of their function have been extensively reviewed elsewhere (Ornitz and Marie, 2019; Xie et al., 2020). In brief, several FGFs are present in the

developing growth plate, the surrounding perichondrium and endochondral bone, including FGF2, FGF7. FGF8, FGF9, FGF17 and FGF18 (Finch et al., 1995; Garofalo et al., 1999; Krejci et al., 2007; Liu et al., 2002; Xu et al., 1999). Of their receptors, *FGFR1* is mostly expressed by hypertrophic chondrocytes, whilst *FGFR3* is expressed in proliferating chondrocytes (Deng et al., 1996; Jacob et al., 2006). FGFR3 has been demonstrated to negatively control chondrocyte proliferation and regulate their differentiation. This is particularly relevant as the most common form of dwarfism in humans, achondroplasia, is caused by heterozygous gain-of-function mutations of *FGFR3* (Rousseau et al., 1994; Shiang et al., 1994). Depending on their exact location and specific genotype, mutations in *FGFR3* cause several disorders, including hypochondroplasia, that are collectively termed the achondroplasia family of skeletal disorders. The delicacy of balanced FGF signalling is illustrated by CATSHL (campodactylyl, tall stature and hearing loss) syndrome which is characterised by tall stature as well as skeletal deformities, and LADD (lacrimoauriculodentodigital) syndrome, which involves deformities of the hands and feet. Both result from heterozygous loss-of-function mutations of *FGFR2, FGFR3* and *FGF10* (Makrythanasis et al., 2014; Rohmann et al., 2006; Toydemir et al., 2006), highlighting that both too much as well as too little FGF signalling has detrimental consequences during skeletal development.

Similar to the FGF family, the transforming growth factor β superfamily with over 40 members, including TGFβ1, GDFs and BMPs, plays a major role in skeletal development. Their relevance for skeletal development and homeostasis has been described in detail previously (Rys et al., 2016; Thielen et al., 2019; W. Wang et al., 2020).

Typically, TGFβ ligands interact with their receptors TGFBR type I and II, which initiate signalling via SMAD2 and SMAD3 to induce chondrogenesis as well as osteoblastogenesis, but repress the last step of both chondrocyte hypertrophy and osteoblast maturation. BMP ligands as well as GDF ligands bind to BMPR type I and II, initiating signalling via SMAD1, SMAD5 and SMAD8, which stimulate chondrocyte proliferation and all steps of osteoblastogenesis. It is no surprise that activating mutations in parts of the TGFβ signalling pathway result in Loeys-Dietz syndrome, characterised by skeletal deformities and overgrowth, Fibrodysplasia Ossificans Progressiva, which leads to heterotopic endochondral ossification as well as various

other disorders (Loeys et al., 2005; Martinez-Garcia et al., 2016; Shore et al., 2006; Stange et al., 2015).

Another large family of signalling factors, the Wnt signalling pathways comprise 19 different ligands that act via three distinct signalling pathways – the Wnt/β-catenin pathway (canonical) and two non-canonical pathways (reviewed in (Huybrechts et al., 2020; Maeda et al., 2019)). When Wnt ligands bind to a receptor (and, depending on the pathway, co-receptor) the canonical pathway leads to the translocation of β-catenin into the nucleus, and activation of Wnt target genes. In the absence of Wnt ligands, β-catenin is degraded via the proteasome. The non-canonical pathways act either via small G proteins and Jun kinase (JNK) or via intracellular Ca^{2+} release and the activation of calcium-sensitive enzymes. In cartilage, the canonical Wnt pathway inhibits cartilage formation from mesenchymal stem cells, favouring osteogenesis (Day et al., 2005). It also promotes chondrocyte hypertrophy by inhibiting PTHrP (Guo et al., 2009).
Mutations in Wnt ligands are associated with various forms of skeletal dysplasia, for example osteogenesis imperfecta type XV (caused by mutations of *WNT1*), and autosomal dominant Robinow syndrome which presents with short-limbed dwarfism (Lu et al., 2018; Person et al., 2010). Similarly, defects in Wnt receptors, caused by mutations of their respective genes, lead to a variety of diseases, including autosomal dominant omodysplasia (facial deformities and shortness of upper extremities), osteosclerosis (thickening of trabecular bone), osteoporosis (increased fragility of the bone), autosomal recessive Robinow syndrome and autosomal dominant brachydactyly type B (malformations of the fingers and toes) (Afzal and Jeffery, 2003; Korvala et al., 2012; Kwee et al., 2005; Saal et al., 2015).

Notch signalling is also known to inhibit chondrogenesis (Chen et al., 2013). Furthermore, Notch signalling represses early and late osteoblast differentiation, but induces the differentiation of osteoprogenitor cells into osteoblast precursors (Engin et al., 2008; Hilton et al., 2008). In brief, the binding of a ligand (members of the jagged and delta-like family) to a Notch receptor triggers the cleavage of the receptor and the release of the Notch Intracellular domain (NICD) which subsequently becomes part of a protein complex acting as a transcription factor (Siebel and Lendahl, 2017). Mutations in components of the Notch signalling pathway lead to Hajdu-Cheney syndrome, characterised among others by short stature and bowing of

the long bones, as well as the phenotypically related lateral meningocele syndrome (short stature, facial dysmorphism and vertebral anomalies), Alagille syndrome (abnormal shape and segmentation of the vertebrae) and spondylocostal dysostosis (segmentation defects of the vertebrae and malalignment and fusion of the ribs) (Bulman et al., 2000; Gripp et al., 2015; Isidor et al., 2011; Oda et al., 1997).

Several signalling pathways described here interact and affect each other in regulating skeletal development (Figure 1.1). Interestingly, they often ultimately act on one (or both) of two transcription factors, SOX9 and RUNX2, which are frequently regarded as master regulators of endochondral ossification (Figure 1.2).

The transcription factor SOX9 is essential for commitment to chondrogenesis (Bi et al., 1999) in MSCs and growth plate chondrocyte differentiation (Dy et al., 2012); and loss of *Sox9* in a mouse model effectively prevented mesenchymal condensation and subsequent endochondral ossification (Akiyama et al., 2004, 2002). Both Wnt and Notch signalling pathways suppress chondrogenesis via their control of *SOX9* expression (Akiyama et al., 2004; Chen et al., 2013) whilst phosphorylated SMAD3 appears to enhance SOX9 transcriptional activity (Furumatsu et al., 2005). Within the growth plate, SOX9 is expressed by proliferating chondrocytes and itself controls the expression of several markers of chondrogenesis, including *COL2A1* and *ACAN*, whilst inhibiting hypertrophy by direct regulation of *RUNX2*. Mutations in *SOX9*, and resulting haploinsufficiency, cause campomelic dysplasia (Foster et al., 1994; Wagner et al., 1994), characterised by shortness and bowing of bones formed by endochondral ossification.

As chondrocytes differentiate towards hypertrophy, the lower concentration of PTHrP no longer represses *RUNX2* expression, which subsequently induces expression of several hypertrophy markers including collagen type X (Guo et al., 2006). When *Runx2* was inactivated in mice, ossification was blocked and chondrocyte differentiation severely impaired (Komori et al., 1997). Additionally, the specific inactivation in chondrocytes not only altered chondrocyte differentiation, but also affected vascular invasion, osteoclast differentiation and periosteal bone formation (Stricker et al., 2002). In agreement with these findings, mutations of *RUNX2* in humans lead to cleidocranial dysplasia (Mundlos et al., 1997; Zhang et al., 2000)

which includes symptoms such as short stature, open skull sutures, scoliosis and *coxa vara*.

In terminal hypertrophic chondrocytes RUNX2 also initiates expression of VEGF (Zelzer et al., 2001). VEGF expression attracts blood vessels, osteoblasts and osteoclasts resulting in the removal of terminal hypertrophic chondrocytes (Zelzer et al., 2004), resorption of the calcified cartilage matrix and deposition of type I collagen-containing bone ECM (Gerber et al., 1999; Hu and Olsen, 2017).

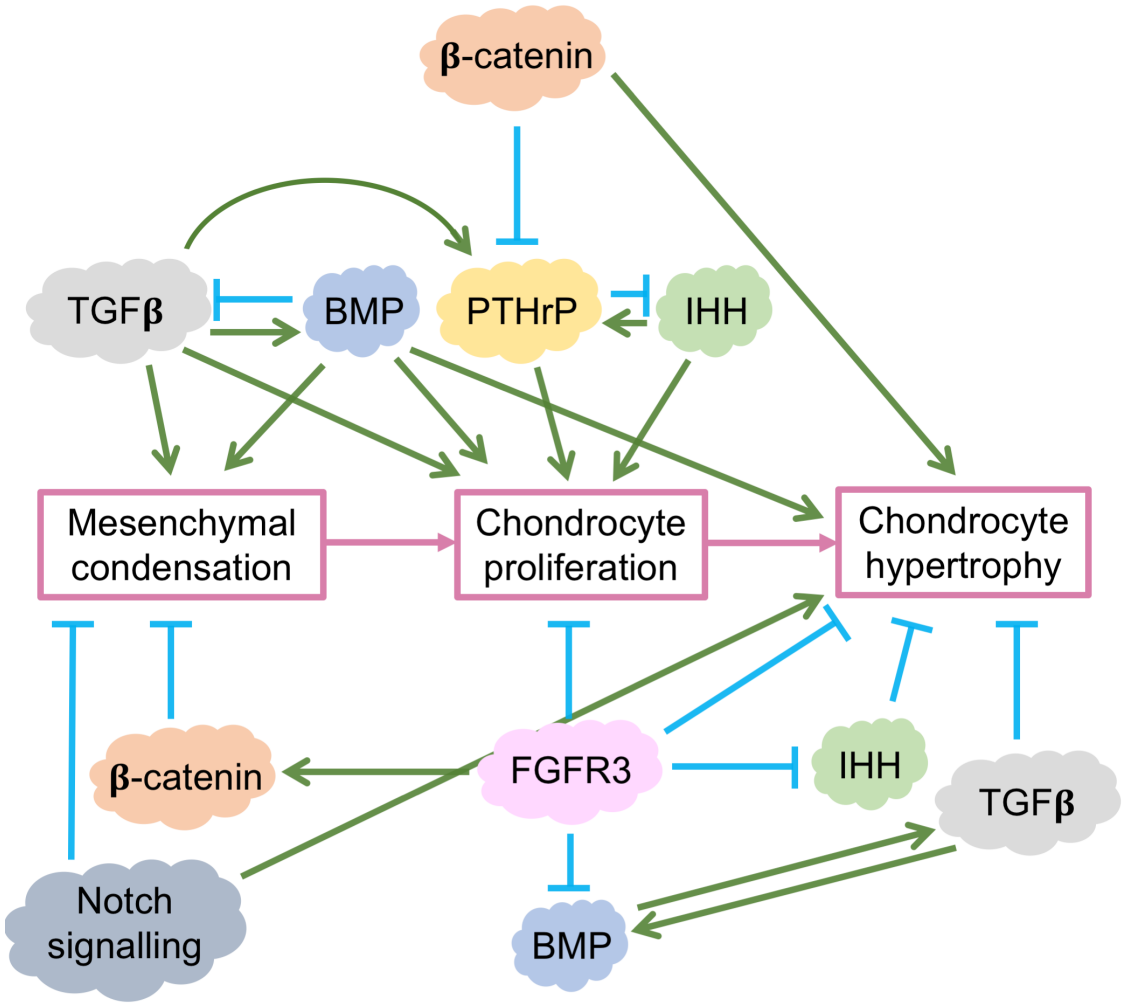

Figure 1.1 – Simplified representation of selected signalling pathways involved in the regulation of endochondral ossification. Green arrows indicate positive regulation, blue bars negative regulation/inhibition.

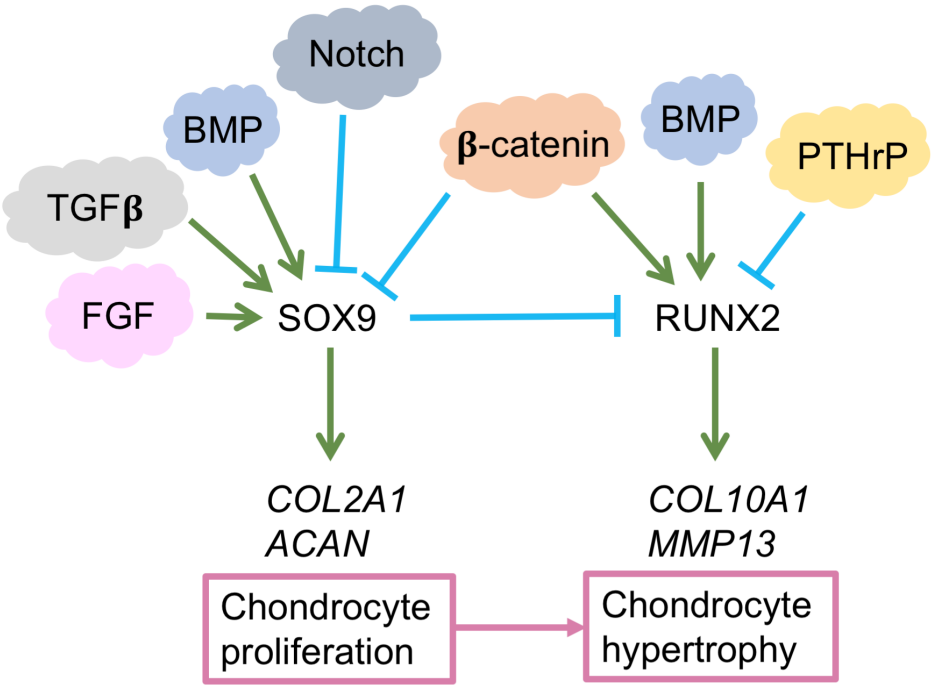

Figure 1.2 – By integrating the signals from various pathways, the two transcription factors SOX9 and RUNX2 act as master regulators of endochondral ossification. Green arrows indicate positive regulation, blue bars negative regulation/inhibition.

1.4 The cartilage extracellular matrix

Endochondral ossification and skeletal development are tightly regulated by numerous signalling factors, but their effects are often dependent on biological context. For example, β-catenin is known to inhibit the differentiation of MSCs into chondrocytes, but stimulates hypertrophy at later stages of development (Day et al., 2005; Guo et al., 2009).

Cartilage itself contains only a single cell type, namely chondrocytes, and is generally considered a tissue of low cellularity, but rich in ECM (Krishnan and Grodzinsky, 2018). The ECM comprises a network of proteoglycans, collagenous components and glycoproteins (Figure 1.3) secreted by chondrocytes (Krishnan and Grodzinsky, 2018). Besides its structural function as a tissue scaffold, the ECM interacts with various molecules, including secreted growth factors and signalling molecules, thereby altering their ability to bind to inhibitors as well as their receptors. For example, TGFβ ligands are secreted as inactive forms, associated with their respective latency-associated pro-peptides (LAPs) and often associated with latent-TGFβ-binding proteins (LTBPs) (Rys et al., 2016). They illustrate the importance of the extracellular environment for their signalling action, since their activation is dependent on interactions with specific components of the ECM, and thus the composition of the ECM directly influences TGFβ bioavailability and activity (Buscemi et al., 2011; Crawford et al., 1998). In other cases, for example BMP7, the pro-domain may target the growth factor to components of the ECM, resulting in sequestration of the growth factor until it is cleaved and released by MMPs (Furlan et al., 2021; Wohl et al., 2016). These findings emphasise the relevance of the ECM and its architecture in the regulation of signalling events during development (S.-H. Kim et al., 2011; Loeser, 2014). Depending on the developmental stage of cartilage, and the differentiation state of the chondrocyte, different matrix proteins are expressed and secreted. The ECM might therefore be considered ‘the context’ of chondrocytes with different ECM compositions being characteristic for distinct differentiation stages. Chondrocytes detect and also respond to changes in the ECM by interacting with their surrounding ECM via cell-surface receptors, such as integrins, and transmembrane proteins (Dieterle et al., 2021; Loeser, 2014).

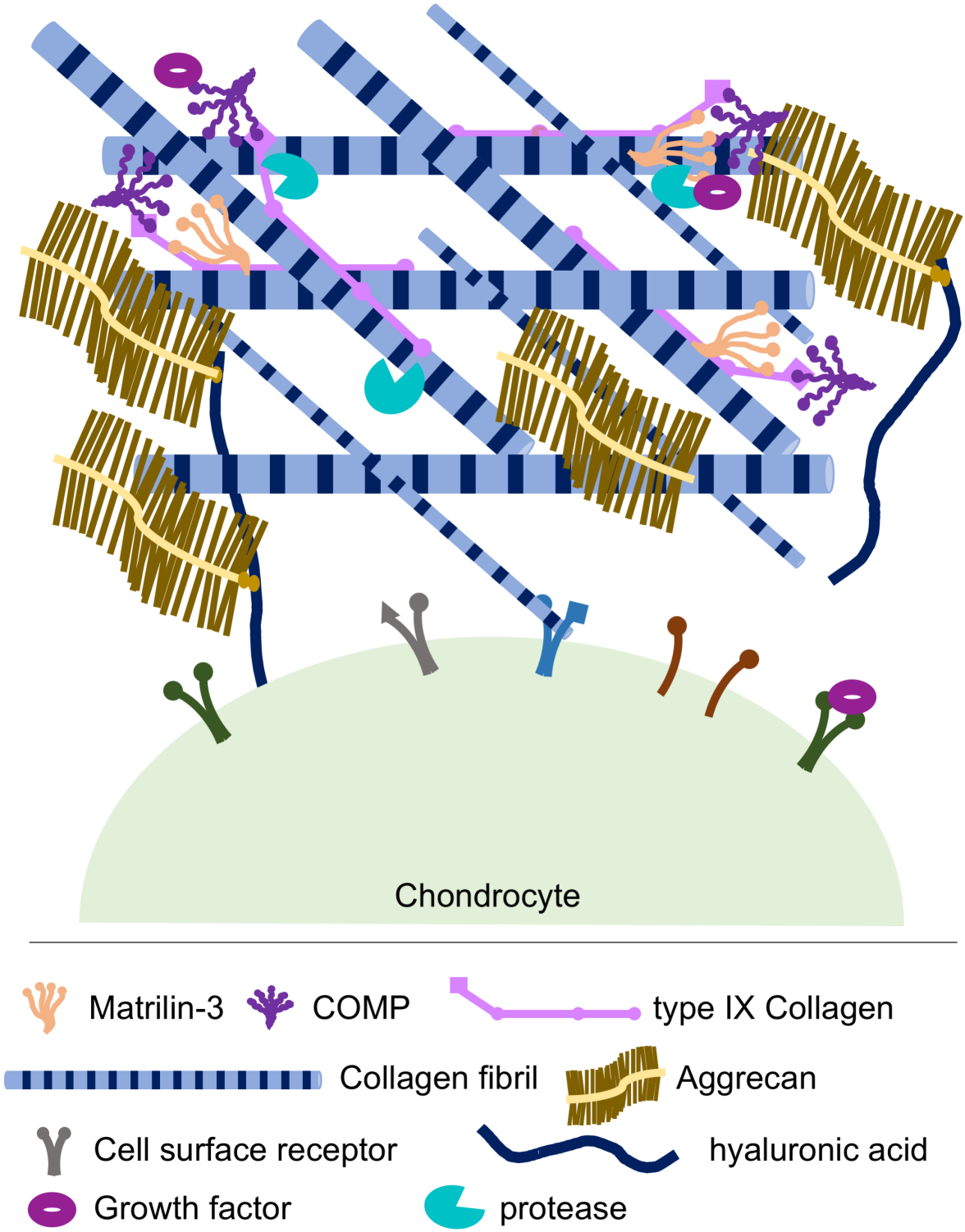

Figure 1.3 – Simplified schematic representation of the cartilage ECM. Aggrecan and collagen fibrils are the two major components of the cartilage ECM. Collagens are extensively decorated with FACIT collagens and adaptor proteins such as matrilin-3 and COMP. Aggrecan forms larger aggregates by interacting with hyaluronic acid. Chondrocytes interact with the ECM via cell surface receptors, for example integrins. The ECM also interacts with various signalling molecules, such as growth factors, to regulate their bioavailability. Proteases play a role in ECM turnover as well as remodelling and contribute to growth factor availability by cleaving them or proteins that sequester them.

1.4.1 Proteoglycans

Proteoglycans (PGs) are one of the major structural components of the cartilage ECM (Knudson and Knudson, 2001). They consist of a central protein core to which single or multiple glycosaminoglycan (GAG) side chains are attached. These GAG chains consist of repeating disaccharide units of one amino sugar (N-acetylglucosamine or N-acetylgalactosamine) and one iduronic sugar (glucuronic acid or iduronic acid) or galactose, often further modified by sulphation. Depending on the sugar composition, GAGs are divided into four classes: chondroitin sulphate (CS), heparan sulphate (HS), keratan sulphate (KS) and hyaluronic acid (Knudson and Knudson, 2001). Whilst the core protein is synthesised in the endoplasmic reticulum (ER), the attachment and modification of GAG chains is a multi-step process that is mediated by enzymes present in the Golgi (Sasarman et al., 2016). CS and HS are attached to their core protein via O-linked glycosylation, whereas KS can be attached either via O- or N-linked glycosylation (Caterson and Melrose, 2018; Couchman and Pataki, 2012; Multhaupt and Couchman, 2012). The mature PG is then secreted via the secretory pathway. Hyaluronic acid, however, is the only non-sulphated GAG, consisting exclusively of glucuronic acid and N-acetylglucosamine. In contrast to other GAGs, hyaluronic acid is not attached to a core protein, but synthesised directly into the extracellular space by three transmembrane synthases, explaining the lack of sulphation (Couchman and Pataki, 2012).

Since GAGs carry a strong negative charge, they attract sodium ions into the tissue, which in turn facilitate the influx of water (Heinegård, 2009). Because cartilage is a tissue that has to withstand physiological loading and compression, PGs contribute extensively to its function and their loss or degradation is commonly regarded as an early sign of cartilage degeneration (Horkay et al., 2017).

Aggrecan is one of the major components of intact cartilage and its most abundant PG, with side chains of CS and KS (Heinegård, 2009). It interacts with hyaluronic acid to form large aggregates (Melrose et al., 2016). The importance of aggrecan is highlighted by several naturally occurring mutations in mice, chicken and cattle, but also by several diseases that are associated with mutations in *ACAN* in humans, including spondyloepimetaphyseal dysplasia (SEMD), spondyloepiphyseal dysplasia (SED) type Kimberley, osteochondritis dissecans (OCD) and idiopathic short stature (reviewed in detail by (Gibson and Briggs, 2016)). Interestingly, some mutations in *ACAN* are thought to lead to haploinsufficiency whilst others appear to have a dominant-negative effect. This emphasises the variety and complexity of skeletal

dysplasia, with multiple disorders arising from mutations in a single gene (i.e. allelic series) and illustrates the need to study gene function as well as specific effects of individual mutations in the context of diseases.

Apart from aggrecan, there are several other PGs that constitute part of the cartilage extracellular matrix (Hwang and Halper, 2021). Small leucine rich repeat proteoglycans (SLRRPs), such as decorin and biglycan, have important regulatory roles in collagen fibril assembly. Decorin, for example, controls the diameter of collagen fibrils, regulates growth factor availability (Knudson and Knudson, 2001; Melrose et al., 2016) and has recently been revealed to regulate cartilage aggrecan content by connecting aggrecan molecules with each other, but also with collagen fibrils (Han et al., 2019).
Remarkably, mutations in *DCN* have been identified in cases of rare, autosomal dominant congenital stromal corneal dystrophy (CSCD), a disease that leads to bilateral corneal clouding, but surprisingly does not cause anomalies of connective tissues (Mellgren et al., 2015). It has been speculated by others (Hwang and Halper, 2021) that this results from individuals with CSCD carrying point mutations of *DCN*, often leading to premature termination codons and a truncated gene product, but not experiencing complete loss of decorin. Interestingly, in a study that attempted to address this, cells isolated from human CSCD corneas were found to be able to secret the truncated decorin, whilst in a mouse model, truncated decorin was found to be retained intracellularly (Mellgren et al., 2015). This finding highlights the need to validate diseases models, and – if possible – to compare different types of model systems.

1.4.2 Collagens

Collagens are a family of large, trimeric proteins that are either secreted or integrated into the plasma membrane (Gelse et al., 2003). Each collagen is composed of three α chains that depending on the collagen type may be products of the same (for example type II collagen from *COL2A1*) or different genes (type IX collagen from *COL9A1, COL9A2* and *COL9A3*). To date 28 collagens have been described (Ricard-Blum, 2011) and depending on their structural and functional properties they have been divided into several subgroups such as 1) fibril-forming, 2) fibril-associated with interrupted triple helices (FACIT) and 3) network-forming (Figure 1.4). However, all collagen α chains contain characteristic Gly-X-Y repeats with

proline and 4-hydroxyproline frequently occupying the X and Y positions respectively (Ricard-Blum, 2011).
These repeats are crucial for the formation of the collagen triple helix, which assembles from the C-terminus in a zipper-like fashion. When formed correctly, the triple helical structure is highly resistant to strain as well as several proteases (Gelse et al., 2003). Since glycine is the smallest amino acid, its presence at every third position is crucial for proper formation of the triple helix. Accordingly, mutations that result in an amino acid substitution at the position of glycine in the triple helical region disrupt the formation of a stable triple helix and are thus frequently found to be disease-causing, for example in osteogenesis imperfecta (OI) (Forlino and Marini, 2016), vascular Ehlers-Danlos syndrome (EDS) (Omar et al., 2021; Pepin et al., 2014), Bethlem myopathy and Ulrich congenital muscular dystrophy (UCMD) (Butterfield et al., 2013).

In cartilage, type II, III, VI, IX, X, XI, XII and XIV collagen are present, with type II collagen being the most abundant form (Mackie et al., 2011; Ricard-Blum, 2011; C. Wang et al., 2020). Type II collagen, together with type XI collagen, forms fibrillar structures with their surface decorated with the FACIT collagen type IX collagen. Type IX collagen consists of three collagenous domains (COL1-3) that are interrupted by several non-collagenous (NC) domains (Ricard-Blum, 2011). Its most N-terminal NC domain, NC4, and the following COL3 domain project away from the collagen fibril surface, facilitating interactions with other, non-collagenous proteins such as matrilins and cartilage oligomeric matrix protein (COMP), and thus connecting the collagenous protein network with other components of the ECM (Ricard-Blum, 2011).
The importance of type II collagen for cartilage integrity is highlighted by the various diseases that arise from heterozygosity for different mutations in *COL2A1*, including spondyloepiphyseal dysplasia congenita, achondrogenesis type II, Stickler syndrome type I, Kniest dysplasia and spondyloepimetaphyseal dysplasia (Kannu et al., 2012; Mortier et al., 2019). Symptoms include disproportionate short stature, various joint deformities and sometimes incomplete ossification of parts of the skeleton, but anomalies are also found in the eyes and ears (Kannu et al., 2012). Although differing in disease severity, multiple disease-causing mutations appear to result in substitution of a glycine residue in the Gly-X-Y repeats of the type II collagen molecule, preventing successful folding of the triple helix (Kannu et al., 2012).

Misfolded type II collagen is subsequently retained in the ER, inducing ER stress, which may ultimately drive apoptosis and abnormal chondrocyte differentiation (Chakkalakal et al., 2018; Chung et al., 2009; Liang et al., 2014).

It is noteworthy that mutations in *COL2A1* and OI-causing mutations in *COL1A1* as well as *COL1A2* may be mechanistically very similar to each other. As it is the major type of collagen in bone, skin, tendons and ligaments, type I collagen disorders differ from type II collagen diseases in the tissues and cell types that are involved and accordingly result in distinct phenotypes (Bateman et al., 2009). However, amongst the various reported mutations of type I collagen, glycine substitutions are relatively common and have been demonstrated to cause not only misfolding and reduced collagen secretion, but also ER stress in osteoblasts, ultimately resulting in fragile bones, which is the most prominent feature of OI (Besio et al., 2018; Garibaldi et al., 2021; Marini et al., 2007; Mirigian et al., 2016).

In addition to mutations in *COL2A1*, mutations in *COL9A1, COL9A2* and *COL9A3* also cause Stickler syndrome (Baker et al., 2011; Faletra et al., 2014; Nixon et al., 2019; Van Camp et al., 2006). In contrast to *COL2A1* mutations, Stickler syndrome caused by mutations in the genes encoding for type IX collagen is an autosomal-recessive disease. The main symptoms of autosomal-recessive Stickler syndrome include hearing difficulties, myopia and epiphyseal dysplasia. Mutations in all three genes encoding the three chains of type IX collagen are also associated with autosomal dominant multiple epiphyseal dysplasia (EDM6, EDM2 and EDM3 respectively) (Czarny-Ratajczak et al., 2001; Muragaki et al., 1996; Paassilta et al., 1999). These mutations are typically found at splice donor or acceptor sites (Lohiniva et al., 2000). Conflicting observations have been reported as to whether mutant type IX collagen is retained intracellularly in these cases (Bönnemann et al., 2000; Spayde et al., 2000).

Whilst most collagens, including type II and type IX, are expressed throughout cartilage, the network forming type X collagen is expressed exclusively by hypertrophic chondrocytes (Rosati et al., 1994; Schmid and Linsenmayer, 1983). Type X collagen is a homotrimer and its α chain is encoded by the *COL10A1* gene (Figure 1.5) which is composed of three exons; exon 1 encodes for the 5'-UTR, exon 2 for a part of the 5'-UTR, the signal peptide and a part of the non-collagenous (NC)

2 domain and exon 3 contains the rest of the protein sequence as well as the 3'-UTR (Apte et al., 1991; Bogin et al., 2002; Thomas et al., 1991).

Mutations in type X collagen cause metaphyseal chondrodysplasia type Schmid (MCDS) marked by widened, irregular growth plates and short stature (Bateman et al., 2004, 2005; Bogin et al., 2002; Forouhan et al., 2018b; Rajpar et al., 2009). Interestingly, the vast majority of MCDS-causing mutations in *COL10A1* are found in exon 3 regions encoding the NC1 domain, with only two mutations reported in exon 2 in the coding sequence of the signal peptide (Ikegawa et al., 1997).

The restricted expression of type X collagen to hypertrophic cartilage complicates the design and interpretation of experiments. In principal, there appear to be two distinct disease mechanisms: nonsense-mediated RNA decay (NMD) due to premature termination codons between codon 582 and 673 of *COL10A1* appears to cause haploinsufficiency for type X collagen in patient-derived chondrocytes (Bateman et al., 2003; Tan et al., 2008), whilst amino acid substitutions impair protein folding and secretion, resulting in type X collagen retention in the ER as demonstrated in various *in vitro* and *in vivo* models (Forouhan et al., 2018b; Ho et al., 2007; Rajpar et al., 2009; Wilson et al., 2005). Furthermore, the expression and intracellular retention of mutant type X collagen was shown to interfere with chondrocyte differentiation *in vivo* since hypertrophic chondrocytes appeared to 'revert' differentiation and re-express *Col2a1* (Ho et al., 2007; Rajpar et al., 2009). Indeed, the retention of mutant type X collagen and the induction of ER stress and the unfolded protein response (UPR) has been identified as a crucial part of the disease mechanism and a potential therapeutic target (Forouhan et al., 2018b; Ho et al., 2007; Mullan et al., 2017; Rajpar et al., 2009; Wang et al., 2018). Importantly, the induction of ER stress alone in hypertrophic chondrocytes is sufficient to induce the MCDS-typical expansion of the hypertrophic zone, and the delayed recruitment of osteoclasts to the vascular invasion front (Ho et al., 2007; Kung et al., 2012; Rajpar et al., 2009).

The significance of intracellular mutant type X collagen retention is further highlighted by the lack of major skeletal defects in mice deficient for type X collagen (Ho et al., 2007; Rosati et al., 1994) although loss of type X collagen caused *coxa vara* in the right femur in one mouse model (Kwan et al., 1997). The very limited phenotype in knock-out mouse models of type X collagen also calls into question potential

haploinsufficiency caused by NMD. This apparent discrepancy might be due to different model systems (mouse models vs patient-derived cells) or the methods used for analysis. Remarkably, NMD only occurred in patient-derived chondrocytes, but not osteoblasts or lymphoblasts, both expressing extremely low amounts of *COL10A1* transcript (Bateman et al., 2003). Furthermore, a mutation that has been demonstrated to cause transcript degradation via NMD in patient-derived chondrocytes was shown to be expressed in a knock-in mouse model of MCDS (Forouhan et al., 2018b). These findings demonstrate the need for diverse model systems to study MCDS *in vitro* and *in vivo,* taking into consideration potential species- and tissue-specific differences.

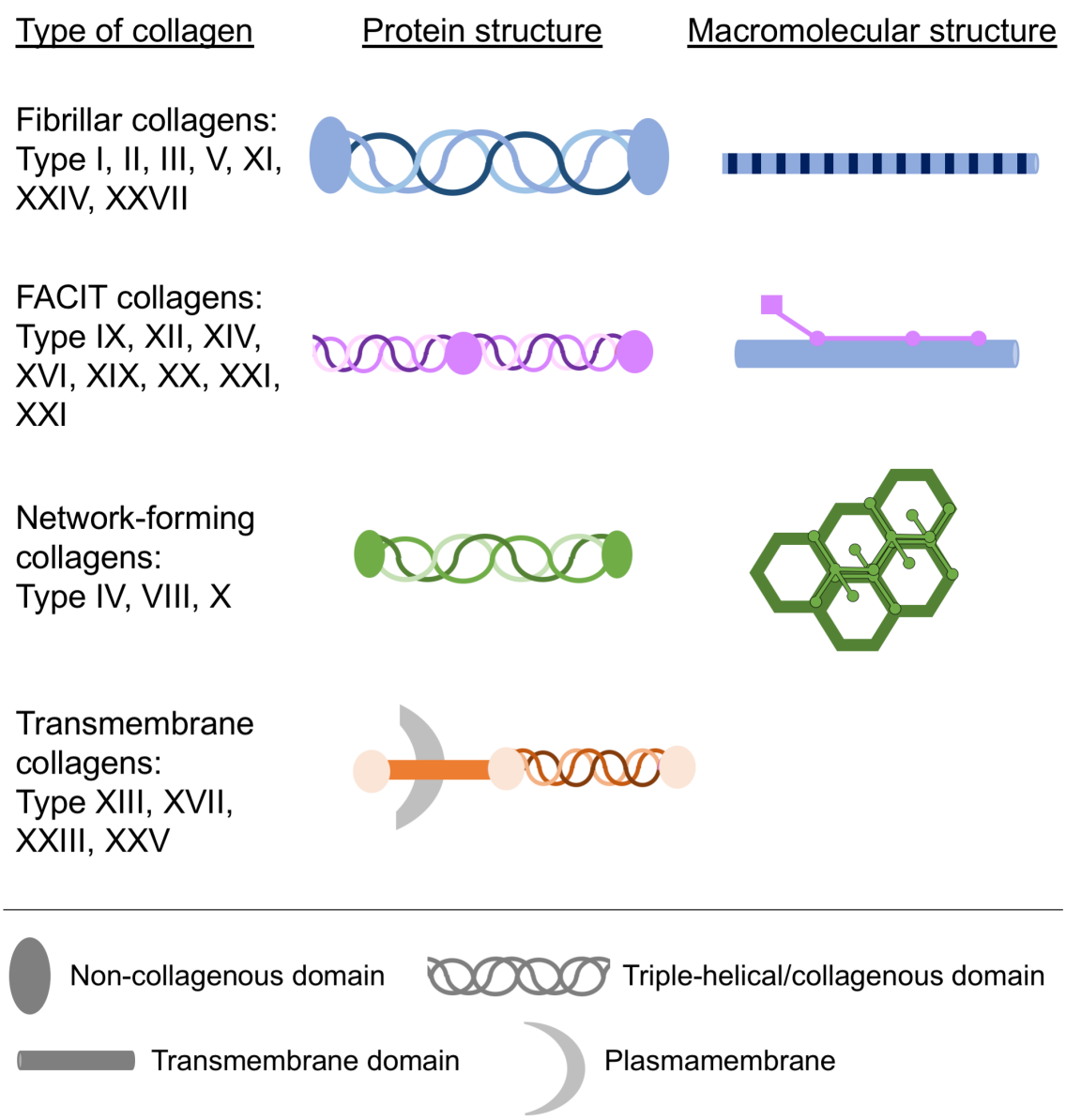

Figure 1.4 – Cartilage collagens differ in their protein structure and their resulting macromolecular assembly. Simplified schematic representation of some major groups: fibrillar, FACIT, network-forming and transmembrane collagens. By decorating the surface of fibrillar collagens, FACIT collagens regulate the assembly into larger fibres. Network-forming collagens assemble into various types of networks, for example the hexagonal-lattice type network that is formed by type X collagen. Transmembrane collagens are anchored to the cell surface by their transmembrane domain.

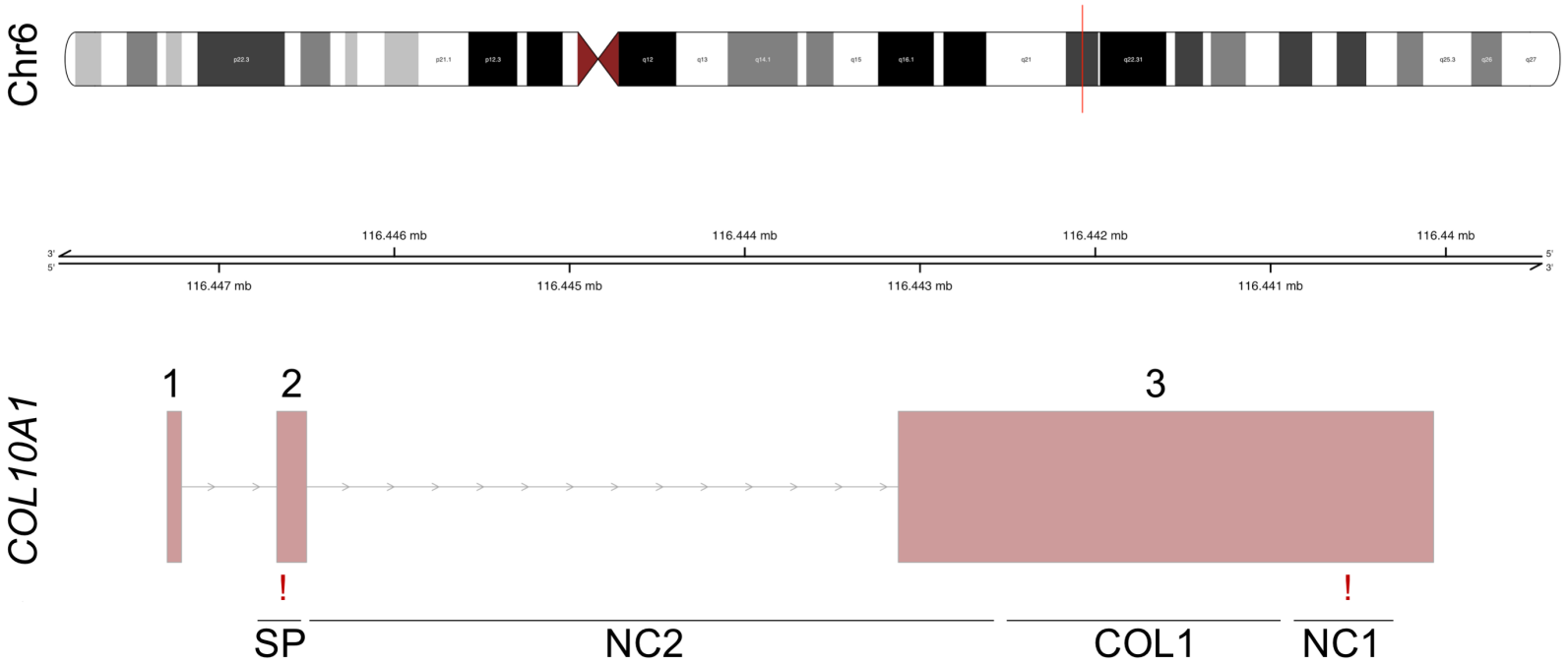

Figure 1.5 – Location and structure of the *COL10A1* gene and corresponding protein domains. Chr: Chromosome. SP: signal peptide. NC: Non-collagenous domain. COL: collagenous (triple-helical) domain. Exons in which disease-causing mutations have been identified are marked with !.

1.4.3 Non-collagenous glycoproteins

In addition to proteoglycans and collagens, the cartilage ECM contains numerous non-collagenous, often glycosylated proteins, such as the matrilin protein family (Klatt et al., 2011) and thrombospondins (TSPs) (Adams and Lawler, 2011). These proteins interact with various members of the collagen family as well as proteoglycans, thereby serving as adaptor proteins and connecting the two networks together in the cartilage ECM (Di Cesare et al., 2002; Mann et al., 2004; Otten et al., 2010; Pihlajamaa et al., 2004; Rosenberg et al., 1998; Wiberg et al., 2003). Besides their function as adaptor molecules, these proteins also regulate growth factor or protease activity or facilitate the secretion of other ECM molecules (Haudenschild et al., 2011; Ishida et al., 2013; Schulz et al., 2016; X. Yang et al., 2014). Matrilin-3 and COMP (also known as TSP-5) are of particular interest since mutant forms of these proteins have been identified as causes of multiple epiphyseal dysplasia (MED) and pseudoachondroplasia (PSACH) (Briggs et al., 1995; Chapman et al., 2001; Jackson et al., 2004). Whilst PSACH is caused exclusively by mutations in *COMP*, MED is a heterogenous disease with mutations identified not only in type IX collagen genes (see section 1.4.2) but also *COMP* and *MATN3* in autosomal dominant MED (Jackson et al., 2012; Mortier et al., 2001) and *CANT1* as well as *DSTD* in autosomal recessive MED (Balasubramanian et al., 2017; Superti-Furga et al., 1999). Both MED and PSACH result in delayed or irregular ossification of the epiphysis and thus lead to disproportionate dwarfism, joint pain and restricted movement with phenotypes ranging from mild (MED) to severe (PSACH) (Jackson et al., 2012). Many patients require joint replacement of the knee or hips in early adulthood (Chapman et al., 2001; Mäkitie et al., 2004; Mortier et al., 2001). On a cellular level the dilation of ER cisternae in affected chondrocytes is a classical feature of these diseases (Dinser et al., 2002; Fresquet et al., 2008). Dilation of the ER is caused by the retention of mutant proteins which presents a common disease mechanism in many types of skeletal dysplasia (Leighton et al., 2007; Nundlall et al., 2010; Suleman et al., 2012).

1.4.4 Cartilage Oligomeric Matrix Protein (COMP)

The *COMP* gene is located on human chromosome 19. Its product COMP, a pentameric glycoprotein, was first described in 1992 (Hedbom et al., 1992), followed by descriptions of its cDNA (Oldberg et al., 1992) and chromosomal location in 1994 (Newton et al., 1994). Only one year later, in 1995, mutations causing PSACH and MED were first mapped to *COMP* (Briggs et al., 1995; Hecht et al., 1995).

COMP consists of 19 exons, encoding the signal peptide, the N-terminal coiled coil domain, four EGF-like – or type 2 – repeats, followed by eight so called type 3 repeats and a C-terminal domain (Figure 1.6). Within the cartilage ECM, COMP is known to interact with several other structural proteins as well as growth factors and proteases (extensively reviewed in (Acharya et al., 2014)). Remarkably, COMP binds to the two other proteins known to be involved in autosomal dominant MED, type IX collagen and matrilin-3. Whilst COMP interacts via its C-terminal domain (CTD) with the N-terminal NC4 domain of type IX collagen, matrilin-3 appears to bind to the COL3 domain through its single Von Willebrand Factor A domain (Figure. 1.8). Together, these proteins play a critical role in establishing and maintaining the cartilage ECM and cartilage integrity (Blumbach et al., 2008; Budde et al., 2005; Groma et al., 2012).

Since 1995, numerous mutations that cause either MED or PSACH have been identified in *COMP*. PSACH is generally considered to be a more severe form of skeletal dysplasia than MED, with symptoms including the typical short stature, laxity of the ligaments, scoliosis as well as early-onset osteoarthritis (Briggs et al., 1995). The majority of mutations (about 85 %) are found within the type 3 repeats of COMP, encoded by exons 8-15, with a smaller number of mutations occurring in the C-terminal domain encoded by exons 16-19 (Figure 1.7). Curiously, about 30 % of PSACH cases appear to be caused by the p.D469del (or p.D473del) mutation, in which one of five aspartic acid residues is missing (Jackson et al., 2012). Substitution of this aspartic acid residue (or indeed, other aspartic acid residues) can also cause disease. The type 3 repeats of COMP are known to be calcium-binding domains, and mutations in the type 3 repeats have been demonstrated to modify the number of bound calcium ions (Thur et al., 2001). This has been proposed to interfere with protein folding, resulting in intracellular retention. Early *in vitro* studies using cartilage and tendon samples of patients showed protein retention within the rough ER, although no difference in the amount of secreted protein was observed (Délot et al., 1999, 1998).

Since then, various mouse models of PSACH, several of which express p.D469del COMP, have been generated (Piróg-Garcia et al., 2007; Posey et al., 2009; Schmitz et al., 2008; Suleman et al., 2012); however, they differ in the level of protein expression (transgene vs knock-in) and mimic the human PSACH phenotype to

varying degrees. The knock-in model of the p.D469del *Comp* mutation resembles the human phenotype in that homozygous animals developed short-limbed dwarfism after birth as well as progressive hip dysplasia (Suleman et al., 2012). The growth plate was found to be extensively disorganized and displayed regions of hypocellularity. Furthermore, chondrocyte proliferation was reduced and apoptosis was both increased and spatially dysregulated (Suleman et al., 2012). In contrast to individuals with PSACH, however, heterozygous animals exhibited a much milder phenotype.
Another knock-in model, expressing *Comp* with the C-terminal p.T583M mutation (equivalent to human p.T585M), exhibited a reduction in post-natal growth and hip dysplasia (Piróg-Garcia et al., 2007). Consistent with individuals carrying the p.T585M mutation displaying mild PSACH, heterozygous animals showed a less severe phenotype than homozygous animals. In addition to that, phenotypic severity was influenced by the genetic background of the p.T583M mouse model, suggesting that genetic modifiers may contribute to disease severity of PSACH and/or MED (Piróg et al., 2014). The identity of these modifiers and/or the pathways they are involved in remain to be investigated.

Expression of rat mutant (p.D469del) COMP in a transgenic mouse model led to reduced post-natal growth in male, but not female mice. Interestingly, this effect was aggravated by crossing transgenic animals onto a *Comp*-deficient background (Schmitz et al., 2008).
The results of studies employing a mouse model overexpressing human p.D469del COMP (MT-COMP mice) when induced with doxycycline have indicated that mutant COMP may interact with other ECM proteins within the ER and form large aggregates (Posey et al., 2009). Interestingly, the genetic ablation of *Comp* in mice did not appear to have major consequences for cartilage development (Svensson et al., 2002), but COMP has been demonstrated to be required for secretion of type I collagen in dermal fibroblasts (Schulz et al., 2016). Accordingly, there may also be a role for COMP in skeletal muscle and tendon, especially since collagen fibrils in tendon appeared irregular and myopathy was observed in PSACH knock-in mouse models carrying the p.D469del or the p.T583M mutation (Piróg et al., 2013).

Importantly, the disease mechanism for mutations that occur in the type 3 repeats is thought to be distinct from the mechanism of mutations within the C-terminal domain

of COMP. Typically, mutations in the C-terminal domain of COMP do not prevent protein secretion, but affect collagen fibril formation (Chen et al., 2008; Hansen et al., 2011; Piróg-Garcia et al., 2007; Schmitz et al., 2006). Because the C-terminal domain is thought to be responsible for collagen binding as well as the interaction with other ECM components, impairment of these interactions and disruption to the ECM architecture has been proposed as the underlying mechanism for MED and PSACH caused by mutations in the C-terminal domain.

In contrast, the 'archetypal' mutation of the type 3 repeats, p.D469del interferes with COMP secretion, thus driving ER stress that is likely the cause for dysregulated apoptosis. For other mutations located in the type 3 repeats, only a limited number of studies have investigated their secretion *in vitro*, and the observed effects varied between mutations (i.e. genotype specific) (Chen et al., 2008; Schmitz et al., 2006; Thur et al., 2001). The disease mechanisms may therefore also vary between different mutations, even within the type 3 repeats. Milder phenotypes may be associated with incomplete protein retention, and thus less pronounced ER stress (Chen et al., 2008). Notably, conflicting observations have been reported as to how chondrocytes respond to mutant COMP (Posey et al., 2009; Suleman et al., 2012). Some studies report activation of the PERK branch of the UPR, a signalling cascade aiming to reduce protein folding load onto the ER by reducing translation and simultaneously to increase chaperone capacity within the ER to improve protein folding (see section 1.5/1.5.2).
Others did not detect signs of an active UPR on gene expression or proteomic level for the same mutation (Bell et al., 2013; Hartley et al., 2013; Suleman et al., 2012). This discrepancy is likely due to the different types of mouse model used in the studies. Still, both mouse models exhibited signs of oxidative stress and inflammation (Posey et al., 2012; Suleman et al., 2012). Notably, although p.T583M COMP was not retained in growth plate chondrocytes *in vivo*, a mild and transient activation of the UPR was observed (Piróg-Garcia et al., 2007).

How exactly the oxidative response to p.D469del COMP is mediated remains somewhat unclear, although some research using the MT-COMP mouse model has suggested the involvement of CHOP (*Ddit3)*, tumor necrosis factor (TNF) α and mammalian target of rapamycin complex 1 (mTORC1) (Posey et al., 2019, 2015). Considering that the p.D469del knock-in mouse model did not display altered CHOP

levels, it appears likely that other factors are involved in driving oxidative stress and inflammation. In fact, previous microarray analysis of the p.D469del knock-in mouse model has indicated a possible role for nuclear factor kappa b (NFκB) in PSACH (Suleman et al., 2012). NFκB has been identified as a central regulator of inflammation via both canonical and non-canonical pathways, following the activation of TNF receptor, interleukin-1 (IL-1) receptor or Toll-like receptors by ligand binding (Hayden and Ghosh, 2012; Kracht et al., 2020).

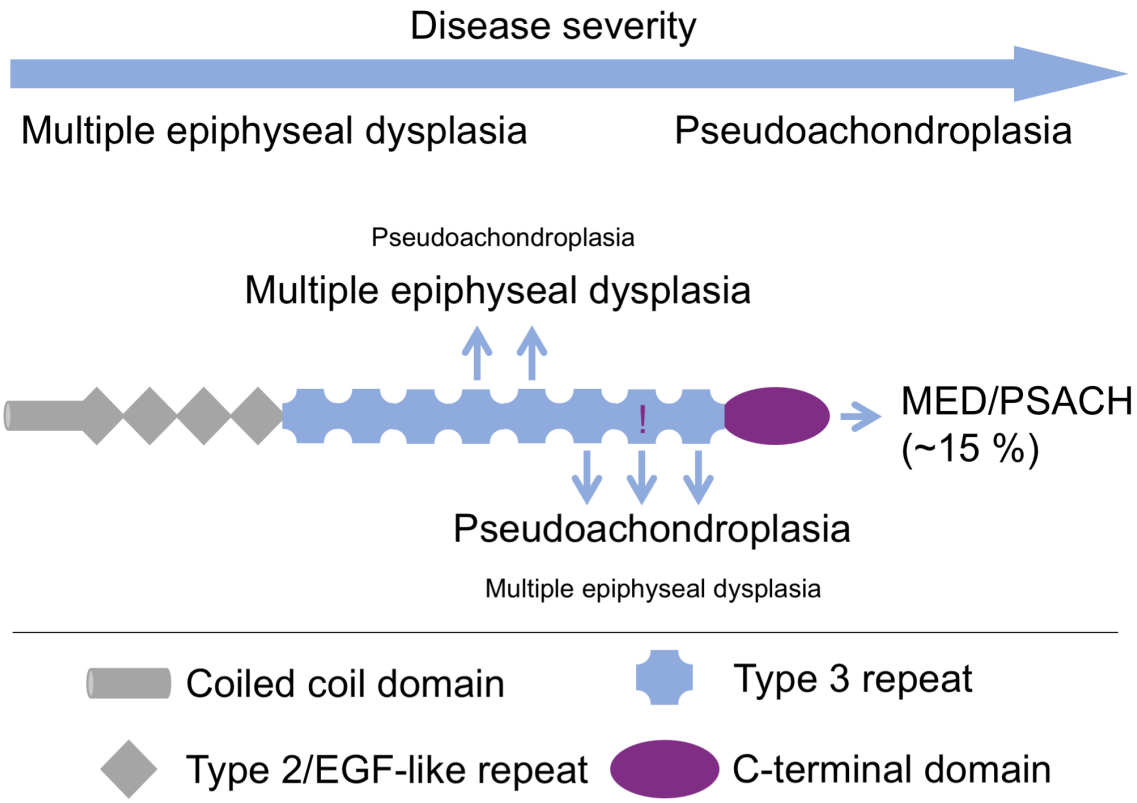

Figure 1.6 – Schematic depicting disease severity of COMPopathies and known correlations between the domain in which a mutation occurs and disease severity. The location of the particularly common p.D469del mutation is marked with !.

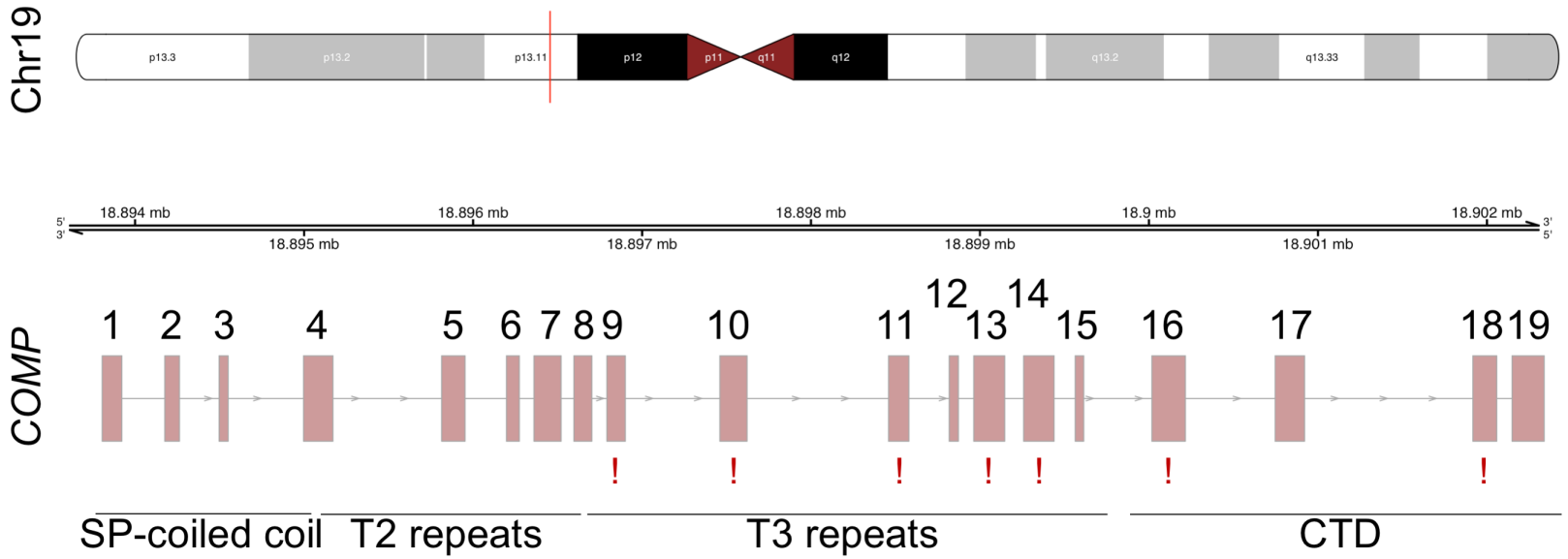

Figure 1.7 – Location and structure of the *COMP* gene and corresponding protein domains. Chr: Chromosome. SP: signal peptide. T2 repeats: EGF-like repeats (T2 repeats 2 and 3 bind Ca^{2+}). T3 repeats: Thrombospondin type 3 repeats. CTD: C-terminal domain. Exons in which disease-causing mutations have been identified are marked with !.

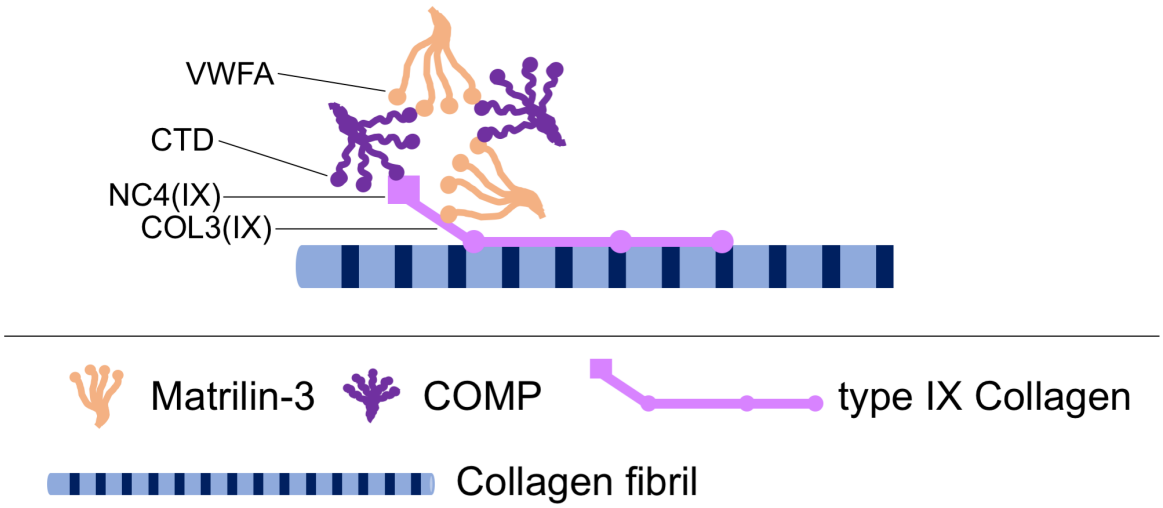

Figure 1.8 – Interaction of COMP with type IX collagen and matrilin-3. COMP binds to the N-terminal non-collagenous domain 4 (NC4) of collagen IX via its C-terminal domain (CTD), and matrilin-3. The von Willebrand factor A domain (VWFA) of matrilin-3 interacts not with the NC4(IX) domain, but with the collagenous domain 3 (COL3) of type IX collagen. Mutations in *COMP, MATN3* and the three genes encoding type IX collagen are associated with MED.

1.4.5 Matrilin-3

Similar to COMP, matrilin-3 is an oligomeric, glycosylated ECM protein. Matrilin-3 is part of the matrilin protein family, which comprises four members (matrilin-1-4). All matrilins are present in cartilage; however, matrilin-2 and -4 are also found in various other tissues, including tendon and ligament, brain, and intestine. Structurally, all matrilins have at least one Von Willebrand Factor A domain (VWFA) domain, one or more EGF-like domains and a C-terminal coiled coil domain that facilitates oligomerisation into trimers or tetramers. By interacting with several components of the cartilage ECM, including collagens and SLRRPs, matrilins function as adaptor proteins.

Structurally, *MATN3* consists of eight exons, that encode for an N-terminal VWFA domain, followed by four EGF-like domains, and a C-terminal coiled coil domain responsible for the assembly of the matrilin-3 tetramer (Figure 1.7). In contrast to all other matrilin family members which contain 2 VWFA domains, matrilin-3 contains a single VWFA domain. Matrilin-3 has been demonstrated to interact with COMP and type IX collagen, the latter being required for matrilin-3 incorporation into the cartilage ECM (Budde et al., 2005; Mann et al., 2004; Otten et al., 2010).

Remarkably, the loss of *Matn3* (or *Matn1* or *Matn2*) did not result in obvious skeletal defects (Aszódi et al., 1999; Ko et al., 2004; Mátés et al., 2004), reduced growth or osteoarthritis in mice. This prompted the suggestion that some matrilins may be functionally redundant, and other members of the matrilin family may be able to compensate for the loss of a matrilin in the ECM. This is at least partially supported by an apparent increase in matrilin-4 in cartilage from *Matn1*-deficient mice (Aszódi et al., 1999) and elevated matrilin-2 levels in *Matn4*-deficient mice (Li et al., 2020). It is noteworthy that both *Matn4*-deficient as well as *Matn1-4*-deficient mice were susceptible to severe spontaneous osteoarthritis (Li et al., 2020), indicating that other matrilins may not completely compensate for the loss of matrilin-4. So far, no disease-causing mutations of *MATN1, MATN2* or *MATN4* have been identified in humans.

In contrast, mutations of *MATN3* are known to cause MED (Chapman et al., 2001; Mäkitie et al., 2004), similar to some mutations of *COMP* (Briggs et al., 1995; Jackson et al., 2012). Whilst PSACH is considered to be more severe, MED patients

usually display milder symptoms, including but not limited to, joint stiffness and pain, mild short stature and early-onset osteoarthritis (Briggs et al., 1995). Notably, mutations of *MATN3* are typically found in the second exon, encoding the VWFA domain, which appears responsible for the interaction with type II and type IX collagen as well as COMP (Fresquet et al., 2007). Whilst MED is linked to heterozygous mutations in *MATN3*, homozygous mutations in exon 2 or 3 result in the more severe disease spondyloepimetaphyseal dysplasia (SEMD) (Borochowitz et al., 2004; Das et al., 2020; Shyamasundar et al., 2020).
Together with the generally normal development of matrilin-deficient mice, the observation that mutant matrilin-3 accumulates within the ER (Cotterill et al., 2005; Fresquet et al., 2008; Jackson et al., 2004) contributed to the hypothesis that the disease mechanism of MED may be a dominant-negative effect, rather than the loss of matrilin-3 as an adaptor protein of the cartilage ECM. Indeed, when a knock-in mouse model of MED was generated, short-limbed dwarfism after birth was observed. The growth plates of mutant mice were disorganised, and chondrocytes exhibited pronounced intracellular retention of matrilin-3 (Leighton et al., 2007). Further studies revealed that mutations may interfere with accurate disulphide-bridge formation, driving aggregation of mutant matrilin-3 in the ER as well as formation of multi-protein complexes containing several chaperones and protein disulphide isomerases (PDIs) (Cotterill et al., 2005; Hartley et al., 2013).

In contrast to the knock-in mouse model of PSACH, analysis of the MED knock-in mouse model revealed elevated levels of chaperones, and activation of the UPR (Bell et al., 2013; Nundlall et al., 2010; Piróg et al., 2019). Subsequently, several transgenic mouse models overexpressing misfolding proteins that are not typically expressed by chondrocytes, and therefore do not play a role in the cartilage extracellular matrix, were generated (Gualeni et al., 2013; Kung et al., 2015; Rajpar et al., 2009). Compellingly, despite normal cartilage ECM composition and organisation, these mouse models exhibited chondrodysplasia-like phenotypes illustrating the significance of ER stress and the UPR cascade for skeletal development and the disease mechanisms of skeletal dysplasia.

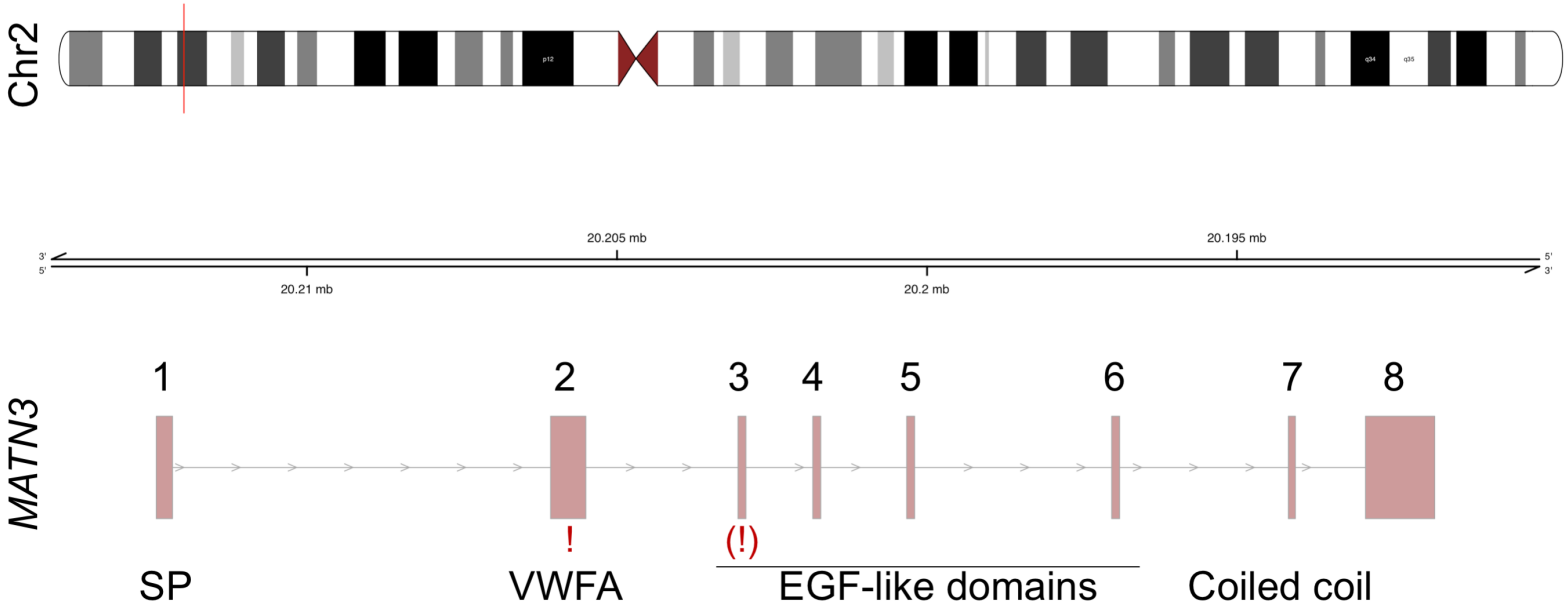

Figure 1.9 – Location and structure of the *MATN3* gene and corresponding protein domains. Chr: Chromosome. SP: signal peptide. VWFA: von Willebrand factor A domain. Exons in which disease-causing mutations have been identified are marked with !. Mutations in exon 3 marked with (!) have been described to predispose to hand osteoarthritis. Homozygous missense mutations in exon 2 (marked with !) and exon 3 (marked with (!)) result in a form of spondyloepimetaphyseal dysplasia (SEMD).

1.5 The Unfolded Protein Response (UPR)

Secreted proteins like matrilin-3 and COMP are inserted into the ER lumen co-translationally, where they are folded and if necessary modified (Hetz and Papa, 2018). Various proteins and enzymes assist in protein folding: Some bind to transiently exposed hydrophobic surfaces of the incompletely folded protein to prevent its aggregation, others bind to incompletely folded proteins to retain them in the ER lumen for correct folding, and yet others actively participate in the formation of correct disulphide bonds by facilitating disulphide exchange reactions (Hetz and Papa, 2018). Misfolded proteins are recognized by various quality control mechanisms and are cleared by either the ER-associated degradation pathway (ERAD) or autophagy (Wang and Kaufman, 2012). The accumulation of misfolded proteins leads to the activation of the UPR, initiating a signal cascade that attenuates protein translation, but selectively increases expression of chaperone proteins (Hughes et al., 2017). Whilst in principle aiming to restore the homeostasis of the ER, continuous activation of the UPR can ultimately lead to the induction of apoptosis (Morishima et al., 2002; Piróg et al., 2014; Tabas and Ron, 2011). The UPR comprises three genetic pathways, all of which involve immunoglobulin heavy chain binding protein (BiP/Grp78), which is a chaperone of the Hsp70 family.

1.5.1 The IRE1 pathway

IRE1 (in humans also known as ERN1) is a transmembrane serine/threonine kinase that also shows endoribonuclease activity. In the absence of misfolded or unfolded proteins BiP is bound to the luminal domain of IRE1, thereby inhibiting its activation. When BiP dissociates from IRE1 to bind to unfolded proteins, IRE1 dimers form and are activated by auto-phosphorylation (Lebeaupin et al., 2020). Activated IRE1 triggers unconventional splicing of *X-box binding protein 1* (*XBP1*) mRNA. The product of unspliced (XBP1u), as well as the spliced mRNA (XBP1s), acts as a transcription factor; however, whilst XBP1u serves as a transcriptional repressor of UPR-associated genes, XBP1s upregulates these genes (Hetz and Papa, 2018). Additionally, IRE1 is able to degrade mRNA during ER stress in a process called RIDD (regulated IRE1-dependent decay), thereby reducing the protein load on the ER folding machinery (Hollien et al., 2009).

The UPR, including IRE1, is particularly important in tissues that experience a high secretory load, for example the pancreas. It is therefore not surprising that ablation of *Ire1* in a mouse model resulted in reduced body weight, reduced pancreatic mass and hypoinsulinemia as well as hyperglycaemia (Iwawaki et al., 2010).

In cartilage, the ablation of *Xbp1* in mice led to a chondrodysplasia phenotype with dysregulated chondrocyte proliferation and shortening of the hypertrophic zone (Cameron et al., 2015b), indicating that this branch of the UPR is important during skeletal development. In Japanese rice fish, also known as medaka or *Oryzias latipes*, defects caused by either the absence of XBP1 or IRE1 were fully rescued by constitutive expression of the spliced form of *Xbp1* (Ishikawa et al., 2017). These results indicate that although IRE1 can act independently of XBP1 (Hollien et al., 2009; Urano et al., 2000), these pathways might not be relevant to skeletal development.

It is noteworthy that the involvement of specific branches of the UPR appears to be modulated by chondrocyte differentiation and thus differ between ER stress-related disorders. Whilst genetic ablation of *Xbp1* did not significantly impact the disease-severity of a MCDS mouse model expressing mutant type X collagen (Cameron et al., 2015a), loss of *Xbp1* in a mouse model of matrilin-3 MED significantly exacerbated the phenotype (Piróg et al., 2019). As the authors of the latter study suggest, this difference may arise from type X collagen being exclusively expressed by hypertrophic chondrocytes, whereas matrilin-3 is synthesised by proliferative chondrocytes.

1.5.2 The PERK pathway

PERK is also a transmembrane protein kinase in the ER membrane. Similar to IRE1, the dissociation of BiP leads to the activation of PERK by oligomerization and autophosphorylation (Lebeaupin et al., 2020). Activated PERK phosphorylates eIF2α which participates in the initiation of translation and is inhibited by phosphorylation, resulting in a reduction of mRNA translation (Shi et al., 1998; Sood et al., 2000). Importantly, phosphorylation of eIF2α by PERK, but also other kinases is also at the centre of the integrated stress response (ISR), a signalling pathway responding to various stressors, such as ER stress, amino acid starvation and viral infection (Pakos-Zebrucka et al., 2016).

Apart from attenuation of general translation, activation of PERK causes an increase in *ATF4* translation (Hetz and Papa, 2018). ATF4 in turn acts as a transcription factor on C/EBP homologous protein (CHOP) which has pro-apoptotic properties (Marciniak et al., 2004).

Loss of *Atf4* resulted in skeletal defects including delayed ossification and short stature in mice (Wang et al., 2009). By binding directly to its promoter, ATF4 was shown to positively regulate *Ihh* expression and, accordingly, the ablation of *Atf4* caused a shortened proliferative zone with disorganized columns and a transient expansion of the hypertrophic zone of the cartilage growth plate (Wang et al., 2009).

Loss-of-function mutations in PERK lead to Wolcott-Rallison syndrome (Delépine et al., 2000), characterised by diabetes, growth retardation and skeletal dysplasia, all of which are recapitulated by ablation of *Perk* in mice (Wei et al., 2008; Zhang et al., 2002). The absence of PERK appears to predominantly affect cells that have a high protein synthesis and secretion load, such as pancreatic cells and osteoblasts. This finding highlights the importance of the UPR under physiological circumstances.

The role of CHOP in the disease mechanisms of PSACH has been studied in more detail in two different mouse models, firstly the MT-COMP (inducible overexpression of human p.D469del COMP) and secondly the knock-in p.T583M Comp mouse model. Loss of *Ddit3/*CHOP did not affect levels of apoptosis in the proliferative or hypertrophic zone in p.T583M COMP mice, indicating that another mechanism is primarily responsible in this case. Additionally, ablation of *Ddit3* further impaired long bone growth, but remarkably ameliorated hip dysplasia in p.T583M COMP (Piróg et al., 2014). In the MT-COMP mouse model, COMP retention and chondrocyte apoptosis at the age of one month was ameliorated by loss of CHOP, but unfortunately long bone lengths were not analysed (Posey et al., 2012). Whether or not ablation of *Ddit3* provides beneficial effects on skeletal growth in this model therefore remains unclear.

1.5.3 The ATF6 pathway

Similar to IRE1 and PERK, ATF6 is a transmembrane protein in the ER membrane. However, binding to BiP retains ATF6 in the ER (Lebeaupin et al., 2020). Upon dissociation of BiP, ATF6 is transported into the Golgi apparatus where the cytosolic

part of ATF6 is cleaved by site-1-protease and site-2-protease, which allows the translocation of the N-terminal, cytosolic part into the nucleus (Hetz and Papa, 2018). Cleaved ATF6 can dimerise and bind to the ER-stress response element (ERSE), ERSE-II and the ATF6-binding element in promoter sequences (Yamamoto et al., 2004). As a heterodimer with XBP1, ATF6 can also bind to unfolded protein response element (UPRE)-like elements and thereby regulate transcription of various factors, including BiP and CHOP (Yamamoto et al., 2007, 2004).

ATF6 exists in two isoforms (ATF6α and ATF6β) and studies in medaka and mice have provided evidence for – to some extent – a redundant function of both isoforms (Ishikawa et al., 2013; Yamamoto et al., 2007). There is however some evidence that both isoforms have additional unique roles during ER stress, for example in the context of diabetes. Ablation of *Atf6α* combined with a high-fat diet resulted in mild glucose intolerance and insulin deficiency, suggesting that *Atf6β* cannot fully compensate for the loss of *Atf6α* (Usui et al., 2012).

In cartilage, a reduction in chondrocyte proliferation was observed in ATF6β-deficient, but not ATF6α-deficient mice (Forouhan et al., 2018a). The elevated expression of *BiP* and *Creld2* in a mouse model of MCDS, for example, was dependent on ATF6α, but not ATF6β (Forouhan et al., 2018a), suggesting at least, to some extent, distinct roles of both isoforms. Furthermore, loss of ATF6α intensified PERK- and IRE1-mediated signalling in MCDS mice, illustrated by increased *Xbp1* splicing and elevated levels of ATF4. In contrast to this, *Atf6β* ablation in MCDS mice not only decreased *Xbp1* splicing and ATF4 protein levels, suggestive of a reduction in ER stress, but also alleviated the characteristic expansion of the hypertrophic zone. Accordingly, ablation of *Atf6β* ameliorated the MCDS phenotype, whereas loss of *Atf6α* increased disease severity (Forouhan et al., 2018a). The authors of this study suggest that the ratio of activated ATF6α and activated ATF6β determines the level of transcriptional activity, with homodimers of ATF6α being most active, followed by heterodimers and lastly ATF6β homodimers.

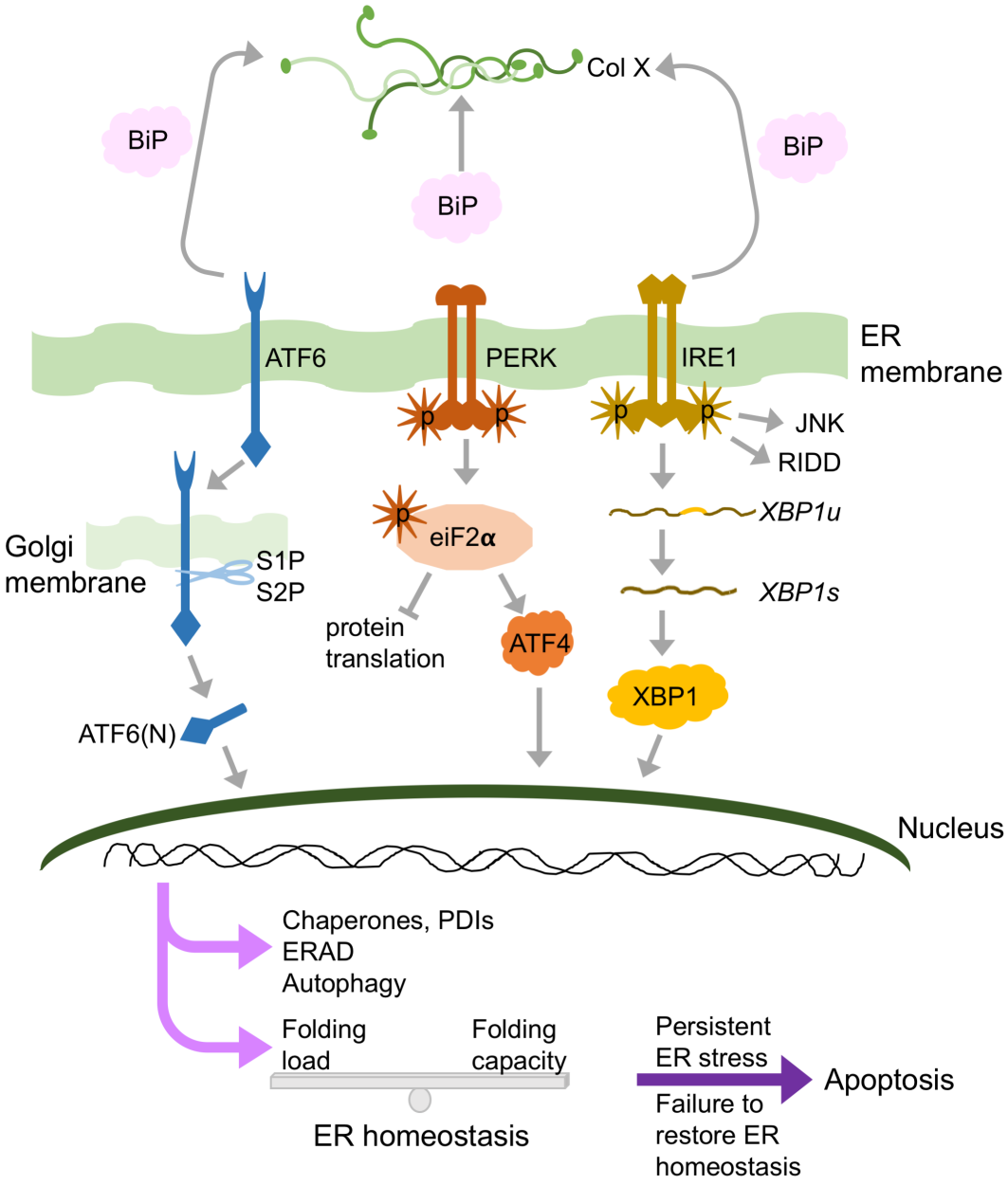

Figure 1.10 – Accumulation of unfolded proteins in the endoplasmic reticulum (ER) triggers the unfolded protein response (UPR) to reinstate ER homeostasis. The three main branches of the UPR cascade – Activating Transcription Factor 6 (ATF6), PKR-like endoplasmic reticulum kinase (PERK) and Inositol-requiring enzyme 1 (IRE1) – are activated by dissociation of binding immunoglobulin protein (BiP), which binds to unfolded proteins in the ER lumen. Subsequently, ATF6 translocation to the Golgi compartment is initiated alongside phosphorylation of eukaryotic translation initiation factor 2A (eiF2α) by PERK and unconventional splicing of *X-box binding protein 1 (XBP1)* by IRE1. In the Golgi, ATF6 is cleaved by Site-1- and Site-2-proteases (S1P, S2P), releasing the active transcription factor ATF6(N). Phosphorylation of eiF2α drives a reduction in general protein translation, whereas *Activating Transcription Factor 4 (ATF4)* selectively escapes this action. IRE1 also controls mRNA degradation during ER stress (Regulated IRE1-dependent decay, RIDD) and interacts with the JNK-signalling pathway. Whilst in principal aimed at restoring ER homeostasis, failure to clear unfolded proteins, and continuous UPR activity eventually triggers apoptosis.

1.6 Role of UPR in disease

The significance of ER homeostasis for skeletal development and cartilage integrity is highlighted by several disease models displaying mutant protein retention in the ER, and the chondrodysplasia-like phenotype caused by targeted induction of ER stress in chondrocytes (Table 1.1) (Nundlall et al., 2010; Dinser et al., 2002; Wilson et al., 2005; Rajpar et al., 2009; Gualeni et al., 2013; Kung et al., 2015; Piróg et al., 2019). The extent to which the UPR is activated and which branches are involved appears to differ between individual disorders and may depend on the specific mutation causing ER stress, the type/differentiation status of the cells suffering from ER stress, and when during development mutant proteins are expressed and start to accumulate (Cameron et al., 2015a; Gualeni et al., 2013; Kung et al., 2015, 2012; Piróg et al., 2019; Suleman et al., 2012).

Apart from skeletal disorders, ER stress and the UPR have also been studied extensively in other types of disorders, for example neurodegenerative diseases such as Parkinson's, Alzheimer's, and Huntington's disease (PD, AD and HD, respectively) as well as amyotrophic lateral sclerosis (ALS) (Bell et al., 2016; Duran-Aniotz et al., 2017; Hetz et al., 2009; Vidal et al., 2012).

Whilst the accumulation of amyloid-β fibrils and the formation of amyloid plaques in the AD brain typically occurs extracellularly, amyloid-β oligomers can interfere with cellular calcium homeostasis, resulting in ER stress, the activation of the UPR and simultaneous inhibition of proteasome activity (Gerakis and Hetz, 2018). In turn, the UPR and PERK in particular have been reported to promote production of amyloid-β oligomers creating a vicious cycle (Yoon et al., 2012). A second factor involved in AD, tau has been shown to block the ERAD pathway, preventing clearance of misfolded protein and also inducing ER stress (Abisambra et al., 2013).

Obstruction of protein clearance via ERAD and prevention of the degradation of misfolded proteins, also leads to ER stress and apoptosis in early stages of ALS (Montibeller and de Belleroche, 2018; Saxena et al., 2009). Ultimately, this results in loss of motor neurons in the brain and spinal cord (Saxena et al., 2009). Indeed, one study found that whilst increased ER stress is present in both AD and ALS, the extent to which individual branches of the UPR are activated appears to be disease-specific (Montibeller and de Belleroche, 2018), similar to what has been described for skeletal

disorders. A phase II clinical trial to target ER stress in ALS by treatment with sodium phenylbutyrate (4-PBA) and tauroursodeoxycholic acid (TUDCA), both chemical chaperones, revealed a 6.5 months increase in median survival (Paganoni et al., 2021) and a phase III trial is currently ongoing.

In HD, expansion of a glutamine repeat region of the huntingtin protein causes misfolding, aggregation, and disruption of ERAD, driving ER stress (Duennwald and Lindquist, 2008).
Promising results have been obtained in a clinical trial for pridopidine (McGarry et al., 2020), an agonist of the sigma-1 receptor which is involved in the regulation of ER stress by controlling calcium flux from the ER to mitochondria as well as interacting with monomeric IRE1 (Hayashi, 2019; Mori et al., 2013). Although the total functional capacity scores of individuals treated with pridopidine did not differ from individuals that received placebo after 26 weeks, the scores were improved in individuals receiving treatment for 52 weeks (McGarry et al., 2020; Reilmann et al., 2019). In particular in individuals with early-stage HD, the decline of total functional capacity was diminished.

The accumulation of α-synuclein and other proteins in Lewy's bodies within a specific neuron type is a hallmark of PD and also occurs in the ER (Kurtishi et al., 2019). As a consequence, ERAD function and the transport from the ER towards the Golgi apparatus are compromised, leading to ER stress but also preventing the activation of the ATF6 pathway of the UPR (Credle et al., 2015). ATF4 has been found to be upregulated in patient samples and cell models of PD, and appears to protect neurons from cell death following ER stress (Bellucci et al., 2011; Sun et al., 2013).

Furthermore, ER stress and the UPR have been implicated in pancreatic β-cell death and diabetes (Dhounchak et al., 2021; Sharma et al., 2021; Thomas et al., 2010; Zhu et al., 2013). Indeed, treatment with TUDCA improved blood glucose levels and body weight in a mouse model of diabetes (Dhounchak et al., 2021) and also appeared to ameliorate insulin sensitivity in muscle and liver, but not adipose tissue of obese individuals (Kars et al., 2010).

Model	Gene	Mutation	Mutant ECM protein	UPR	Disease onset	Irregular growth plate	Reference
MED	*Matn3*	p.V194D	Yes	Yes *Xbp1*/ATF6	2 weeks	Disrupted cellular organisation and column formation	(Bell et al., 2013; Leighton et al., 2007; Nundlall et al., 2010)
PSACH	*Comp*	p.D469del	Yes	No	6 weeks	Disorganised with areas of hypocellularity	(Bell et al., 2013; Suleman et al., 2012)
PSACH-MED	*Comp*	p.T585M	Yes	Transient ATF6/p-eiF2a	9 weeks	Disrupted chondrocyte alignment, expanded proliferative zone	(Bell et al., 2013; Piróg-Garcia et al., 2007)
Col2-RDW	*Col2-RDW*	p.G2320R	No	No	birth	Disorganised with areas of hypocellularity	(Gualeni et al., 2013)
Col2-cog	*Col2-Cog*	p.L2263P	No	Yes *Xbp1*/p-eiF2a	3 weeks	No	(Kung et al., 2015)
MCDS	*Col10A1*	p.N617K	Yes	Yes *Xbp1*/ATF6	1 week	Expanded hypertrophic zone	(Cameron et al., 2011; Rajpar et al., 2009)
Col10-cog	*Col10-Cog*	p.L2263P	No	Yes *Xbp1*/ATF6	1 week	Expanded hypertrophic zone	(Cameron et al., 2011; Rajpar et al., 2009)

Table 1.1 – Comparison of genetically engineered chondrodysplasia mouse models with regards to UPR involvement, disease onset and growth plate architecture.

1.7 Treatment options for skeletal dysplasia

For some types of skeletal dysplasia, treatment options have already been developed. For chondrodysplasia arising from gain-of-function mutations in *FGFR3*, several clinical trials are currently ongoing (Table 1.2) including approaches to limit aberrant FGF signalling through a soluble form of FGFR3 or tyrosine kinase inhibitors and approaches to restore normal bone growth by treatment with C-natriuretic peptide (CNP) which inhibits overactive MAPK signalling and thereby restores ECM synthesis (Garcia et al., 2013; Komla-Ebri et al., 2016; Legeai-Mallet and Savarirayan, 2020; Yasoda et al., 2004). Additionally, a recent study described improved growth plate organisation and chondrocyte proliferation alongside increased cellular volume of hypertrophic chondrocytes in a mouse model of achondroplasia treated with (-)-epicatechin, a compound probably directly interacting with downstream components of the FGFR signalling pathway (Martin et al., 2022).

Mutations of the sulphate/chloride importer *SLC26A2* can lead to severe phenotypes, such as achondrogenesis 1 B or to the milder diastrophic dysplasia (DTD) and recessive multiple epiphyseal dysplasia, depending on the specific mutation and the residual activity of the transporter (Rossi and Superti-Furga, 2001). In chondrocytes, the sulphation of proteoglycans (and other proteins) is heavily dependent on the import of extracellular sulphate. Interestingly, treatment with N-acetylcysteine, a widely used drug, partially restored proteoglycan sulphation and ameliorated the phenotype of a mouse model of DTD by acting as an intracellular sulphate donor (Paganini et al., 2021). A further study found that ablation of *Slc26a2* in mice resulted in enhanced FGFR3 activity and repurposing a tyrosine kinase inhibitor initially developed for treating FGFR3-related disorders could ameliorate the phenotype (Zheng et al., 2019).

Bisphosphonate therapy can be used to treat OI caused by type I collagen defects. This therapy aims to prevent fractures by slowing bone turnover and increasing bone mineral density; however, its effectiveness in reducing fracture incidence is debated (Dwan et al., 2016). Furthermore, clinical trials are currently ongoing to treat individuals with OI with monoclonal sclerostin or TGFβ antibodies. Sclerostin is known to prevent bone formation by inhibiting Wnt signalling. Inhibition of sclerostin by monoclonal antibodies was shown to promote bone formation and reduce bone

resorption in OI (Glorieux et al., 2017). Inhibition of TGFβ signalling by monoclonal antibodies has been demonstrated to slow bone turnover and improve biomechanical properties in several mouse models of OI (Bi et al., 2017; Greene et al., 2021).

A different approach directly targets protein accumulation, and thus the cause of the disease rather than consequences of the mutation by RNA interference (RNAi). This approach has previously been studied *in vitro* for type VI collagen-related muscular dystrophy, in which mutations in *COL6A3* interfere with collagen VI assembly (Bolduc et al., 2014). RNAi has been applied to reduce mutant *COMP* and *Comp* expression in a mouse model of PSACH. In this mouse model, human *COMP* can be overexpressed in chondrocytes by treatment with doxycycline. However, using a non-allele-specific approach the treatment appeared to significantly reduce only endogenous (wild type) murine *Comp*, but not the overexpressed human *COMP* (Posey et al., 2017). The authors claim that mutant COMP may exhibit a stronger cytotoxic effect in the presence of endogenous wild type COMP and thus a general reduction of Comp protein may have beneficial consequences in PSACH. They base this claim on a reduction in apoptosis when endogenous COMP is reduced, and conclude that for therapeutic approaches the total protein level should be reduced. They support this claim with the observed reduction in disease severity after crossing the inducible transgenic mouse model with a COMP-deficient strain. However, they ignore earlier studies using a transgenic mouse model carrying the same mutation which displayed a more severe phenotype after being crossed with a COMP-deficient strain (Schmitz et al., 2008).

However, developing a treatment for one specific rare disease is time- and resource-consuming and may be regarded as inefficient. Identifying common underlying disease mechanisms of numerous, individually rare diseases is crucial to allow the development (or repurposing) of drugs that are appropriate for more than one mutation or gene defect, thereby accelerating drug development and improvement of quality of life for affected individuals. Furthermore, in skeletal disorders treatment has to be initiated during childhood, when skeletal growth is still active, but could be terminated once skeletal maturity is reached. Repurposing drugs that are already being used for treatment of children or drugs that do not have known adverse effects in children could accelerate clinical trials, and is therefore especially attractive for treatment of rare skeletal disorders.

Substance	Name	Mechanism	Stage	ClinicalTrial.gov number	Reference
Soluble FGFR3	TA-46 (recifercept)	Decoy receptor binds to FGF, preventing its interaction with FGFR3	Phase 1 (completed) Phase 2 (recruiting)	NCT04543344, NCT04638153, NCT05116046	(Garcia et al., 2013)
Tyrosine kinase inhibitors	BGJ398 (infigratinib)	Small molecule tyrosine kinase inhibitor	Phase 1 (completed) Phase 2 (ongoing)	NCT04035811, NCT04265651 NCT05145010	(Komla-Ebri et al., 2016; Kunova Bosakova et al., 2019)
C-natriuretic peptide (CNP)	BMN111 (vosoritide)	Analogue of CNP, inhibits MAPK signalling and improves bone growth	Phase 2 (ongoing) Phase 3 (ongoing)	NCT02055157, NCT03197766 NCT02724228, NCT03424018 NCT03583697, NCT03989947 NCT04554940	(Lorget et al., 2012; Yasoda et al., 2009, 2004)
	TransCon CNP	CNP conjugated to a carrier molecule	Phase 1 (completed) Phase 2 (ongoing)	NCT04085523, NCT05246033	
FGFR3-Antibody	B-701 (vofatamab)	Monoclonal antibody binds and interferes with ligand binding ability and dimerisation	Efficacy has been reported in bladder cancer models (FGFR3-dependent tumors)		(Trudel et al., 2006; Yin et al., 2016)
FGF aptamer	APT-F2P (RBM-007)	Nucleic acid molecule that binds and neutralises FGFs	Preclinical studies in ACH mouse model using an aptamer targeting FGF2		(Jin et al., 2016)
(-)epicatechin	NA	Interacts with ERK1/2 and p38 MAPK	Preclinical		(Martin et al., 2022)

Table 1.2 - Current therapeutic approaches for achondroplasia.

1.7.1 Targeting protein homeostasis in skeletal dysplasia

Having demonstrated the central role of ER stress, and the UPR, for cartilage pathology in skeletal dysplasia, targeting the UPR and ER homeostasis has emerged as a potential drug therapy.

Selective inhibition of the Perk branch of the UPR by treatment with ISRIB (Integrated Stress Response InhiBitor) ameliorated the skeletal phenotype in a mouse model of MCDS (Wang et al., 2018). Importantly, by preventing enhanced translation of *Atf4*, treatment with ISRIB was demonstrated to block the SOX9-mediated re-expression of *Col2a1* and prevent the disruption of chondrocyte hypertrophy observed in MCDS (Wang et al., 2018).

Furthermore, a clinical trial (mcds-therapy.eu) is currently ongoing for the treatment of MCDS with carbamazepine (CBZ). CBZ enhances mutant collagen X degradation, thus relieving cells from ER stress. In human cell lines as well as in two mouse models, treatment with CBZ enhanced clearance of mutant type X collagen, thereby mitigating ER stress, improving chondrocyte differentiation and alleviating the skeletal phenotype (Mullan et al., 2017; Forouhan et al., 2018b). Curiously, CBZ enhanced protein clearance, although the specific pathway of degradation was genotype specific, with both ERAD and autophagy implicated (Mullan et al., 2017).

Remarkably, although both MCDS and MED are linked to ER-stress and UPR activation, CBZ did not appear to ameliorate ER stress in a cell model of MED (Dennis et al., 2021). As others have suggested previously (Piróg et al., 2019), this difference may stem from the distinct differentiation stages of type X collagen-expressing chondrocytes compared to chondrocytes expressing mutant matrilin-3.

It is noteworthy that – in contrast to CBZ – the chemical chaperone 4-PBA was neither able to attenuate ER stress in a cell model of MCDS (Mullan et al., 2017), nor improved the skeletal phenotype of a MED mouse model. Although protein levels of BiP, ERp72 and GRP94 were significantly downregulated at the age of three weeks, suggesting a reduction in ER stress, the skeletal phenotype, as well as chondrocyte proliferation and apoptosis remained the same as in untreated animals (Nundlall et al., 2010).

In contrast to that, 4-PBA treatment ameliorated the phenotype in a mouse model of moderate to severe OI (*Aga2*), as indicated by reduced fracture incidence and increased body length as well as weight (Duran et al., 2022). In a second mouse model of OI (*Col1a2*^{G610C}), treatment with 4-PBA did not improve bone fragility, but augmented long bone growth (Scheiber et al., 2022). Compellingly, the authors of the latter study revealed that the effect to 4-PBA was largely mediated by reducing UPR/BiP-mediated ER stress in hypertrophic chondrocytes, but not the UPR/BiP-independent ER stress in osteoblasts. Consequently, 4-PBA treatment potentially improved the trans-differentiation of hypertrophic chondrocytes to osteoblasts, thereby enhancing bone growth without affecting bone fragility. Together with the study performed in the *Aga2* mouse model, this study highlights how mutations affecting the same protein may act via distinct mechanisms. In contrast to osteoblasts from the *Col1a2* ^{G610C} mouse model, osteoblasts from the *Aga2* mouse model exhibited an increase in BiP protein levels as well as the phosphorylation of PERK (Duran et al., 2022), explaining why treatment with 4-PBA reduced the fracture incidence in this model. These studies also profoundly demonstrate the need for a detailed understanding of the ER stress response elicited in a disease model, the different cell types that are involved and their relative contribution to the phenotype.

In an attempt to target the inflammatory and oxidative stress observed in the MT-COMP mouse model of PSACH, anti-inflammatory drugs (aspirin, ibuprofen) and antioxidants (notably resveratrol) have been tested (Posey et al., 2015). Resveratrol improved chondrocyte survival, proliferation and long bone growth in mice via stimulation of autophagy (Hecht et al., 2021a). Whether these findings will translate into individuals with PSACH and/or MED is currently unclear since the MT-COMP mouse model may not be the most physiological relevant mouse model.

The specific reason why p.D469del COMP elicits a distinct type of ER stress, compared to either mutant matrilin-3 or mutant type X collagen, and also p.T583M COMP, currently remains unclear. Whether this is also the case for other (missense) mutations located in type 3 repeats of COMP currently remains unknown.

Furthermore, before potential drugs can be tested *in vitro* and later *in vivo*, biomarkers are required that allow the evaluation of a potential treatment. Whilst there are many different types of biomarkers - for example predictive, prognostic or

monitoring biomarkers (Califf, 2018) - for most skeletal dysplasias there are no relevant biomarkers available. Most importantly, to assess a potential treatment a pharmacodynamic biomarker is required.

In vitro, as well as in animal models, interventions can be analysed for example by determining the levels of cell stress, apoptosis and/or the activity of specific signalling pathways. In individuals, however, cartilage and bone are relatively inaccessible tissues, because biopsies are invasive and painful and it would be unethical to surgically interfere with an infant's growth plate. Analysis of cell stress, apoptosis or a signalling molecule of interest in patient-derived tissue is therefore not feasible. Due to restricted expression, more accessible tissues may however not exhibit elevated levels of cell stress or apoptosis. In the case of skeletal dysplasias, ideal biomarkers should be secreted either themselves in the affected tissue, or respond to a factor secreted from the affected tissue, enabling detection of the potential biomarker in body fluids, such as blood or urine. Furthermore, any biomarker needs to exhibit specificity as well as sensitivity. These specifications depend on the type of biomarker and the required application. In order to successfully develop biomarkers for skeletal dysplasias and their treatment, understanding and being able to distinguish between different types of disease mechanism is necessary.

Disease/Gene/Mutation	**Stress Response**	**Potential Treatment**
MCDS/*Col10a1*/multiple	(IRE1) PERK/ATF6	CBZ
MCDS/*Col10a1*/FCdel	PERK/ATF6	ISRIB
OI/*Col1a2*/G610C	UPR/BiP-dependent (hypertrophic chondrocytes), UPR/BiP-independent (osteoblasts)	4-PBA
OI/*Col1a1*/*Aga2* (frameshift in the C-terminal pro-peptide)	PERK-mediated UPR/ISR (osteoblasts)	4-PBA
PSACH/*COMP*/p.D469del (MT-COMP mouse model)	PERK/oxidative/inflammatory	Resveratrol
MED/*Matn3*/p.V194D	IRE1/ATF6	?

Table 1.3 – Potential treatment strategies in models of skeletal dysplasia.

1.8 The UPR and the epigenome/DNA methylation

The relation of the UPR and the epigenome is poorly understood. The epigenome is defined as heritable changes of the genome, that do not alter the actual nucleotide sequence of DNA and comprises DNA methylation, histone post-translational modifications, non-coding RNAs and chromatin structure (van Meurs et al., 2019). All of those can modify the accessibility of genes, promoters and enhancers and thus influence gene expression.

During DNA methylation, DNA-methyltransferases (DNMTs) add a methyl group to cytosine residues followed by a guanine residue (Figure 1.10 A). Generally, high levels of DNA methylation and transcription-repressive histone marks are associated with transcriptional repression (Figure 1.10 B) (Morgan and Shilatifard, 2020; Prakash and Fournier, 2018). Whilst most CpG sites within the genome are methylated, long stretches containing high levels of CpG sites (CpG islands) typically remain unmethylated (Dor and Cedar, 2018; Jones, 2012). Increased methylation of CpG islands within promoter regions has traditionally been linked to a reduction in gene expression, whilst DNA methylation within gene bodies is typically found in transcriptionally active genes (Greenberg and Bourc'his, 2019). However, there is emerging evidence that the role of DNA methylation is more complex (Figure 1.10 C), and that some transcription factors may also bind methylated motifs or that within a certain region, the specific motif that a transcription factor binds to may depend on its methylation status (Zhu et al., 2016). Enhancer regions display highly variable levels of methylation and the functional consequences of DNA methylation within enhancers are not entirely understood (Angeloni and Bogdanovic, 2019; Jones, 2012). In contrast to DNMTs, Ten-Eleven-Translocation enzymes (TETs) actively remove methyl groups. DNMT1 is the main enzyme responsible for maintaining DNA methylation patterns during cell division, whilst DNMT3a and DNMT3b are *de novo* methyltransferases. Cartilage-specific *Dnmt3b* ablation results in altered chondrocyte maturation and a reduction in the size of the hypertrophic zone (Xu et al., 2018). Additionally, DNA methylation changes have been observed in osteoarthritis by numerous studies (Reynard et al., 2014, 2011; van Meurs et al., 2019; Young et al., 2022). Although not all changes in DNA methylation may always be functionally relevant, these data demonstrate the involvement of DNA methylation in chondrocyte differentiation and cartilage integrity.

Recently, a role for dysregulated DNA methylation in one skeletal dysplasia was unravelled by a study that reported a GGC repeat expansion in the promoter of *XYLT1,* an enzyme involved in proteoglycan synthesis (LaCroix et al., 2019). Mutations in *XYLT1* cause Baratela-Scott syndrome, symptoms of which include facial dysmorphism and severe short stature (Baratela et al., 2012; Bui et al., 2014; Schreml et al., 2014). Remarkably, this expansion was associated with hypermethylation of the first exon, which was found to be incompatible with transcription. In some individuals, both alleles were affected by this expansion resulting in a complete loss of *XYLT1* expression, whilst in others, the second allele contained point mutations, frame shift mutations or larger deletions (LaCroix et al., 2019). Notably, carriers of one expanded allele associated with hypermethylation appeared to be unaffected, as did carriers of other mutations in *XYLT1*, suggesting that Baratela-Scott syndrome results from loss-of-function rather than dominant-negative effects.

As described previously, the UPR has been implicated in skeletal diseases as well as in neurodegenerative disorders and, amongst others, diabetes. In addition to the UPR, epigenetic alterations and especially changes in DNA methylation have been suggested to play a role in predisposition and progression of these disorders (De Jager et al., 2014; Gasparoni et al., 2018; Nilsson and Ling, 2017; van Heesbeen and Smidt, 2019). Fascinatingly, a common DNA methylation signature was identified in samples from four different neurodegenerative diseases (Sanchez-Mut et al., 2016) including Alzheimer's and Parkinson's disease, both of which are also linked to ER stress. The authors postulated a common disease mechanism that develops into different clinical manifestations (Sanchez-Mut et al., 2016). Whether a similar common signature or distinct methylation patterns exist in skeletal dysplasia is currently not known. Indeed, to what extent DNA methylation is affected by various types of skeletal dysplasia pathology has not yet been investigated.

Whilst the existence of ER stress response elements and unfolded protein response elements in promoter sequences is well established (Kokame et al., 2001; Mori et al., 1992; Yoshida et al., 1998), if and to what extent the UPR can modify epigenetic marks to regulate gene expression is currently unknown. A previous study has reported that induction of the UPR results in methylation of the promoter of *cystic fibrosis transmembrane conductance regulator* (*CFTR)* and its transcriptional

repression (Bartoszewski et al., 2008b), suggesting that DNA methylation may be specifically altered by ER stress. This is particularly interesting since a mutant form of CFTR (ΔF508 CFTR) is known to cause cystic fibrosis and activates the UPR when expressed recombinantly (Bartoszewski et al., 2008a).
As the importance of DNA methylation and the UPR is continuously revealed, it raises the question of how they interact during development and disease. Effects of the UPR on DNA methylation (or vice versa) could account for the phenotypic variability that is frequently observed within patients. Studying the relationship between ER stress, the UPR and DNA methylation might therefore reveal novel disease modifiers in the future.

Furthermore, previous studies have attempted to use DNA methylation in blood samples as biomarkers for diabetes (Davegårdh et al., 2018; Willmer et al., 2018). Blood samples offer the advantage of being relatively easy to obtain and rapidly analysed. An emerging approach is the methylation analysis of circulating, cell-free DNA as a marker for tissue degeneration. When cells undergo cell death, for example pancreatic cells in diabetes, they release DNA which can then be detected using tissue-specific methylation patterns (Lehmann-Werman et al., 2016). For skeletal disorders, identification of a possible DNA methylation signature could result in the development of a 'methylation biomarker' to enable development and rapid monitoring of future treatments.

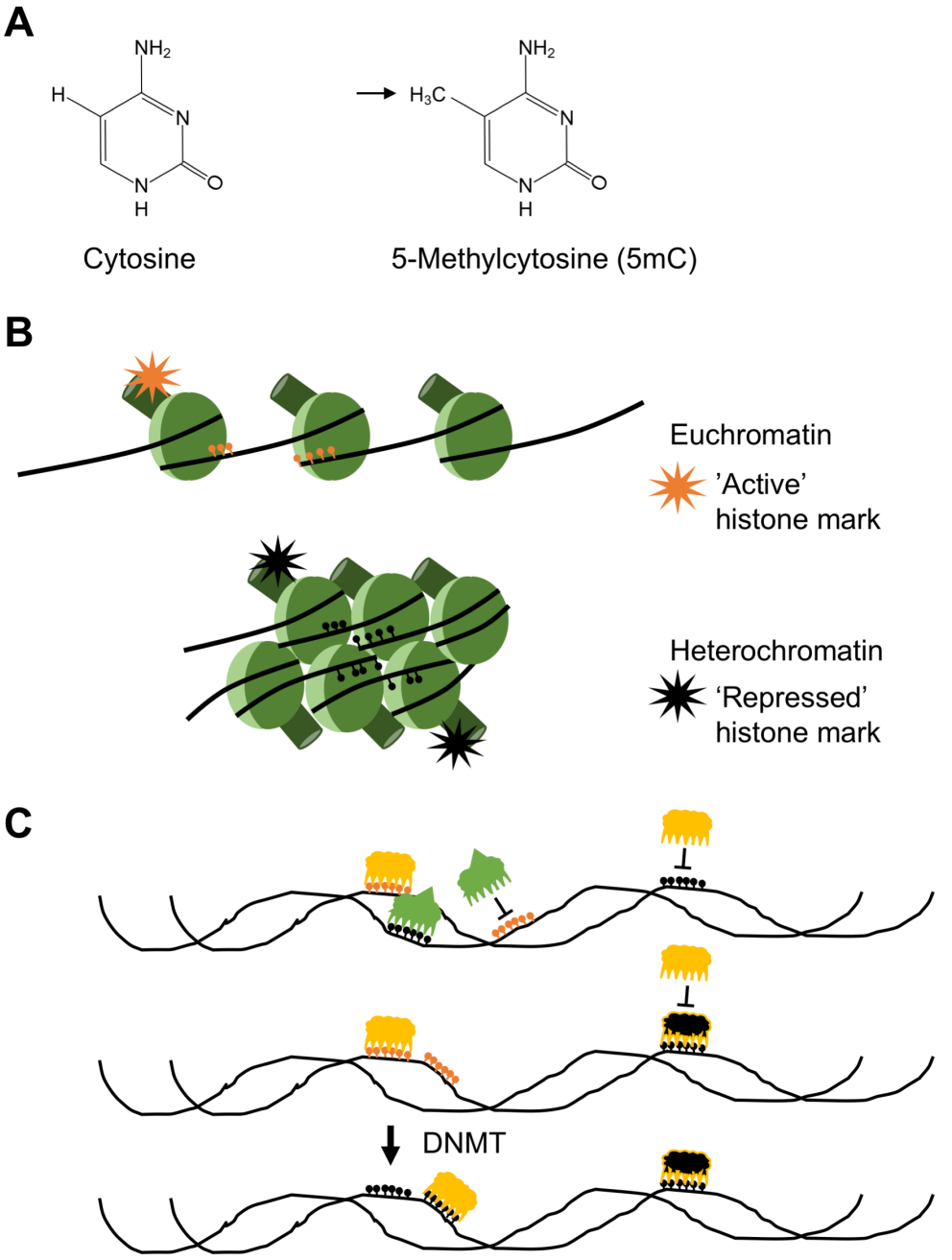

Figure 1.11 – DNA methylation affects gene expression both directly and indirectly. (A) Chemical structure of cytosine and 5-methylcytosine (5mC). The position of the added methyl group is indicated by a black arrow. (B) DNA methylation levels differ depending on chromatin accessibility. Typically, low levels of global methylation are associated with transcriptionally active euchromatin and active histone marks, whereas high methylation levels and repressive histone marks indicate densely packed heterochromatin. (C) DNA methylation can affect gene expression directly by modulating transcription factor binding. Transcription factors may have varying affinities for large unmethylated (orange) and heavily methylated (black) regions (upper panel). Methyl-binding proteins (black) may compete with transcription factors for binding to heavily methylated regions (middle panel, right) or the exact binding site within a region may be modified by DNA methylation content (middle/bottom panel left).

1.9 Aims

Concerning skeletal disorders, their mechanism and potential treatments, several questions remain to be answered.

1) Do changes in DNA methylation occur in ER-stress related skeletal dysplasia, as they do in neurodegenerative diseases? Could DNA methylation play a role as disease modifier and/or biomarker?

2) Why does p.D469del COMP appear to elicit a distinct stress response in PSACH compared to other, closely related chondrodysplasias and is this the case for all type 3 *COMP* mutations?

3) Are there differences in the cellular response to MED- and PSACH-causing COMP mutations? Is there a common biomarker for COMP-induced stress, that could advance future drug screenings?

To investigate whether DNA methylation is altered by ER stress in the context of skeletal dysplasia, an appropriate model system had to be identified and therefore the suitability of human induced pluripotent stem cells (hiPSCs) to study DNA methylation in skeletal dysplasia was examined. Furthermore, the suitability of HT1080 cells overexpressing wild type or p.D469del COMP as a disease model of PSACH for the study of DNA methylation was evaluated.

DNA methylation was then analysed using the Illumina Infinium Methylation EPIC array. The cellular response to p.D469del COMP was explored and potential biomarker genes identified using transcriptomic analysis. Subsequently, it was investigated whether the UPR-independent ER stress that is observed in p.D469del COMP expressing cells is a common feature to other *COMP* mutations, and whether there are distinct cellular responses to PSACH and MED-causing mutations. Lastly, biomarker candidates identified in p.D469del COMP cells were assessed in multiple cell models of PSACH and MED.

Chapter 2. Materials and Methods

2.1 Reagents and suppliers

All reagents were purchased from Sigma unless otherwise stated.

Antibody suppliers are stated in table 2.1, primers were purchased from Eurofins Scientific Ltd and sequences are provided in table 2.2.

Dulbecco's modified eagle medium/nutrient mixture F12 (DMEM/F12), sterile PBS, tissue culture plates, acetic acid, hydrochloric acid, methanol, xylene, coverslips and Superfrost Plus microscopy slides were obtained from VWR International.

Foetal bovine serum (FBS), non-essential amino acids, Trypsin/EDTA solution, OptiMem, G418 Geneticin, Penicillin-Streptomycin, DNA-free kit, ethidium bromide, MitoTracker Red CM-H_2Xros, methanol-free paraformaldehyde, Pierce BCA protein assay kit, dithiothreitol (DTT), glycerol, Novex 4-12 % Bis-Tris precast gradient gels, NuPAGE MES running buffer, paraffin wax, isopropanol, ethanol, RNase H and Power SYBR Green Master Mix were obtained from ThermoFisher.

ReliaPrep RNA tissue miniprep system, DeadEnd Fluorometric TUNEL system, GoScript Reverse Transcription System and ethylenediaminetetraacetic acid (EDTA) were obtained from Promega.

Cell proliferation labelling reagent bromodeoxyuridine (BrdU) was purchased from GE Healthcare.

Precision Plus Protein Dual colour protein standard was obtained from Bio-Rad.

Fluoroshield mounting medium with DAPI and thapsigargin were purchased from Abcam.

BioMix red and HyperLadders 1 kb and 100 bp were obtained from Bioline Reagents.

Agarose was purchased from Melford Laboratories Ltd.

RNeasy Mini kit and QIAprep Spin Miniprep kit were obtained from Qiagen.

E.Z.N.A DNA/RNA Isolation Kit was purchased from Omega Bio-Tek.

2.1.1 DNA constructs

The *hCOMP*-pEGFP-N3 plasmids encoding human wild type and p.D469del COMP were described previously (Suleman et al., 2012). *MATN3*-FLAG-pcDNA3.1 plasmids encoding wild type and p.V194D matrilin-3 were kindly provided by Dr Ella Dennis, Newcastle University. The *hCOMP*-pEGFP-N3 plasmids encoding p.C312Y, p.D385N, p.D440R, p.D473H and p.D511Y COMP were generated by Dr Beth Gibson by site-directed mutagenesis using the wild type *COMP*-pEGFP-N3 plasmid as template.

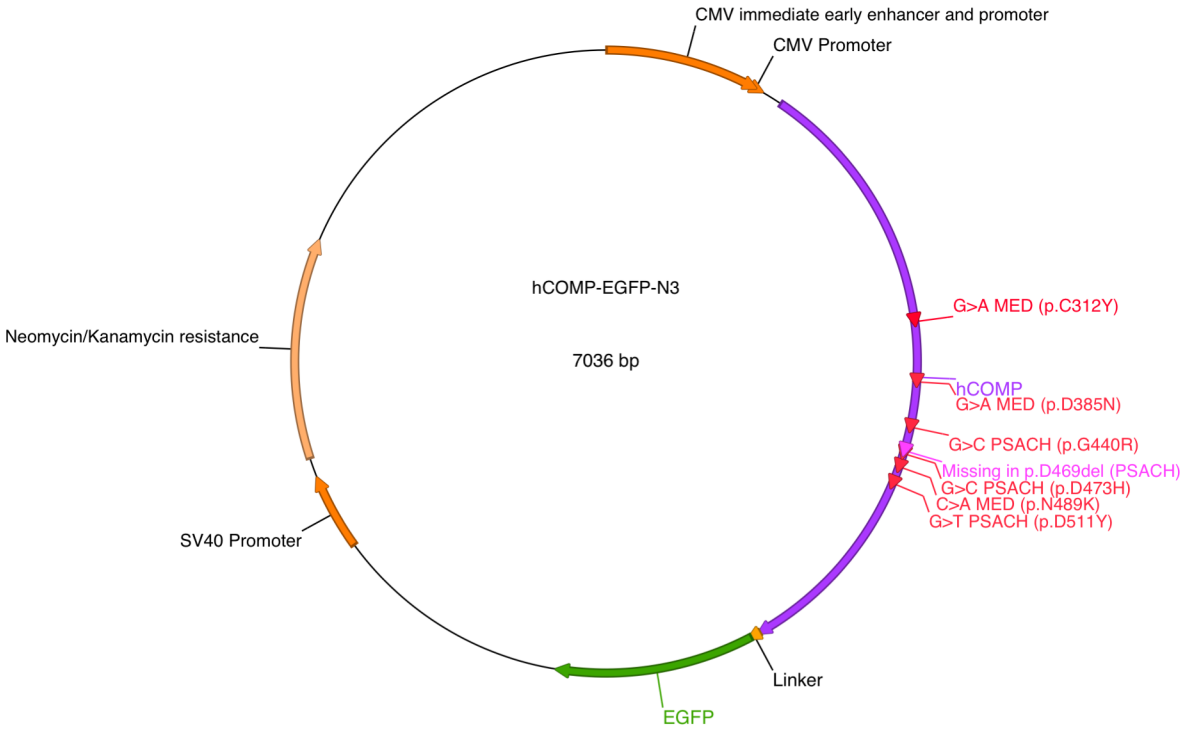

Figure 2.1 – Plasmid map of hCOMP-EGFP-N3 constructs encoding wild type and mutant COMP. The coding sequence of COMP is shown in purple, nucleotide substitutions are marked in red and the p.D469del deletion is marked in pink. EGFP is shown in green, other plasmid features are shown in orange.

2.1.2 Antibodies

Primary and secondary antibodies for western blotting and immunofluorescence staining (IF) and the appropriate dilutions are listed below (Table 2.1).

Antigen	Host	Dilution	Product code	Company/Reference
Pan AKT	Rabbit	1:1000	#9272	Cell Signalling Technologies
Phospho- AKT (Ser473)	Rabbit	1:1000	#9271	Cell Signalling Technologies
AMPK	Rabbit	1:1000	#2603	Cell Signalling Technologies
pAMPK (Thr172)	Rabbit	1:1000	#2535	Cell Signalling Technologies
BiP	Rabbit	1:1000	#3177	Cell Signalling Technologies
BrdU	Rat	1:200 (IF)	ab6326	Abcam
Calnexin	Rabbit	1:1000	ADI-SPA 860	Enzo LifeSciences
Collagen X	Rabbit	1:500 (IF)	N/A	Raised against recombinant human collagen X (Wilson et al., 2005)
COMP	Rabbit	1:1000	GTX14515	GeneTex
FLAG-HRP	mouse	1:1000	A8592	Sigma
Phospho-eiF2α	Rabbit	1:1000	#9721	Cell Signalling Technologies
Total eiF2α	Rabbit	1:1000	#9722	Cell Signalling Technologies
GAPDH	Mouse	1:40 000	AB2302	Merck Millipore
GFP	Rabbit	1:2000 1:500 (IF)	ab290	Abcam
HIF1α	Rabbit	1:500	#14179	Cell Signalling Technologies
LC3B	Rabbit	1:1000	#2775	Cell Signalling Technologies
PRDX2	Rabbit	1:1000	10545	Proteintech
pSMAD2	Rabbit	1:1000	#18338	Cell Signalling Technologies
pSMAD3	Rabbit	1:1000	#9520	Cell Signalling Technologies
SMAD2/3	Rabbit	1:1000	#8685	Cell Signalling Technologies

Rabbit IgG AlexaFluor488	goat	1:200 (IF)	ab150081	Abcam
Rat IgG AlexaFluor594	goat	1:200 (IF)	ab150160	Abcam
Mouse IgG	goat	1:2000	P0447	Dako
Rabbit IgG	goat	1:2000	P0448	Dako

Table 2.1 – Primary and secondary antibodies used in this study.

2.1.3 Primer sequences

Primers for genotyping, cloning and qRT-PCR were obtained from Eurofins Genomics. Sequences are stated below (Table 2.2).

Primer	**Sequence (5'-3')**
Comp Genotyping F	CAT CAC ATG TCC CTT TGG GC
Comp Genotyping R	GTT GGA GTA TAG GGA AGG TC
HT1080 qRT-PCR	
DDIT3 qPCR F	GCG CAT GAA GGA GAA AGA AC
DDIT3 qPCR R	TCT GGG AAA GGT GGG TAG TG
GALNT18 qPCR F	GGT GGA TGA CAA CAG CAG TAA CG
GALNT18 qPCR R	GCT TGC TGT GAC GCA CGA CTT T
GFP qPCR F	AAG CAG CAC GAC TTC TTC AA
GFP qPCR R	CGG CCA TGA TAT AGA CGT TG
HSPA5 qPCR F	GCT AAT GCT TAT GGC CTG GA
HSPA5 qPCR R	CGC TGG TCA AAG TCT TCT CC
MMP1 qPCR F	ATG AAG CAG CCC AGA TGT GGA G
MMP1 qPCR R	TGG TCC ACA TCT GCT CTT GGC A
MMP9 qPCR F	GCC ACT ACT GTG CCT TTG AGT C
MMP9 qPCR R	CCC TCA GAG AAT CGC CAG TAC T
SOX9 qPCR F	CCC ATG TGG AAG GCA GAT G
SOX9 qPCR R	TTC TGA GAG GCA CAG GTG ACA
XBP1 F	GAA GCC AAG GGG AAT GAA GT

XBP1 R	CCA GAA TGC CCA ACA GGA TA
18S qPCR F	GGC CCT GTA ATT GGA ATG AGT C
18S qPCR R	CCA AGA TCC AAC TAC GAG CTT

hiPSC qRT-PCR	
ACTNB F	AAG TCC CTT GCC ATC CTA AAA
ACTNB R	ATG CTA TCA CCT CCC CTG TG
BGLAP F	GCA GCG AGG TAG TGA AGA GAC
BGLAP R	GGG GAC CCC ACA TCC ATA GG
COL1A1 F	GCT TCA CCT ACA GCG TCA CT
COL1A1 R	AAG CCG AAT TCC TGG TC TGG
COL10A1 F	AAA GGC CCA CTA CCC AAC AC
COL10A1 R	GGA CTT CCG TAG CCT GGT TT
DDIT3 F	GAG GAA GAC CAA GGG AGA ACC
DDIT3 R	GAT TTC CTG CTT GAG CCG TTC
HSPA5 F	AGC TGT AGC GTA TGG TGC TG
HSPA R	AAG GGG ACA TAC ATC AAG CAG T
XBP1 F	GGA GTT AAG ACA GCG CTT GG
XBP1 R	ACT GGG TCC AAG TTG TCC AG

Mitochondrial DNA content	
nuDNA human qPCR F	AGG GTA TCT GGG CTC TGG
nuDNA human qPCR R	GGC TGA AAA GCT CCC GAT TAT
mtDNA human qPCR F	ACA CCC TCC TAG CCT TAC TAC
mtDNA human qPCR R	GAT ATA GGG TCG AAG CCG C

Murine tissue qRT-PCR	
Canx qPCR F	TGA TTT CCT CTC CCT CCC CTT
Canx qPCR R	CAC TGG AAC CTG TTG ATG GTG
Comp qPCR F	GTG CCC AAC TTT GAC CAG AGT G

Comp qPCR R	ACA GGC ATC ACC CAC AAA GTC G
Ddit3 qPCR F	CTG CCT TTC ACC TTG GAG AC
Ddit3 qPCR R	CGT TTC CTG GGG ATG AGA TA
Grp94 qPCR F	GCA CCA TGA GGG TCC TGT
Grp94 qPCR R	CAT CAT CAG CTC TGA CGA ACC
Grp78 qPCR F	GGC ACC TTC GAT GTG TCT CTT C
Grp78 qPCR R	TCC ATG ACC CGC TGA TCA A
18S qPCR F	GTA ACC CGT TGA ACC CCA TT
18S qPCR R	CCA TCC AAT CGG TAG TAG CG

Table 2.2 - Primer sequences.

2.2 Methods

2.2.1 Molecular Biology methods

2.2.1.1 PCR for genotyping

PCR set up and cycling conditions used for genotyping of wild type and p.D469del *Comp* mice are described below (Table 2.3 and 2.4).

2 x BioMix Red	10 µL
Primer (10 µM stock)	0.8 µL each
DNA	1.5 µL
Water	7.1 µL

Table 2.3 – Typical PCR reaction for genotyping.

Temperature	Duration	
95°C	5 min	
95°C 63°C 72°C	1 min 1 min 1 min	30 x
72°C	5 min	

Table 2.4 - PCR cycling conditions for genotyping.

Samples were stored at 4°C prior to electrophoresis.

2.2.1.2 Agarose gel electrophoresis

DNA was separated using agarose gels of the appropriate percentages in 1 x Tris-Acetate-EDTA (TAE) buffer. For genotyping, typically 1.5 % (w/v) agarose gels were used. A final concentration of 0.5 µg/mL ethidium bromide was used to visualise DNA under UV light. Samples were mixed with 5 x loading dye prior to electrophoresis and 5 µL of a DNA molecular weight standard was used. The gel was run for 30 min at 90 V in 1 x TAE buffer or until the dye front had reached 2/3 of the gel.

1 X Tris-Acetate-EDTA buffer: 40 mM Tris-base
20 mM Glacial acetic acid
1 mM EDTA pH 8.0

2.2.1.3 Determination of DNA/RNA concentration

DNA and RNA concentrations were determined using a NanoDrop spectrophotometer. The $A_{260/280}$ ratio was used to assess DNA/RNA purity.

2.2.1.4 Transformation of competent cells with plasmid DNA

DH5α competent cells were thawed on ice and 1 µL of plasmid DNA added. The mix was then incubated for 30 min on ice prior to heat shock at 42°C for 30 sec. After 2 min incubation on ice, 250 µL SOC medium was added and cells allowed to recover for 1 h at 37°C with shaking. 50 – 100 µL of the cell suspension was plated onto LB agar plates containing either kanamycin (50 µg/mL) or ampicillin (100 µg/mL) depending on the transformed plasmid and plates incubated at 37°C overnight.

LB agar: 1 % (w/v) Tryptone
0.5 (w/v) Yeast extract
1 % (w/v) NaCl

1.5 (w/v) Agar

The mixture was boiled on a hot plate prior to autoclaving. Antibiotics were added immediately before use in appropriate concentration.

2.2.1.5 Culturing bacteria

Colonies were picked from LB agar plates using a sterile tip and cultured in 10 mL LB broth containing the appropriate antibiotic. Cultures were grown overnight at 37°C in a shaker.

LB broth: 1 % (w/v) Tryptone
0.5 % (w/v) Yeast extract
1% (w/v) NaCl

The broth was boiled on a hot plate prior to autoclaving. Antibiotics were added immediately before use in appropriate concentration.

2.2.1.6 Plasmid DNA extraction

Plasmid DNA was extracted from bacterial cultures using the QIAprep Spin Miniprep kit. Each 10 mL culture was divided into two tubes and centrifuged for 10 min. Plasmid DNA extraction was then carried out according to manufacturer's instructions. In brief, 250 µL buffer P1 was added to each pellet and the pellet resuspended. 250 µL buffer P2 was added and the tubes inverted to mix. 350 µL buffer N3 was added and again the tubes were inverted to mix. After centrifuging for 10 min at 13 000 x g, 800 µL of the supernatant was applied to a spin column and the column centrifuged for 1 min at 13 000 x g. The column was then washed with 500 µL buffer PB and centrifuged for 1 min at 13 000 x g, prior to washing with 750 µL buffer PE. After the column was centrifuged for 1 min at 13 000 x g, it was centrifuged 1 min at 13 000 x g again. The column was transferred into a clean microcentrifuge tube and 30 µL distilled water was used to elute DNA from the column. After adding the water to the column and incubating for 1 min at room temperature, the column was centrifuged for 1 min at 13 000 x g to elute the DNA.

2.2.1.7 Simultaneous DNA/RNA extraction from cells

Simultaneous DNA/RNA extraction from cell culture samples was performed using the EZNA DNA/RNA system. In brief, cells were trypsinised and pelleted as described in section 2.2.2.8. After pelleting, the supernatant was removed and the pellet snap frozen in liquid nitrogen. Samples were then stored at -80°C until RNA

extraction. Immediately before use, 20 µL of 2-mercaptoethanol was added to each 1 mL of GTC lysis buffer required, for example 60 µL 2-mercaptoethanol for 3 mL lysis buffer. 350 µL of GTC lysis buffer was added to each sample. Tubes were vortexed and incubated for 5 min at room temperature. The lysate was then added to the DNA column and centrifuged for 1 min at 13 000 rpm. The DNA column was placed into a new collection tube and set aside. 350 µL of 70 % ethanol was added to the flow through and mixed by pipetting. The solution was transferred onto an RNA column and centrifuged for 1 min at 13 000 rpm. 500 µL of RNA wash buffer I was added to the RNA column and centrifuged as before. After that, 500 µL of RNA wash buffer II was added to the column and centrifuged as before. The wash with RNA wash buffer II was repeated once, before the column was transferred to a new collection tube and centrifuged for 2 min at 13 000 rpm. The RNA column was transferred into a fresh tube and incubated at room temperature for 5 min. 50 µL of preheated DEPC water was added to the column and incubated for 5 min at room temperature, before the RNA was eluted by centrifugation at 13 000 rpm for 1 min.

The DNA column was then washed with 500 µL HBC buffer, centrifuged for 1 min at 13 000 rpm and the filtrate discarded. 700 µL DNA wash buffer was added to the column before the column was centrifuged for 30 sec at 12 000 rpm. The wash step was repeated once. The empty column was centrifuged for 2 min at 10 000 rpm before being transferred to a clean tube. The membrane was dried for 5 min at room temperature with the lid open before 100 µL preheated elution buffer was added to the column and the column incubated at 70°C for 5 min. The column was centrifuged for 1 min at 13 000 rpm and the eluate added back onto the column. It was incubated for 5 min at room temperature and centrifuged as before. Quality of RNA and DNA was assessed by nanodrop measurements and agarose gel electrophoresis.

2.2.1.8 RNA extraction from hiPSCs

When hiPSCs were collected for RNA extraction, the supernatant was removed and 1 mL of Trizol added to each well. After pipetting up and down several times, the sample was transferred into a microcentrifuge tube and incubated for 10 min at room temperature while shaking (600 rpm). For cartilage-like pellets, frozen samples were homogenised before being transferred into Trizol. The sample was then either frozen at -80°C or RNA isolated directly. For RNA isolation, 200 µL of chloroform was added and the tube shaken vigorously for 15 sec, prior to 5 min incubation at room temperature. The sample was then centrifuged for 15 min at 4°C and no more than

12 000 x g. The aqueous phase (top phase) was transferred into a tube containing 10 µg glycogen and the extraction repeated with the organic phase.
500 µL of isopropanol was then added to the tube containing glycogen and both aqueous phases. After mixing, the sample was incubated for 10 min at room temperature and subsequently centrifuged for 10 min at 4°C and no more than 12 000 x g. The supernatant was removed and the pellet washed with 1 mL 75 % (v/v) ethanol. The pellet was mixed carefully prior to centrifuging at 7 500 x g and 4°C for 10 min. The supernatant was removed and the wash step repeated. The supernatant was then removed entirely and the pellet air-dried for 5-10 min at room temperature prior to resuspension in water. 1 µL of sample was used for nanodrop measurements.

2.2.1.9 Reverse transcription and qPCR (hiPSCs)

Reverse transcription of RNA isolated from hiPSCs was performed using the QuantiTect Reverse Transcription Kit (Qiagen) according to the manufacturer's instructions. In brief, 100 ng of RNA was brought to a volume of 12 µL with RNase-free water and incubated with 2 µL of gDNA wipeout buffer (7 x) for 2 min at 42°C. A reverse transcription mix of 4 µL Quantiscript RT buffer (5 x), 1 µL Primer Mix and 1 µL reverse transcriptase was added to each reaction and incubated for 30 min at 42°C and subsequently for 3 min at 95°C. The reaction was then stored at -20°C until qPCR was performed.
For qPCR, three genes were measured in parallel and every cDNA sample run in duplicate. 2 µL of every cDNA were diluted with 5 µL water and 1 µL of this dilution used per well. 5 µL/well of SYBR green master mix (Agilent) were added. A primer stock was prepared, containing each forward and reverse primer at 1 µM. 4 µL of the primer stock was used per well. Besides cDNA samples, negative controls containing water instead of DNA and a standard curve were measured. The standard curve consisted of pooled cDNA which had been serially diluted 1:5 for five times. qPCR was performed in a 384-well plate which was briefly centrifuged prior before starting the cycling program (Table 2.5).

Temperature	Duration	Step
95 [°C]	3 min	Pre-incubation
95 [°C] 60 [°C]	5 sec 10 sec	amplification
95 [°C] 65 [°C] 97 [°C]	5 sec 1 min continuous	Melting curve
40 [°C]	30 sec	cooling

Table 2.5 - Cycling program used for qRT-PCR of hiPSC cDNA.

2.2.1.10 RNA extraction using Promega ReliaPrep RNA Mini Prep System

RNA extraction from femoral head cartilage (1 week) and from p.C312Y, p.D385N, p.D473H, p.G440R, p.D511Y and wild type COMP cells was carried out using the ReliaPrep RNA Tissue Miniprep System according to the manufacturer's protocol for fibrous tissue. Cell samples were collected 72 hrs after confluency as described in section 2.2.2.12.

For RNA extraction from femoral head cartilage, cartilage was dissected as described in section 2.2.4.3. For each sample, cartilage from 3 animals was pooled prior to extraction. A Sartorius Micro Dismembranator S tissue homogeniser vessel was cooled in liquid nitrogen, before 500 µL of LBA + TG buffer and the frozen tissue were added. The frozen tissue was then ground using the tissue homogeniser for 1 min at 2 000 rpm. The sample was allowed to thaw and DNA sheared by pipetting up and down multiple times. For snap frozen cell pellets, 500 µL of LBA + TG buffer was added/pellet before the pellets were allowed to thaw in buffer. All following steps were identical for tissue and cell samples.

500 µL of RNA dilution buffer was added and the samples mixed by vortexing, before samples were centrifuged for 3 min at 10 000 x g. The supernatant was then transferred to a fresh tube. 340 µL of isopropanol was added and the samples mixed, before half of the sample was transferred to a Minicolumn. After centrifuging for 1 min at 14 000 x g, the remaining sample was loaded onto the Minicolumn and the centrifugation repeated. The Minicolumn was washed with 500 µL RNA wash solution before DNase I digestion was performed according to the manufacturer's protocol. After DNase I treatment, 200 µL of column wash solution was added and the column centrifuged. The column was then washed twice with RNA wash solution, before

RNA was eluted in nuclease-free water. The obtained eluate was passed through the column a second time to elute any remaining RNA.

2.2.1.11 Reverse transcription and qPCR

Reverse transcription of RNA isolated from mouse tissue or HT1080 cells was performed using the Promega GoScript Kit according to the manufacturer's instructions. In brief, for HT1080 cells, 1 µg of RNA was added to 0.5 µg of random primer and 0.5 µg of Oligo-dT-primer. Water was added to a volume of 5 µL. The mix was incubated at 70°C for 5 min before it was chilled on ice immediately. A reverse transcription mix of 4 µL GoScript 5X reaction buffer, 2.5 µL $MgCl_2$ (final concentration 3.125 mM) 1 µL PCR Nucleotide Mix (final concentration 0.5 mM each dNTP), 0.5 µL RNasin (20 U) and 1 µL GoScript reverse transcriptase per reaction was prepared. The volume was adjusted to 15 µL, added to the RNA/primer mix and briefly centrifuged before being incubated for 5 min at 25°C and subsequently for 60 min at 42°C. The reverse transcriptase was inactivated by incubating at 70°C for 15 min. The reaction was then stored at -20°C until qPCR was performed. In case of RNA extracted from murine tissues, 50 - 100 ng were transcribed, depending on the yield of the extraction.

Prior to qPCR, all samples were treated with 1 U RNaseH for 20 min at 37°C.

For qPCR, RNaseH treated cDNA was diluted to 5 ng/µL prior to setting up the reaction. Per well, each reaction contained 1 µL of diluted cDNA, 2 µL primer mix (final concentration 0.5 µM), 5 µL PowerUp SYBR green master mix and 2 µL water. The plate was briefly centrifuged before qPCR was performed using a QuantStudio3 qPCR cycler (Table 2.6).

Relative quantification was performed using the $2^{-\Delta\Delta CT}$ method (Livak and Schmittgen, 2001).

Temperature [°C]	Duration	Step
94	2 min	Pre-incubation
94 60 72	30 sec 30 sec 30 sec	Amplification – 40 cycles
72	10 min	
55-95	continuous	Melt curve

Table 2.6 – Cycling program used for qRT-PCR of cell and murine tissue cDNA.

2.2.1.12 RT-PCR for XBP1 splicing analysis

To visualise the long and short form of *XBP1,* 5 µL of diluted cDNA was added to a BioMix reaction (see section 2.2.1.1). The amount of water was reduced accordingly, keeping the reaction volume at 20 µL. The cycle number was reduced to 28 cycles. Long and short forms of the *XBP1* transcript were then visualised using agarose gel electrophoresis as described in section 2.2.1.2.

2.2.1.13 Quantification of mitochondrial and nuclear DNA

Because mitochondria carry their own genome, the ratio of mitochondrial (mt) to nuclear (nu) DNA may be used to compare the amount of mitochondria between samples. To quantify mtDNA and nuDNA, DNA extracted from wild type and D469del COMP cells was analysed by qPCR. For each sample, reactions were measured in triplicate with 0.25 ng of template DNA. The total reaction volume was 20 µL, using 10 µL PowerSYBR Green Master mix and with final primer concentrations of 0.5 µM.

2.2.1.14 DNase I treatment and RNA sequencing

For transcriptomic analysis, 10 µg of RNA extracted as described previously (see section 2.2.1.7) were diluted to a volume of 30 µL and digested using the DNA-free kit according to the manufacturer's instructions. RNA was mixed with 0.1 volume of 10X DNase I buffer and 1 µL of recombinant DNAse I and subsequently incubated at 37°C for 30 min. After the incubation, 0.1 volume of DNase I Inactivation Reagent was added and the reactions mixed well. After incubating at room temperature for 2 min and occasional mixing, the samples were centrifuged at 10 000 x g for 1.5 min before the RNA was transferred into a fresh tube. RNA sequencing was then performed by the Genomics Core Facility at Newcastle University using the Illumina NextSeq500 platform.

2.2.1.15 Infinium MethylationEPIC array

500 ng of DNA (see section 2.2.1.7) was used to carry out methylation analysis using the Illumina Infinium MethylationEPIC array. Bisulfite conversion and methylation analysis was carried out at Edinburgh Clinical Research Facility, Wellcome Trust CRF, Western General Hospital, Edinburgh.

2.2.2 Cell culture methods

2.2.2.1 Maintenance of feeder-free human induced pluripotent stem cells (ff-hiPSCs)

ff-hiPSCs were cultured on 6-well plates precoated with Matrigel in Essential 8 medium with supplements as supplied by the manufacturer. To coat one well of a 6-well plate, 14 µL Matrigel was diluted in 2 mL DMEM/F12 medium and mixed well. The coating solution was then added to one 6-well and incubated for up to 24 h at 37°C. After cells were added (see below), the plates were kept at 37°C with 5 % CO_2 and the medium changed daily.

2.2.2.2 Passaging of ff-hiPSCs

Medium was carefully aspirated and 2 mL PBS used to wash the cell layer. After PBS was removed, the cells were incubated with 1 mL of EDTA dissociation reagent for 4 min at 37°C. The EDTA dissociation reagent was carefully aspirated and 1 mL of fresh medium added directly to the cell surface, dislodging the cells. Medium and dislodged cells were then transferred to a Falcon tube. Again, 1 mL of medium was added, cells dislodged from the plate and transferred into the tube. This was repeated one more time before the cell suspension was mixed with the appropriate amount of fresh medium and 2 mL/well added to a Matrigel-coated plate.

EDTA dissociation reagent: 0.5 mM EDTA in sterile PBS

2.2.2.3 Osteogenic differentiation of ff-hiPSCs

Differentiation was performed on 12-well plates. At least 1 h prior to use, wells were coated with 1 mL of 0.1 % (v/v) gelatin solution. Immediately before seeding cells, the coating solution was removed and 1 mL of differentiation medium added.
To seed cells for differentiation, ff-hiPSCs were counted using an automated cell counter (countess). In brief, old medium of one well was removed and that well washed with 2 mL PBS. After PBS was removed, cells were incubated with 1 mL TrypLE for 3 min at 37°C. 2 mL of Essential 8 medium was added and cells resuspended. 10 µL of the cell suspension was mixed with 10 µL Trypan blue and counted.
Subsequently, medium of all wells that were collected was removed. All wells were washed with 2 mL of PBS and incubated with 1 mL EDTA dissociation solution for 4 min at 37°C. EDTA dissociation solution was aspirated and the cells dislodged using 3 x 1 mL differentiation medium. Cells were diluted to the appropriate concentration

(typically 400 000 cells/mL) and plated at the desired density (400 000 cells/well on a 12-well plate). To enhance osteoblastic differentiation, 200 nM of AM580, a retinoic acid receptor agonist, was added to the differentiation medium and the osteogenic medium.

Differentiation medium:

80 % (v/v) osteogenic medium
20 % (v/v) Essential 8
10 µM Y-27632 (Rock inhibitor)

Osteogenic medium:

DMEM GlutaMax + pyruvate, 4.5 g/L glucose
20 % (v/v) KnockOut serum replacement
10 mM β-Glycerophosphate
1 nM Dexamethasone
0.1 mM 2-Mercaptoethanol
50 µg/mL Ascorbate-2-phosphate
1 x non-essential amino acids

On day 2, day 7 and day 10, medium was replaced with fresh 100 % (v/v) osteogenic medium.

During optimisation, plates were coated with gelatin and Matrigel in parallel and differentiation assessed after seven days of culture by alizarin red staining. Additionally, cells were seeded directly in differentiation media or allowed to attach overnight in Essential 8 medium prior to differentiation. Besides AM580, 1 µM all trans retinoic acid (ATRA) was used to induce osteogenesis.

2.2.2.4 Maintenance of feeder dependent human induced pluripotent stem cells (hiPSCs)

For feeder dependent cultures, culture vessels (typically T25 flasks) were pre-treated with feeder medium overnight before use.

Feeder medium:

10 % (v/v) FBS
50 U/mL Penicillin

50 µg/mL Streptomycin
2 mM GlutaMAX
In DMEM high glucose

Subsequently, mitotically inactivated primary mouse embryonic fibroblasts (pMEFs) were thawed and seeded onto the culture vessels. For thawing, 5 mL of feeder medium was prepared in a falcon tube and 2 x 10^6 pMEFs thawed in a water bath. The pMEFs were added to the falcon tube and centrifuged for 3 min at 1500 rpm at 4°C. They were then resuspended at a concentration of 1 x 10^6/mL and 0.5 mL used for the preparation of each T25 flask. pMEFs were allowed to attach for 1-4 h before use.

Feeder dependent hiPSCs were cultured in hiPSC medium, containing the following components:

20 % (v/v) KnockOut serum replacement
1 x non-essential amino acids
2 mM GlutaMAX
0.1 mM 2-Mercaptoethanol
50 ng/mL basic FGF
In DMEM/F12

2.2.2.5 Passaging of feeder-dependent hiPSCs

Medium was carefully aspirated and 2.5 mL PBS used to wash the cell layer. After PBS was removed, the cells were incubated with 1 mL of EDTA dissociation reagent for 3 min at 37°C. The EDTA dissociation reagent was carefully aspirated and 3 mL of fresh medium added directly to the cell surface. The cells were dislodged by tapping against the flask. 1 mL of cell suspension was then transferred onto a new flask coated with pMEFs. 4 mL of fresh hiPSC medium was added and the flask placed back into the incubator.

2.2.2.6 Osteogenic differentiation of feeder-dependent hiPSCs

To induce osteogenic differentiation, feeder-dependent cells were cultured as feeder-free cells on Matrigel in E8 for one passage prior to differentiation. They were then differentiated as described in section 2.2.2.3.

During optimisation, feeder-dependent hiPSCs were also differentiated on pMEFs in the same medium as described in section 2.2.2.3.

2.2.2.7 Maintaining HT1080 cells

HT1080 fibrosarcoma cells (Rasheed et al., 1974) were cultured in DMEM/F12 supplemented with 10 % FBS, 50 µg/mL Streptomycin, 50 U/mL Penicillin and 1 x non-essential amino acids (from a 100X stock). Cells were cultured at 37°C with 5 % CO_2.

HT1080 cells overexpressing wild type and D469del COMP with a C-terminal GFP tag were previously described (Suleman et al., 2012). HT1080 cells overexpressing wild type, p.C312Y, p.D385N, p.G440R, p. D473H and p.D511Y COMP were generated by Dr Beth Gibson, Newcastle University.

2.2.2.8 Passaging cell lines

When cells reached 70-80 % confluency, the old medium was removed and cells were washed with 10 mL of PBS. After removal of PBS, 1.5 mL of Trypsin/EDTA was added and incubated at 37°C for 5 min. Cell detachment was confirmed visually. After addition of 8.5 mL fresh medium, cells were gently resuspended prior to transfer into a 15 mL falcon tube. The cell suspension was centrifuged at 500 x g for 5 min and the supernatant discarded. The cell pellet was resuspended in 10 mL of fresh medium and 1-2 mL of the cell suspension was transferred into a new T75 flask, containing 12 mL of fresh medium. For cells overexpressing COMP constructs, 500 µg/mL Geneticin was added to the culture medium.

2.2.2.9 Seeding cells for experiments

Cells were passaged according to section 2.2.2.8. After resuspension of the pellet, 9 µL of cell suspension was transferred to a haemocytometer and cells counted. Cells were then seeded with the appropriate density, for HT1080 cells typically 200 000 cells/well for a 6-well plate in media containing 500 µg/mL Geneticin (where appropriate), 2 mM L-Glutamine and 50 µg/mL ascorbate-2-phosphate.

For in-gel zymography, cells were cultured on 6-well plates until confluent, washed with PBS and then cultured in serum-free media for another 72 hrs.

For immunocytochemistry experiments, cells were seeded onto 8-well chamber slides at the appropriate density (typically 15 000 cells/well for HT1080 cells).

2.2.2.10 Transfections

Cells were seeded into 6-well plates on the day before transfection. Confluency at the time of transfection was approximately 70 %.

1 µg of plasmid DNA was mixed with 150 µL OptiMEM serum-free medium. In a second tube, 4 µL Lipofectamine2000 was mixed with 150 µL OptiMEM serum-free medium. Both tubes were incubated 5 min at room temperature before being mixed

and incubated for another 30 min. During this incubation period, cells were washed once with PBS and fresh medium added.

2.2.2.11 Collection of cells for RNA extraction

To extract RNA from cells, the media was removed and cells washed with 1 mL sterile PBS. Cells were then detached from the culture plate by incubating with 250 µL of Trypsin/EDTA at 37°C for 5 min. Trypsin/EDTA was inactivated by adding 1 mL of fresh media. Cells were resuspended and subsequently centrifuged at 1 000 x g for 5 min. The supernatant was removed and cells washed with 1 mL of sterile PBS. Cells were centrifuged again, the supernatant removed and the pellet snap frozen in liquid nitrogen until RNA extraction.

2.2.2.12 MitoTracker Red CM-H_2XROS labelling of mitochondria

MitoTracker labelling was carried out using chamber slides. Prior to labelling, medium was removed and the cell layer washed with serum-free DMEM medium. MitoTracker Red CM-H_2XROS (in DMSO) was diluted in serum-free media to a final concentration of 500 nM. DMSO was used as negative control. Cells were labelled for 45 min, washed several times with serum-free media and fixed in 4 % (v/v) methanol-free paraformaldehyde in PBS for 15 min. Cells were washed 3 x 5 min with PBS before being incubated in DAPI containing fluorescence mounting medium for 5 min. Slides were mounted, left to dry for 1 h at room temperature and imaged on a confocal microscope (A1R Nikon).

2.2.2.13 TUNEL labelling of cell lines

For TUNEL labelling, cell lines were seeded onto 8-well chamber slides. After 24 h, media was removed and cells were fixed with 4 % (v/v) methanol-free paraformaldehyde in PBS for 10 min at room temperature. After fixation, cells were washed multiple times with sterile PBS. Cells were then permeabilised with 0.25 % (v/v) TritonX100 in PBS for 5 min, washed with PBS for 3 x 5 min and treated with equilibration buffer for 10 min. Each well was then treated with a reaction mixture of 180 µL equilibration buffer, 20 µL nucleotide mix and 4 µL TdT enzyme. The reaction was performed in a humidified chamber at 37 C for 1 h. After stopping the reaction by incubating with 2 x SSC solution (in water) for 15 min, cells were washed with PBS 3 x 5 min and mounted using Fluoroshield mounting medium with DAPI. Microscopy was carried out using a Zeiss AxioImager3 fluorescence microscope.

2.2.2.14 BrdU-labelling of cell lines

To assess effects on cell proliferation, cell lines were seeded onto 8-well chamber slides. After 24 h, media was removed and fresh media containing BrdU labelling

reagent (diluted 1:1000) was added to the cells. Cells were incubated for 2 h at 37°C with 5 % CO_2 before being fixed in 95 % (v/v) Ethanol, 5 % (v/v) acetic acid for 10 min at room temperature. Slides were washed with sterile PBS several times before antigen retrieval was performed by treating with 4 M hydrochloric acid for 10 min, followed by incubating in 0.1 M borate buffer pH 8.5 for 20 min. After washing cells 3 x 5 min with PBS, cells were incubated with primary antibody overnight at 4°C. Cells were then washed 3 x 5 min with PBS, followed by incubation with respective secondary antibodies for 2 h at room temperature. After washing 3 x 5 min with PBS, slides were mounted with Fluoroshield mounting medium with DAPI. Microscopy was performed using a Zeiss AxioImager3 fluorescence microscope.

1 X PBS (not sterile): 5 tablets PBS/1 L water

2.2.2.15 Immunocytochemistry

For immunocytochemistry, cells were typically fixed in 95 % (v/v) Ethanol, 5 % (v/v) acetic acid, washed with sterile PBS several times before immunocytochemistry was performed (Table 2.7).

Step	Duration
Permeabilise 0.25 % TritonX100 in PBS	10 min
PBS	3 x 5 min
Block in 10 % (v/v) normal donkey serum or 1 % (w/v) BSA/PBS	1 h
Incubate with primary antibody (see Table 2.1)	Overnight, 4°C
PBS	3 x 5 min
Incubate with secondary antibody in the dark (see Table 2.1)	2 h
PBS	3 x 5 min
Mount with Fluoroshield mounting medium	5 min

Table 2.7 – General procedure for immunocytochemistry.

Slides were left to dry at room temperature (protected from light) before being imaged using a Zeiss AxioImager3 fluorescence microscope.

2.2.2.16 Treatment with tunicamycin or thapsigargin

To induce the activation of the UPR in wild type and D469del COMP cells, 3 wells per cell line were seeded as described in section 2.2.2.9. The following day, media were removed and replaced with media containing either DMSO (diluted 1:2500), 2 µg/mL tunicamycin (stock: 5 mg/mL in DMSO) or 2 µM thapsigargin (stock: 5 mM in DMSO). Cells were then left for 16 h, before being collected for analysis as described in section 2.2.2.12 and 2.2.2.18.

2.2.2.17 Detection of superoxide anions using nitroblue tetrazolium chloride (NBT)

To compare the amount of superoxide anions, a specific type of reactive oxygen species (ROS), a modified NBT assay (Esfandiari et al., 2003; Sim Choi et al., 2006) was used. Typically, phagocytes that produce large amounts of ROS are stained with NBT and the staining is then analysed visually. In this study, the formazan crystals formed by the reduction of NBT by superoxide anions were extracted and the absorbance measured at 620 nm (based on reference (Sim Choi et al., 2006)). In brief, cells were seeded at the appropriate density onto 12-well tissue culture plates (typically 100 000 cells/well for HT1080 cells). 24 h after seeding, the medium was replaced with fresh culture medium. Another 24 h after refreshing the medium, the medium was removed and replaced with 0.5 mL PBS containing 0.1 % (w/v) NBT (sterile-filtered). The cells were incubated for 40 min at 37°C with 5 % CO_2. After staining, the NBT solution was removed, cells were washed twice with ice-cold PBS and subsequently washed with ice-cold 100 % methanol once. The wells were air-dried before 120 µL of 2 M KOH solution was added per well. After adding 140 µL DMSO, the plates were incubated 10 min in the dark on a shaker. 100 µL of each sample was transferred onto 96-well plate (each extracted well was measured in duplicate) and absorbance was measured at 620 nm.

As a positive control, several wells of each cell line were also treated with 50 µM menadione for 15 min at 37°C with 5 % CO_2 prior to NBT staining. Empty wells with and without menadione treatment treated with NBT solution served as negative controls.

Absorbance was then normalised to cell numbers. To count cells, 3 wells of each cell line were washed with PBS once and detached from the plate by incubating with Trypsin/EDTA solution for 5 min at 37°C. 0.8 mL of cell culture medium was added to each well and cells were collected by centrifugation at 500 x g for 5 min. The pellets

were resuspended in 1 mL cell culture medium each and counted using a haemocytometer.

2.2.2.18 Protein extraction from cells

Samples were collected 72 hrs after confluency. If serum free conditioned media was to be analysed, cells were seeded in serum containing media and cultured until confluent. The medium was then removed, cells were washed with PBS and fresh, serum free media added.

To analyse cell culture supernatants and cell lysates by western blotting, the cell culture supernatant was removed and cleared by centrifugation at 500 x g for 5 min. The cleared supernatant was then transferred into a fresh tube and stored at -80°C. The cell layer was washed once with 1 mL PBS prior to adding 150 µL 2 x SDS loading buffer containing protease inhibitors. Cells were scraped into Eppendorf tubes (on ice) and passed through an insulin needle before centrifuging at 14 000 rpm for 15 min at 4°C. The cleared lysate was then transferred into a fresh tube and stored at -80°C.

5 x SDS loading buffer:	625 mM Tris-base
	50 % (v/v) Glycerol
	10 % (w/v) SDS
	0.025 (w/v) Bromophenol blue
	pH 6.8

Prior to use, the buffer was diluted to working concentration (2 x) and protease inhibitors (complete EDTA free Mini) were added.

2.2.3 Biochemical methods

2.2.3.1 BCA assay

To determine protein concentration, protein samples were measured by BCA assay. Samples were diluted appropriately (typically 1:20). BSA solution with concentrations from 0 to 2 000 µg/mL were used as a standard. 10 µL of each standard and all samples were used per well. All standards and samples were measured in duplicate. The two reagents were mixed in a 1:50 ratio and 200 µL of the working reagent added to each well. After incubating for 30 min at 37°C, the absorbance was measured at 562 nm. A standard curve was generated using the absorbance of the

BSA standards and the slope used to calculate the protein concentrations of the samples.

2.2.3.2 SDS-PAGE and western blotting

Typically, 18 µL of cell lysate/lane was mixed with DTT (final concentration: 100 mM) and heated to 95°C for 10 min. After briefly centrifuging, samples were loaded onto a 4-12 % Bis-Tris NuPAGE gel in a gel tank filled with 1 x MES running buffer. 5 µL of a molecular weight standard was loaded alongside the samples. The gel was run for 60 min at 180 V.

A transfer stack consisting of filter paper – membrane – gel – filter paper was assembled. The transfer stack was placed between sponges soaked in transfer buffer and transferred for 90 min at 30 V in transfer buffer.

After transfer, the stack was disassembled, ponceau stained for a maximum of 3 min and background staining removed by rinsing the membrane in water. After imaging, the membrane was blocked for 1 h in 3 % (w/v) BSA in TBS-T at room temperature. Incubation with primary antibody (diluted according to table 1 in blocking solution) was carried out overnight at 4°C. After washing 3 x 5 min in TBS-T, the membrane was incubated with secondary antibody (diluted according to table 1 in 5 % (w/v) milk/TBS-T solution) for 1 h at room temperature. After washing 3 x 15 min with TBS-T and rinsing the membrane in TBS, the protein of interest was detected using enhanced chemiluminescent reaction (ECL). Reagents A and B of the SuperSignal West Pico Plus Chemiluminescent Substrate were mixed in a 1:1 ratio and the membrane incubated in the solution for approximately 5 min. Detection was carried out using an Azure c600 system with a cumulative exposure of 10 x 30 sec. If necessary, the membrane was then re-incubated with another primary antibody overnight and the procedure repeated. For GAPDH detection, incubation with primary antibody was carried out at room temperature for 1 h.

20 X Transfer buffer: 1 M Tris-Base
0.77 M Glycine
0.72 % (w/v) SDS

Prior to use, the transfer buffer was diluted to 1 x and 20 % methanol added.

10 X TBS: 100 mM Tris
1.5 M NaCl

The pH was adjusted to 7.4 with hydrochloric acid followed by adjusting the final volume to 1 L.

TBS-T 50 mL 10 X TBS
450 mL water
0.5 mL Tween-20

2.2.3.3 Dot blot of conditioned media

2 µL of conditioned media from wild type and D469del COMP cells treated with DMSO, tunicamycin or thapsigargin was loaded onto a nitrocellulose membrane. The membrane was allowed to dry completely before ponceau staining was performed for 3 min. After removing background staining by rinsing with water, the membrane was imaged and subsequently blocked in 3 % (w/v) BSA in 0.1 % (v/v) TBS-T at room temperature. Incubation with rabbit-anti-GFP primary antibody (diluted according to table 1 in blocking solution) was carried out overnight at 4°C. After washing 3 x 5 min in 0.1 % (v/v) TBS-T, the membrane was incubated with goat-anti-rabbit secondary antibody (diluted according to table 1 in 5 % (w/v) milk/TBS-T solution) for 1 h at room temperature. After washing 3 x 15 min with TBS-T and rinsing the membrane in TBS, GFP-tagged COMP was detected using ECL. Reagents A and B were mixed in a 1:1 ratio and the membrane incubated in the solution for approximately 5 min.

2.2.3.4 In-gel zymography

To assess the activity of gelatinases, in-gel zymography of concentrated cell culture supernatant was performed. 1 mL of serum-free cell culture supernatant was concentrated to 25 µL using VivaSpin columns with a molecular weight cut-off of 10 kDa for 10 min at 12 000 x g. The concentrated sample was then mixed with an appropriate amount of 5 x SDS loading buffer (without DTT) and incubated for 10 min at room temperature. Each sample was then loaded onto a 0.3 % (w/v) gelatin-containing 7.5 % SDS polyacrylamide gel as well as a standard 7.5 % SDS polyacrylamide gel. The gels were run in parallel, on ice, at 140 V until the dye front had reached the bottom of the gel. The gelatin gel was then incubated 3 x 15 min in 0.25 % (v/v) TritonX100 to allow MMPs to be renatured after SDS-PAGE. Subsequently, the gelatin gel was incubated in reaction buffer (see appendix) for 20 h at 37°C and 60 rpm to allow MMPs to digest the gelatin. The reaction was stopped by incubating the gelatin gel in Coomassie G250 solution for 60 min at room

temperature. The gelatin gel was then incubated in de-staining solution until bands were clearly visible and imaged on the Azure c600 system.
As a loading control, the SDS polyacrylamide gel was rinsed briefly in distilled water before being stained with Coomassie G250 solution for 60 min at room temperature. The gel was then incubated in de-staining solution until bands were clearly visible and imaged on the Azure c600 system.

Separating gel solution:

2.3 mL 40 % (v/v) Acrylamide/Bis-Acrylamide solution
3 mL 1.5 M Tris-HCl pH 8.8
60 µL 20 % (w/v) SDS solution
2.4 mL 1.5 % (w/v) gelatin solution (replaced with water for loading control)
Ad 12 mL

The 1.5 % (w/v) gelatin solution was made fresh and incubated for 30 min at 37°C and 60 rpm prior to use.

60 µL of 20 % (w/v) ammonium persulfate (APS) and 20 µL of TEMED were added just before casting the gel.

Stacking gel solution:
0.75 mL 40 % (v/v) Acrylamide/Bis-Acrylamide solution
1.5 mL 0.5 M Tris-HCl pH 6.8
30 µL 20 % (w/v) SDS solution
Ad 6 mL

30 µL of 20 % (w/v) APS and 10 µL of TEMED were added just before casting the gel.

Coomassie staining solution:
40 % (v/v) Methanol
10 % (v/v) Glacial acetic acid
0.2 % (w/v) Coomassie Brilliant Blue G250

Coomassie de-staining solution:
40 % (v/v) Methanol
10 % (v/v) Glacial acetic acid

Reaction buffer: 50 mM Tris-HCl pH 7.4
10 mM $CaCl_2$
0.02 % (w/v) NaN_3

2.2.4 In vivo methods

All experiments involving the use of animals were carried out according to Directive 2010/63/EU of the European Parliament under project licence P8A8B649A. Local ethical approval was provided under The Animals (Scientific Procedures) Act 1986.

2.2.4.1 HotShot extraction of DNA for genotyping

Ear punches were incubated in 75 µL of lysis buffer for 30 min at 95°C, followed by 10 min at 4°C. Following the addition of 75 µL of neutralising buffer, each sample was vortexed and centrifuged for 2 min. 1.5 µL of the supernatant was used for PCR.

Lysis buffer: 25 mM NaOH
0.2 mM EDTA pH 8.0

Neutralising buffer: 40 mM Tris pH 5.0

2.2.4.2 Dissection, fixation and decalcification of tissue for histology

For histology, hind limbs were dissected by dislocation of the hip and fixed in 10 % (v/v) neutral buffered formalin solution for 24 h at room temperature. The following day the samples were rinsed in water and decalcified in Formical overnight at room temperature. Decalcified samples were then processed prior to wax embedding as described in section 2.2.5.1.

2.2.4.3 Dissection of femoral head cartilage for RNA isolation

For RNA isolation, hind limbs were dissected by dislocation of the hip. Following that, the cartilage was separated from the subchondral bone of the femoral head and immediately frozen in liquid nitrogen. The cartilage was then stored at -80°C until RNA extraction.

2.2.4.4 Isolation of primary chondrocytes from femoral head cartilage

For experiments using primary chondrocytes, cartilage was dissected as described above (Section 2.2.4.3). The cartilage was immersed in warm PBS until all cartilage was dissected (typically 3 animals/genotype). The tissues were then transferred into

1.5 mL collagenase and digested for 3-4 h at 37°C. During this period, samples were vortexed every 30 min. After digestion, 3.5 mL fresh DMEM4 medium was added and the suspension mixed by pipetting. The suspension was then passed through a 70 µM cell strainer, followed by 10 mL of fresh medium. The cell suspension was centrifuged at 350 x g for 5 min and the pellet resuspended in 10 mL of PBS. After centrifuging again, cell pellets were resuspended in 1 mL of trizol before samples were snap frozen in liquid nitrogen.

DMEM4 medium: 40 mL DMEM
8 mL FBS
0.5 mL Penicillin/Streptomycin
100 µL ascorbate 25 mg/mL

2.2.5 Histological methods

2.2.5.1 Tissue processing

Decalcified samples were wax-embedded using a Thermo Scientific Spin Tissue Processor according to the protocol shown below (Table 2.8). Samples were then embedded in Fisher wax and sectioned.

Solution	Duration
70 % (v/v) Ethanol	6 h
90 % (v/v) Ethanol	45 min
95 % (v/v) Ethanol	45 min
100 % (v/v) Ethanol	45 min
100 % (v/v) Ethanol	45 min
100 % (v/v) Ethanol	45 min
Xylene	30 min
Xylene	30 min
Xylene	30 min
Paraffin wax	1 h
Paraffin wax	1 h

Table 2.8 - Tissue processing protocol.

2.2.5.2 Sectioning

Samples were cut into 6 µM sections using a microtome (Microm Cool-Cut HM355) and heated water bath. Sections were wet mounted onto Superfrost Plus microscope slides and dried overnight.

2.2.5.3 Toluidine Blue staining

Slides of formalin-fixed tissues were dewaxed, rehydrated and stained with Toluidine Blue and Nuclear Fast Red (Table 2.9).

For Toluidine blue staining of sections from hiPSC pellets (kindly provided by Prof John Bateman, Murdoch Children's Research Institute, Melbourne, Australia), nuclear fast red was replaced with fast green staining solution.

Toluidine blue staining solution: 0.04 g Toluidine Blue O
100 mL 0.1 M Sodium acetate buffer pH 4.0

The pH was adjusted to 3.75 with acetic acid and the final volume adjusted to 100 mL.

Solution	Duration
Xylene	2 x 5 min
100 % (v/v) Ethanol	3 min
90 % (v/v) Ethanol	3 min
70 % (v/v) Ethanol	3 min
50 % (v/v) Ethanol	3 min
dH_20	2 x 5 min
Toluidine blue (0.04 % Toluidine blue in 0.1 M sodium acetate, pH 3.75)	10 min
dH_20	2 x 5 min
Nuclear fast red (Sigma)	5 min
dH_20	2 x 5 min
100 % (v/v) Ethanol	5 min
Xylene	2 x 5 min
DPX	Dried overnight

Table 2.9 - Toluidine Blue staining protocol.

2.2.5.4 Collagen X staining of iPSC pellets after chondrogenic differentiation

Sections were kindly provided by Prof John Bateman, Murdoch Children's Research Institute, Melbourne, Australia. Sections were baked for 60 min at 60°C prior to immunostaining (Table 2.10). In brief, after dewaxing, heat-induced epitope retrieval (HIER) was combined with enzymatic antigen retrieval by hyaluronidase digestion to facilitate the recognition of the antigen by the antibody. The sections were then blocked and subsequently incubated with a primary antibody specific to collagen X. After washing, the sections were incubated with secondary antibody directed against the species the primary antibody was raised in. After washing, nuclei were counterstained with DAPI before mounting.

Process	Step	Duration [min], Temperature
Dewaxing	Xylene	2 x 5 min, RT
Dewaxing	100 % (v/v) Ethanol	1 x 5 min, 1 x 2 min, RT
Dewaxing	90 % (v/v) Ethanol	2 min, RT
Dewaxing	70 % (v/v) Ethanol	2 min, RT
Dewaxing	Tap water	5 min, RT
	PBS	5 min, RT
Antigen retrieval	0.01 M citrate buffer, pH 6.0, 0.05 % (v/v) Tween	30 min, 60°C 30 min, RT
Antigen retrieval	Wash with PBS	3 x 2 min
Antigen retrieval	0.2 % (w/v) hyaluronidase in PBS	30 min, 37°C
Antigen retrieval	Wash with PBS	3 x 2 min
Block	2 % normal goat serum in 1 % (w/v) BSA in PBS OR 3 % (w/v) BSA	1 h, RT
Primary antibody	1:500 in blocking solution	o/N, 4°C
Wash	PBS	3 x 2 min
Secondary antibody	Rabbit IgG Alexa Fluor488 in blocking solution	1 h, RT
Wash	PBS	2 x 2 min
Nuclei staining	DAPI 0.5 µg/mL	5 min, RT
Wash	PBS	3 x 2 min
Mount	Immuno-Mount	

Table 2.10 - Immunostaining for type X collagen of hiPSC pellets.

2.2.5.5 Alizarin Red staining of iPSCs after osteogenic differentiation

Medium was removed and cells washed with 1 mL PBS. PBS was removed and the cell layer was fixed with 1 mL ConFix green for 1 h at room temperature. After removal of ConFix green, the wells were covered with PBS and stored in the cold room until staining.

For staining, the PBS was removed and wells washed with 2 mL of water, prior to staining with 2 mL alizarin red solution for 20 min at room temperature. The staining

solution was taken off and the wells washed three times with water. 2 mL of water was added to the wells and imaged using an inverted microscope.

Alizarin Red staining solution: 2 g Alizarin Red S
100 mL water

The pH was adjusted to 4.1-4.3 using 0.1 % ammonium hydroxide prior to filtering the solution.

2.2.6 Bioinformatical analysis

2.2.6.1 RNA sequencing analysis

The analysis of RNA sequencing data was performed using the Galaxy platform (Afgan et al., 2018). Adaptor sequences were removed using Cutadapt (Martin, 2011). Quality control was performed using the FastQC (Andrews, 2019) and MultiQC (Ewels et al., 2016) tools. HISAT2 was then used to align reads to the transcriptome (Kim et al., 2019), before the featureCounts tool (Liao et al., 2014) was used to generate counts from reads. Limma-voom (Law et al., 2014; Ritchie et al., 2015) was then used to compare expression between groups and generate a list with differentially expressed genes. Volcano plots were generated in R studio using the package 'EnhancedVolcano' (Blighe et al., 2022). KEGG pathway analysis was performed using the Enrichr tool (Kuleshov et al., 2016).

2.2.6.2 DNA methylation analysis

The analysis of Illumina Infinium EPICMethylation array data was performed in R studio (RStudio Team, 2016) using a Bioconductor workflow (Maksimovic et al., 2016). In brief, after removing poor quality probes, 865859 probes were used for normalisation using the *preprocessQuantile* function (Touleimat and Tost, 2012) in *minfi* (Aryee et al., 2014). PreprocessQuantile was chosen for normalisation, as it assumes no global differences between samples (for example, they are derived from the same tissue). Probes were then filtered to remove poor performing probes, probes affected by common SNPs, probes binding to the sex chromosomes and known cross-reactive probes, before probe-wise differential methylation analysis was carried out on the remaining 690594 probes. These results were then further examined to reveal differentially methylated regions using *DMRcate* (Peters et al., 2015). Gene set analysis was performed on DMPs using the gometh function in

missMethyl (Phipson et al., 2016). Visualisation of differentially methylated probes and regions was performed using *Gviz* (Hahne and Ivanek, 2016).

2.2.6.3 Statistical testing

Western blot intensities were quantified in ImageJ/Fiji (Schindelin et al., 2012) using GAPDH as loading control. Gene expression was evaluated by qRT-PCR using 18S as housekeeping gene. Fold changes were calculated from C_T values and statistical testing was performed on $\log_2$ fold changes (Livak and Schmittgen, 2001). Differences were deemed statistically significant if their *P*-value was smaller than 0.05. Statistical testing was generally performed using R studio. Where appropriate, paired/unpaired student's *t*-tests were used. Where multiple groups were compared, ANOVA was performed followed by Tukey's post-hoc test.

Chapter 3. Use of human induced pluripotent stem cell derived cartilage pellets as an *in vitro* model of MCDS

3.1 Introduction

The development of induced pluripotent stem (iPS) cells (Takahashi et al., 2007; Takahashi and Yamanaka, 2006) provides potentially exciting new opportunities to study cartilage-related disorders *in vitro*, although the robust differentiation of those cells into chondrocyte-like cells remains challenging and time-consuming.
Human iPS cell (hiPSC) lines previously generated by John Bateman's laboratory, Murdoch Children's Research Institute, Melbourne, Australia, were used to generate cartilage-like pellets from control and MCDS-patient hiPSCs using their previously establish protocols. This particular differentiation protocol included an additional step to induce hypertrophic differentiation *in vitro.*

Additionally, some control and MCDS-patient derived pellets were treated with CBZ prior to collection. CBZ has been demonstrated to induce degradation of mutant type X collagen in other models of MCDS (Forouhan et al., 2018b; Mullan et al., 2017). A clinical trial to explore treatment with CBZ as a therapy for MCDS is currently ongoing. These data were used to determine whether MCDS-patient hiPSC derived cartilage-like pellets display a robust activation of the UPR after induction of hypertrophy and thus could be a suitable model system to study ER stress associated changes in DNA methylation *in vitro.*

3.1.1 Chapter aims

- To confirm the successful differentiation of hiPSCs into chondrocyte-like cells.

- To confirm the expression of type X collagen mRNA after induction of hypertrophy and evaluate protein levels with and without CBZ treatment.

- To assess UPR activation in cartilage-like pellets and determine whether CBZ reduces the activation of the UPR in cartilage-like pellets derived from hiPSCs.

- To determine whether hiPSC derived cartilage-like pellets could be a suitable model system to study DNA methylation.

3.2 MCDS-patient derived and control hiPSCs form cartilage-like pellets

MCDS-patient derived and control hiPSCs underwent chondrogenic differentiation prior to the induction of hypertrophy (Figure 3.1). Multiple pellets per cell line were

established for differentiation. Cartilage-like pellets were then treated with CBZ for 48 hrs before collection. To perform histology, as well as gene expression analysis, pellets were cut in half during collection.

Firstly, histological analysis was performed to confirm that both control and MCDS-patient derived pellets successfully differentiated into cartilage-like nodules using the previously established protocol. Toluidine blue staining was used to confirm the presence of proteoglycans, one of the key elements of the cartilage extracellular matrix, as a first indicator of successful differentiation. Since hypertrophy had to be induced in the cartilage-like pellets of both control and MCDS-patient derived hiPSCs, two MCDS-patient derived cartilage-like pellets without induction were also analysed as a control. Both MCDS-patient and control derived hiPSCs differentiated into chondrocyte-like cells and formed cartilage-like tissue, as indicated by purple staining (Figure 3.2). This was independent of induction of hypertrophy, as pellets without induction (Figure 3.2 A) showed a comparable Toluidine staining to all other samples.

Similarly, CBZ treatment for 48 hours before collection did not affect cartilage formation (Figure 3.2 B, B' and C, C'). Notably, the overall morphology (e.g. size) of the pellets cannot be assessed based on this staining alone since the pellets had to be cut in half to allow for simultaneous RNA extraction and histological processing. However, in addition to the successful Toluidine blue staining morphological features characteristic for chondrocytes were also observed. All pellets contained small, rounded cells that sometimes appeared to be stained purple. They also contained large, white cells that appeared to be almost rectangular, indicating that some cells may differentiate towards hypertrophy in all pellets. Most pellets contained flattened cells that were arranged in a column-like fashion characteristic of proliferative chondrocytes (Figure 3.2, red arrows). Neither induction of hypertrophy nor treatment with CBZ appeared to dramatically influence the cell morphology. A quantification of columns or hypertrophic chondrocyte-like cells was not performed, as this was likely to depend on both the way the pellets were cut in half prior to collection as well as the plane of sectioning. In contrast to most tissues, pellets do not contain any marks that could indicate a comparable plane of sectioning. Therefore, quantification of the proliferative columns in each pellet was not deemed appropriate.

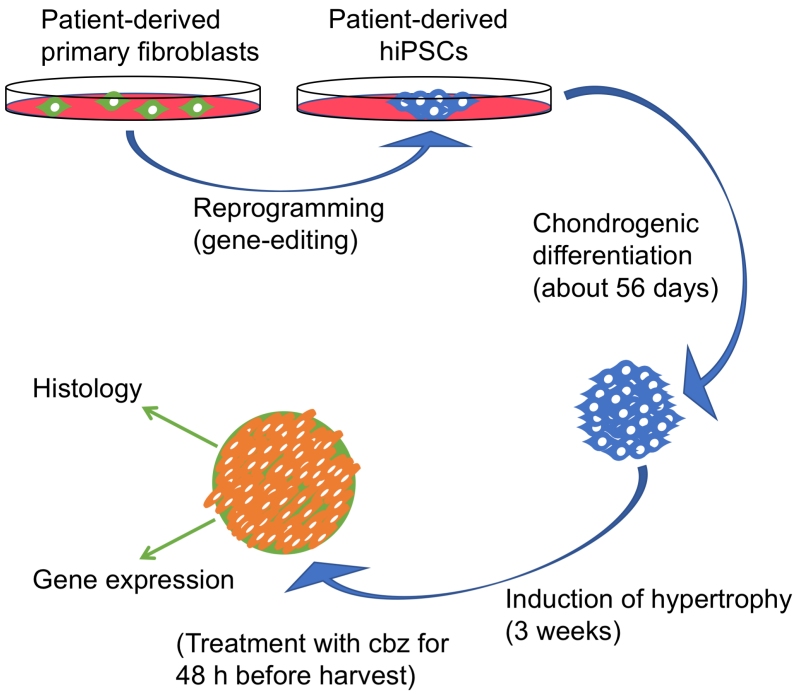

Figure 3.1 – Schematic representation of the differentiation of control and MCDS-patient derived hiPSCs into cartilage-like pellets. Chondrogenic differentiation was performed in pellet culture for about 56 days prior to induction of hypertrophy for three weeks. CBZ was added 48 hrs before collection. Analysis was performed by histology and qRT-PCR of extracted RNA.

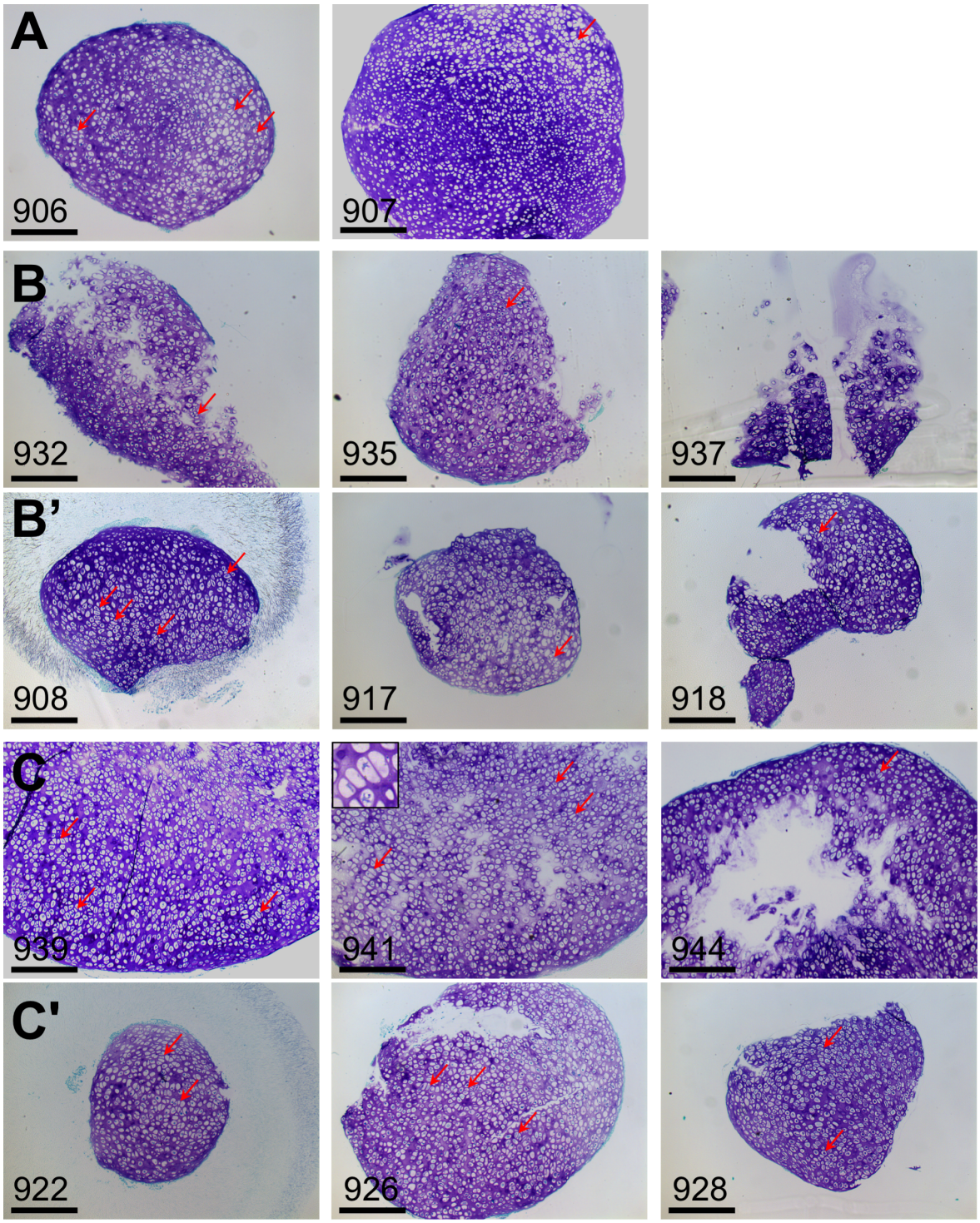

Figure 3.2 – Histological analysis of hiPSC derived cartilage-like pellets. Toluidine Blue staining of (A) two MCDS-patient cartilage-like hiPSC pellets without induction of hypertrophy, (B) three control cartilage-like hiPSC pellets after induction of hypertrophy, (B') three MCDS-patient cartilage-like hiPSC pellets after induction of hypertrophy, (C) three control cartilage-like hiPSC pellets after induction of hypertrophy and treatment with CBZ, insert shows one of the column-like structures in higher magnification, (C') three MCDS-patient cartilage-like hiPSC pellets after induction of hypertrophy and treatment with CBZ. Red arrows indicate columnar structures. Numbers refer to individual pellets, derived from the same control or MCDS-patient hiPS cell line. Scale bar: 500 µM.

3.3 Cartilage-like pellets express type X collagen after induction of hypertrophy

Next, the expression of type X collagen without induction of hypertrophy was assessed at the protein level by immunohistochemistry (IHC). Detection of type X collagen protein was chosen over evaluation of gene expression at this stage as the UPR is activated by the misfolded mutant protein. The presence of the *COL10A1* mRNA transcript could indicate the presence of the protein, however, protein levels could still be small enough for the cells to cope with the resulting ER stress, as observed previously during early stages of cartilage development (Kung et al., 2012). As expected, without induction of hypertrophy no staining for type X collagen was detected (Figure 3.3 B and C) in both pellets analysed. Although some unspecific staining was observed in these samples, this appeared mainly around the nuclei allowing the clear distinction between specific extracellular staining and unspecific nuclear staining.

The expression of type X collagen was then evaluated after hypertrophy was induced. As expected, type X collagen was detected within the extracellular matrix of both control and MCDS-patient cartilage-like hiPSC pellets after induction of hypertrophy (Figure 3.4). No obvious difference in either localisation or staining intensity was observed between control and MCDS-patient cartilage-like hiPSC pellets, although slight variations of staining intensity within the pellets and between replicates occurred. Remarkably, even columnar structures characteristic of proliferative chondrocytes that do not usually express type X collagen were stained positively in this experiment. Although it was to some extent surprising to see no obvious differences, it is noteworthy that protein retention in MCDS has predominantly been studied in cell lines and mice models. The actual extent of protein retention in patient cells *in vivo* is therefore somewhat unclear. In contrast to many mouse models of human disease, which are usually bred to homozygosity, in humans MCDS is an autosomal dominant disease and patients usually carry one normal allele as well as the mutated allele. Therefore, the MCDS-patient derived hiPSCs also carry one functional allele and one disease-causing allele. To visualise differences, more powerful imaging techniques may therefore be required. The study was therefore continued, although no obvious differences in type X collagen localisation were detected at this point.

Type X collagen expression was further assessed in the cartilage-like pellets of both control and MCDS-patient derived hiPSCs that were treated with CBZ (Figure 3.4). While in general, cartilage-like pellets from control hiPSCs treated with CBZ seemed larger than MCDS-patient derived hiPSC pellets, again no quantitative measurements were taken due to the fact that pellets were cut in half prior to collection to allow for simultaneous RNA extraction. Type X collagen staining intensity and localisation seemed to be unchanged between pellets from control and MCDS-patient hiPSCs treated with CBZ (Figure 3.5). Columnar structures typical for proliferative chondrocytes were observed in both control and MCDS-patient derived hiPSC pellets treated with CBZ and were stained positively for type X collagen, similar to what was observed without CBZ treatment previously (Figure 3.4). In MCDS, CBZ has been shown to enhance degradation of intracellular mutant type X collagen. A side by side comparison of images obtained from control hiPSC pellets with and without CBZ treatment did not show any pronounced differences in staining intensity (Figure 3.6 A and B). Similarly, MCDS-patient derived hiPSC pellets did not display prominent differences in staining intensity. Whilst protein extraction and further analysis by immunoblot may be necessary to quantify protein levels, these results demonstrate the successful differentiation of both control and MCDS-patient derived hiPSCs into cartilage-like pellets and the successful induction of hypertrophy as demonstrated by the presence of type X collagen.

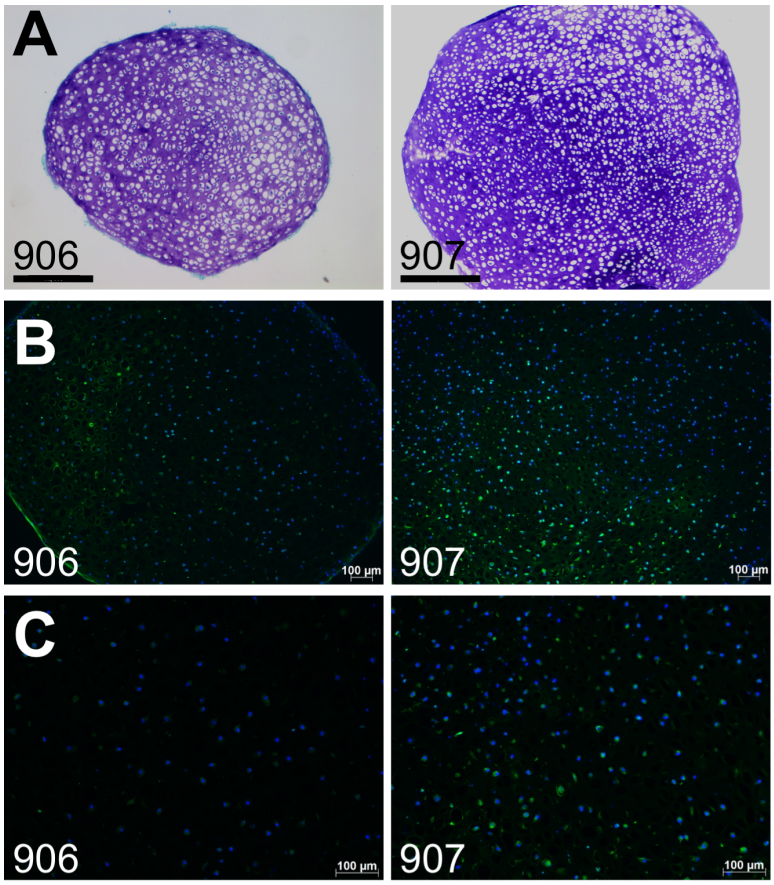

Figure 3.3 – Immunohistochemical detection of type X collagen in cartilage-like pellets without induction of hypertrophy. (A) Toluidine blue staining (Images from Figure 3.2) of two MCDS-patient derived hiPSC cartilage-like pellets confirmed the successful differentiation into cartilage-like tissue, included for reference. Scale bar: 500 µM. (B) Immunohistochemical staining of the same samples for type X collagen (green). Scale bar: 100 µM. (C) Higher magnification of (B). Scale bar: 100 µM. Nuclei were stained with DAPI (blue).

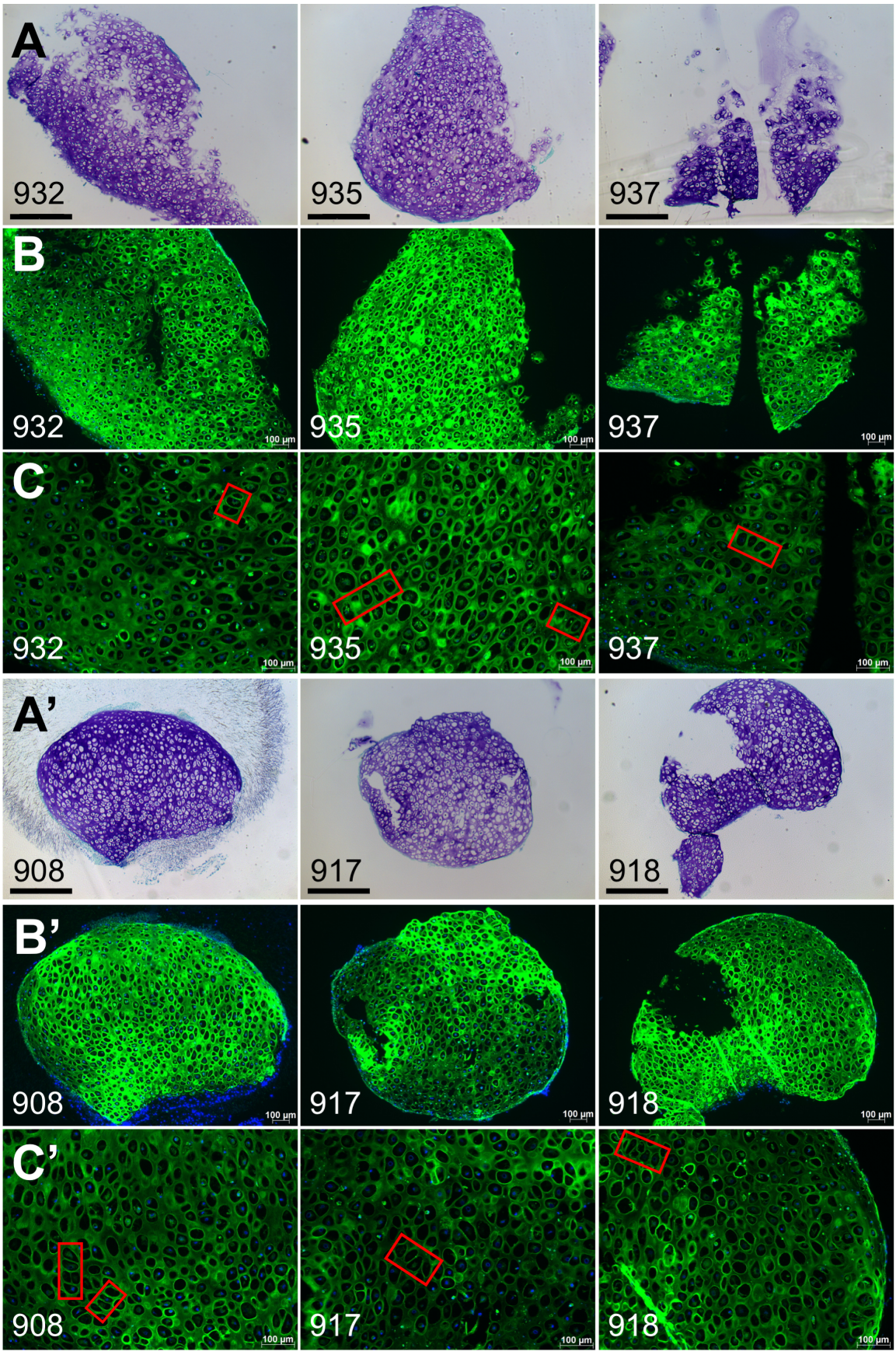

Figure 3.4 – Histological analysis of control and MCDS-patient cartilage-like hiPSC pellets. (A) three control cartilage-like hiPSC pellets and (A') MCDS-patient cartilage-like hiPSC pellets were stained with Toluidine blue (Images from Figure 3.2) for proteoglycans to confirm differentiation. Scale bar: 500 µM. (B) Immunofluorescence staining for type X collagen (green) in cartilage-like

pellets derived from control hiPSC. (C) Higher magnification of (B). (B') Immunofluorescence staining for type X collagen (green) in cartilage-like pellets derived from MCDS-patient hiPSC. (C') Higher magnification of (B'). Scale bar: 100 µM. Red boxes indicate columns of proliferative chondrocytes. Nuclei were stained with DAPI (blue). Numbers refer to individual pellets, derived from the same control or MCDS-patient hiPS cell line.

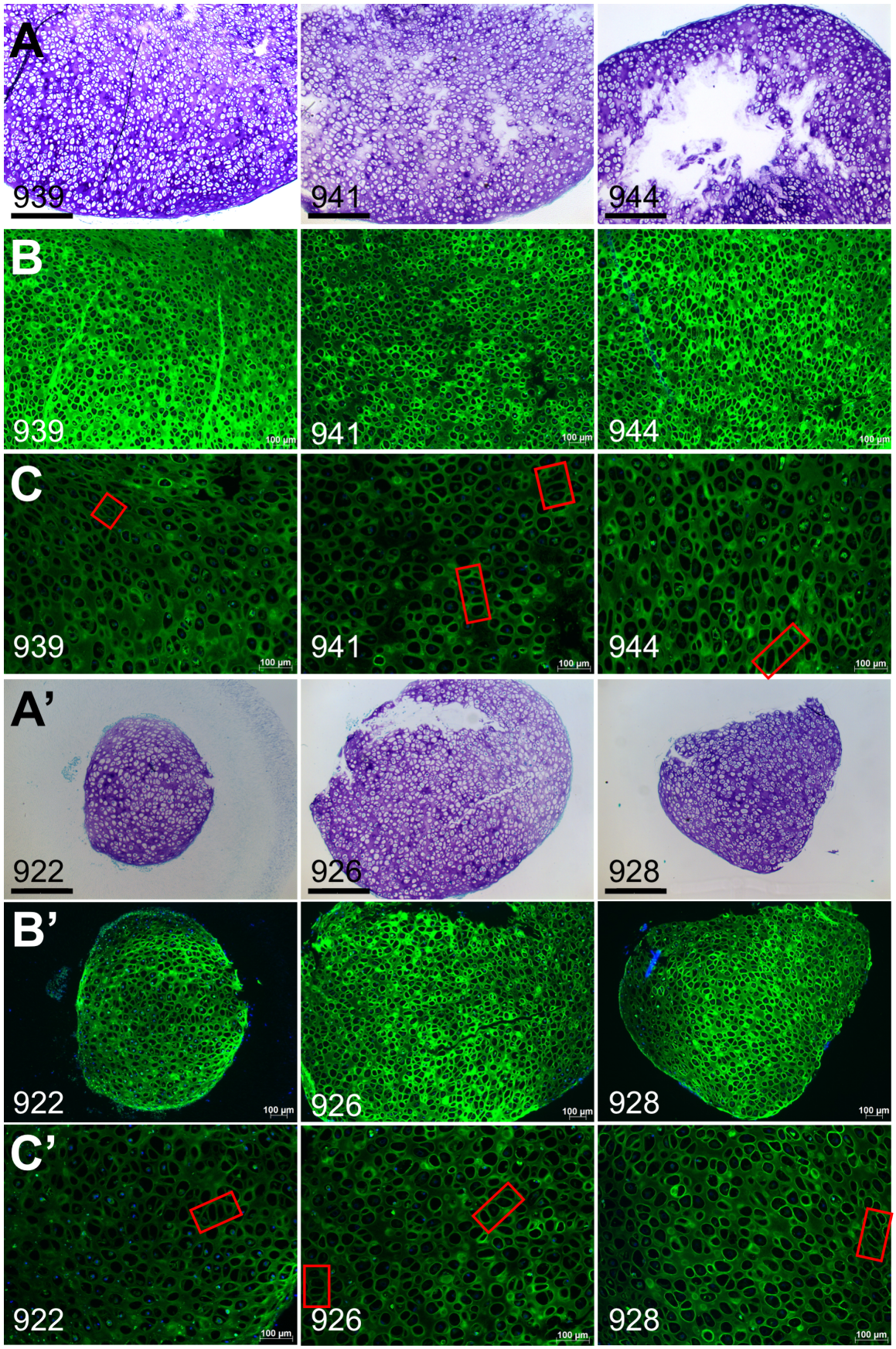

Figure 3.5 – Histological analysis of control and MCDS-patient cartilage-like hiPSC pellets after treatment with CBZ. (A) three control cartilage-like hiPSC pellets and (A') MCDS-patient cartilage-like hiPSC pellets treated with CBZ were stained with Toluidine blue (Images from Figure 3.2) for proteoglycans to confirm differentiation. Scale bar: 500 µM. (B) Immunofluorescence staining for

type X collagen (green) in cartilage-like pellets derived from control hiPSC treated with CBZ. (B') Immunofluorescence staining for type X collagen (green) in cartilage-like pellets derived from MCDS-patient hiPSCs treated with CBZ. Red boxes indicate columns of proliferative chondrocytes. Nuclei were stained with DAPI (blue). Scale bar = 100 µM. Numbers refer to individual pellets, derived from the same control or MCDS-patient hiPS cell line.

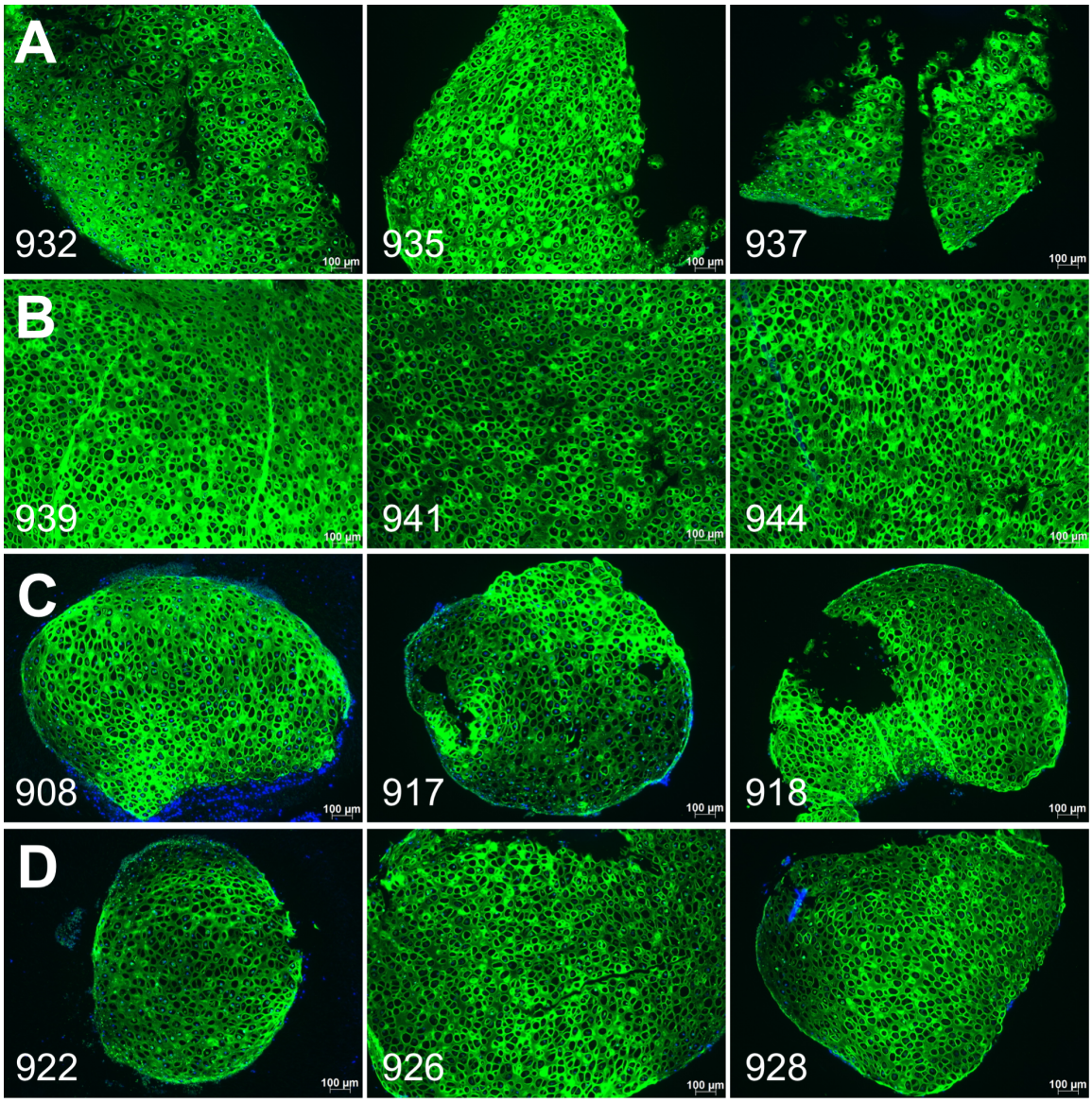

Figure 3.6 – Side by side comparison of immunohistochemical staining of type X collagen (green) in (A) control cartilage-like hiPSC pellets without CBZ; (B) control cartilage-like hiPSC pellets with CBZ treatment; (C) MCDS-patient cartilage-like hiPSC pellets without CBZ; (D) MCDS-patient cartilage-like hiPSC pellets with CBZ treatment. Images from Figure 3.3 and Figure 3.4 were rearranged for side by side comparison. Nuclei were stained with DAPI (blue). Scale bar: 100 µM.

3.4 Evaluation of UPR activation in hiPSC derived cartilage-like pellets

The UPR recognises ER stress via three main sensors: IRE1, PERK and ATF6. All sensors interact with the chaperone BiP (encoded by its gene *HSPA5)* unless the load of unfolded protein within the ER lumen exceeds a certain threshold, leading to the dissociation of BiP from the sensors and the activation of the sensors. The activation of IRE1 can be specifically measured by quantification of *XBP1* splicing. *XBP1* is unconventionally spliced by activated IRE1 and subsequently increases expression of ER chaperones and ERAD components to protect the cell from ER stress induced apoptosis. The activation of the PERK branch can be evaluated by measuring protein levels of ATF4 and its downstream target *DDIT3* (CHOP), however, *DDIT3* is - to a lesser extent - also regulated by XBP1 and ATF6. CHOP regulates various genes involved in apoptosis and a reduction of CHOP levels can protect cells from ER stress induced apoptosis.

In MCDS, elevated expression levels of *HSPA5* and *DDIT3* have been found as well as an increase in *XBP1* splicing. Elevated protein levels of ATF4 and BiP have also been reported alongside increased activation of ATF6. Upon activation of PERK, translation generally decreases, whilst some specific transcripts escape this inhibition of translation. For this reason, *ATF4* transcript levels are not usually used to determine the activation of the PERK branch of the UPR. Due to the limited sample size of this experiment, only RNA, but not protein was extracted from the hiPSC derived cartilage-like pellets. The expression of *HSPA5, DDIT3* and *COL10A1* was then examined by qRT-PCR (Figure 3.7) to examine the activation of the UPR in MCDS-patient derived hiPSC cartilage-like pellets with and without treatment with CBZ. *For COL10A1* (Figure 3.7 A), no pronounced differences were observed. Unfortunately, the qRT-PCR revealed huge variations between expression levels of individual replicates. This was especially the case for the MCDS-patient hiPSC derived cartilage-like pellets. Even if there was a difference in *COL10A1* expression between the groups, it would likely be unrecognisable due to the huge variation. Similarly, the variation within the groups for *HSPA5* (Figure 3.7 B) would likely be masking any effect of CBZ. For *DDIT3* (Figure 3.7 C) the variation between replicates appeared very high as well, not allowing any conclusions to be made at this point. Previous studies have found *DDIT3* expression to be decreased after CBZ treatment (Mullan et al., 2017). As another indication of ER stress, *XBP1* splicing was analysed using PCR and densitometry (Figure 3.8). Similar to the results of qRT-PCR, a high

variation in *XBP1* splicing between samples within the same group was observed (Figure 3.8). Due to the high
variation between replicates no conclusions could be drawn at this point.

Taken together, *COL10A1* expression has been confirmed by qRT-PCR. However, the activation of the UPR in MCDS-patient hiPSC derived cartilage-like pellets could not be demonstrated sufficiently by examination of *HSPA5* and *DDIT3* expression and assessment of *XBP1* splicing. The observed variation between replicates of same group did not allow any conclusions to be made. Furthermore, the effect of CBZ treatment on hiPSC derived cartilage-like pellets could not be examined adequately due to the large variation within groups.

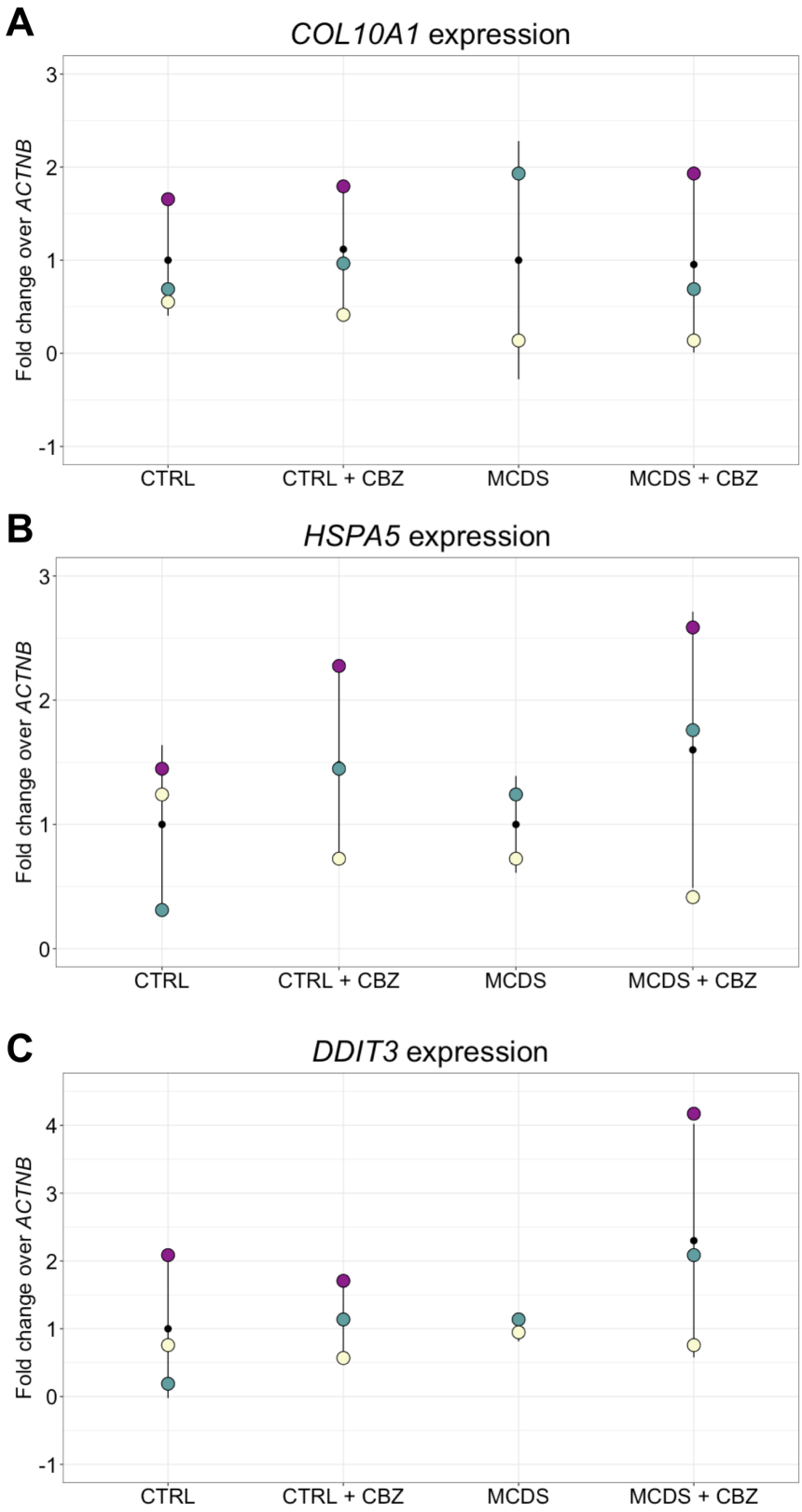

Figure 3.7 - Gene expression analysis of cartilage-like pellets derived from control or MCDS-patient hiPSCs with or without CBZ treatment by qRT-PCR. Changes in (A) *COL10A1* expression, (B) *HSPA5* or (C) *DDIT3* expression were compared between untreated pellets and pellets treated with CBZ. *ACTNB* was used as housekeeping gene. Colours represent technical replicates (n = 3, except for MCDS n = 2), mean and standard deviation are shown in black.

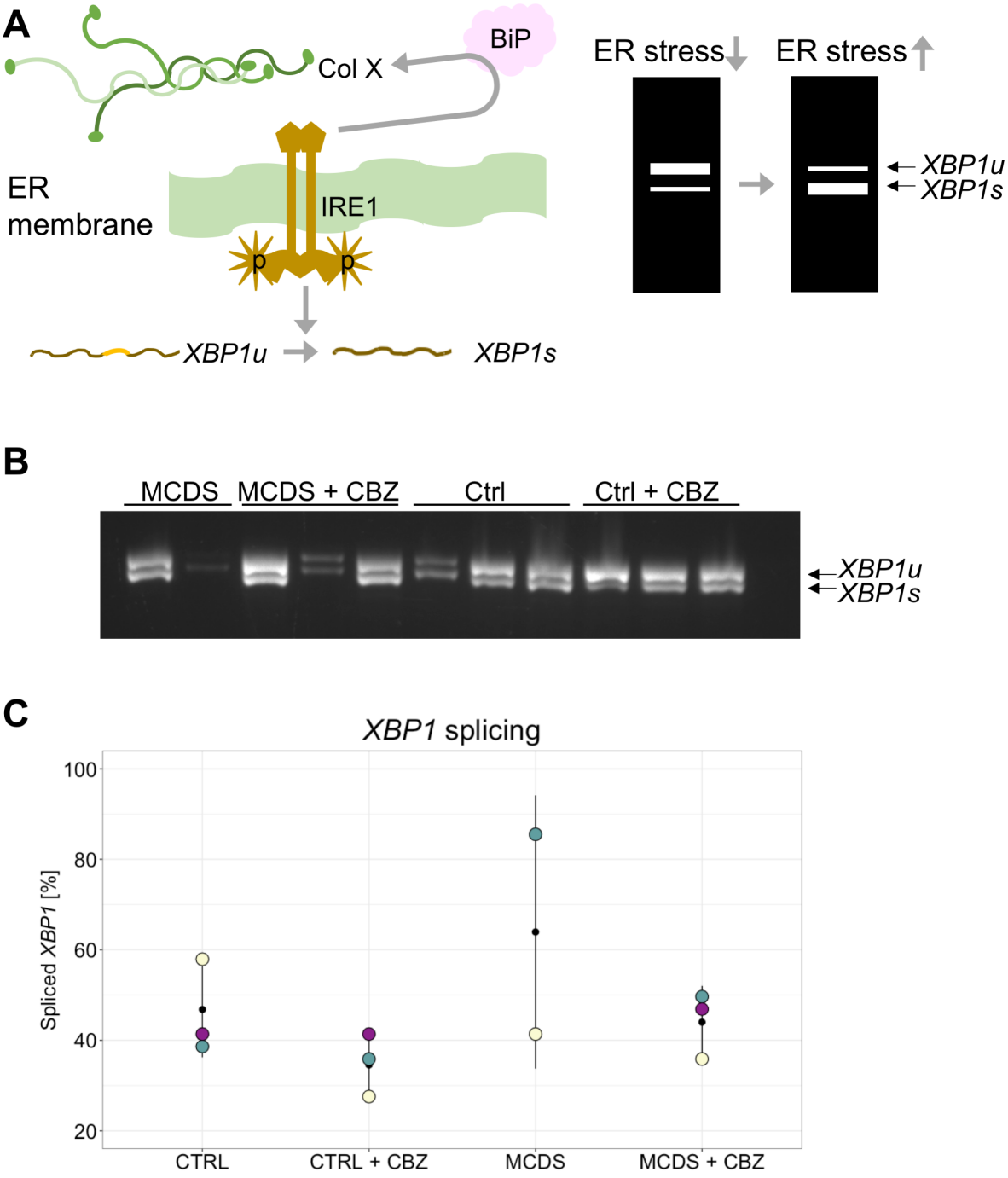

Figure 3.8 - *XBP1* splicing analysis in hiPSC derived cartilage-like pellets with or without CBZ treatment. (A) *XBP1* is processed by IRE1 when it is activated during ER stress, which can be detected as a shift in migration during agarose gel electrophoresis after PCR. (B) PCR was used to amplify both the unspliced and spliced transcript (*XBP1u* and *XBP1s* respectively). Products were visualised by agarose gelelectrophoresis (brightness was adjusted for better visualisation) and (C) the ratio between spliced and total *XBP1* determined using densitometry. Colours represent technical replicates (n = 3, except for MCDS n = 2), mean and standard deviation are shown in black.

3.5 hiPSC derived cartilage-like pellets as an *in vitro* model system to study DNA methylation in MCDS

As described previously, MCDS has so far mostly been studied by plasmid overexpression in cell lines (Mullan et al., 2017; Wilson et al., 2005) and in mouse models (Forouhan et al., 2018b; Ho et al., 2007; Rajpar et al., 2009). Whilst mouse models have contributed greatly to further the understanding of the disease mechanism, they can never replicate all aspects of a disease. For instance, MCDS is an autosomal dominant disease, however mice are usually bred to homozygosity before analysis. Furthermore, some mutations in *COL10A1* have been linked to nonsense-mediated mRNA decay (Bateman et al., 2003) which is not replicated in a mouse model (Forouhan et al., 2018b). Similarly, transient plasmid overexpression in cell lines has been successfully used to study the disease mechanism of MCDS and identify CBZ as potential drug treatment. As most cell lines are derived from cancer cells, they carry anomalies in their genome and display genome instability. Apart from that, ER stress has previously been shown to be involved in carcinogenesis and has emerged as a potential drug target in various cancers. Careful selection of cell lines used for the study of ER stress is therefore crucial. The use of hiPSCs could not only overcome the difficulties associated with the *in vitro* study of chondrocytes, but could also offer an alternative to the routine use of cancer cell lines.

It was therefore determined whether hiPSC derived cartilage-like pellets could present an alternative *in vitro* model system to study DNA methylation in MCDS. Unfortunately, the variation between cartilage-like pellets of the same differentiation was found to be very high at this stage of the study. The variation in gene expression was so high that activation of the UPR as described in previous publications could not be convincingly demonstrated. Subsequently, no effect of CBZ treatment on MCDS-patient hiPSC derived cartilage-like pellets could be established. It is therefore likely that DNA methylation analysis would not produce meaningful results due to large variation between technical replicates.

3.6 Discussion

In this chapter, the suitability of hiPSC derived cartilage-like pellets as an *in vitro* model system of MCDS was examined. It was also evaluated whether they could be used to study DNA methylation changes in ER stress associated diseases, such as MCDS.

As type X collagen is exclusively expressed by hypertrophic chondrocytes, *in vitro* studies of mutations in *COL10A1* have been extremely challenging. Previous studies investigating protein retention have therefore employed plasmid overexpression in cell lines for *in vitro* approaches (Mullan et al., 2017; Wilson et al., 2005). This chapter describes the successful differentiation of both control and MCDS-patient derived hiPSCs into cartilage-like pellets. Surprisingly, even the characteristic columnar structures of proliferative chondrocytes were observed within the pellets demonstrating that chondrocytes derived from hiPS cell lines undergo maturation in cartilage-like pellets at least to some extent, even without chemical induction of hypertrophic differentiation. The formation of cartilage-like pellets and columns of proliferative chondrocytes observed in this study were unaffected by induction of hypertrophy and treatment with CBZ. As chondrocytes undergo hypertrophy, they change their gene expression profile as well as their morphology. The cell volume increases, leading to the appearance of large, white cells within the Toluidine blue stained extracellular matrix. Remarkably, cells that matched the morphology of hypertrophic chondrocytes were observed in most pellets, even without induction of hypertrophy. In contrast to this, detection of type X collagen by immunofluorescence staining was only possible after induction of hypertrophy.

As many iPSC studies have aimed for a more articular cartilage-like phenotype for the study of osteoarthritis (Diekman et al., 2015, 2012; M.-J. Kim et al., 2011; Willard et al., 2014), the extent to which hiPSC derived cartilage-like pellets display growth plate characteristics is only poorly characterised. A recent study however observed some signs of chondrocyte maturation, such as small amount of type X collagen, in cartilage-like pellets and the authors speculated that those pellets may eventually undergo endochondral ossification (Dicks et al., 2020). This is in accordance with the observation that some cells appear hypertrophic, even without induction of hypertrophy. Apart from cell morphology, hypertrophic chondrocytes are characterised by expression of type X collagen. Immunohistochemical staining of type X collagen protein established that despite the morphological appearance of

some cells within the pellets, type X collagen protein was only present after induction of hypertrophy. Finding that type X collagen is not expressed without induction of hypertrophy contradicts some previous studies that have observed expression of *COL10A1/Col10a1* (Dicks et al., 2020; Diekman et al., 2015, 2012); however, others have reported a stable articular cartilage-like phenotype of hiPSCs with low expression of *COL10A1* (Diederichs et al., 2019). There are multiple explanations for those differences. Firstly, some of these studies have been performed using murine iPSCs which may differ in their maturation properties. Furthermore, those studies employed cell sorting to enrich for cells expressing either type II collagen or $CD146^+$, $CD166^+$, and PDGFRβ prior to setup of pellet cultures. As these cells are considered to already be chondroprogenitor-like cells, they may not necessarily require further induction of hypertrophy to express type X collagen in contrast to the unsorted hiPSCs used to perform the chondrogenic differentiation and subsequent hypertrophic differentiation in this study.

Remarkably, columns of proliferative chondrocytes were still observed after induction of hypertrophy and displayed an extracellular matrix containing type X collagen protein. This was an unexpected finding and draws into question whether the induction of hypertrophy was performed at an optimal timepoint during differentiation. In a recent study of hiPSCs with mutations in *COL10A1* and isogenic controls (Pretemer et al., 2021), staining for type X collagen appeared to also extend to some parts of columnar structures, however, cells arranged in columns appeared larger and less flattened. Within the growth plate, type X collagen expression is restricted to hypertrophic chondrocytes and not normally found around the columns of proliferative chondrocytes. It would be interesting to examine the distribution of other collagens within the cartilage extracellular matrix, such as type II, IX and XI collagen which are found in the proliferative zone of the growth plate. A previous study found that within the extracellular matrix of cartilage-like pellets differentiated from $CD146^+$, $CD166^+$, and $PDGFR\beta^+$ triple-positive subset of hiPSCs, type X collagen presence was closely associated with the pericellular localisation of type VI collagen (Dicks et al., 2020). The authors suggested this may indicate maturation of their cartilage-like pellets and speculated that they could undergo further hypertrophic differentiation *in vitro*. Thus, it would be interesting to investigate the localisation of type VI collagen after induction of hypertrophy in control and MCDS-patient hiPSC derived cartilage-like pellets.

Within the murine growth plate, differentiation of chondrocytes is controlled by several factors including the PTHrP/IHH axis (Guo et al., 2006; Nishimori et al., 2019) and the expression of RUNX2 (which controls both *COL10A1* (Zheng et al., 2003) and *VEGF* (Zelzer et al., 2001) expression by hypertrophic chondrocytes). To gain a more detailed understanding of the *in vitro* differentiation of hiPSCs into chondrocyte-like cells, the distribution of these factors within the pellets could be examined. Findings of a previous study suggest, however, that increased *RUNX2* expression alone is not necessarily associated with hypertrophic differentiation (Adkar et al., 2019) in iPSC derived cartilage-like pellets and *RUNX2* must therefore be analysed alongside another marker of hypertrophy, such as *COL10A1* or *MMP13*.

No pronounced differences were found in location or staining intensity of type X collagen between control and MCDS-patient cartilage-like pellets. Whilst somewhat surprising, this could be explained by the fact that the MCDS-patient derived hiPSCs are heterozygous carriers of the disease-causing mutation and could therefore still express one functional copy of the gene. Allele-specific expression could be evaluated using qRT-PCR to assess the contribution of normal and mutated allele to total amount of *COL10A1* transcript. In addition, retained protein may require more refined imaging methods, such as co-stainings with ER markers to identify retained protein by microscopy. This could be complemented by a pulse-chase style experiment to analyse protein secretion in more detail. However, a detailed investigation of type X collagen secretion will require the extraction of protein from the cartilage-like pellets in future experiments.

QRT-PCR analysis performed to investigate the activation of the UPR in cartilage-like pellets derived from control or MCDS-patient hiPSCs revealed a high extent of variation between replicates. This was not only seen for the activation of the UPR, but also for *COL10A1* expression itself. However, immunohistochemistry had failed to detect larger variations in type X collagen protein level between replicates. This could indicate that after induction of hypertrophy and upregulation of *COL10A1*, some cartilage-like pellets may start to downregulate *COL10A1*. In the mouse model of MCDS, it has been reported previously that chondrocyte differentiation is disrupted and instead of expressing *COL10A1*, some hypertrophic chondrocytes revert differentiation and start to re-express *COL2A1,* the main fibrillar collagen of cartilage

(Rajpar et al., 2009). It could also be that control cells express large quantities of type X collagen protein after induction of hypertrophy, inducing slight ER stress and causing a subsequent decrease in protein production. As these events may occur during later stages of hypertrophic induction, a considerable amount of type X collagen may be already deposited in the extracellular matrix. Another possibility would be that the induction of hypertrophy leads to variable expression of type X collagen within every cartilage-like pellet, depending on the exact properties and conditions for this exact cartilage-like pellet. As the induction of hypertrophy was performed for three weeks prior to immunohistochemical examination of type X collagen deposition, comparable levels of type X collagen may have accumulated within the extracellular matrix of all cartilage-like pellets regardless of variable expression.

The observed variation and the discrepancies to previous studies could have several causes. Firstly, as the control and MCDS-patient hiPSCs are not isogenic cell lines, biological differences in their ability to differentiate into chondrocyte-like cells and undergo hypertrophy may be inherently different. In this work, formation of cartilage-like nodules was therefore assessed histologically prior to any gene expression analysis. Whilst there were no prominent morphological differences observed, this would not discover more subtle aspects of chondrocyte characteristics, e.g. differences in the level of *COL2A1* expression which could potentially affect differentiation.

Furthermore, the differentiation of hiPSCs into hypertrophic cartilage-like pellets involves a multi-step protocol and about 80 days of culture (in total). It is possible that during these long culture periods, some pellets develop faster/slower than others and therefore, following steps (e.g. the induction of hypertrophy) exhibit varying degrees of efficiency. For instance, it is currently not known whether an induction of hypertrophy at earlier timepoints induces extracellular type X collagen deposition to the same extent. It is also not known whether the presence of columns indicative of proliferative chondrocytes is required for successful induction of hypertrophy. Finally, whether the timescale of differentiation is comparable between control and MCDS-patient derived hiPSCs is unknown. The induction of hypertrophy therefore may have to be further optimised in terms of timing, duration and concentration of the hypertrophy-inducing agent. Notably, previous research that was not focused

primarily on type X collagen reported variations in *COL10A1* expression in cartilage-like pellets depending on the passage number prior to pellet formation (Diekman et al., 2015, 2012). However, these pellets were derived from mouse iPS cells and sorted for apparent chondroprogenitor cells prior to passaging and pellet formation. This finding may therefore not apply to the hiPSCs used in this study, as they were not sorted for type II collagen expression prior to chondrogenic differentiation in pellet culture. Adopting a similar approach as Dicks et al., 2020 (Dicks et al., 2020) who sorted hiPSCs for a specific set of cell surface markers may allow for a more uniform chondrogenic differentiation and subsequent induction of hypertrophy.

Interestingly, it has been demonstrated by previous research that the ER stress response of chondrocytes is dependent on their differentiation state (Piróg et al., 2019). Inducing hypertrophy to varying degrees in the hiPSC derived cartilage-like pellets may therefore cause an activation of a subset of the UPR in some pellets. Another reason for the high variation observed in the qRT-PCR results could be physiologically occurring ER stress during differentiation. It is well accepted that the UPR is activated under physiological conditions to preserve the ER homeostasis, especially in professionally secreting cells such as chondrocytes. Therefore, the UPR may be activated in the cartilage-like pellets during *in vitro* differentiation, potentially to varying degrees, leading to high variation between pellets. Additionally, a potentially limited activation of the UPR by type X collagen in MCDS-patient hiPSC derived cartilage-like pellets may be masked. The *in vitro* situation may also lead to transient shortages of factors within the culture media, e.g. ascorbate. Ascorbate is a vitamin C derivative, necessary for proper post-translational modification of many collagens. In the absence of ascorbate, collagens cannot be hydroxylated properly which leads to impaired secretion and subsequent ER stress. While ascorbate was added to the culture media regularly, the cells still may experience temporary suboptimal ascorbate concentrations due to a limited biological half-life.

Lastly, as MCDS is an autosomal dominant disease the hiPSC line is also a heterozygous carrier of this mutation. This presents a much more disease-relevant setting compared to a plasmid overexpression, however, it may also introduce difficulties in dissecting more delicate differences between control and disease model. Future work should firstly focus on the optimisation of the differentiation protocol, including the induction of hypertrophy. Evaluation of the allele-specific

expression could indicate to what extent the mutant allele is actually expressed in MCDS-patient hiPSC derived cartilage-like pellets. It would also be interesting to perform co-stainings of type X collagen and markers for the ER and Golgi compartment. Retention of secreted proteins due to mutations mostly retains proteins within the ER, whereas correctly folded proteins are secreted into the extracellular space, usually via the Golgi compartment. Furthermore, co-stainings of type X collagen and UPR markers, such as CHOP, could be used to identify if high levels of CHOP (*DDIT3)* correlate with higher levels of intracellular type X collagen in cartilage-like pellets derived from MCDS-patient hiPSCs. A pulse-chase style experiment could examine alterations in protein secretion in cartilage-like pellets derived from control and MCDS patient hiPSCs. The activation of all three branches of the UPR, as previously reported for other MCDS models (Ho et al., 2007; Mullan et al., 2017; Rajpar et al., 2009), could be confirmed by examination of ATF6 cleavage and ATF4 protein levels, in addition to evaluation of *DDIT3* and *HSPA5* expression, and *XBP1* splicing as performed in this study. Examination of *COL2A1* expression, potentially by *in situ* hybridisation, alongside immunohistochemistry for type II collagen could reveal whether cells in cartilage-like pellets from MCDS patient hiPSCs may upregulate *COL2A1* after induction of hypertrophy has induced ER stress by expression of type X collagen. Analysis of the distribution of factors involved in chondrocyte differentiation, such as SOX9, PTHrP, IHH and RUNX2 could also provide insight into the process of *in vitro* differentiation of hiPSCs into chondrocyte-like cells. Unfortunately, due to time constraints I was not able to perform all these experiments during my three-month secondment in Melbourne.

The overall aim of this chapter was to investigate whether hiPSC derived cartilage-like pellets could serve as a physiologically relevant *in vitro* model system of MCDS and of ER stress induced changes in DNA methylation. Taken together, the results obtained to date demonstrate that both control and MCDS-patient derived hiPSCs successfully differentiate into chondrocyte-like cells and express type X collagen when hypertrophy is induced. Accordingly, the most basic requirements to study MCDS are met. The results also indicate that further optimisation of the protocol and more detailed analysis of the cartilage-like pellets are required to ensure uniform differentiation of cells throughout the cartilage-like pellet, robust induction of hypertrophy within the cartilage-like pellets, and that the UPR is effectively activated in response to ER stress caused by the mutation in *COL10A1,* but not as a response

to the differentiation itself. Reducing the variation between replicates is also necessary to reliably detect any meaningful changes in gene expression or DNA methylation with or without treatment of CBZ. Whilst the potentially lengthy optimisation process may not be feasible for this project at this time, the use of hiPSC derived cartilage-like pellets offers exciting new perspectives for the future study of ER stress associated chondrodysplasias in a disease-relevant setting.

3.7 Summary

- Both control and MCDS patient derived hiPSC are able to differentiate into chondrocyte-like cells and form cartilage-like pellets.

- Both control and MCDS patient hiPSC derived cartilage-like pellets express and deposit type X collagen within the extracellular matrix when hypertrophy is induced.

- The high variation between replicates of the same experimental group did not allow assessment of the activation of the UPR in cartilage-like pellets.

- The protocol of differentiation and hypertrophy induction requires further optimisation before hiPSC derived cartilage-like pellets can be used for DNA methylation analysis.

Chapter 4. Using hiPSC as an *in vitro* model for ER stress related bone diseases

4.1 Introduction

Apart from various chondrodysplasias, skeletal dysplasias also comprise diseases that involve the bone. Mutations in *COL1A1* or *COL1A2*, the genes encoding the two α chains of type I collagen, lead to osteogenesis imperfecta (OI), more commonly known as brittle bone disease (Forlino and Marini, 2016). Previous studies have found that intracellular retention of mutant type I collagen induces ER stress, mainly via the PERK branch of the UPR, although the IRE1 branch appears to be activated by some mutations, particularly mutations of *COL1A2*, as well (Besio et al., 2018). Similarly, BiP (*HSPA5)* appears upregulated mostly in mutations located within the C-terminal pro-peptide, although elevated BiP levels were also observed in some mutations located in the triple-helical region of both α chains (Besio et al., 2018; Chessler and Byers, 1993).

The same study that detected activation of the PERK branch also observed increased autophagy and apoptosis in fibroblasts from OI patients. Interestingly, treatment with the chemical chaperone 4-PBA was found to normalise levels of p-PERK and reduce apoptosis *in vitro* (Besio et al., 2018). However, this study employed OI patient fibroblasts and while fibroblasts naturally express type I collagen, some features of OI such as the naturally occurring mineralisation of the bone are not reflected in this model. Furthermore, the UPR is thought to play a role in the differentiation of several cell types, including osteoblasts (Saito et al., 2011; Tohmonda et al., 2011; Tsang et al., 2010). The response to mutant type I collagen may therefore differ between osteoblasts and other cell types. These limitations affect not only the study of disease pathology, but also potential *in vitro* drug screens.

The use of hiPSCs could potentially overcome some of the difficulties associated with the study of OI; however, before comparisons between patient and control cells are possible, a suitable protocol for osteogenic differentiation needs to be developed. Osteogenic differentiation of hiPSCs would not only allow the confirmation of ER stress in a disease relevant model system, but also potentially allow the study of ER stress associated changes in DNA methylation. In this chapter, the osteogenic differentiation of hiPSCs were therefore analysed to determine whether DNA methylation analysis of OI patient derived hiPSCs after osteogenic differentiation would be feasible.

4.1.1 Chapter aims

- Develop a suitable protocol for osteogenic differentiation of hiPSCs:
    - Treatment with retinoic acid and the retinoic acid receptor α agonist AM580
    - Comparison of different coating substrates
    - Comparison of different control cell lines

- Determine whether hiPSCs after osteogenic differentiation could be used as a model to study DNA methylation changes associated with ER stress in OI.

4.2 A timecourse of osteogenic differentiation of O27 hiPS cells with and without a retinoic acid receptor α agonist

A recently published protocol (Kawai et al., 2019) described the use of either retinoic acid or a retinoic acid receptor α agonist to induce rapid osteogenic differentiation of hiPSCs *in vitro*. The first step therefore was to replicate this study using the retinoic acid receptor α agonist AM580. O27 hiPSCs, generated by reprogramming and simultaneous gene correction of fibroblasts from an individual with OI (Howden et al., 2019), were seeded onto gelatin coated culture dishes and differentiated for up to 14 days. Mineralisation was evaluated by alizarin red staining (Figure 4.1, Table 4.1) and gene expression of two osteogenic marker genes (*COL1A1* and *BGLAP*) analysed by qRT-PCR (Figure 4.2). However, only very limited staining was observed, beginning with some areas of slightly darker colour at day 7 (Figure 4.1 A). Even after 14 days of differentiation in the presence of AM580, no intense staining was observed (Figure 4.1 A). Without AM580, at day 10 and 14 some dark red clusters appeared (Figure 4.1 A). Quantification of the mineralised area revealed that at day 2 and day 4 of differentiation, the proportion of mineralised area was very small in both groups (Table 4.1), but significantly increased in AM580 treated samples compared to control samples. At day 7 of the differentiation process, the alizarin red stained area of the well appeared to have slightly increased in the absence of AM580. No significant difference could be observed between groups due to very high variation in the AM580 treated samples. Nevertheless, at day 10 of differentiation, about 16 % of the total well area was stained by alizarin red - indicating mineralisation - in the absence of AM580. In the presence of AM580, the mineralised area was significantly increased, covering about 30 % of the area of the

well. Surprisingly, at day 14 of the differentiation, the mineralised area was slightly smaller in both groups, and day 14 was also the only timepoint were a larger proportion of the well appeared mineralised in the absence, rather than in the presence, of AM580.

For a more detailed evaluation of the differentiation process, expression of osteogenic marker genes was examined by qRT-PCR. Analysis of *COL1A1* expression (Figure 4.2 A) revealed it was slightly, but significantly upregulated by treatment with AM580 from day 1 to day 7 of differentiation (Figure 4.2 A, table 4.2). From day 10 of differentiation, a drastic increase in *COL1A1* expression was observed. Surprisingly, it was significantly stronger upregulated in the absence of AM580 (Figure 4.2 A). On day 14 of differentiation, the induction of *COL1A1* appeared to be similar between cells differentiated in the presence or absence of AM580 (Figure 4.2 A,).

While at day 10 the absence of AM580 seemed to increase *COL1A1* expression considerably, mineralisation was more enhanced in the presence of AM580. It is noteworthy that while gene expression is regulated by complex pathways, it measures the amount of transcript at the time of RNA extraction. However, mineralisation requires the formation of an organic substrate via protein production and secretion and the subsequent mineralisation of the organic substrate by secretion of calcium phosphate containing vesicles. Changes in the differentiation state may therefore be apparent on gene expression level before changes in the mineralised area are observed. Additionally, expression of *BGLAP*, a marker of mature osteoblasts, was examined (Figure 4.2 B, Table 4.2). Strikingly, no pronounced induction of *BGLAP* expression was observed either in the presence or absence of AM580. Rather, expression appeared to be consistently reduced in both groups compared to day 0 of differentiation (Figure 4.2 B). However, at day 1 and day 10 of differentiation, *BGLAP* was significantly higher expressed in the absence of AM580 compared to AM580 treated samples (Figure 4.2 B).

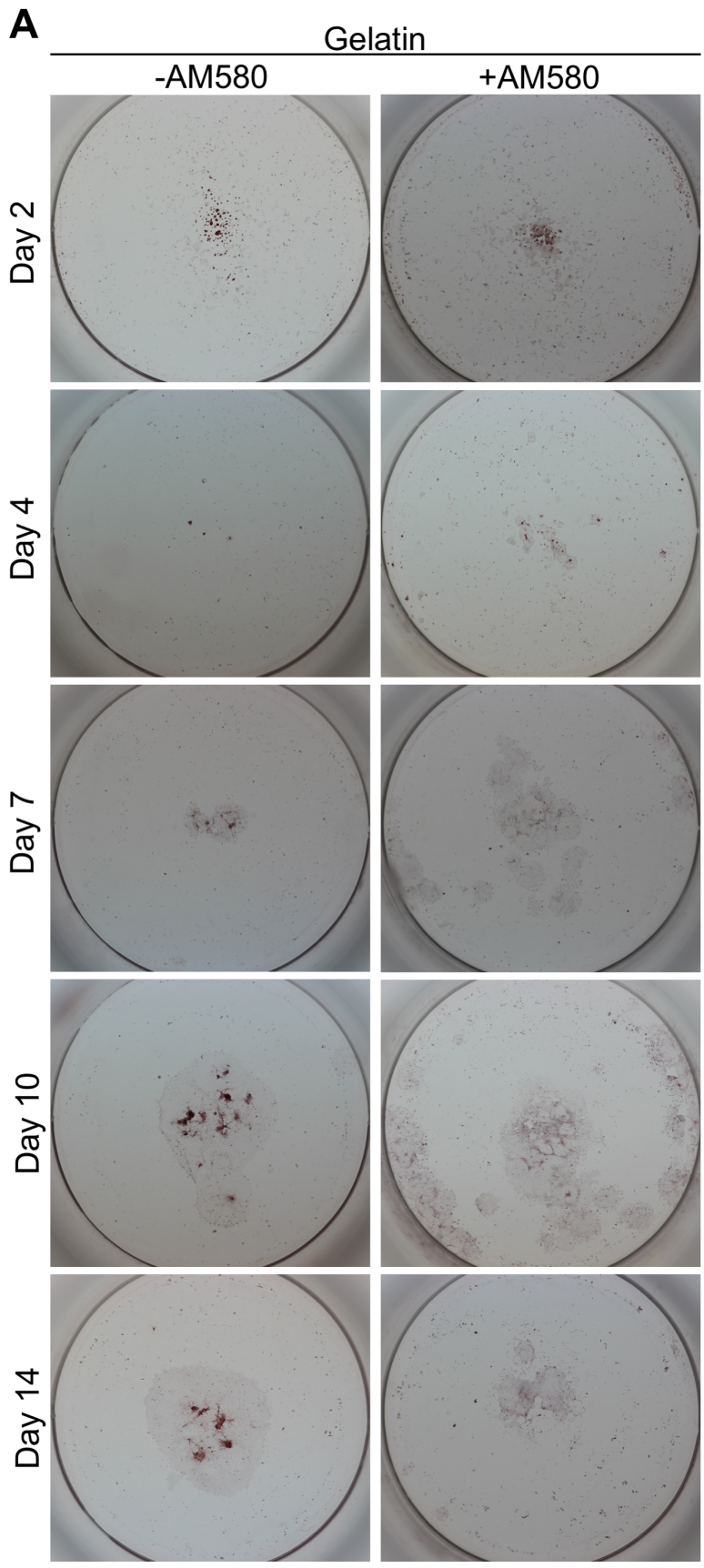
A
Gelatin
-AM580
+AM580
Day 2
Day 4
Day 7
Day 10
Day 14

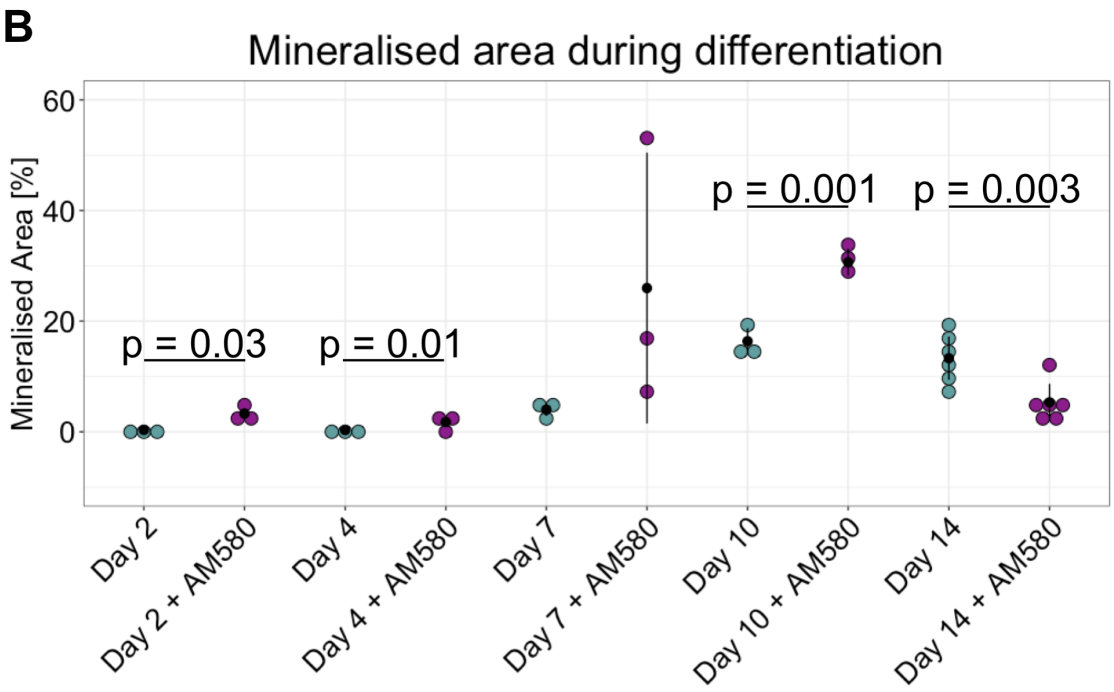

Figure 4.1 – Osteogenic differentiation of the hiPS cell line O27 over time. O27 cells were seeded onto gelatin coated dishes and differentiated for up to 14 days in the presence or absence of the retinoic acid receptor α agonist AM580. (A) Alizarin red staining was performed to assess the extent of mineralisation. Representative images are shown. (B) Quantification of the alizarin red stained portion of the well. The mineralised area is given as percentage of the entire well. Black dots represent mean, error bars represent SD, n = 3, except for D14 (n = 6).

Timepoint	-AM580	+AM580
Day 2	0.32 % ± 0.07 %	3.3 % ± 0.96 %,
Day 4	0.3 % ± 0.33 %	1.78 % ± 0.53 %
Day 7	4.01 % ± 1.13 %	25.98 % ± 24.48
Day 10	16.37 % ± 2.37 %	30.65 % ± 2.44 %
Day 14	13.29 % ± 3.9 %	5.33 % ± 3.35 %

Table 4.1 – Percentage of alizarin red stained proportion of the well during osteogenic differentiation.

Timepoint	-AM580	+AM580	Gene
Day 1	2.65 ± 0.56	4.0 ± 0.25,	*COL1A1*
Day 2	2.71 ± 0.38	7.39 ± 0.11	*COL1A1*
Day 4	1.2 ± 0.26	5.96 ± 0.87	*COL1A1*
Day 7	2.97 ± 0.08	5.81 ±1.09	*COL1A1*
Day 10	80.34 ± 16.25	26.16 ± 5.06	*COL1A1*
Day 14	114.53 ± 8.74	106.74 ± 28.24	*COL1A1*
Day 1	0.55 ± 0.13	0.17 ± 0.02	*BGLAP*
Day 2	0.35 ± 0.18	0.33 ± 0.1	*BGLAP*
Day 4	0.52 ± 0.2	0.42 ± 0.05	*BGLAP*
Day 7	0.23 ± 0.08	0.31 ± 0.17	*BGLAP*
Day 10	0.84 ± 0.26	0.24 ± 0.08	*BGLAP*
Day 14	0.38 ± 0.03	0.21 ± 0.14	*BGLAP*

Table 4.2 – Fold changes of *COL1A1* and *BGLAP* expression in cells differentiated over 14 days in the absence or presence of AM580.

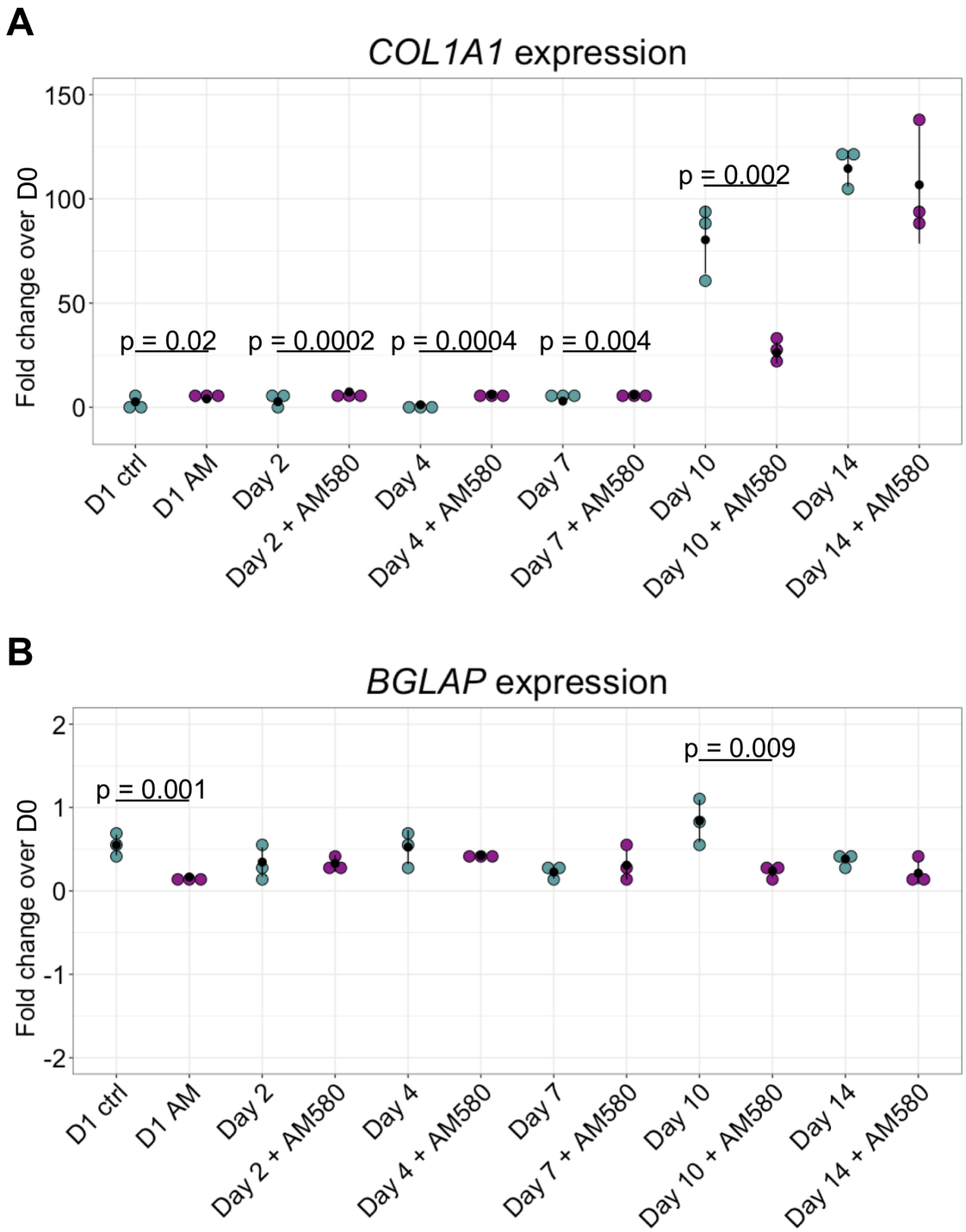

Figure 4.2 - Changes in expression of osteogenic marker genes during osteogenic differentiation. O27 cells were seeded onto gelatin and differentiated in the presence or absence of AM580 for up to 14 days. (A) *COL1A1* expression was measured by qPCR as one marker of osteogenic differentiation. (B) *BGLAP* expression was analysed by qPCR as a marker of late-stage osteoblast differentiation. The mean is shown in black, error bars represent SD, n = 3.

4.3 Influence of different coating substrates on osteogenic differentiation

The originally published protocol contained conflicting information about the substrate used for differentiation of feeder-free cell lines. Since the O27 cell line used for differentiation was cultured on Matrigel prior to differentiation, the differentiation was repeated using both gelatin and Matrigel as a substrate during differentiation. Analysis was performed using alizarin red staining. Because a slight increase in alizarin red stained area was first detected in both the presence and absence of AM580 on day 7, the differentiation on Matrigel and gelatin was performed for seven days. In addition to AM580, retinoic acid was also used to induce osteogenesis. Since it could not be excluded that the hiPSCs would lose their ‘stemness’ when seeded onto gelatin or Matrigel in differentiation medium directly, the differentiation was also performed after seeding the hiPSCs onto the substrate in stem cell medium (E8). The cells were then allowed to attach overnight, before the medium was changed to differentiation medium containing either DMSO, retinoic acid or AM580. Alizarin red staining revealed that both retinoic acid and AM580 had a comparable effect on cells seeded directly in differentiation medium (Figure 4.3). No staining at all could be observed for cells seeded onto gelatin in E8. In contrast to cells seeded directly in differentiation medium, only a very small number of cells attached when seeded in E8 which is likely the reason for the complete absence of staining. When seeded onto Matrigel, some wells exhibited large orange patches. This appeared to be specifically the case for cells treated with DMSO after seeding onto Matrigel in differentiation medium and cells treated with retinoic acid that had been seeded onto Matrigel in E8. However, some bright red staining could be observed in the cells that had been seeded onto Matrigel in E8 and then treated with either retinoic acid or AM580. Cells that had been seeded onto Matrigel in differentiation medium and treated either with DMSO or AM580 showed a fainter staining; however, in the case of the DMSO treated wells this was much more dispersed. Unfortunately, none of the conditions were able to replicate the results of the original study.

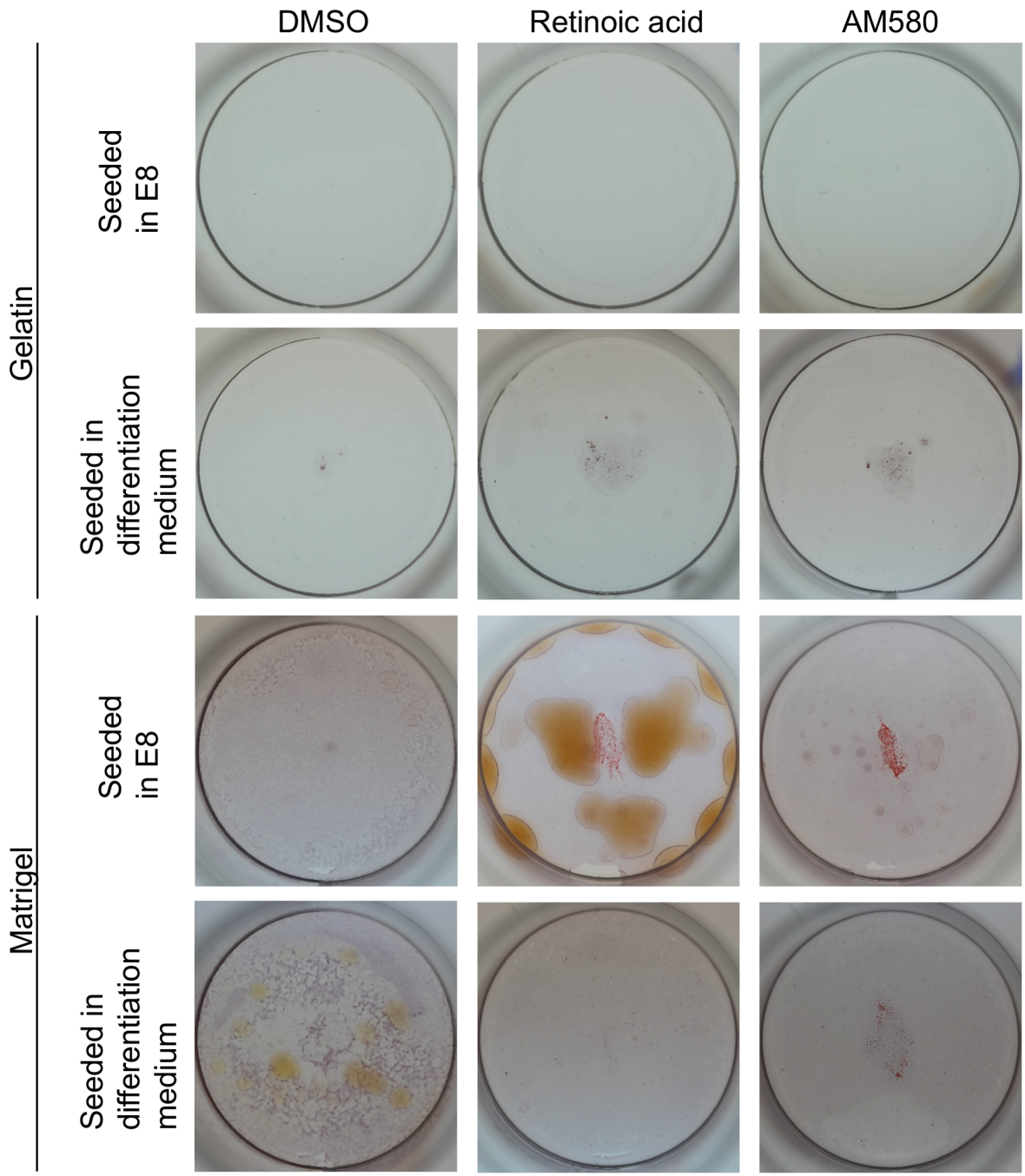

Figure 4.3 – Alizarin red staining of O27 hiPSCs after seven days of differentiation. O27 hiPSCs were seeded either in stem cell medium ('seeded in E8') or directly into differentiation medium, both on gelatin and Matrigel. Cells were treated with DMSO, retinoic acid or AM580 for seven days during differentiation before mineralisation was assessed using alizarin red staining, n = 2 (one of the replicates is shown).

4.4 Influence of hiPS cell line on osteogenic differentiation

O27 cells were cultured under feeder-free conditions, on Matrigel, before differentiation. Human iPSCs in general can be cultured either on protein substrates, such as Matrigel or on feeder-cells (primary murine embryonic fibroblasts, pMEFs). It was therefore possible that a feeder-dependent cell line would behave differently. For this reason, the differentiation was repeated using the feeder-dependent RM3.5c hiPSC line (Hosseini Far et al., 2019), derived from reprogrammed peripheral blood mononuclear cells. Differentiation was performed for seven days on gelatin, Matrigel and feeder cells in the presence of DMSO, retinoic acid or AM580. Again, cells were either seeded directly in differentiation medium or allowed to attach overnight in stem cell medium. Cells that were differentiated on gelatin or Matrigel were cultured on Matrigel for one passage prior to differentiation (as described in the original study). Interestingly, under all conditions RM3.5c cells stained more intensely than previously observed with O27 cells [(Figure 4.4 - 4.6) compared to Figure 4.1 A and 4.3)]. When cells were seeded onto feeder cells in differentiation medium (Figure 4.4), treatment with retinoic acid or AM580 seemed to have little effect on staining intensity. With either retinoic acid or AM580, there seemed to be some darker spots compared to the DMSO control and the staining pattern appeared to be more defined. When cells were seeded onto feeder cells in stem cell medium (Figure 4.4), this effect was even more pronounced. In some areas, the staining also appeared to be darker; however, some areas presented with a complete absence of alizarin red staining and there also seemed to be a strong variation between duplicates. Both retinoic acid and AM580 appeared to lead to a more defined and slightly more intense staining, suggesting some positive effect on mineralisation. The most striking difference compared to the previous experiments using O27 cells was the spread of the staining. Whilst the staining of O27 cells after differentiation had been confined to small areas of the well and a large portion of the well remained unstained, the differentiation of RM3.5c cells led to staining that covered a much larger proportion of the well, but with varying intensity. Examination of RM3.5c cells differentiated on Matrigel (Figure 4.5) demonstrated that this was also the case for this substrate. In general, the staining on Matrigel appeared to be pinker, but less well defined. In contrast to the differentiation performed on feeder cells (Figure 4.4), Matrigel as a substrate for differentiation lead to a larger area of the well that exhibited less intense staining (Figure 4.5). Moreover, the effects of retinoic acid and AM580, previously observed on feeder cells, failed to occur during differentiation on Matrigel. When cells

were seeded onto Matrigel in differentiation medium and only treated with DMSO, large white spots appeared after staining with alizarin red. This was not the case for cells treated with retinoic acid or AM580. When cells were seeded in differentiation medium, staining seemed to be most intense for the DMSO treated cells. On Matrigel, no positive effect of retinoic acid or AM580 on mineralisation could be observed.

Finally, the staining of RM3.5c cells differentiated on gelatin (Figure 4.6 A) reflected the staining pattern previously observed with O27 cells after differentiation (Figure 4.1 A and 4.3). Some areas of the culture dish were stained, whilst others remained completely unstained. However, the staining of differentiated RM3.5c cells was much more intense. Interestingly, only minor differences were observed between DMSO, retinoic acid and AM580 treated cells when seeded in stem cell medium. In general, the observed staining was very irregular and only small areas of staining were observed. Retinoic acid and AM580 treatment seemed to increase the number of areas that were stained with alizarin red. In contrast, when seeded directly in differentiation medium, alizarin red stained areas seemed more coherent. Still, a large area of the culture dish remained completely unstained especially after retinoic acid treatment during differentiation. Strikingly, cells treated with AM580 seemed to mineralise to a greater extent. The staining involved a larger area and appeared to be a coherent layer instead of multiple stained spots in close proximity. Quantification of the stained area (Figure 4.6 B) confirmed that only AM580, but not retinoic acid, appeared to affect mineralisation when cells were seeded in differentiation medium (86.69 % ± 12.35 % vs 31.66 % ± 9.4 % respectively compared to 43.04 % ± 16.84 % with DMSO). Furthermore, both retinoic acid and AM580 seemed to have a positive effect on mineralisation (Figure 4.6 B) when cells where seeded in hiPSC medium (25.93 % ± 0.25 % vs 29.65 % ± 1.16 % respectively compared to 8.05 % ± 5.99 % with DMSO); however, the stained area remained relatively small. Although RM3.5c hiPS cells in general appear to possess a higher potential for osteogenic differentiation than O27 cells, the efficacy of differentiation seems to strongly depend on the substrate used for the coating of culture dishes, the seeding procedure, treatments with retinoic acid or AM580 and the exact combination of these conditions.

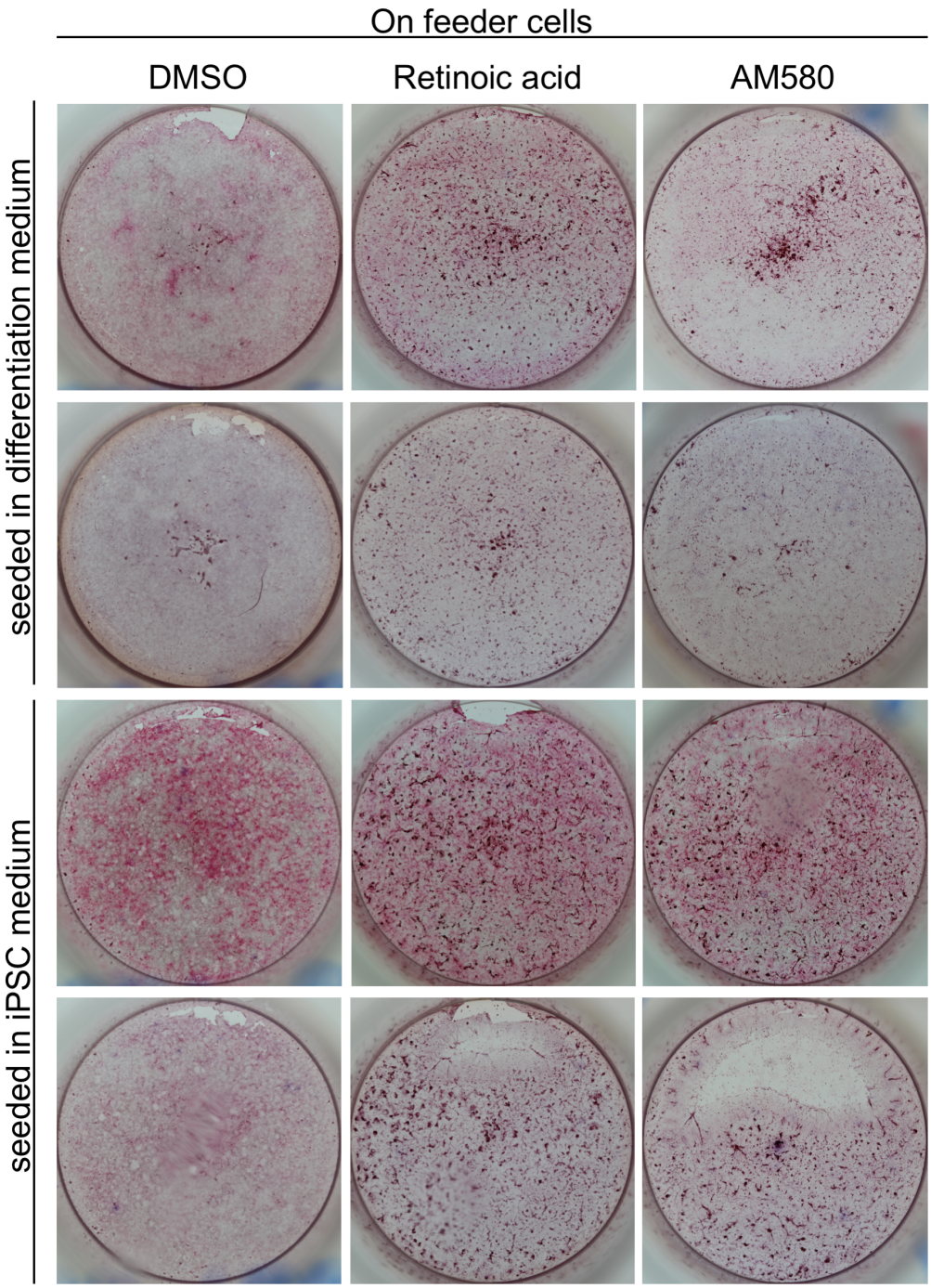

Figure 4.4 - Mineralisation of hiPSCs after seven days of osteogenic differentiation on feeder cells. RM3.5c cells were seeded on feeder cells, either directly in differentiation medium or allowed to attach in stem cell medium prior to inducing osteogenesis. Cells were treated with DMSO, retinoic acid or AM580 for seven days during differentiation before mineralisation was assessed using alizarin red staining. Both technical replicates are shown (n=2).

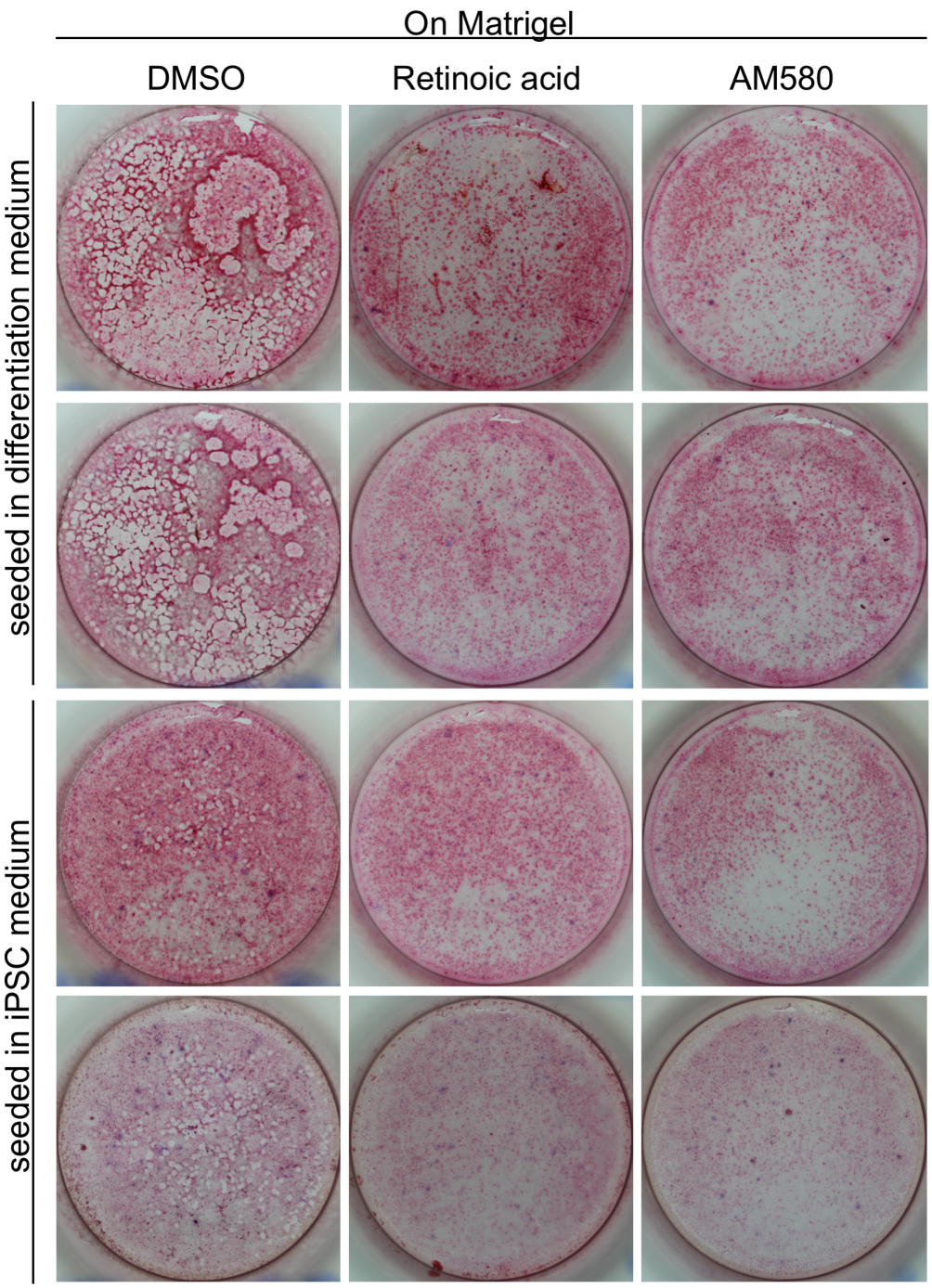

Figure 4.5 - Mineralisation of hiPSCs after seven days of osteogenic differentiation on Matrigel. RM3.5c cells were seeded on Matrigel, either directly in differentiation medium or allowed to attach in stem cell medium prior to inducing osteogenesis. Cells were treated with DMSO, retinoic acid or AM580 for seven days during differentiation before mineralisation was assessed using alizarin red staining. Both technical replicates are shown (n=2).

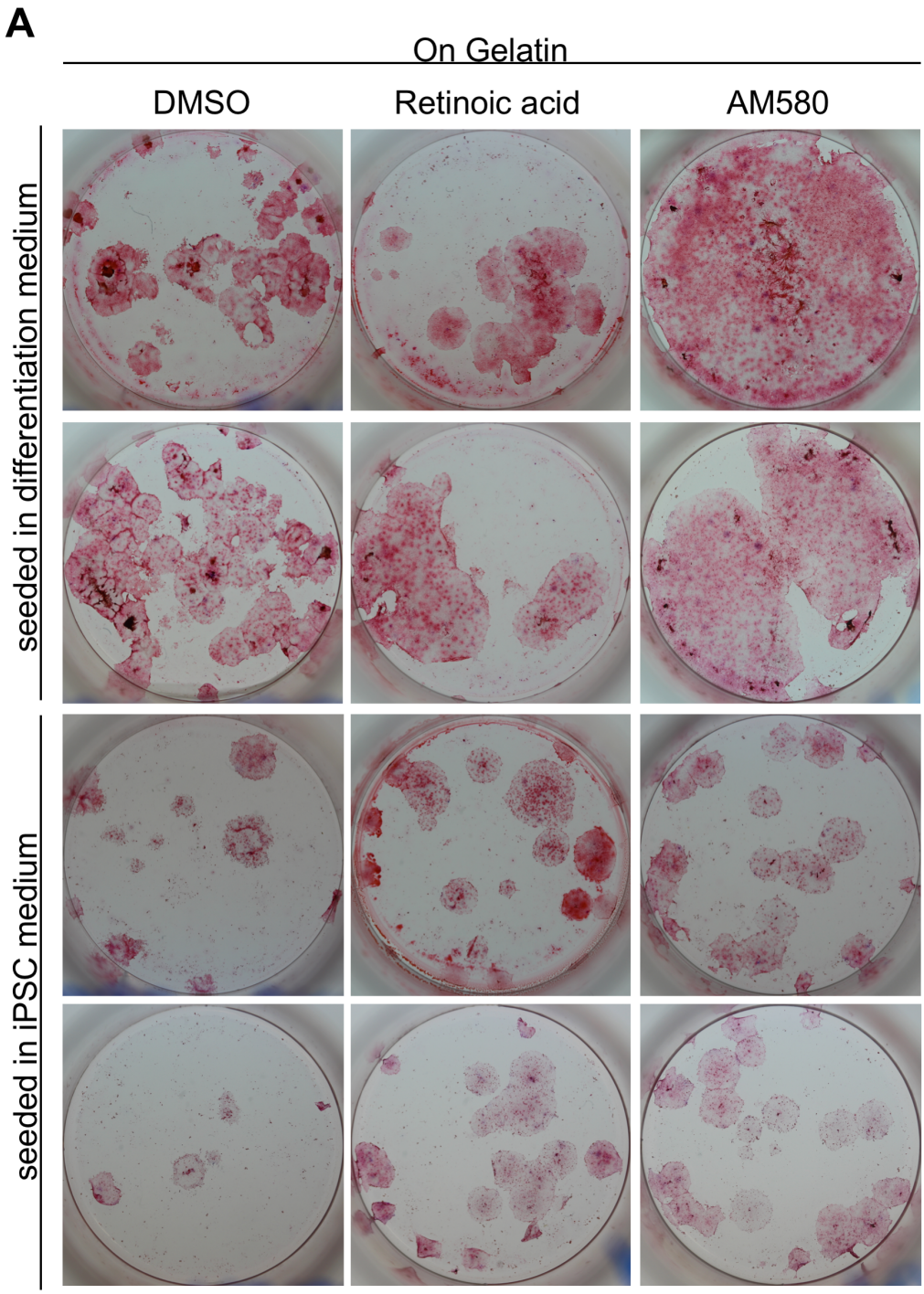
A
On Gelatin
DMSO
Retinoic acid
AM580
seeded in differentiation medium
seeded in iPSC medium

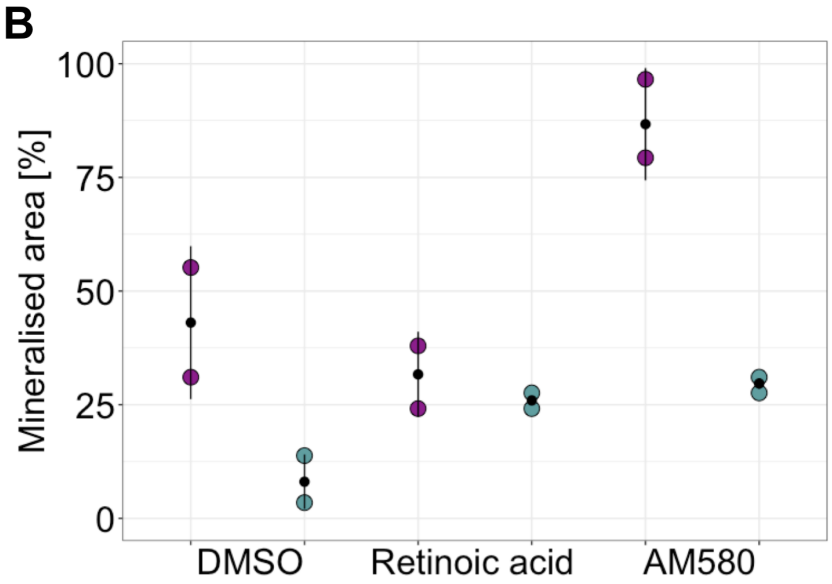

Figure 4.6 - Mineralisation of hiPSCs after seven days of osteogenic differentiation on gelatin. (A) Alizarin red staining after seven days of differentiation in the presence of DMSO, retinoic acid or AM580. RM3.5c cells were seeded on gelatin, either directly in differentiation medium or allowed to attach in stem cell medium prior to inducing osteogenesis. Both technical replicates are shown. (B) Quantification of the stained area of the well. The mineralised area is given as percentage of the total surface area of a well after seeding in differentiation medium (purple) or stem cell medium (blue), n = 2. Error bars represent SD, black dots indicate mean.

4.5 Suitability of hiPS cells to study ER stress associated changes in DNA methylation in OI

The aim of this chapter was to investigate whether the osteogenic differentiation of hiPS cells into osteoblast-like cells could facilitate the study of ER stress associated DNA methylation changes in OI. Before DNA methylation could be investigated, the model system had to be validated and the presence of ER stress in an OI-patient derived hiPS cell line had to be confirmed.

These data indicate that control hiPSCs are able to differentiate into osteoblast-like cells; however, this seems to be strongly cell line dependent. More detailed analysis of the differentiated RM3.5c samples is still required to conclusively demonstrate their osteoblast-like phenotype, e.g. by gene expression analysis. Since the process of differentiation potentially impacts DNA methylation, the course of differentiation has to be compared between patient derived cells and controls. Furthermore, the characterisation of ER stress and potential for UPR activation in the OI-patient derived hiPS cell line following differentiation is required prior to DNA methylation analysis.

4.6 Discussion

Previous studies have suggested an involvement of ER stress in the disease mechanism of OI; however, this seems to be mutation specific (Besio et al., 2018; Chessler and Byers, 1993; Mirigian et al., 2016). It remains difficult to study OI in a disease-relevant context since patient derived cells are difficult to obtain and studies are often limited to fibroblasts. The osteogenic differentiation of hiPSCs might overcome these problems as patient derived cells could be differentiated into the disease relevant cell types (Csobonyeiova et al., 2017). A recently published protocol (Kawai et al., 2019) appeared to offer a relatively straightforward approach using retinoic acid (or a retinoic acid receptor α agonist, AM580), introducing limited variation between differentiations. However, before patient derived hiPSCs could be differentiated and compared to control hiPSCs, the protocol first had to be validated.

Indeed, conflicting findings regarding the properties of retinoic acid and its role in osteogenic differentiation have been reported previously. Whilst some studies described a disruption of pro-osteogenic Wnt signalling which resulted in impaired osteoblast differentiation (Green et al., 2017; Roa et al., 2019), others reported enhanced osteogenesis and mineralisation during treatment with retinoic acid

(Skillington et al., 2002; Weng et al., 2019). It has also been suggested that retinoic acid promotes the differentiation of osteoblasts to pre-osteocytes, thus enhancing mineralisation but not osteoid deposition (Jeradi and Hammerschmidt, 2016).

Initially a time course of differentiation for the O27 feeder-free hiPSC line was performed following the protocol. Surprisingly, only minor mineralisation of up to 30 % of the total well area was observed by alizarin red staining, with a peak at day 10 of differentiation. Whilst the expression of *COL1A1* was prominently increased from day 10 of differentiation, no pronounced elevation of *BGLAP* expression levels was observed over time. Surprisingly, at day 1 and day 10 of differentiation, *BGLAP* levels were significantly decreased in the AM580 treated samples. Furthermore, *COL1A1* expression was significantly higher in the absence of AM580 on day 10, but not day 14 of differentiation. This could potentially indicate that the presence of AM580 caused a delay in osteogenic differentiation that was overcome by day 14, but not by day 10. However, from day 1 to day 7 of differentiation *COL1A1* expression was consistently elevated in AM580 treated samples. The small but consistent upregulation of *COL1A1* in the first week of differentiation could also indicate that by day 10, perhaps even day 7, the protein levels of type I collagen were sufficient to allow matrix mineralisation. Indeed, recent research suggests that not all collagen is secreted rapidly (within 2-2.5 hrs) via the classic ER/Golgi secretory pathway, but that some collagen and procollagen is stored in lysosomes with a half-life of around 70 hrs prior to secretion and collagen fibril formation (Pickard et al., 2022). It is therefore tempting to speculate that AM580 treated cells commit to an osteoblastic lineage earlier during differentiation, and increase expression of *COL1A1* less dramatically later on. Examination of the expression of stem cell marker genes, such as *NANOG* and *OCT4* could reveal whether this hypothesis is accurate. Additionally, other osteoblastic marker genes could be analysed to gain a more comprehensive understanding of the differentiation process in the presence and absence of AM580. In the original study, gene expression analysis of hiPSCs differentiated in the presence of retinoic acid indicated a drastic acceleration of osteogenesis by retinoic acid. In untreated samples, genes associated with either hiPSCs (such as *NANOG)* or osteoprogenitor cells (such as *RUNX2)* were upregulated throughout differentiation (Kawai et al., 2019) with hiPSC associated genes decreasing from day 7. Retinoic acid treated samples however upregulated osteoprogenitor genes as

early as day 1, and expressed genes consistent with mature osteoblasts or even osteocytes (such as *BGLAP, PHEX* and *SOST)* by day 10 of differentiation.

A potential influence of the culture dish coating was also investigated by repeating the differentiation for seven days on Matrigel or gelatin. Whilst the protocol states that the osteogenic differentiation was performed after seeding cells on gelatin, a chart within the manuscript suggested that feeder-free cells were actually differentiated on laminin. Nevertheless, alizarin red staining revealed very limited mineralisation on Matrigel. No improvement of mineralisation was observed after cells were allowed to attach to the culture dish coated with either gelatin or Matrigel overnight, prior to induction of differentiation.

For mesenchymal stem cells (MSCs) it is well accepted that cells from various donors behave differently during differentiation (Gray et al., 2016; Kim et al., 2018; McLeod and Mauck, 2017). A second hiPSC line, RM3.5c was therefore chosen and the differentiation process repeated. Additionally, in contrast to O27, RM3.5c cells are feeder-dependent hiPSCs which could also influence their osteogenic differentiation potential. Osteogenic differentiation of RM3.5c cells was performed on feeder cells, gelatin and Matrigel in the presence of DMSO, retinoic acid or AM580. Indeed, the alizarin red staining observed under all conditions was more intense than for previous experiments using O27. Furthermore, the staining observed with RM3.5c involved a much larger area of the culture dish: for Matrigel and feeder cell coated dishes the staining covered almost the entire culture dish. Interestingly, the patchy staining pattern observed for O27 cells seeded onto gelatin was indeed replicated by RM3.5c cells; however, RM3.5c cells displayed a more intense alizarin red staining than O27 cells after differentiation. Furthermore, alizarin red staining of RM3.5c cells seeded onto gelatin and treated with AM580 covered about 86.69 % $\pm$ 12.35 % of the total well area after seven days of differentiation compared to about 25.98 % $\pm$ 24.48 % of the well area covered after differentiation of O27 cells. This indicates that hiPS cell lines may differ in their osteogenic potential and highlights the importance of isogenic control cell lines for studies involving patient mutations. However, whilst the alizarin red staining appears promising, induction of genes involved in osteogenesis, such as *COL1A1* and *BGLAP,* remains to be investigated. Additionally, examination of the expression of stem cell marker genes such as *NANOG* and *OCT4* could increase the confidence in the differentiation protocol. RNA was isolated from

RM3.5c hiPSCs after seven days of differentiation and transcribed into cDNA; however, qRT-PCR has not been conducted yet. These preliminary data suggest that, using this protocol, O27 hiPSCs have a lower osteogenic differentiation potential than RM3.5c hiPSCs. For RM3.5c hiPSCs, the differentiation appears to be most successful either when differentiated in the presence of retinoic acid or AM580 after allowing them to attach to feeder cells in hiPSC medium overnight, or when differentiated on gelatin in the presence of AM580 after seeding them directly in differentiation medium. This could be explained by improved attachment of the cells to the plate prior to differentiation. Possibly, hiPSCs kept in hiPSC medium adhere better to the feeder cells than hiPSCs seeded in differentiation medium directly. Consequently, as fewer cells attach, fewer cells therefore differentiate. In contrast to that, hiPSCs seem to have only a limited capacity to adhere to gelatin. Seeding hiPSCs directly in differentiation medium may therefore improve their ability to attach to the gelatin coating, leading to more cells that attach successfully and differentiate. Indeed, an alternative approach for the osteogenic differentiation of hiPSCs also utilises gelatin-coated culture plates, following an initial differentiation step from hiPSC to MSCs (Panicker et al., 2018). MSCs are likely to adhere better to the gelatin coating than hiPSCs, leading to improved differentiation results. The fact that only AM580 but not retinoic acid appeared to enhance mineralisation in RM3.5c cells on gelatin after seeding in differentiation medium could result from differences in affinity for different retinoic acid receptors. Whilst AM580 activates the retinoic acid receptor α, retinoic acid receptor β stimulation also enhanced osteogenic differentiation of hiPSCs (Kawai et al., 2019); however, induction of retinoic acid receptor β by retinoic acid treatment has also been linked to the disruption of osteogenesis (Roa et al., 2019).

In the case that future qRT-PCR data confirms the induction of osteogenic marker genes such as *COL1A1* in RM3.5c hiPSCs differentiated on feeder cells and on gelatin in the presence of AM580, it would then be interesting to compare an isogenic OI hiPSC line after differentiation under these conditions. Retention of type I collagen within the ER could be demonstrated by immunohistochemistry and immunoblot analysis. The induction of ER stress and the UPR could be analysed on gene expression level by qRT-PCR and on protein level by immunoblot and immunohistochemistry before DNA is extracted and DNA methylation analysed. Whilst non-isogenic hiPS cell lines have successfully been used to study disease

mechanisms *in vitro* (Panicker et al., 2018, 2014), this work highlights the differences in osteogenic differentiation potential of hiPS cell lines from different donors.

A novel, recently published approach uses the direct differentiation of osteoblasts from primary fibroblasts by treatment with IGFBP7, eliminating the need for reprogramming and differentiation of hiPSCs (Lu et al., 2020). This is an exciting approach for tissue engineering purposes and therapeutic approaches, since it reduces the risk of teratoma formation *in vivo*. Still, at the moment it remains unclear whether the differentiation of fibroblasts in response to IGFBP7 treatment is as donor-dependent as hiPSC differentiation. This has important implications for the study of genetic bone diseases *in vitro*, e.g. isogenic primary fibroblasts may be required to produce meaningful results. In this case, the generation of hiPSCs would most likely remain the preferable approach for *in vitro* studies due to their capacity for self-renewal.

Unfortunately, due to the time constraints, the completion of experiments was not possible during the three-month secondment in Melbourne. A main limitation of these results is therefore the lack of gene expression data to confirm the successful differentiation of RM3.5c cells. Furthermore, these data imply that before OI patient derived and control hiPSCs can be compared after differentiation, the progress of differentiation itself will have to be evaluated. Only after it is confirmed that both the control and patient derived cell line display a comparable osteogenic differentiation potential, further experiment examining differences e.g. in DNA methylation can be performed. Previous studies have sometimes used control hiPS cell lines from healthy individuals and compared these to patient-derived hiPS cell lines. The results of these experiments clearly demonstrate that isogenic control lines, or at least the careful evaluation of osteogenic differentiation potential of all studied cell lines, are required to make meaningful conclusions.

4.7 Summary

- The potential to differentiate into osteoblast-like cells is hiPS cell line dependent.

- The substrate used for coating of cell culture dishes influences the osteogenic differentiation and the response to retinoic acid and AM580 treatment.

- In O27 cells, AM580 treatment during osteogenic differentiation leads to an early upregulation of *COL1A1* and a less pronounced increase later during differentiation while *BGLAP* expression is not induced.

- RM3.5c cells appear to have a higher osteogenic differentiation potential than O27 cells according to alizarin red staining.

Chapter 5. Overexpression of p.D469del COMP in HT1080 fibrosarcoma cells as an *in vitro* model of pseudoachondroplasia

5.1 Introduction

The data obtained in chapter 3 and chapter 4 indicated that whilst hiPSC offer exciting new opportunities, for the experiments of this study, a more conventional approach may be necessary. Aside from the established mouse model of pseudoachondroplasia (PSACH), a previously established cell model was used to study transcriptional and epigenetic changes. In this cell model, wild type and mutant COMP are overexpressed in HT1080 fibrosarcoma cells. Both wild type and mutant COMP carry a green fluorescent protein (GFP) tag at the C-terminus, which allowed the cells to be FACS sorted by GFP fluorescence to ensure high levels of expression. In some experiments, a cell line that expressed only the relatively small GFP tag, but not recombinant COMP was used as an additional control.

5.1.1 Chapter aims

- Confirm some of the observations previously made in the mouse model of PSACH in a HT1080 cell model:
    - Intracellular retention of mutant COMP
    - Decreased Proliferation and increased apoptosis

- Assess the activation of the UPR in the D469del COMP cell model.

- Compare D469del COMP cell model to the PSACH mouse model.

- Examine the response of D469del COMP cells to chemically induced ER stress.

5.2 D469del COMP cells mimic hallmarks of pseudoachondroplasia

Hallmarks of PSACH pathology were identified in previous studies using a range of mouse and cell-based models (Suleman et al., 2012; Schmitz et al., 2008; Posey et al., 2009; Piróg-Garcia et al., 2007; Holden et al., 2005; Chen et al., 2004). The retention of COMP inside the ER of chondrocytes, a reduction in postnatal growth, reduction in chondrocyte proliferation, increased and spatial dysregulation of chondrocyte apoptosis within the growth plate, lack of a conventional UPR and a gene signature that has been attributed to oxidative and/or inflammatory stress are some of the most prominent features (Posey et al., 2015, 2009; Suleman et al.,

2012). Before HT1080 cells overexpressing wild type or mutant p.D469del COMP could be used to study PSACH *in vitro*, it was necessary to confirm that the molecular pathology of PSACH was replicated in this model, although some characteristics of PSACH, such as a reduction in growth, could not be examined *in vitro.* Instead, the intracellular retention of mutant p.D469del COMP was assessed, followed by investigation of cell proliferation and apoptosis as well as the lack of activation of classical UPR markers.

Firstly, the retention of mutant COMP within the cells was confirmed by western blot. For both cell lines, GFP-tagged COMP protein was observed in the cell lysate samples. Notably, mutant p.D469del COMP was strongly reduced or absent from the media whilst GFP-tagged wild type COMP was successfully detected in these samples (Figure 5.1 A). Ponceau staining of the membrane was used to confirm the presence of protein in media of D469del COMP samples. Additionally, since GAPDH levels in the cell lysates were found to be comparable, the lack of mutant p.D469del COMP in the cell culture media was not due to strongly decreased cell numbers or excessive cell death prior to sample collection (Figure 5.1 A). There was no significant difference in the amount of intracellular COMP (Figure 5.1 B), but the relative amount of intracellular COMP protein was markedly increased in the D469del COMP cells (Figure 5.1 C). As expected, the relative extracellular amount of p.D469del COMP was strongly decreased compared to wild type COMP (Figure 5.1 D).

Expression of GFP-tagged COMP was also analysed by immunocytochemistry (Figure 5.2). Both wild type and mutant p.D469del COMP were detected inside the cells when cells were permeabilised during staining. However, compared to the wild type overexpressing cells, the staining seemed to be much more prominent in D469del COMP overexpressing cells. Furthermore, mutant p.D469del COMP staining appeared to cover a larger area around the nucleus of individual cells. These data demonstrate that mutant p.D469del COMP is retained intracellularly when overexpressed in HT1080 cells, which confirms findings of previously published experiments.

Previous studies performed on murine growth plate cartilage sections demonstrated a marked reduction in chondrocyte proliferation rate and an increase as well as

spatial dysregulation of apoptosis (Posey et al., 2009; Schmitz et al., 2008; Suleman et al., 2012). To investigate whether this is replicated in the D469del COMP cell model, TUNEL and BrdU labelling of cells overexpressing wild type COMP or p.D469del COMP was performed (Figure 5.3). In wild type COMP cells only 4.0 ± 0.8 % TUNEL-positive cells were observed. In D469del COMP cells, 8.5 ± 0.2 % of all cells were TUNEL-positive, which represents a 2.1-fold increase in apoptosis (Figure 5.3 A and B). For comparison, in the murine growth plate, the increase in apoptosis has been reported to be increased from 2.88-fold at five days up to 5-fold at three weeks (Suleman et al., 2012).

To analyse cell proliferation, both wild type and D469del COMP overexpressing cells were treated with BrdU, which is a thymidine analogue that is incorporated into newly synthesised DNA. As expected, only nuclear BrdU staining was observed in both cell lines (Figure 5.3 C). BrdU incorporation was significantly reduced in D469del COMP compared to wild type COMP cells in three labelling experiments (Figure 5.4 D). On average, wild type COMP overexpressing cells showed a proliferation rate of 39.5 ± 5.0 % whereas D469del COMP cells showed a rate of only 31.2 ± 5.8 %. This corresponds to an approximately 20.6 % reduction in cell proliferation, which is close to the observed decrease of 17 % in the murine growth plate of three-week old animals (Suleman et al., 2012). These results suggested that overexpression of p.D469del COMP in HT1080 cells lead to a similar imbalance of proliferation and apoptosis as observed in the murine model, and that the major hallmarks of PSACH pathology were replicated in the HT1080 cell model.

Next, levels of several markers of ER stress were assessed to confirm the absence of a classical unfolded protein response. The first protein of interest was BiP (or GRP78, encoded by the *HSPA5* gene), which is known to control all three branches of the UPR. Interestingly, a mild but significant increase in BiP protein level was detected in mutant D469del COMP cells (Figure 5.4 A and B) compared to wild type COMP cells. It is worth noting that BiP levels for both wild type and D469del COMP cells appeared raised compared to cells expressing only GFP (Figure 5.4 C). Both wild type and p.D469del COMP are considerably larger proteins than GFP and require posttranslational modifications such as N-glycosylation. The rise in BiP protein level compared to cells expressing only GFP demonstrates that even producing wild type COMP can strain the ER considerably.

Next, expression of the gene encoding for BiP (*HSPA5)* and the gene encoding for CHOP (*DDIT3)* was analysed alongside *GFP* expression by qRT-PCR (Figure 5.5 A). As each molecule of COMP carries a GFP tag, the level of *GFP* expression is equivalent to COMP overexpression. *HSPA5* was selected due to its prominence as a master regulator of the UPR and *DDIT3* was chosen specifically because previous studies have reported conflicting results as to whether *DDIT3/Ddit3* is upregulated in cell and mouse models of PSACH (Coustry et al., 2012; Posey et al., 2012; Suleman et al., 2012). Interestingly, no statistically significant difference was observed between wild type and D469del COMP cells for both *HSPA5* and *DDIT3* expression, although a slight increase in BiP protein levels was previously observed by western blotting. *GFP* expression however was decreased in D469del COMP cells compared to wild type COMP cells. Under ideal circumstances p.D469del COMP would be expressed to the same extent as wild type COMP; however, given the considerable amount of stress that p.D469del COMP causes, the decrease in expression was not surprising. The reported reduction in proliferation alongside higher numbers of apoptotic cells in mouse models of PSACH as well as in the D469del COMP cells demonstrate the detrimental effect of p.D469del COMP expression.
Next, induction of *XBP1* splicing was investigated as a marker for the activation of the IRE1 branch of the UPR (Figure 5.5 B). In agreement with previous reports, no increase in *XBP1* splicing was observed in D469del COMP cells. Surprisingly, a slight, but significant decrease in the proportion of spliced *XBP1* was observed during quantification (Figure 5.5 C).

Having already examined expression levels of *DDIT3,* potential activity of the PERK branch was further investigated by evaluating phosphorylation of eiF2α by western blotting (Figure 5.6 A, B). No significant difference in phosphorylation was observed between wild type and D469del COMP cells, suggesting that the PERK branch of the UPR is not activated in response to p.D469del COMP expression. Finally, levels of calnexin were evaluated using western blotting (Figure 5.6 C, D). Calnexin was specifically chosen as it plays a role in the folding of glycosylated proteins such as COMP. Whilst calnexin levels were significantly higher in D469del COMP cells, this was not observed on transcript level (see Chapter 6.4). The increase in BiP and calnexin protein level may therefore be caused by a structural expansion of the ER in the case of D469del COMP retention. Taken together, these data indicated that whilst D469del COMP cells displayed the expected protein retention, as well as

alterations in proliferation and apoptosis, the expression of p.D469del COMP did not trigger the UPR.

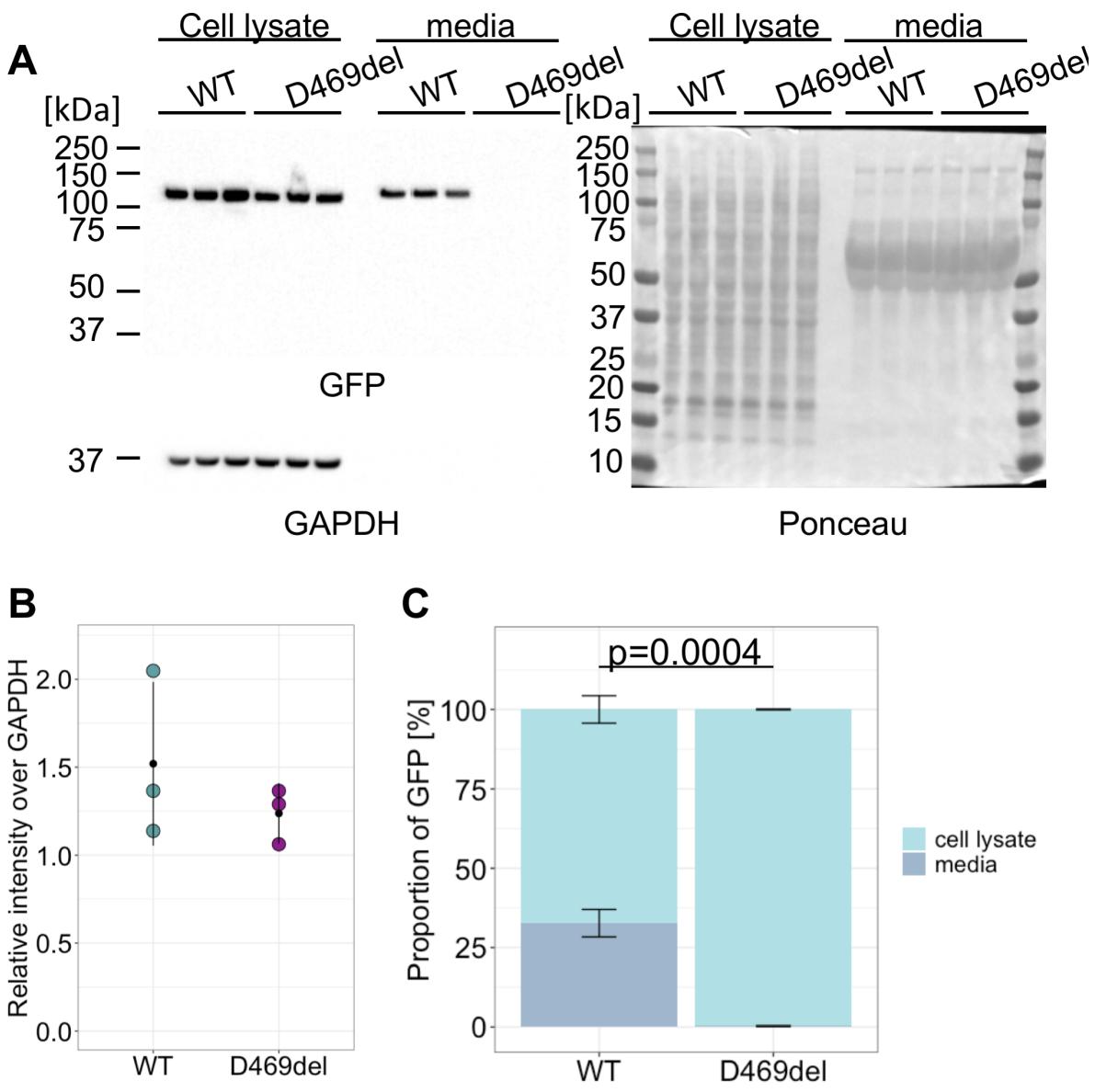

Figure 5.1 – Intracellular retention of p.D469del COMP in HT1080 cells. (A) Western Blot of cell lysates and media from HT1080 cells overexpressing wild type COMP (WT) or mutant p.D469del COMP (D469del). COMP proteins were detected via the C-terminal GFP tag. GAPDH was used as loading control for cell lysates. To demonstrate equal loading of media, a ponceau staining of the membrane is shown. (B) Quantification of total intracellular COMP protein levels. (C) Quantification of relative intracellular (cell lysate) and extracellular (media) proportion of COMP protein. N = 3 experiments. Black dots represent mean values, bars show standard deviation, *P*-values were determined using student's t-test.

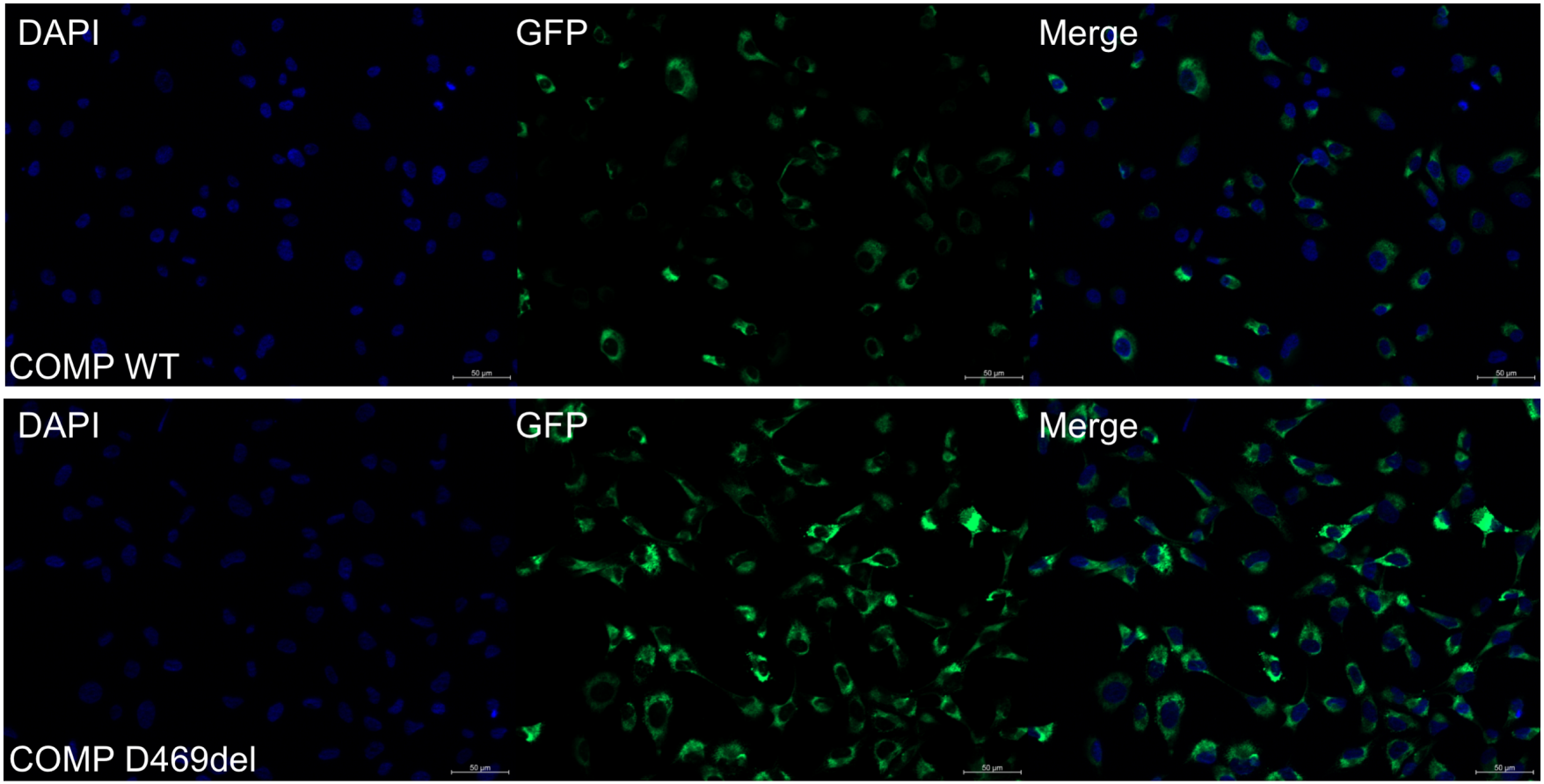

Figure 5.2 – Immunofluorescence of GFP-tagged wild type COMP and p.D469del COMP in HT1080 cells. Cells were stained with an antibody against GFP. Nuclei were visualised using DAPI. Scalebar: 50 μm.

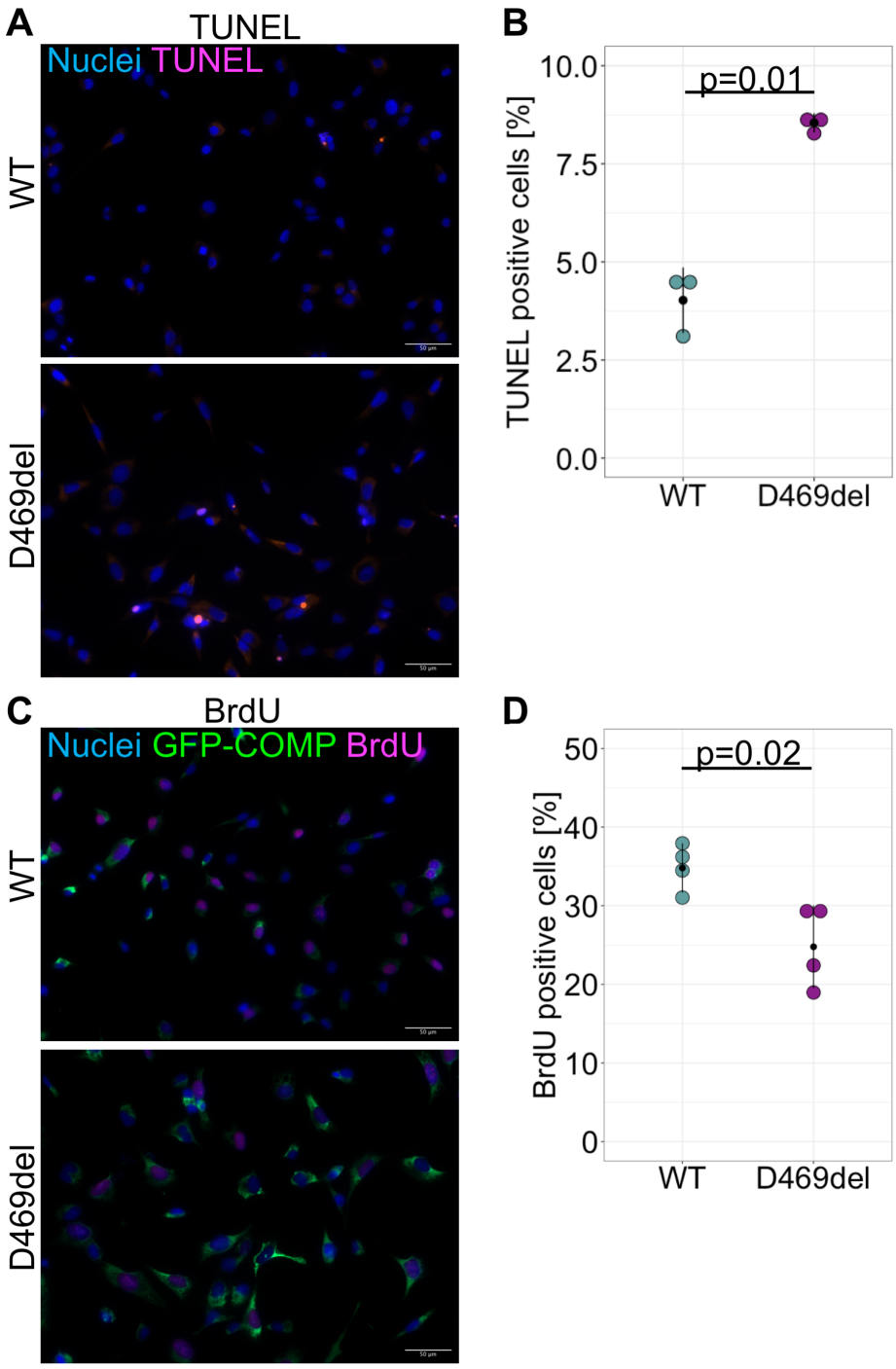

Figure 5.3 – Analysis of apoptosis and cell proliferation in D469del COMP cells. (A) TUNEL assay of wild type (WT) or D469del COMP (D469del) cells. Nuclei were visualised using DAPI (blue). A representative image is shown. (B) Quantification of TUNEL staining from one experiment. n = 1 experiment, 3 replicates, *P*-value determined using student's t-test. (C) Wild type (WT) or D469del COMP cells were stained for GFP (green) and BrdU (magenta) using specific antibodies following BrdU-labelling. Nuclei were visualised using DAPI (blue). A representative image is shown. (D) Quantification of BrdU positive cells from one experiment (n=4), labelling was repeated three times. *P*-value calculated using student's t-test. Black dots represent mean value, black bars display standard deviation.

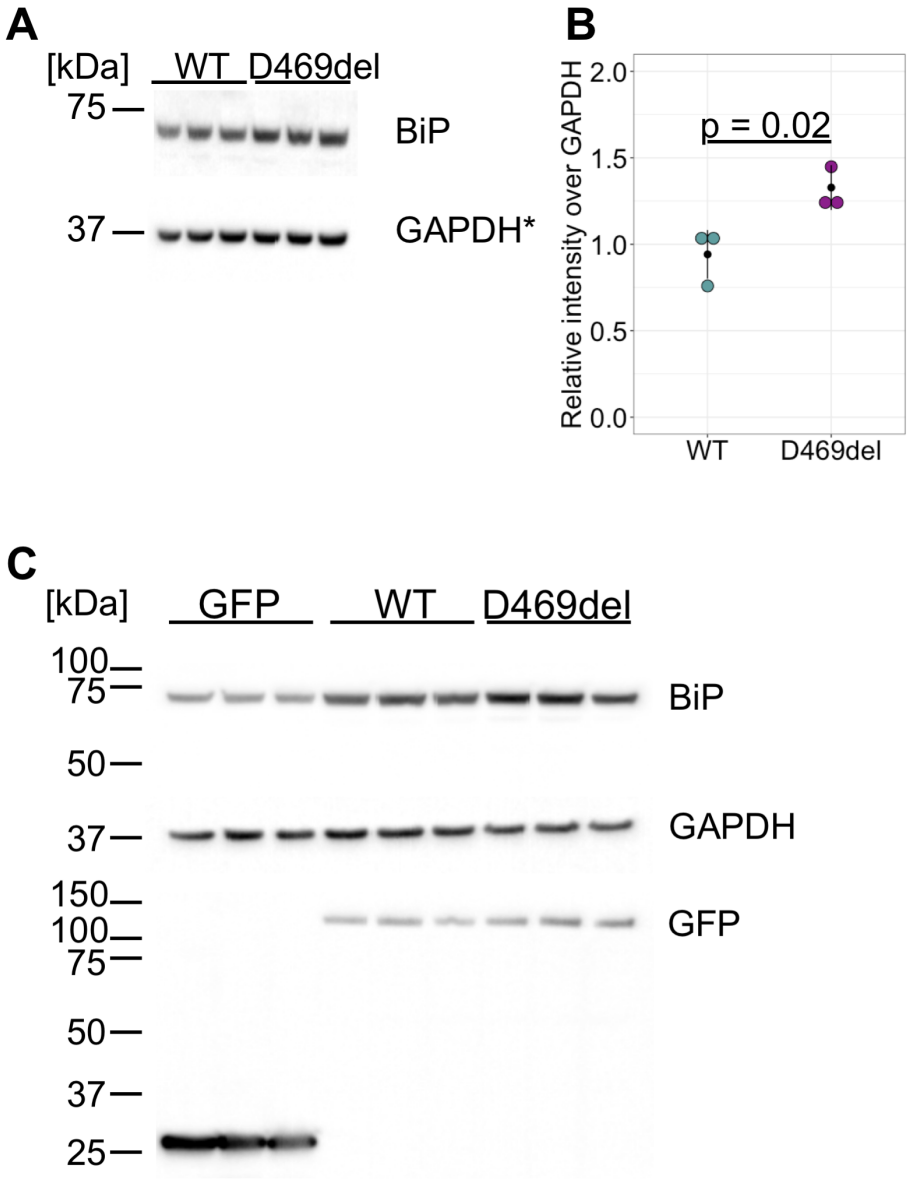

Figure 5.4 – D469del COMP cells display only a mild increase in BiP protein level. (A) Western Blot and (B) quantification of BiP levels in wild type COMP (WT) or mutant D469del COMP (D469del) cells. *The same membrane used for Figure 5.1 A was re-probed with an antibody specific for BiP, the same GAPDH is shown as loading control; n = 3 experiments, *P*-value was determined using student's t-test. (C) Western Blot of HT1080 cells overexpressing GFP alone, wild type COMP (WT) or p.D469del COMP using BiP- and GFP-specific antibodies. GAPDH was used as loading control, n = 2 experiments.

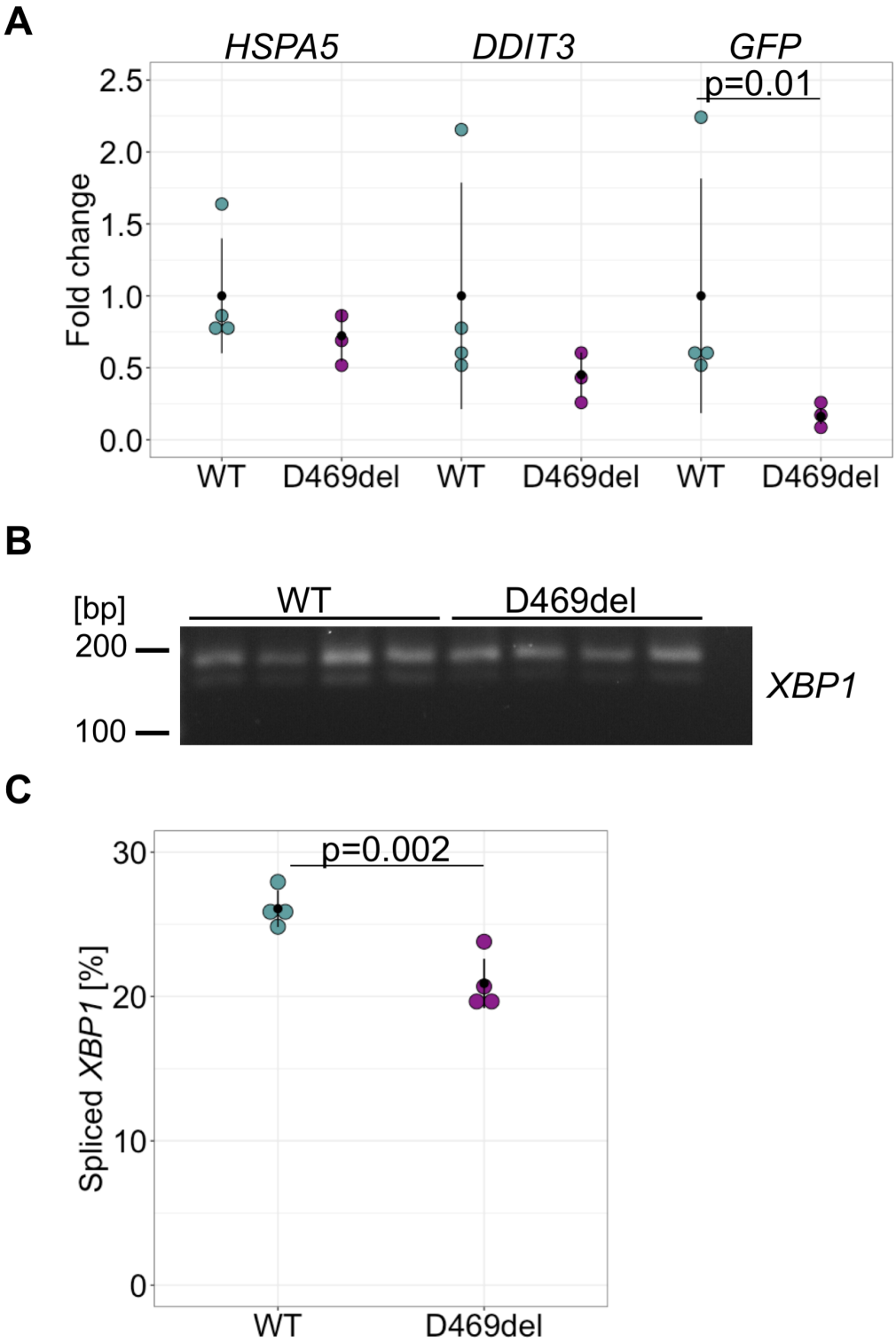

Figure 5.5 – Expression of selected UPR markers and analysis of *XBP1* splicing in D469del COMP cells. (A) Gene expression of *GRP78*, *DDIT3* and *GFP*. 18S was used as housekeeping gene. n = 3-4. (B) *XBP1* splicing was analysed by RT-PCR and subsequent agarose gel electrophoresis. The top band corresponds to unspliced form, the lower band to the spliced form of *XBP1*. (C) Densitometric quantification of *XBP1* splicing, n = 4. Black dots represent mean value, black bars display standard deviation, *P*-value was determined using student's t-test

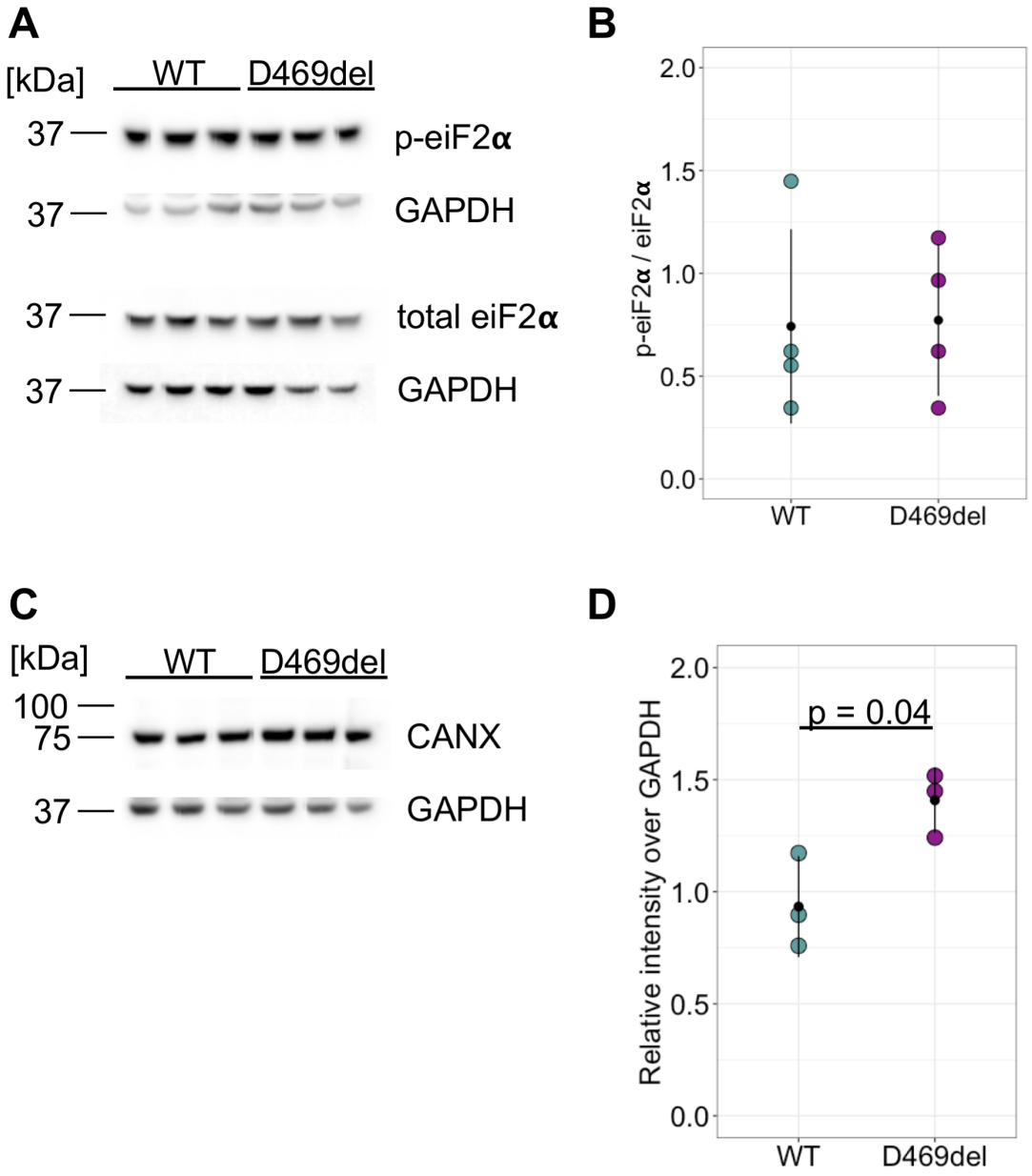

Figure 5.6 – Phosphorylation of eiF2α and calnexin protein levels in D469del COMP cells. (A) Western blot and (B) quantification of phosphorylated (p-eiF2α) and total eiF2α in wild type (WT) and D469del COMP cells. n = 4 experiments. (C) Western blot and (D) quantification of calnexin (CANX) protein levels. n = 3 experiments. GAPDH was used as loading control. Black dots represent mean values, bars show standard deviation, *P*-values were determined using student's t-test.

5.3 Comparison of D469del COMP cells with femoral head cartilage

In D469del COMP cells, expression of recombinant COMP was lower than in wild type COMP cells. This was not observed in previous studies using a mouse model of PSACH; however, the expression of *Comp* was not analysed after the age of three weeks. To examine how closely D469del COMP cells resemble the characteristics of chondrocytes at earlier and later stages of skeletal development, the expression of *Ddit3, Grp94* (which encodes the chaperone Hsp90b1), *Grp78* (BiP) and *Canx* as markers of the UPR, as well as *Comp* was analysed in femoral head cartilage obtained at the age of one and six weeks from wild type and D469del *Comp* mice. The age of six weeks was chosen specifically because male p.D469del *Comp* mice were found to be significantly lighter, and their tibias shorter at this age (Suleman et al., 2012). To exclude that p.D469del Comp would affect the development of the femoral head at the age of six weeks, Toluidine Blue staining was performed on femoral head cartilage sections from male animals (Figure 5.7). In both genotypes, Toluidine Blue staining was most intense in the growth plate but also evenly distributed in the femoral head cartilage. No signs of ossification were observed in both genotypes; thus, six weeks was deemed a suitable age to proceed with chondrocyte and RNA extraction.

At the age of one week, no significant difference in the expression of *Ddit3, Grp94* and *Canx* was found (Figure 5.8). *Grp78*, the gene that encodes for BiP, was slightly upregulated in samples from D469del *Comp* mice. There was also no significant difference in *Comp* expression at this timepoint, in agreement with previous reports (Suleman et al., 2012). This finding demonstrates that the lack of UPR activation at the transcriptional level at this time point is not driven by a reduction of *Comp* expression. At the age of six weeks, no difference in the expression of *Ddit3, Grp94* and *Canx* was detected. *Grp78* expression was still significantly elevated. Surprisingly, *Comp* expression was significantly decreased in samples from D46del *Comp* mice at the age of six weeks (Figure 5.9). This indicates that the difference in expression of recombinant COMP observed in D469del COMP cells has – at least to some extent – a physiological relevance. It also suggests that the expression of *Comp* itself has little influence on *Ddit3, Grp94, Grp78* and *Canx* expression, since a reduction in *Comp* did not drive a relative reduction of their transcripts.

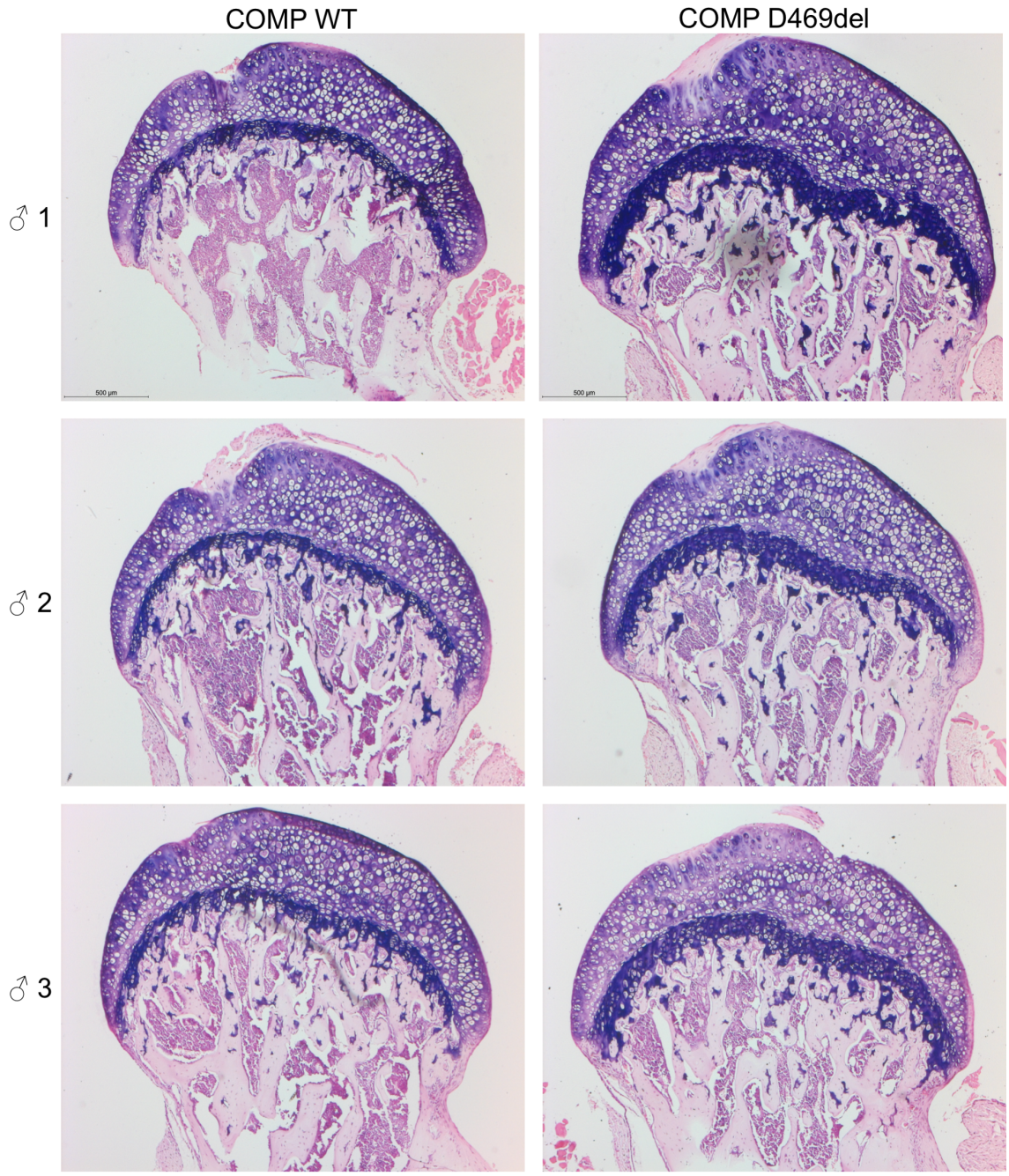

Figure 5.7 – Toluidine Blue staining of femoral head cartilage in male mice at the age of six weeks. Proteoglycans are stained purple. Nuclei are stained pink. Male mice from three litters/genotype were analysed. No signs of ossification are observed in both genotypes. Scale bar: 500 µm.

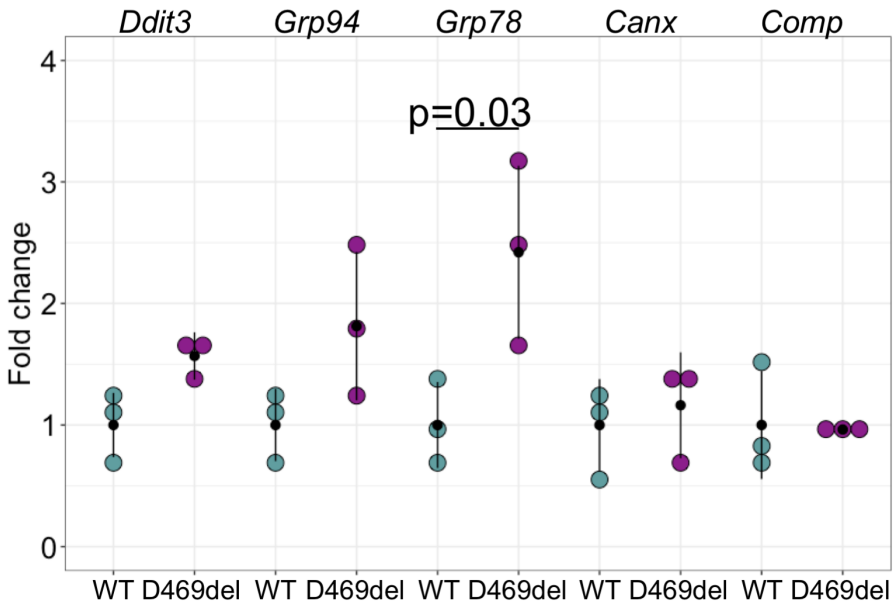

Figure 5.8 – Expression of selected UPR markers in femoral head cartilage at the age of one week. Gene expression was analysed by qRT-PCR and is presented as fold change relative to wild type. 18S was used as housekeeping gene. Black dots represent mean values, bars show standard deviation, *P*-values were determined using student's t-test. Individual data points in teal (wild type) or purple (D469del). N = 3 litters (3 animals/litter were pooled for each extraction).

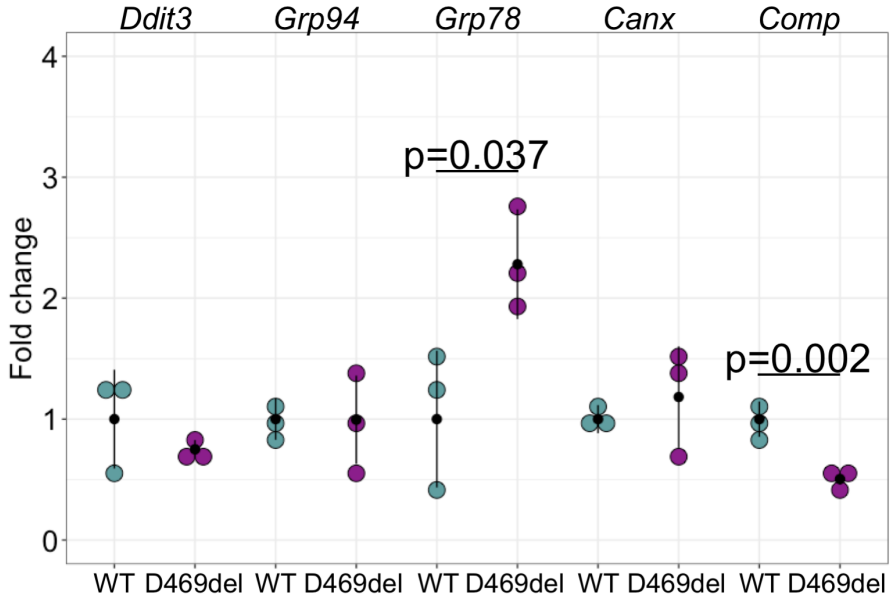

Figure 5.9 – Expression of selected UPR markers in femoral head cartilage chondrocytes at the age of six weeks. Gene expression was analysed by qRT-PCR and is presented as fold change relative to wild type. 18S was used as housekeeping gene. Black dots represent mean values, bars show standard deviation, *P*-values were determined using student's t-test. Individual data points in teal (wild type) or purple (D469del). N = 3 litters (3 animals/litter were pooled for each extraction).

5.4 D469del COMP cells are capable of activating the UPR upon treatment with tunicamycin and thapsigargin

Whilst the UPR is activated in several other skeletal dysplasia types, such as MCDS and *MATN3*-MED, the p.D469del mutation in COMP does not appear to involve the (canonical) UPR. This observation raised the question as to whether cells expressing the p.D469del COMP mutant protein would still be able to activate the UPR. To answer this question, wild type and D469del COMP cells were treated with tunicamycin or thapsigargin to cause ER stress and induce the UPR. Both treatments are commonly used to activate the UPR but act through different mechanisms. Whilst tunicamycin inhibits N-linked glycosylation within the ER (Duksin and Bornstein, 1977) and therefore causes misfolding of proteins, thapsigargin inhibits the enzymes that accumulate calcium within the ER lumen, disrupting Ca^{2+} homeostasis and activating the UPR (Li et al., 2000; Sagara and Inesi, 1991).

After treatment with either chemical, or DMSO as negative control, phosphorylation levels of eiF2α were analysed alongside protein levels of BiP, CHOP and calnexin and splicing of *XBP1* (Figure 5.10). Both wild type and D469del COMP cells displayed noticeably increased levels of BiP, although thapsigargin appeared to cause a greater increase than tunicamycin in both cell lines (Figure 5.10, Figure 5.11 A). Calnexin (CANX) levels were modestly induced by both treatments in wild type as well as D469del COMP cells. No significant differences in BiP or CANX levels after treatment with tunicamycin or thapsigargin were detected between wild type and D469del COMP cells.

Protein levels of CHOP as well as phosphorylation of eiF2α and *XBP1* splicing were also quantified (Figure 5.11 B). Whilst CHOP levels remained below the limit of detection in both cell lines when treated with DMSO only, it was robustly detected in both tunicamycin and thapsigargin-treated cells, although this failed to reach statistical significance. No significant differences were detected between the cell lines. In agreement with elevated CHOP expression, increased phosphorylation of eiF2α was observed in response to treatment with tunicamycin and thapsigargin. Notably, although both cell lines displayed increased phosphorylation levels in response to both chemicals, phosphorylation was only significantly increased in wild type COMP cells after tunicamycin treatment (Figure 5.11 B). Furthermore, no statistically significant difference was observed between the two cell lines in any of

the conditions tested. To investigate the activation of the IRE1 branch of the UPR, XBP1 splicing was evaluated (Figure 5.10 B, Figure 5.11 B). Both cell lines displayed increased *XBP1* splicing after tunicamycin or thapsigargin treatment, however, this was only significant for thapsigargin-treated D469del COMP cells. No difference was observed between wild type and D469del COMP cells.

When COMP levels, following treatment with tunicamycin and thapsigargin, were examined, the expected decrease in apparent molecular weight was observed for tunicamycin-treated samples (Figure 5.12 A), indicating that tunicamycin treatment successfully induced ER stress and the UPR by inhibiting N-linked glycosylation. Surprisingly, when the effects of tunicamycin and thapsigargin treatment on intracellular COMP levels were examined, wild type and p.D469del COMP appeared to behave distinctly different (Figure 5.12 A, B). Whilst tunicamycin caused only a slight reduction in wild type COMP cells, levels of intracellular p.D469del COMP were significantly decreased after treatment with tunicamycin (Figure 5.12 A, B). This was however not associated with an increase in COMP in conditioned media of D469del COMP cells (Figure 5.12 C), indicating that ameliorated secretion is not the reason for reduced intracellular levels of p.D469del COMP. Thapsigargin appeared to prompt an increase in intracellular wild type COMP, although this was not statistically significant (Figure 5.12 A, B). In D469del COMP cells, thapsigargin treatment did not appear to exacerbate COMP retention, although extracellular COMP levels were diminished in both cell lines (Figure 5.12 C).

Taken together, these results indicate that D469del COMP cells are capable of activating the UPR when challenged by treatment with tunicamycin or thapsigargin. The extent of the activation of the UPR does not appear to be different from wild type COMP-overexpressing cells with the exception of thapsigargin-induced *XBP1* splicing, which appears slightly reduced in D469del COMP cells.

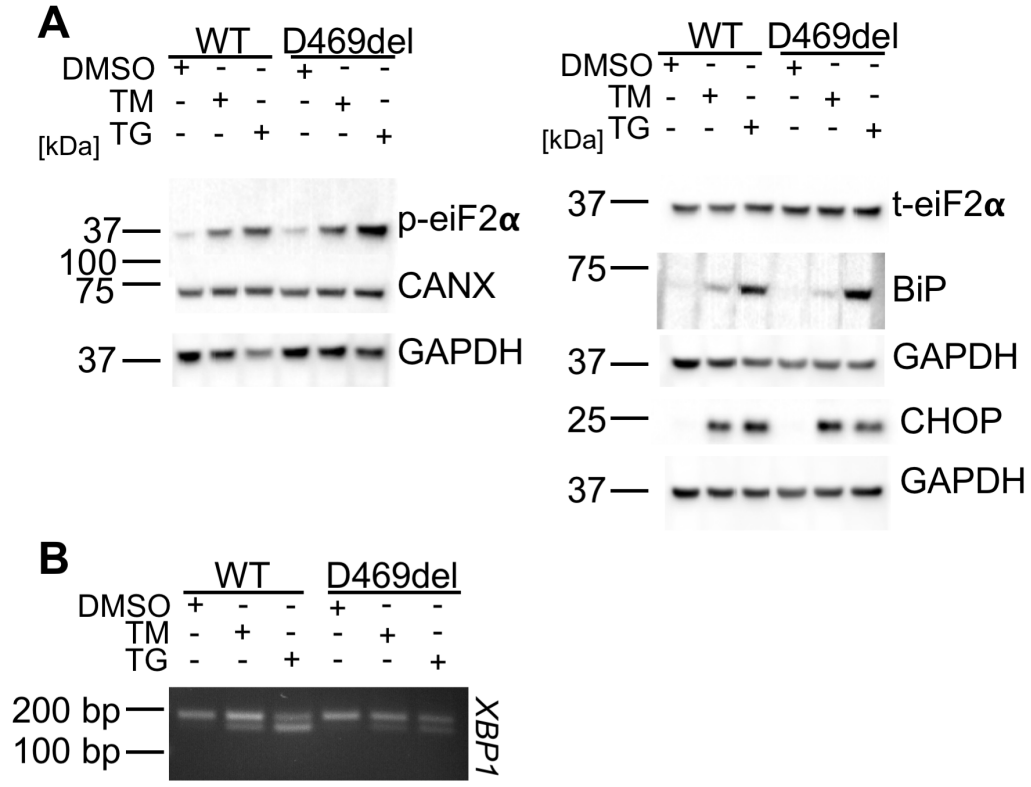

Figure 5.10 – Analysis of UPR markers after treatment of wild type or D469del COMP cells with tunicamycin or thapsigargin. (A) Protein levels of several markers of the UPR (BiP, CANX, CHOP) and ratio of phosphorylated to total eiF2α were assessed after treatment with tunicamycin (TM) or thapsigargin (TG). DMSO served as negative control. GAPDH was used as a loading control. (B) *XBP1* splicing was analysed by RT-PCR and subsequent gel electrophoresis, n = 3 experiments.

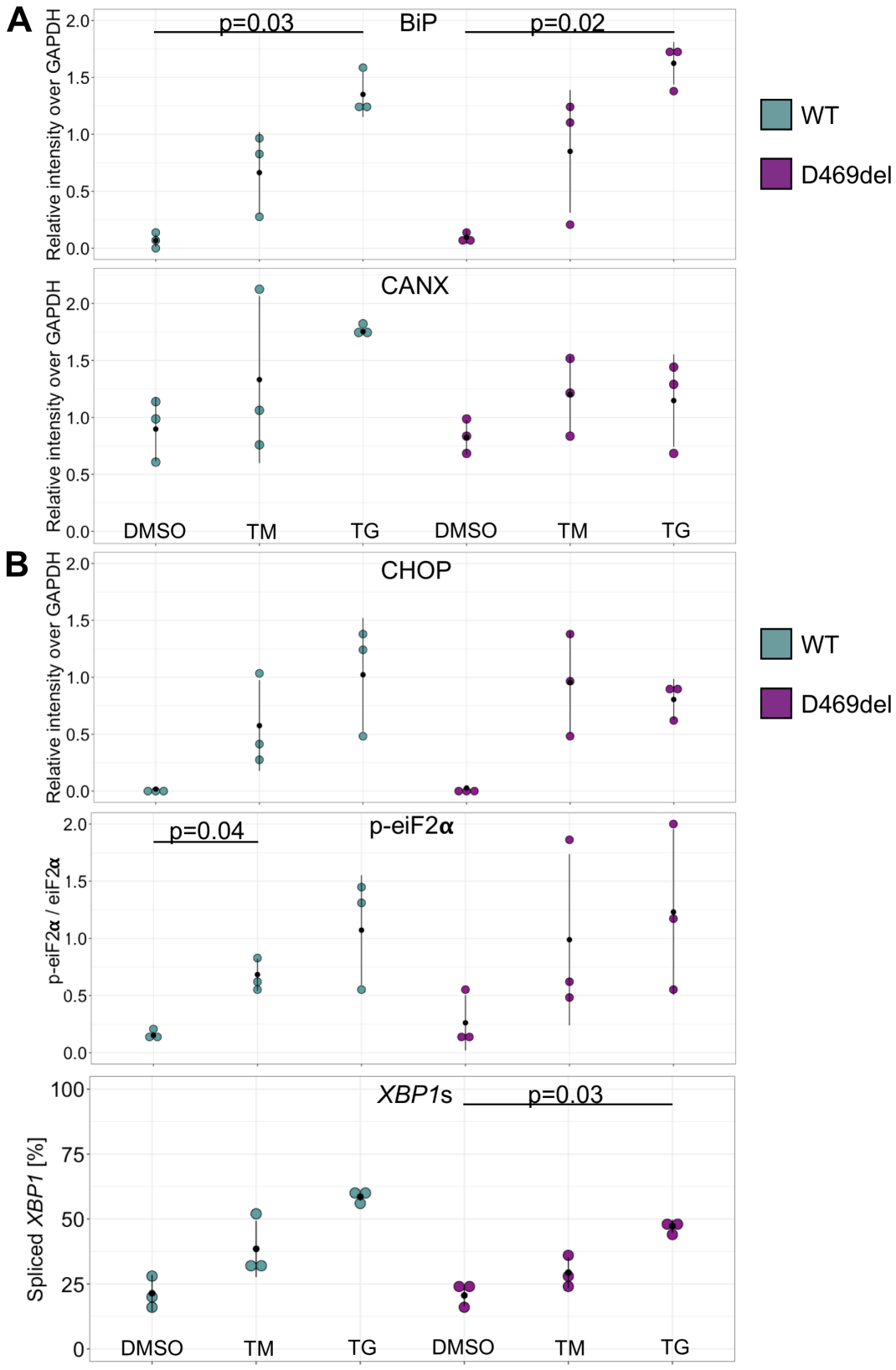

Figure 5.11 – Quantification of UPR activation of wild type and D469del COMP after treatment with DMSO, tunicamycin or thapsigargin. (A) Protein levels of chaperones BiP and CANX were examined as well as (B) downstream effectors of the UPR, such as CHOP, phosphorylated eiF2α and *XBP1s*. Black dots represent mean values, bars show standard deviation, *P*-values were determined using student's t-test (paired for treatments) with Bonferroni multiple test correction, n = 3 experiments.

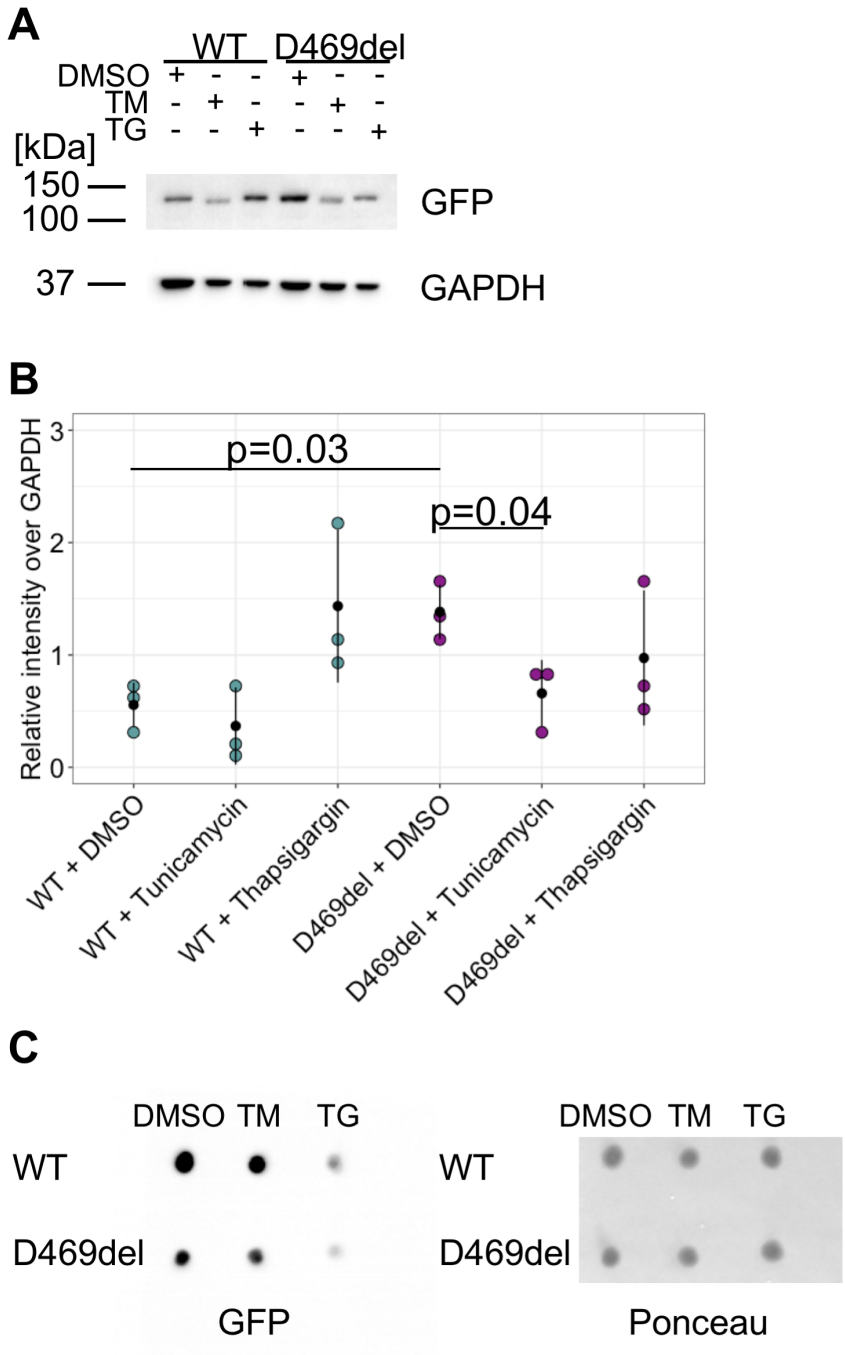

Figure 5.12 – Effect of tunicamycin and thapsigargin on COMP protein levels in wild type and D469del COMP cells. (A) Western blot and (B) quantification of intracellular GFP-tagged COMP levels after treatment with DMSO, tunicamycin or thapsigargin. GAPDH was used as loading control. Black dots represent mean values, bars show standard deviation, *P*-values were determined using student's t-test (paired for treatments) with Bonferroni multiple test correction, n = 3 experiments. (C) Dot blot of conditioned media from cells overexpressing wild type or D469del COMP after treatment with DMSO, tunicamycin or thapsigargin. Ponceau staining prior to GFP detection was used as loading control, n = 2 experiments.

5.5 Discussion

The aim of this chapter was to validate the HT1080 cell model for the study of PSACH by confirming some of the previous findings from other cell and mouse models.

The experiments described confirmed that p.D469del COMP is retained intracellularly in HT1080 cells which leads to decreased cell proliferation and elevated levels of apoptosis. This has also been observed in mouse models of PSACH (Suleman et al., 2012). It was further shown that the involvement of the unfolded protein response is very limited, with only BiP showing significantly increased protein levels in D469del COMP compared to wild type COMP cells. In a knock-in mouse model of PSACH carrying the same mutation, the UPR was also not initiated as evidenced by comparable protein levels and expression of chaperones, and eiF2α phosphorylation (Suleman et al., 2012).

One particular difficulty in the study of ER stress induced by mutant COMP protein corresponds to the differential expression of wild type and mutant protein. Because COMP itself is a relatively large protein, even the expression of wild type COMP may cause mild ER stress, as demonstrated by elevated BiP levels of wild type and D469del COMP cells when compared to a cell line expressing the GFP tag alone. If the mutant protein is not expressed to the same level as the wild type, direct comparison of gene expression and protein levels may be problematic. Nevertheless, a reduction of expression in response to the stress caused by a mutant protein may occur and be relevant *in vivo.* Thus, a mouse model of PSACH was used to compare expression of *Comp* at the age of one and six weeks to the expression of *GFP-COMP* in the cell model. In femoral head cartilage samples *Comp* expression was not changed at one week, but significantly reduced at the age of six weeks. Previous studies reported no statistically significant difference in xiphoid cartilage at the age of three weeks (Suleman et al., 2012). Several explanations are possible, for example, cartilage derived from different parts of the skeleton may have slightly different matrix compositions and thus the effect of mutant Comp may vary between cartilage samples from different sources. Furthermore, expression of mutant *Comp* may only be reduced towards the end of skeletal growth. Notably, at the age of three weeks, D469del *Comp* mice were not yet significantly shorter or lighter than their wild type littermates, but by the age of six weeks, male mice carrying the D469del *Comp*

mutation exhibited decreased tibial length as well as a reduction in body weight compared to wild type littermates (Suleman et al., 2012).

Interestingly, *Grp78* expression was found to be mildly elevated in PSACH mice at the age of one and six weeks. This was not observed in previous studies using rib cage and xiphoid cartilage from five day and three-week-old animals, respectively (Suleman et al., 2012). Again, this could indicate that p.D469del *Comp* expression affects cartilage from various parts of the skeleton differently. It is also possible that, depending on the location of the cartilage, different bio-mechanic forces and strains act on cartilage and chondrocytes and thus modulate matrix composition or expression of matrix proteins. Indeed, cyclic tensile strain has been reported to induce extracellular colocalization of COMP with type II collagen (Bleuel et al., 2015). Together, this suggests that differences in the source of cartilage tissue (and thus potentially different bio-mechanical loading) as well as age influence the extent of COMP-induced ER stress *in vivo*.

In a different mouse model, human p.D469del *COMP* is expressed under the control of doxycycline under the *Col2a1* promoter. In this mouse model, CHOP was consistently increased (Posey et al., 2012). This was not observed in femoral head, xiphoid or rib cage cartilage from a knock-in mouse model of PSACH although there was a tendency for *Ddit3* to be slightly higher in samples from femoral head cartilage of D469del *Comp* mice at the age of one week. *In vitro,* D469del COMP cells appear to mimic the behaviour of juvenile murine PSACH chondrocytes in that *COMP* expression is reduced whilst BiP protein levels are elevated, whereas *Comp* expression seems to be not yet affected in cartilage samples from younger animals. In agreement with the D469del *Comp* knock-in mouse model, no significant difference in *Ddit3* expression was observed in D469del COMP cells.

Work presented in this chapter also indicates that D469del COMP cells retain the ability to activate the UPR when additionally challenged with tunicamycin or thapsigargin. Although the upregulation of several markers of the UPR were clearly visible in both wild type and D469del COMP-overexpressing cells, quantification revealed that the increases were not statistically significant. The variation between experimental repeats was relatively high for some of these analysed markers, suggesting that additional repeats of the experiment could improve the accuracy of

the quantification. Nevertheless, these data indicate that D469del COMP cells remain able to respond to additional ER stress. This is particularly relevant during peak times of protein secretion, for example during development or due to circadian rhythm (Chang et al., 2020; Horiuchi et al., 2016; Matsuzaki et al., 2015; Pickard et al., 2019). In fact, it has been demonstrated that the genetic removal of N-glycans from type I collagen does not affect its folding and secretion until cells are additionally challenged (Li et al., 2021). This finding elegantly illustrates the complexity of protein secretion and the problems that may arise when it is disrupted. A mutation in a specific part of an extracellular protein may be tolerable with regards to its secretion, but may affect ECM formation, or it may not affect its interactions with other ECM proteins, but prevent the protein from being secreted. Even a tolerable mutation may effectively prevent secretion when the secretory load is high, or cells experience other types of stress such as low nutrient levels or hypoxia.

Intriguingly, tunicamycin treatment appeared to reduce intracellular D469del COMP protein levels whilst the amount of secreted COMP remained unchanged. This could indicate that glycosylation potentially plays a role in regulating the degradation of D469del COMP, for example by retaining mutant COMP inside the ER lumen and preventing its degradation. Notably, it has been reported for some proteins that mutations slowed their passage through the secretory pathway and that their prolonged presence in the ER resulted in over-modification. This has been reported, for example, for mutant collagens (Barnes et al., 2019; Makareeva et al., 2018; Winterpacht et al., 1996). In contrast, compared to wild type COMP, D469del COMP did neither display a different band pattern nor different band sizes when detected by western blotting indicating that this mutation did not lead to over-modification.

Earlier studies of the glycosylation of bovine COMP reported distinct glycosylation patterns between foetal and adult cartilage-derived COMP (Zaia et al., 1997). The functional consequences for its secretion have not been characterised, although the authors speculated that differential glycosylation may influence the exact location and modulate protein-protein interactions of COMP within the ECM. Importantly, glycosylation of both foetal and adult COMP is consistent with structures that are attached by enzymes in the Golgi apparatus (Zaia et al., 1997), indicating that native COMP typically passes through the Golgi during secretion instead of being secreted via unconventional protein secretion.

Whilst tunicamycin treatment did not appear to influence COMP secretion, thapsigargin treatment reduced secretion of both wild type and D469del COMP. This was not unexpected, because treatment with thapsigargin reduces the Ca^{2+} levels within the ER, thereby disrupting the folding machinery that many secreted proteins, including wild type COMP, rely on for efficient folding and secretion (Shaheen, 2018). Furthermore, COMP secretion was shown to be effectively abolished upon loss of CAB45, and CAB45-mediated secretion was shown to be dependent on calcium-mediated oligomerisation of CAB45 (Crevenna et al., 2016; von Blume et al., 2012). Whilst this function of CAB45 is restricted to the trans Golgi network (TGN), there are some indications calcium stores within the Golgi are partly derived from the ER (Gallegos-Gómez et al., 2018) and calcium-dependent processes within the Golgi may therefore also be sensitive to thapsigargin treatment.

Whilst model systems are only able to model specific aspects of biology, the comparison of several model systems ensures that they reflect important features of the condition. Validation of this cell model, and comparison to the PSACH knock-in mouse model carrying the identical mutation, revealed that the D469del COMP cell model robustly mimics the characteristics of PSACH. The relative accuracy of this cell model demonstrates its suitability for future studies, including the identification of potential biomarkers and drug screenings. It also offers the opportunity to study some molecular aspects of PSACH in more detail. As primary chondrocytes can be difficult to obtain in large numbers and de-differentiate quickly *in vitro*, a suitable *in vitro* model for the study of PSACH could offer new opportunities and allow the exploration of novel approaches.

5.6 Summary

- HT1080 cells overexpressing wild type or D469del COMP recapitulate molecular characteristics of PSACH.

- Decreased expression of p.D469del COMP occurs in femoral head chondrocytes from male D469del *Comp* knock-in mice at the age of six weeks as well as in the D469del COMP cell model, but not in murine femoral head cartilage at the age of one week.

- D469del COMP cells retain the ability to activate the UPR when treated with tunicamycin or thapsigargin.

- Tunicamycin treatment reduces intracellular COMP levels without improving its secretion.

Chapter 6. Analysis of atypical ER stress in D469del COMP cells

6.1 Introduction

The previous chapter demonstrated that HT1080 cells overexpressing p.D469del COMP are a suitable *in vitro* model to study PSACH. Next, pathways that were previously implicated in PSACH were investigated, before an unbiased RNA sequencing based approach was chosen to identify novel pathways and genes of interest. In contrast to targeted gene expression analysis, such as qRT-PCR, RNA sequencing reveals gene expression changes on a transcriptomic level without prior target selection. Therefore, pathways may be uncovered that have not previously been linked to the molecular mechanism of PSACH.

Furthermore, the effects of p.D469del COMP expression on DNA methylation patterns were investigated to determine whether an epigenetic mechanism like DNA methylation could be affected by skeletal dysplasia.

6.1.1 Chapter aims

- Investigate pathways previously implicated in the disease mechanism of PSACH.
- Perform transcriptomic analysis of D469del COMP cell model.
- Validate a selection of differentially expressed genes identified by RNA sequencing.
- Determine whether DNA methylation is affected by p.D469del COMP expression.

6.2 COMP D469del HT1080 cells display signs of oxidative stress

Since no activation of the UPR has been observed in response to p.D469del COMP expression, oxidative stress and a subsequent inflammatory response have been suggested as the consequence of COMP induced ER stress (Posey et al., 2015; Suleman et al., 2012).

To quantify oxidative stress, superoxide levels were measured using a modified version of the nitroblue tetrazolium chloride (NBT) assay (Section 2.2.2.17). Menadione (vitamin K_3) has been used *in vitro* to stimulate superoxide anion generation (Criddle et al., 2006; Fukui et al., 2012; Thor et al., 1982) and was used to

challenge the oxidative stress response of wild type and D469del COMP cells. Levels of superoxide were significantly higher in D469del COMP compared to wild type COMP HT1080 cells (Figure 6.1 A). This was the case under basal conditions (0.07 ± 0.04 vs 0.22 ± 0.09 absorbance units (AU)/million cells) as well as after inducing additional oxidative stress by treating with menadione prior to carrying out the NBT assay (0.4 ± 0.1 vs 1.0 ± 0.1 AU/million cells respectively). This indicated that in D469del COMP cells, production of reactive oxygen species (ROS) such as superoxide was either increased, or capacity to eliminate ROS was decreased or a combination of both.

One of the sources of ROS are mitochondria. Comparing levels of mtDNA between wild type and D469del COMP cells was therefore used to investigate whether there was a difference in the number of mitochondria (Refinetti et al., 2017). Whilst an increase in mtDNA content could indicate an increased number of mitochondria, a decrease of mtDNA content could indicate advanced oxidative damage by ROS and subsequent degradation of mitochondria. Surprisingly, no change in mtDNA content was observed between wild type and D469del COMP cells (Figure 6.1 B). To examine the integrity of mitochondria in D469del COMP cells, cells overexpressing wild type and p.D469del COMP were stained with MitoTrackerRed-CM-H_2Xros, the accumulation of which is dependent on the mitochondrial membrane potential. The dye is only visible once it is oxidised by mitochondrial enzymes, and so it visualises only functional mitochondria. A loss of staining intensity or area therefore indicates reduced mitochondrial integrity. Interestingly, no apparent difference was observed between wild type and D469del COMP cells in terms of MitoTracker staining intensity (Figure 6.1 C). For both cell lines, cells were found that displayed mitochondrial staining largely around the nucleus as well as cells that displayed a more restrictive staining. In both cell lines, some cells displaying a more punctuate staining pattern than others were observed.

The other explanation for increased superoxide levels could be a decreased capacity of D469del COMP cells to eliminate ROS. Whilst superoxide itself is eliminated by superoxide dismutase enzymes (SODs), several enzyme families have evolved to reverse or protect lipids and proteins from the deleterious effects of ROS, e.g. lipid-peroxidation. Previous work performed on the PSACH mouse model has already reported a downregulation of peroxiredoxin-2 (*Prdx2*) in cartilage (Suleman et al.,

2012). Peroxiredoxins are thiol-specific peroxidases that catalyse the reduction of hydrogen peroxide and organic peroxides, thereby protecting cells from oxidative damage such as lipid peroxidation (Veal et al., 2018). When peroxiredoxin-2 (PRDX2) levels were evaluated in D469del COMP cells, they were found to be drastically and significantly decreased (Figure 6.2 A, B). This indicated that indeed there appeared to be a decreased capacity to cope with oxidative damage caused by ROS in D469del COMP cells. In other organisms and tissues, PRDX2 has been shown to be important for insulin secretion (Oláhová and Veal, 2015) and the loss of PRDX2 in a mouse model was demonstrated to lead to increased levels of circulating insulin with a concomitant decrease in intracellular insulin-signalling activation (Cha et al., 2019). One major element of the insulin and insulin-like growth factor (IGF) signalling pathways is protein kinase B or AKT. The phosphorylation level of AKT was therefore assessed by western blotting. In agreement with reduced PRDX2 levels and a potential decrease in insulin/IGF signalling, a decrease in AKT phosphorylation was observed (Figure 6.2 C, D). AKT signalling is known to be one of the major pro-survival signalling pathways and thus a decrease in AKT activity was consistent with the previously observed decrease in cell proliferation and elevated levels of chondrocyte apoptosis.

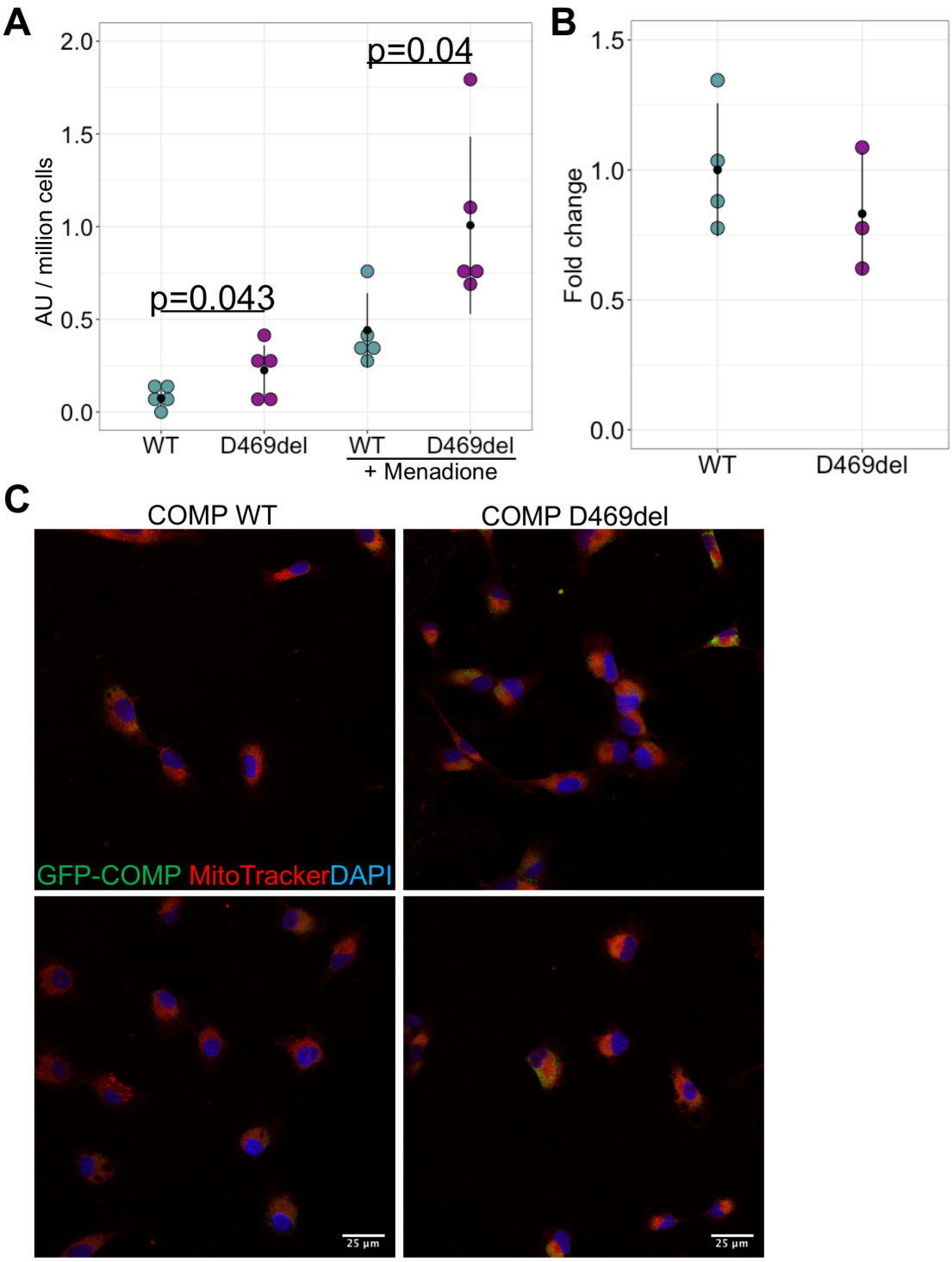

Figure 6.1 – Levels of superoxide and mitochondrial activity in HT1080 cells overexpressing D469del COMP. (A) Increased staining with NBT in D469del COMP cells under basal conditions as well as when additionally challenged with menadione. AU: absorbance units, n = 5 experiments. *P*-values were determined using student's t-test. (B) Mitochondrial DNA (mtDNA) content was examined by qRT-PCR using nuclear DNA (nuDNA) for normalisation. Data is presented as fold change, n = 3-4 technical replicates. *P*-values were calculated using student's t-test. Black dots represent mean values, bars show standard deviation, (C) Mitochondria were visualised using MitoTrackerRed-CM-H_2Xros. The reduced dye becomes visible (red) upon oxidation in the mitochondria. Accumulation is dependent on intact membrane potential, n = 2 experiments.

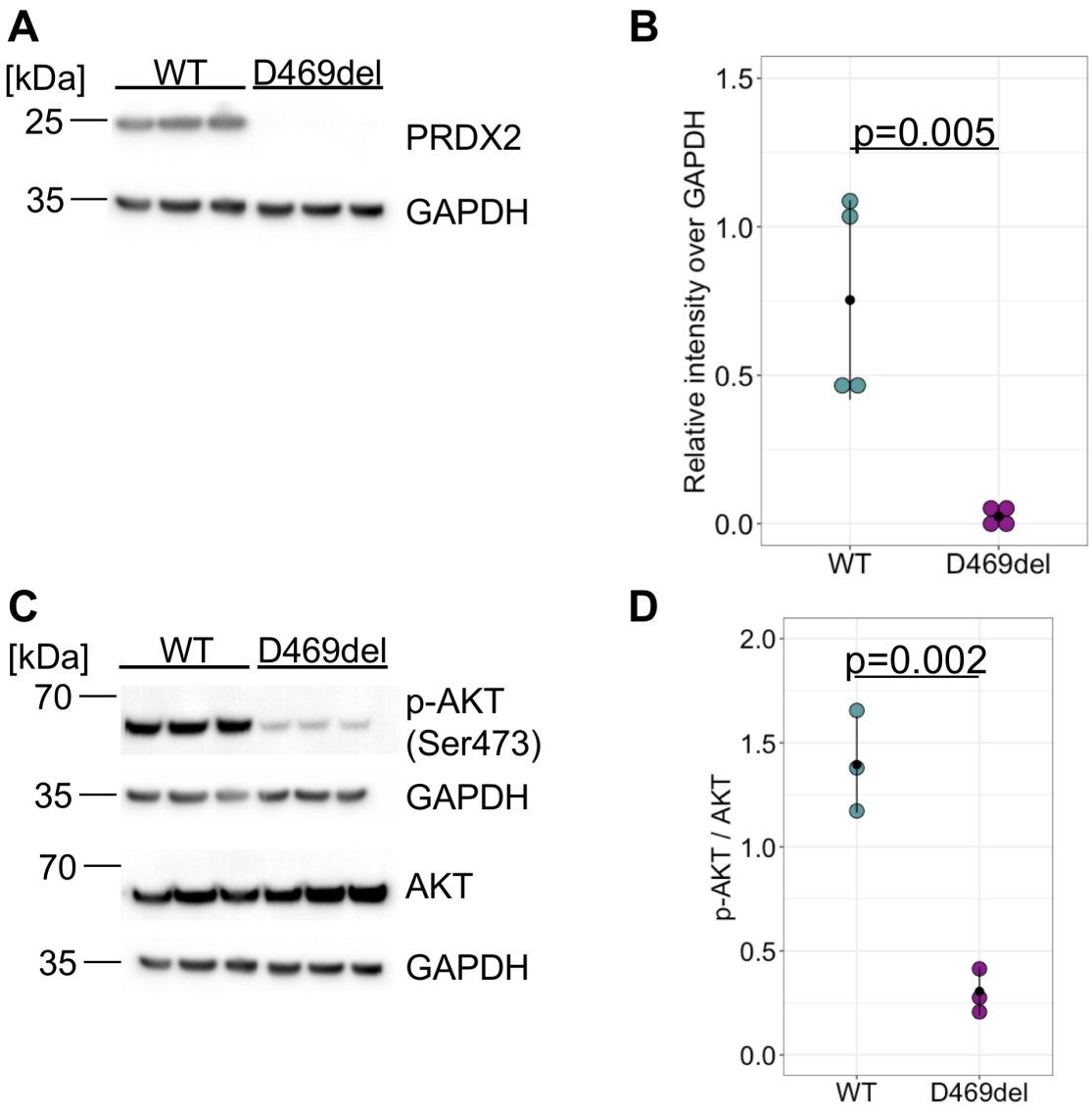

Figure 6.2 – Decreased PRDX2 protein levels and a reduction in phosphorylation of AKT in D469del COMP-overexpressing HT1080 cells. (A) Western blot and (B) quantification of peroxiredoxin-2 (PRDX2) protein levels. PRDX2 was drastically reduced in D469del COMP HT1080 cells, n = 4 experiments. (C) Western blot of phosphorylated and total AKT and (D) quantification of AKT phosphorylation levels, n = 3 experiments. GAPDH was used as loading control. Black dots represent mean values, bars show standard deviation, *P*-values were determined using student's t-test.

6.3 Energy status and oxygen availability in D469del COMP cells

As insulin and insulin-like signalling is closely tied to metabolic regulation, this finding raised the question as to whether the expression of p.D469del COMP affected cellular metabolism. To assess the energy balance in D469del COMP cells, the phosphorylation status of AMP-activated kinase (AMPK) was examined by western blotting (Figure 6.3 A, B). When activated, AMPK increases the uptake of glucose and fatty acids and their oxidation, whilst inhibiting energy-expensive processes such as lipid and protein biosynthesis. AMPK is activated by phosphorylation, and when energy demand is high and ATP is used quicker than it is produced, AMP or ADP binding to AMPK protect its phosphorylation from phosphatases. Conversely, if the concentration of ATP is high, ATP displaces AMP or ADP, allowing access of phosphatases and deactivation of AMPK. Whilst there appeared to be a trend for increased phosphorylation of AMPK in D469del COMP cells, this was not statistically significant (Figure 6.3 B). This indicated that there appeared to be no significant energy deficiency in D469del COMP cells. It has however been demonstrated in the past that ER stress raises the demand for ATP, e.g. to allow chaperones to facilitate protein folding (Yong et al., 2019). Therefore, it was possible that D469del COMP cells adjust metabolic processes, such as increasing oxidative phosphorylation, to overcome this insult. Elevated mitochondrial activity would further explain the increase in ROS.

Whilst the metabolism is regulated by numerous mechanisms, one factor that plays an important role is hypoxia-inducible factor 1 α (HIF1α). Under normoxic conditions, HIF1α is constantly ubiquitinated and degraded. During hypoxic conditions, HIF1α is stabilised and supresses oxygen-expensive processes, such as oxidative phosphorylation whilst activating anaerobic glycolysis. In cartilage development, Hif1α is particularly important for chondrocyte survival in the hypoxic environment (Schipani et al., 2001). When HIF1α was detected by western blotting (Figure 6.3, C and D), a single band of ~120 kDa was detected which corresponded to the expected molecular weight of mature fully post-translationally modified HIF1α. A more diffuse band was also detected at around 180 kDa, potentially corresponding to ubiquitinated HIF1α. No significant difference was observed between wild type and D469del COMP cells, although on average HIF1α_{120} levels appeared slightly lower in D469del COMP-overexpressing cells.

Both oxygen availability as well as nutrient levels are known to regulate autophagy. AMPK is a known regulator of autophagy which can stimulate autophagy by phosphorylating ULK1, linking the cellular energy status directly to autophagosome biogenesis. Furthermore, the retention of misfolded COMP in the ER may affect autophagy. When levels of the autophagy marker LC3B - which is converted from LC3B-I to LC3B-II during active autophagy - were examined (Figure 6.4 A, B), D469del COMP-overexpressing cells displayed only slightly, and not significantly, reduced levels of LC3B-II. This was also observed for the ratio of LC3B-II to LC3B-I (Figure 6.4 C).

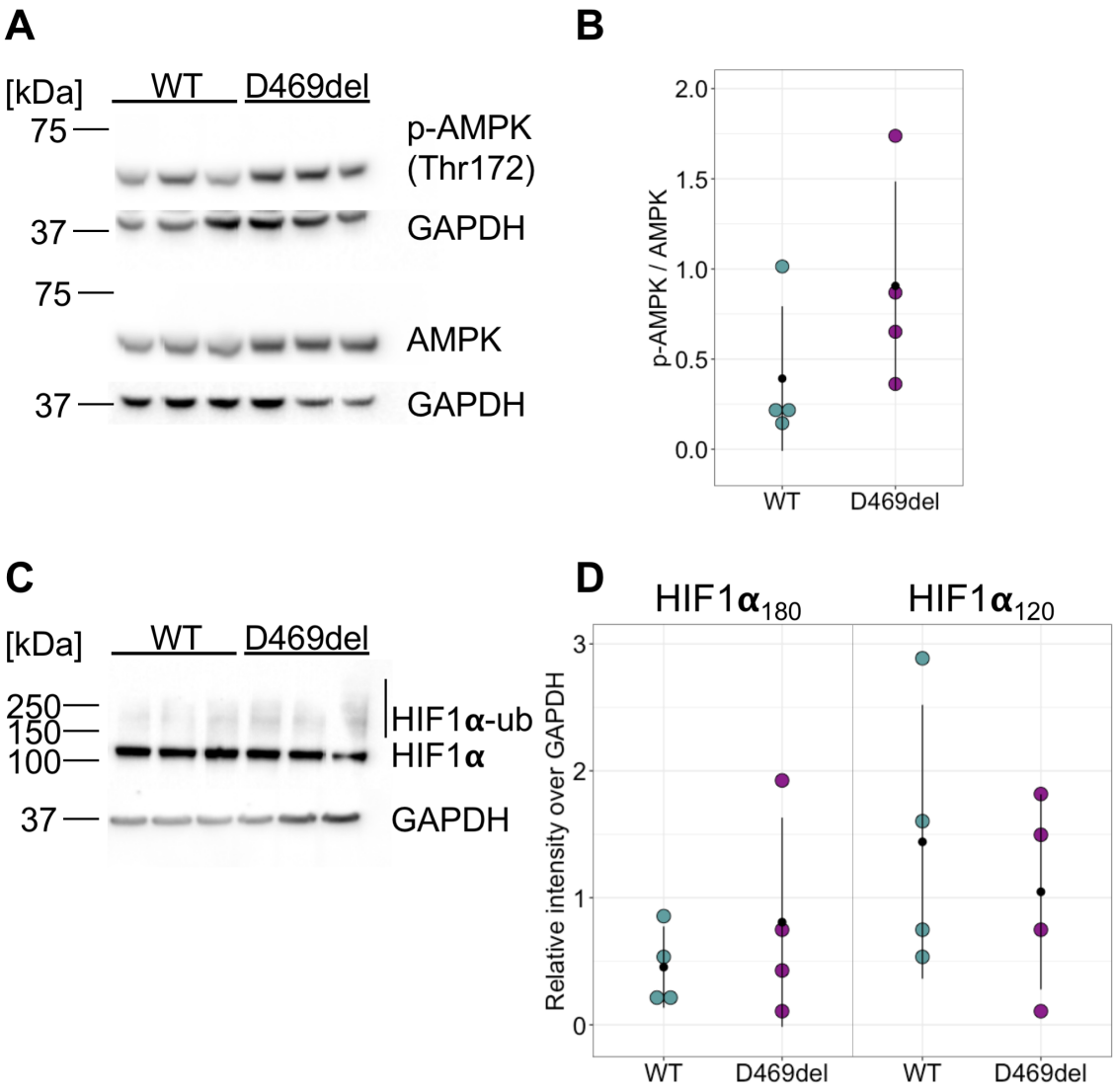

Figure 6.3 – Energy balance as well as oxygen availability appear unaffected by overexpression of D469del COMP. (A) Western blot and (B) quantification of the ratio of phosphorylated to total AMPK. Membranes shown in Figure 5.6 A (p-/total eiF2α) were re-incubated with (p-)AMPK antibodies, therefore the same GAPDH is shown as loading control. (C) Western blot and (D) quantification of HIF1α protein species, n = 4 experiments. GAPDH was used as loading control. Black dots represent mean values, bars show standard deviation, *P*-values were determined using student's t-test.

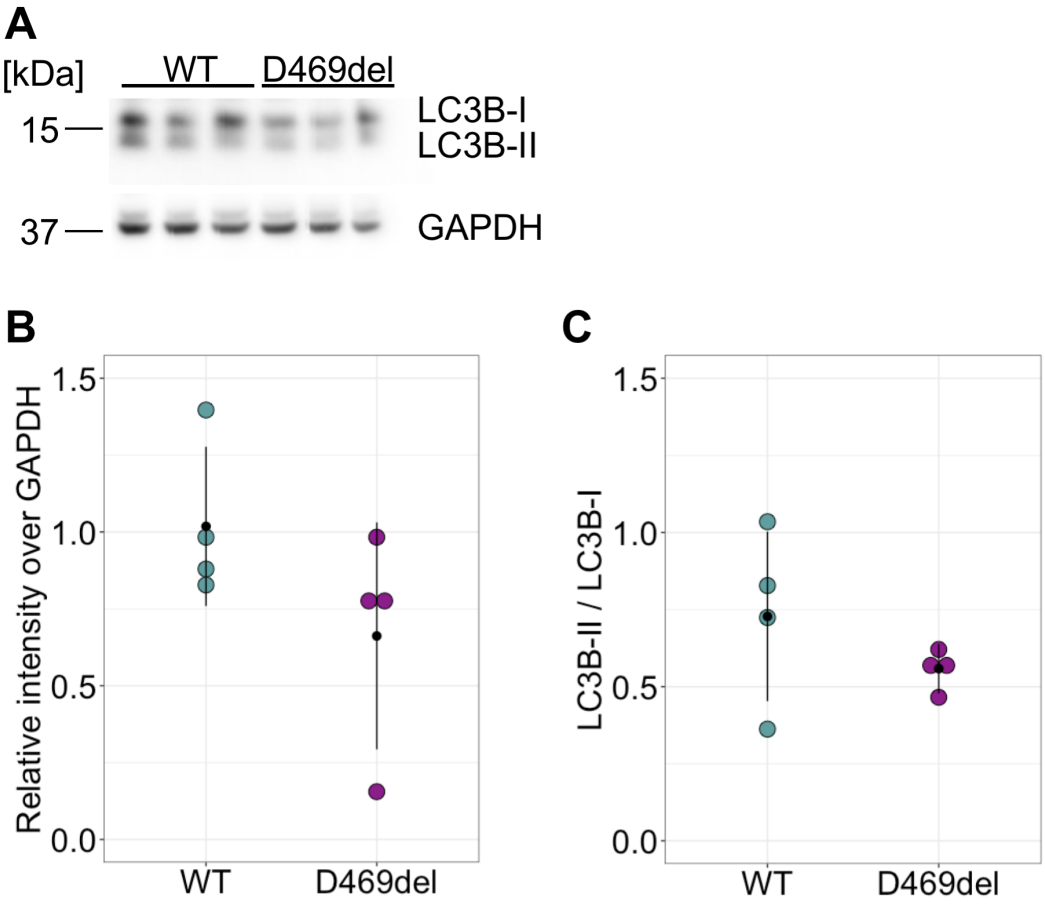

Figure 6.4 – Forms of LC3B in D469del COMP cells. (A) Western blot and (B) Quantification of LC3B-II and (C) the ratio of LC3B-II over LC3B-I. GAPDH was used as loading control, n = 4 experiments. Membrane shown in Figure 5.6 A (total eiF2α) were re-incubated with anti LC3B antibody, therefore the same GAPDH is shown as loading control. Black dots represent mean values, bars show standard deviation, *P*-values were determined using student's t-test.

6.4 Use of RNA sequencing to assess consequences of D469del COMP overexpression

To gain a more comprehensive understanding of the molecular consequences of mutant COMP accumulation, RNA sequencing was performed. RNA was extracted from wild type and D469del COMP overexpressing HT1080 cells at 72 hrs after confluency. Quality of RNA samples (n = 4 per cell line) submitted was assessed initially by non-denaturing agarose gel electrophoresis which demonstrated two distinct bands and no visible signs of degradation (Figure 6.5 A). Quality was also evaluated based on potential protein ($A_{260/280}$) and solvent ($A_{260/230}$) contamination (Figure 6.5 B). Since all $A_{260/280}$ values were higher than 2 the RNA was deemed suitable for RNA sequencing. After RNA was treated with DNase I, samples were submitted to the Genomics Core Facility at Newcastle University for a second step of quality control and subsequent RNA sequencing.

Analysis of RNA sequencing data (n = 3 per cell line) was performed using the Galaxy platform (Afgan et al., 2018). After quality control of the resulting RNA sequencing data, 75 – 80 % of reads mapped uniquely to the reference transcriptome (hg38) using HISAT2 (Kim et al., 2019). Of these, 60 % were assigned to exons. 70 % were unique read pairs. The tool featureCounts (Liao et al., 2014) was used to generate counts before limma-voom (Law et al., 2014; Ritchie et al., 2015) was used to analyse differentially expressed genes (DEGs).

Analysis resulted in the identification of a total of 988 differentially expressed genes (DEGs), with an adjusted *P*-value < 0.05 and fold change > $\pm$1.5 ($\log_2$ fold change > $\pm$0.58), of which 465 were upregulated and 523 downregulated in D469del COMP compared to wild type COMP overexpressing cells (Figure 6.6). KEGG pathway analysis was then performed using Enrichr (Kuleshov et al., 2016) for all DEGs, and up- and downregulated genes separately. KEGG pathways associated with downregulated genes were mainly involved in the PI3K-AKT signalling pathway, pathways in cancer, ECM-receptor interaction and the lysosome (Table 6.1). This was consistent with the previously observed reduction in AKT phosphorylation. Furthermore, a striking decrease in *PRDX2* expression (0.001-fold) was observed, consistent with the previously observed reduction in PRDX2 protein. More KEGG pathways were found to be associated with upregulated genes, including cellular

senescence, cell cycle, NFκB signalling, and various types of cancer pathways (Table 6.2).

When KEGG pathway analysis was performed on all 988 DEGs, a total of 41 pathways were identified (Table 6.3), many of which overlapped with the previous analysis. Some pathways were only identified when all DEGs were analysed together, including focal adhesion, fluid shear stress and atherosclerosis, complement and coagulation cascades as well as rheumatoid arthritis.

None of the terms associated with DEGs indicated the presence of the unfolded protein response or ER stress, confirming previous observations. Instead, it appeared the stress caused by p.D469del COMP expression and the resulting inflammation caused altered cellular signalling via multiple pathways, ultimately leading to changes in cell cycle regulation and senescence.

The receptor NOTCH3 (*NOTCH3)* and the notch ligand JAGGED1 (*JAG1)* were both drastically downregulated (0.002- and 0.27-fold, respectively) in D469del COMP-overexpressing cells. Studies in the context of breast cancer cells have shown that COMP interacts with the NOTCH3-JAGGED1 signalling axis directly (Papadakos et al., 2019). More specifically, secreted COMP facilitates the interaction between NOTCH3 and its ligand JAGGED1 in breast cancer models thereby leading to increased numbers of breast cancer stem cells.

COMP is part of the thrombospondin protein family with *THBS3* and *THBS4* being the most similar to *COMP*. Neither *THBS3* nor *THBS4* were differentially expressed in D469del COMP cells, but both *THBS1* and *THBS2* were upregulated (4- and 2.8-fold, respectively).

In summary, the results of the RNA sequencing experiment suggested that indeed there was no typical ER stress response apparent in D469del COMP HT1080 cells. Instead, a complex interplay between altered ECM organisation, impaired signalling, and increased inflammation was observed. Altered ECM turnover, impaired cellular metabolism and changes in cell cycle regulation may ultimately result in apoptosis. To effectively develop a drug treatment, the identification of a reliable *in vitro* marker for COMP-induced stress is needed.

A

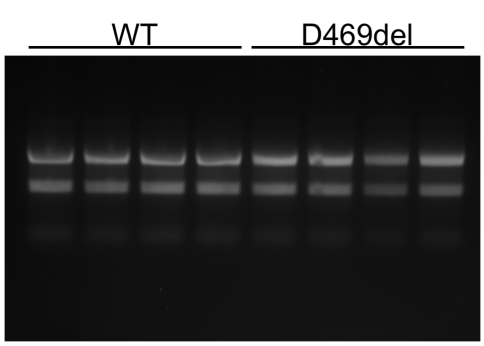

B

Sample	Concentration [ng/µL]	$A_{260/280}$	$A_{260/230}$
WT1	462.5	2.05	2.04
WT2	412.2	2.07	1.45
WT3	461.9	2.05	1.95
WT4	441.1	2.04	2.16
D469del1	412.5	2.07	1.26
D469del2	403	2.05	1.75
D469del3	249.1	2.07	1.88
D469del4	370.9	2.06	1.28

Figure 6.5 – Quality of RNA samples. (A) Non-denaturing agarose gel electrophoresis was performed for initial assessment of RNA quality. Two distinct bands are clearly visible with no smear. (B) Concentrations and $A_{260/280}$ and $A_{260/230}$ scores of RNA samples submitted for RNA sequencing.

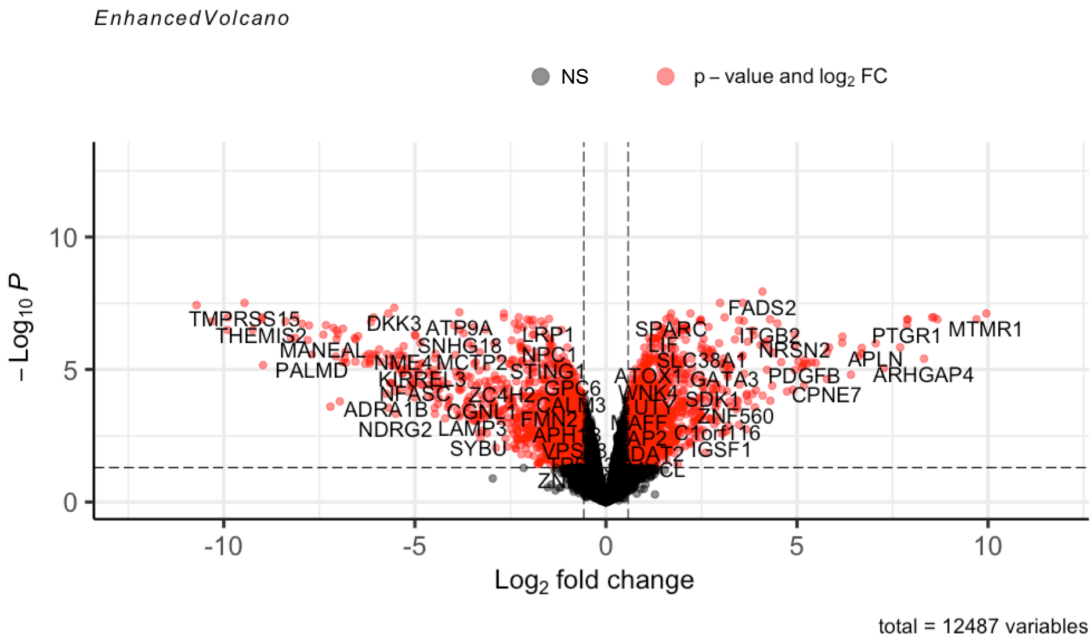

Figure 6.6 – Volcano plot of RNA sequencing results. Differentially expressed genes (Log_2 fold change > 0.58 (fold change of 1.5), adj. *P*-value < 0.05) are represented in red, other genes in grey.

Term	Overlap	Adjusted *P*-value	Genes
PI3K-AKT signalling pathway	24/354	0.003	*CSF1R, ITGA4, BDNF, ITGB4, LAMA1, ITGB3, LAMA3, LPAR3, GNG11, VEGFA, COMP, EFNA1, NR4A1, KITLG, IL6, CCND2, PPP2R2C, CREB3L1, GNG7, DDIT4, ITGA11, IL2RB, SPP1, FGFR3*
Pathways in Cancer	31/530	0.003	*NOTCH3, CSF1R, EPAS1, LAMA1, LAMA3, LPAR3, GLI1, CCND2, RASSF5, GNG7, BDKRB2, BDKRB1, GSTM3, ARNT2, JAG1, GSTM1, JUP, GSTO2, WNT5B, DCC, FOS, GNG11, AGT, VEGFA, TGFBR2, KITLG, IL6, IL2RB, CALM3, PLCB1, FGFR3*
ECM-receptor interaction	9/82	0.022	*COMP, ITGA4, ITGB4, LAMA1, SV2A, ITGB3, LAMA3, ITGA11, SPP1*
Lysosome	11/123	0.23	*ASAH1, GM2A, NPC1, CTSL, SORT1, LAMP3, ACP5, CTSH, NAGA, DNASE2, LITAF*
Apelin Signalling Pathway	11/137	0.046	*NOTCH3, EGR1, JAG1, MRAS, GNG7, ITPR1, SPP1, CALM3, PLCB1, PPARGC1A, GNG11*
Human papillomavirus infection	19/330	0.047	*NOTCH3, JAG1, WNT5B, ITGA4, ITGB4, LAMA1, ITGB3, LAMA3, MX1, TUBG2, VEGFA, OASL, COMP, CCND2, DLG3, PPP2R2C, CREB3L1, ITGA11, SPP1*

Table 6.1 – KEGG pathways associated with downregulated genes. Overlap: The number of genes from the input (i.e. downregulated genes) relative to the total number of genes in this pathway, for example in the PI3K-AKT signalling pathway 24 out of 354 genes are significantly downregulated in D469del COMP cells.

Term	Overlap	Adjusted *P*-value	Genes
Bladder cancer	8/41	0.0008	*CXCL8, CCND1, MMP1, DAPK1, E2F1, THBS1, MMP9, HBEGF*
Small cell lung cancer	11/93	0.0011	*LAMA5, CDK6, CCND1, GADD45B, GADD45A, E2F1, BCL2, RARB, LAMC2, TRAF1, BIRC3*
Pathways in cancer	28/530	0.0035	*LAMA5, CXCL8, PDGFB, LAMC2, ADCY1, CCND1, PLCG2, E2F1, EDN1, TGFB2, SMAD3, GADD45B, DAPK1, TXNRD2, GADD45A, MMP1, TXNRD1, WNT5A, TRAF1, MMP9, BMP2, PLCB4, CDK6, BCL2, RARB, FGFR4, CALM2, BIRC3*
Cellular senescence	13/160	0.0053	*TGFB2, SMAD3, CXCL8, GADD45B, GADD45A, CDC25A, HIPK2, RAD50, CDK6, CCND1, E2F1, MYBL2, CALM2*
Glioma	8/75	0.015	*CDK6, CCND1, GADD45B, GADD45A, PDGFB, E2F1, PLCG2, CALM2*
AGE-RAGE signalling pathway in diabetic complications	9/100	0.018	*TGFB2, EDN1, SMAD3, CXCL8, PLCB4, CCND1, IL1B, PLCG2, BCL2*
Hepatocellular carcinoma	12/168	0.018	*TGFB2, SMAD3, CDK6, CCND1, GADD45B, GADD45A, TXNRD2, TXNRD1, WNT5A, PLCG2, E2F1, DPF3*
Cell cycle	10/124	0.018	*TGFB2, SMAD3, CDK6, CDC45, CCND1, GADD45B, GADD45A, E2F1, MCM4, CDC25A*
Non-small cell lung cancer	7/66	0.02	*CDK6, CCND1, GADD45B, GADD45A, E2F1, PLCG2, RARB*
Malaria	6/49	0.02	*TGFB2, CXCL8, IL1B, ITGB2, THBS2, THBS1*
Transcriptional misregulation in cancer	12/186	0.025	*FUT8, HHEX, CXCL8, GADD45B, GADD45A, PLAT, ETV1, UTY, TRAF1, MMP9, SSX1, BIRC3*
Melanoma	7/72	0.025	*CDK6, CCND1, GADD45B, GADD45A, PDGFC, PDGFB, E2F1*
NF-kappa B signalling pathway	8/95	0.025	*CARD10, CXCL8, GADD45B, IL1B, PLCG2, BCL2, TRAF1, BIRC3*
Amoebiasis	8/96	0.025	*LAMA5, TGFB2, CXCL8, PLCB4, IL1B, ITGB2, LAMC2, ADCY1*

Pancreatic cancer	7/75	0.025	*TGFB2, SMAD3, CDK6, CCND1, GADD45B, GADD45A, E2F1*
Prostate cancer	8/97	0.025	*CCND1, PDGFC, PDGFB, BCL2, E2F1, PLAT, MMP9, CREB5*
Chronic myeloid leukemia	7/76	0.025	*TGFB2, SMAD3, CDK6, CCND1, GADD45B, GADD45A, E2F1*
Parathyroid hormone synthesis, secretion and action	8/106	0.041	*PLCB4, PDE4D, BCL2, GATA3, PTH1R, ADCY1, CREB5, HBEGF*
TNF signalling pathway	8/110	0.049	*EDN1, IL1B, LIF, TRAF1, CXCL3, MMP9, CREB5, BIRC3*

Table 6.2 – KEGG pathways associated with upregulated genes. Overlap: The number of genes from the input (i.e. upregulated genes) relative to the total number of genes in this pathway.

Term	Overlap	Adjusted *P*-value	Genes
Pathways in cancer	59/531	0.0000017	*CXCL8, LAMC2, GLI1, CCND2, CCND1, RASSF5, BDKRB2, BDKRB1, EDN1, GSTO2, WNT5B, DAPK1, DCC, MMP1, WNT5A, FOS, TRAF1, MMP9, TGFBR2, PLCB4, RARB, PLCB1, BIRC3, CSF1R, NOTCH3, LAMA5, EPAS1, LAMA1, LAMA3, PDGFB, LPAR3, ADCY1, GNG7, PLCG2, E2F1, GSTM3, ARNT2, TGFB2, GSTM1, JAG1, SMAD3, JUP, GADD45B, TXNRD2, GADD45A, TXNRD1, GNG11, AGT, VEGFA, KITLG, BMP2, IL6, CDK6, IL2RB, BCL2, CALM3, FGFR4, CALM2, FGFR3*
AGE-RAGE signalling pathway in diabetic complications	17/100	0.00076	*EGR1, TGFB2, EDN1, SMAD3, CXCL8, F3, AGT, TGFBR2, VEGFA, MAPK11, IL6, PLCB4, CCND1, IL1B, PLCG2, BCL2, PLCB1*
Cellular senescence	22/156	0.00076	*TGFB2, SMAD3, CXCL8, GADD45B, GADD45A, ITPR1, CDC25A, TGFBR2, HIPK2, MAPK11, IL6, RAD50, CCND2, CDK6, MRAS, CCND1, RASSF5, E2F1, CALM3, MYBL2, E2F5, CALM2*
Apelin signalling pathway	20/137	0.00086	*NOTCH3, EGR1, JAG1, SMAD3, ITPR1, PLAT, ADCY1, GNG11, PIK3CG, APLN, MRAS, PLCB4, CCND1, GNG7, SPP1, CALM3, CCN2, PLCB1, PPARGC1A, CALM2*
Bladder cancer	10/41	0.001	*CXCL8, CCND1, DAPK1, MMP1, E2F1, THBS1, MMP9, FGFR3, VEGFA, HBEGF*
ECM-receptor interaction	15/88	0.001	*LAMA5, ITGA4, SDC4, ITGB4, LAMA1, ITGB3, LAMA3, LAMC2, THBS2, THBS1, COMP, FRAS1, SV2A, ITGA11, SPP1*
PI3K-AKT signalling pathway	36/354	0.001	*CSF1R, LAMA5, ITGB4, LAMA1, ITGB3, LAMA3, PDGFB, LPAR3, LAMC2, THBS2, THBS1, PIK3CG, COMP, CCND2, CCND1, CREB3L1, GNG7, PDGFC, SPP1, ITGA4, BDNF, GNG11, VEGFA, EFNA1, NR4A1, KITLG, IL6, CDK6, PPP2R2C, DDIT4, ITGA11, IL2RB, BCL2, FGFR4, FGFR3, CREB5*
Rap1 signalling pathway	24/210	0.003	*VAV3, FARP2, CSF1R, ITGB3, ITGB2, PDGFB, LPAR3, ADCY1, THBS1, VEGFA, EFNA1, MAPK11, KITLG, MRAS, PLCB4, RASSF5, PDGFC, CALM3, PLCB1, RAPGEF5, DRD2, FGFR4, CALM2, FGFR3*

Malaria	10/50	0.003	*COMP, TGFB2, IL6, CXCL8, LRP1, IL1B, ITGB2, PECAM1, THBS2, THBS1*
Amoebiasis	15/102	0.003	*SERPINB3, SERPINB4, LAMA5, TGFB2, CXCL8, LAMA1, ITGB2, LAMA3, LAMC2, ADCY1, CXCL3, IL6, PLCB4, IL1B, PLCB1*
Focal adhesion	23/201	0.003	*VAV3, LAMA5, ITGA4, ITGB4, LAMA1, ITGB3, LAMA3, PDGFB, PARVA, LAMC2, THBS2, THBS1, VEGFA, COMP, CCND2, CCND1, PDGFC, ITGA11, SPP1, BCL2, FLNC, MYL9, BIRC3*
Fluid shear stress and atherosclerosis	18/139	0.003	*GSTM3, EDN1, GSTM1, SDC4, GSTO2, ITGB3, PDGFB, PLAT, FOS, MMP9, VEGFA, MAPK11, CTSL, IL1B, BCL2, PECAM1, CALM3, CALM2*
Transcriptional misregulation in cancer	22/192	0.004	*CSF1R, ARNT2, CXCL8, GADD45B, JUP, GADD45A, MMP3, PLAT, ETV1, TRAF1, MMP9, TGFBR2, BAIAP3, FUT8, IL6, HHEX, CCND2, NR4A3, IL2RB, NUPR1, SSX1, BIRC3*
Parathyroid hormone synthesis, secretion and action	15/106	0.004	*EGR1, PDE4D, ITPR1, GATA3, PTH1R, FOS, ADCY1, NR4A2, PLCB4, MMP15, CREB3L1, BCL2, PLCB1, CREB5, HBEGF*
Lysosome	16/128	0.009	*ASAH1, SORT1, FUCA2, CLTC, LAPTM5, NAGA, ABCB9, LITAF, GM2A, NPC1, CTSL, LAMP3, ACP5, CTSH, DNASE2, ARSG*
Small cell lung cancer	13/92	0.009	*LAMA5, GADD45B, LAMA1, GADD45A, LAMA3, LAMC2, TRAF1, CDK6, CCND1, E2F1, BCL2, RARB, BIRC3*
Complement and coagulation cascades	12/85	0.014	*F8, SERPINB2, C1R, PROS1, ITGB2, BDKRB2, ITGAX, BDKRB1, PLAT, F3, CD55, F2RL2*
TNF signalling pathway	14/112	0.018	*EDN1, JAG1, MMP3, LIF, FOS, TRAF1, CXCL3, MMP9, MAPK11, IL6, CREB3L1, IL1B, BIRC3, CREB5*
Renin secretion	10/69	0.026	*EDN1, PLCB4, PDE1C, ITPR1, PDE3A, CALM3, REN, PLCB1, CALM2, AGT*
Human papillomavirus infection	29/331	0.026	*NOTCH3, LAMA5, ITGB4, LAMA1, ITGB3, LAMA3, LAMC2, THBS2, THBS1, OASL, COMP, CCND2, CCND1, CREB3L1, SPP1, E2F1, HES4, JAG1, WNT5B, ITGA4, WNT5A, MX1, TUBG2, VEGFA, CDK6, DLG3, PPP2R2C, ITGA11, CREB5*
Rheumatoid arthritis	10/93	0.026	*TGFB2, IL6, CXCL8, CTSL, MMP1, IL1B, ITGB2, MMP3, ACP5, FOS, CXCL3, VEGFA*

Vascular smooth muscle contraction	15/133	0.029	*EDN1, ITPR1, PLA2G3, PLA2G4A, ADCY1, ADRA1B, AGT, PLCB4, KCNMB4, CALM3, PLCB1, MYL9, MYH10, CALM2, PRKG1*
Proteoglycans in cancer	20/205	0.033	*VAV3, TGFB2, SDC4, WNT5B, ITGB3, WNT5A, ITPR1, MIR21, MMP9, THBS1, VEGFA, MAPK11, MRAS, CCND1, CTSL, PLCG2, HCLS1, FLNC, EZR, HBEGF*
Adrenergic signalling in cardiomyocytes	16/150	0.033	*ADCY1, ATP2B1, ADRA1B, PIK3CG, AGT, MAPK11, CACNB4, PLCB4, PPP2R2C, CREB3L1, BCL2, CALM3, SCN5A, PLCB1, CALM2, CREB5*
Aldosterone synthesis and secretion	10/98	0.033	*NR4A2, NR4A1, PLCB4, CREB3L1, ITPR1, CALM3, ADCY1, ATP2B1, PLCB1, CALM2, AGT, CREB5*
Inflammatory mediator regulation of TRP channels	10/98	0.033	*MAPK11, PLCB4, IL1B, ITPR1, PLCG2, BDKRB2, BDKRB1, PLA2G4A, CALM3, ADCY1, PLCB1, CALM2*
cGMP-PKG signalling pathway	17/167	0.035	*ITPR1, ADCY1, ATP2B1, ADRA1B, PIK3CG, PLCB4, CREB3L1, PDE3A, BDKRB2, KCNMB4, CALM3, PDE5A, PLCB1, MYL9, CALM2, PRKG1, CREB5*
Human cytomegalovirus infection	21/225	0.035	*CXCL8, ITGB3, ITPR1, CGAS, ADCY1, GNG11, VEGFA, MAPK11, IL6, PLCB4, CDK6, STING1, CCND1, CREB3L1, IL1B, GNG7, E2F1, CALM3, PLCB1, CALM2, CREB5*
Hepatocellular carcinoma	17/1678	0.035	*GSTM3, TGFB2, GSTM1, SMAD3, WNT5B, GADD45B, GSTO2, GADD45A, TXNRD2, TXNRD1, WNT5A, TGFBR2, CDK6, CCND1, PLCG2, E2F1, DPF3*
Pancreatic cancer	10/76	0.035	*TGFB2, SMAD3, CDK6, CCND1, GADD45B, GADD45A, E2F1, TGFBR2, ARHGEF6, VEGFA*
Glutamatergic synapse	13/114	0.035	*SLC38A1, HOMER2, ITPR1, PLA2G4A, ADCY1, GNG11, GRK3, PLCB4, GNG7, SLC17A7, PLCB1, GLUL, SHANK3*
Chagas disease	12/102	0.035	*MAPK11, TGFB2, IL6, CXCL8, PLCB4, PPP2R2C, IL1B, BDKRB2, FOS, ADCY1, PLCB1, TGFBR2*
Cortisol synthesis and secretion	9/65	0.035	*NR4A1, PLCB4, CREB3L1, ITPR1, ADCY1, PLCB1, KCNK2, AGT, CREB5*
Purine metabolism	14/129	0.035	*PDE1C, PDE4D, AK3, NME3, NME4, AK5, AMPD3, ADCY1, PDE3A, ENPP1, ENPP4, PDE5A, PDE7B, ADA*

Relaxin signalling pathway	14/129	0.035	*EDN1, MMP1, FOS, ADCY1, GNG11, MMP9, TGFBR2, VEGFA, MAPK11, PLCB4, CREB3L1, GNG7, PLCB1, CREB5*
Regulation of actin cytoskeleton	20/218	0.043	*VAV3, ITGA4, ITGB4, ITGB3, ITGB2, PDGFB, MRAS, SCIN, SPATA13, PDGFC, ITGA11, BDKRB2, ITGAX, BDKRB1, EZR, FGFR4, MYL9, MYH10, FGFR3, ARHGEF6*
Phospholipase D signalling pathway	15/148	0.045	*CXCL8, PDGFB, PLA2G4A, LPAR3, ADCY1, PIK3CG, AGT, KITLG, MRAS, PLCB4, PDGFC, PLCG2, PLPP3, PLCB1, DGKI*
Th17 cell differentiation	12/107	0.045	*MAPK11, IL6, SMAD3, IL1B, IL2RB, RORC, IL21R, AHR, GATA3, FOS, IL27RA, TGFBR2*
IL-17 signalling pathway	11/94	0.045	*FOSL1, MAPK11, IL6, CXCL8, MMP1, IL1B, MMP3, FOS, CXCL3, IL17RC, MMP9*
Hippo signalling pathway	16/163	0.046	*TGFB2, SMAD3, WNT5B, WNT5A, ITGB2, AMOT, TGFBR2, BMP2, CCND2, CCND1, DLG3, PPP2R2C, CCN2, NF2, TEAD2, BIRC3*
Kaposi sarcoma-associated herpesvirus infection	18/193	0.046	*CXCL8, PDGFB, ITPR1, FOS, CXCL3, GNG11, PIK3CG, VEGFA, PREX1, MAPK11, IL6, CDK6, CCND1, GNG7, PLCG2, E2F1, CALM3, CALM2*

Table 6.3 – KEGG pathways associated with DEGs. Overlap: The number of genes from the input (i.e. DEGs) relative to the total number of genes in this pathway.

6.5 Validation of selected targets identified by RNA sequencing

To successfully identify a marker of COMP-induced stress, several DEGs identified by RNA sequencing were firstly validated by qRT-PCR.

Four genes of interest were selected for the initial validation: *GALNT18*, *MMP1, MMP9* and *SOX9*. *SOX9* is a known master regulator of chondrogenesis and is an essential factor for cartilage and bone formation in murine limb buds (Akiyama et al., 2002). *MMP1* and *MMP9* are both secreted matrix metalloproteinases, with roles in remodelling of the extracellular matrix, endochondral ossification and skeletal diseases (Ortega et al., 2004; Pardo and Selman, 2005; Stickens et al., 2004). In addition, secreted enzymes exhibit many desirable characteristics of a biomarker. Firstly, they can be detected readily outside of cells and thus no cell isolation and lysis are necessary. Secondly, MMPs are known to be involved in inflammation and inflammatory diseases, and both *MMP1* and *MMP9* have been shown to be regulated at least in part by NFκB signalling (Di Girolamo et al., 2006; Vincenti and

Brinckerhoff, 2002; Zhu et al., 2014). *GALNT18* was selected because it has been implicated in ER stress although relatively little is known about its function (Jia et al., 2021; Li et al., 2012; Shan et al., 2019). When gene expression was analysed by qRT-PCR, expression of *GALNT18, MMP1* and *MMP9* was found to be elevated (Figure 6.7 A). *SOX9* was not found to be differentially expressed by qRT-PCR (Figure 6.7 A). For *GALNT18, MMP1* and *MMP9,* the Log_2 fold changes obtained by RNA sequencing were 5.38, 2.79 and 3.87, respectively. The Log_2 fold changes obtained by qRT-PCR were 4.2, 1.7 and 3.2, respectively.

The elevated expression of *MMP9* was of particular interest. Firstly, MMP9 is a secreted enzyme, meaning it can be detected extracellularly. For a biomarker, this eliminates the need to isolate cells (in the case of patients) and/or prepare cell lysates and RNA to measure gene expression. Instead, conditioned media (in the case of cells), or more easily obtainable body fluids (in the case of patients) could serve as samples. Secondly, because MMP9 digests collagens of the extracellular matrix, extracellular MMP9 activity can be measured conveniently by gelatin zymography or activity assays employing fluorogenic substrates. Thirdly, MMP9 has been implicated in various disorders by other studies (Gossage et al., 2018; Marshall et al., 2015; Xue et al., 2014), one of which observed increased MMP9 activity after the loss of type IX collagen (Heilig et al., 2020). Notably, the loss of type IX collagen also leads to reduced anchorage of COMP in the cartilage ECM. Therefore, I wished to determine whether the observed change in *MMP9* expression would result in an increase of MMP9 activity in conditioned media of D469del COMP-overexpressing cells. Gelatin zymography of concentrated conditioned media revealed that indeed MMP9 activity was increased in D469del COMP-overexpressing cells (Figure 6.7 B). In contrast, no difference was observed in the activity of the closely related MMP2 (Figure 6.7 B) or *MMP2* expression according to RNA sequencing.

Previous work has demonstrated that TGFβ is able to regulate MMP9 expression via AP1 and NFκb (Safina et al., 2008; Zhu et al., 2014). *TGFB2* and *SMAD3* were found to be upregulated in D469del COMP cells by RNA sequencing, but *TGFBR2,* the gene that encodes for TGFβ type II receptor (TGFBR2), was downregulated. Upon ligand binding, TGFBR2 recruits and phosphorylates the TGFβ type I receptor which then proceeds to phosphorylate downstream targets, including SMAD2 and SMAD3. Therefore, it was investigated whether there was a change in active TGFβ signalling,

using the phosphorylation status of both SMAD2 and SMAD3 as a read-out. A reduction in phosphorylation was observed for SMAD2 (Figure 6.8 A, B), consistent with a downregulation of *TGFBR2*, but not for SMAD3 (Figure 6.8 A, C). There was no significant increase in total SMAD2 protein level (Figure 6.8 A, D), and whilst the increase in *SMAD3* expression observed by RNA sequencing did appear to result in elevated SMAD3 protein levels, this failed to reach statistical significance (Figure 6.8, A, E).

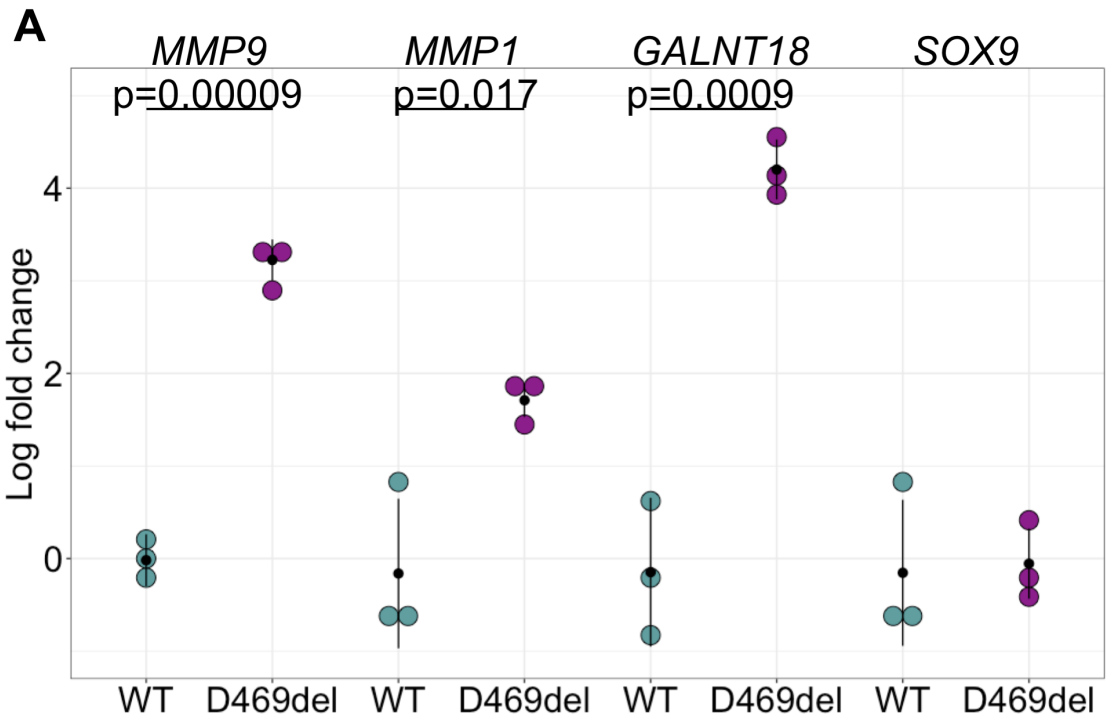

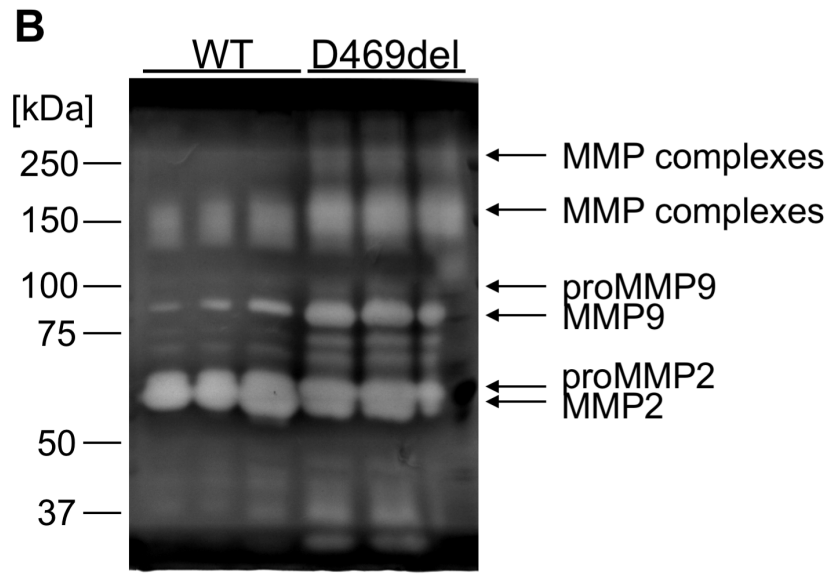

Figure 6.7 – Changes in gene expression originally uncovered by RNA sequencing are also detected by other methods. (A) qRT-PCR analysis of four selected DEGs in wild type (WT) and D469del COMP-overexpressing HT1080 cells. Three out of four selected DEGs display significantly changed expression. Data is presented as Log_2 fold change. 18S was used as housekeeping gene. Black dots represent mean values, bars show standard deviation, *P*-values were determined using student's t-test. (B) Gelatin zymography of concentrated, conditioned media of wild type (WT) and D469del COMP-overexpressing HT1080 cells. Changes in *MMP9* expression translate into increased MMP9.

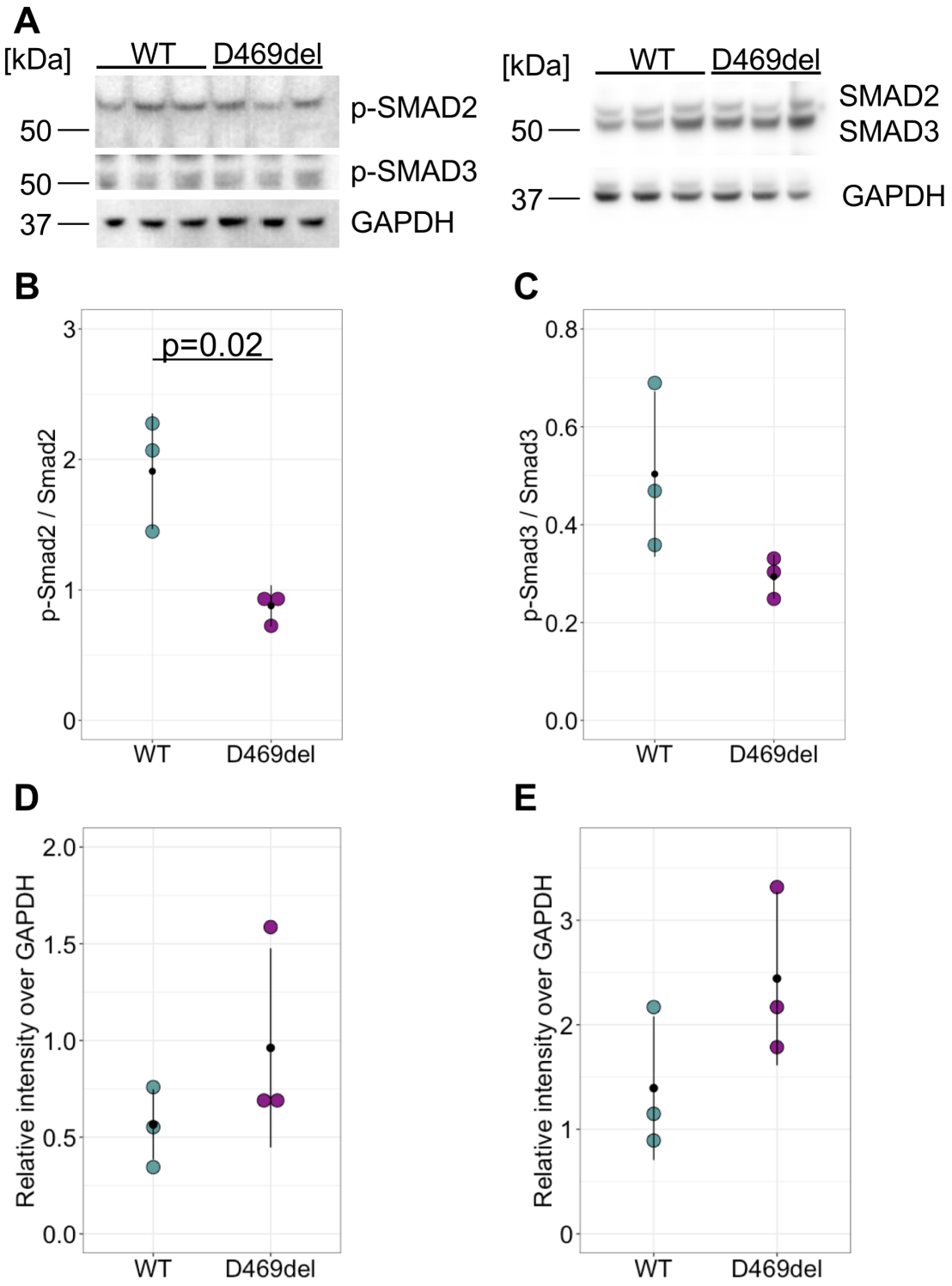

Figure 6.8 – Examination of TGFβ signalling in D469del COMP-overexpressing HT1080 cells. (A) Western blot, (B) quantification of p-SMAD2, (C) quantification of p-SMAD3, (D) quantification of total SMAD2, and (E) quantification of total SMAD3, n = 3 experiments. GAPDH was used as loading control. Black dots represent mean values, bars show standard deviation, *P*-values were determined using student's t-test. To detect SMAD2/3, the membrane shown in Figure 5.6 C (CANX) was re-incubated with anti-SMAD2/3 antibody, therefore, the same GAPDH is shown as loading control.

6.6 DNA methylation is changed dramatically in D469del COMP cells

In cystic fibrosis, the expression of recombinant mutant cystic fibrosis transmembrane conductance regulator (CFTR) is known to cause ER stress. This ER stress was observed to lead to methylation changes in the promoter region of endogenous CFTR, resulting in transcriptional repression (Bartoszewski et al., 2008b). Whilst DNA methylation has been studied in the context of many diseases associated with ER stress, for example Alzheimer's disease and Diabetes (De Jager et al., 2014; Duran-Aniotz et al., 2017; Jerram et al., 2017; Nilsson and Ling, 2017; Santos and Ferreira, 2018; Scheuner and Kaufman, 2008), if and to what extent ER stress and DNA methylation may be linked has not yet been investigated. Furthermore, whether expression of mutant COMP affects DNA methylation has not yet been studied.

DNA methylation was analysed using the Illumina Infinium EPICMethylation array system (n = 4 per cell line) by the Genetics Core Facility at Edinburgh Clinical Research Facility followed by computational analysis (Maksimovic et al., 2016). In brief, 865859 probes passed the threshold of $p < 0.05$ for the mean detection *P*-value (Figure 6.9) and were used for normalisation using the *preprocessQuantile* function (Touleimat and Tost, 2012) in *minfi* (Aryee et al., 2014). PreprocessQuantile was chosen for normalisation (Figure 6.10), as it assumes no global differences between samples (for example, they are derived from the same tissue/cell line). Multiple dimensional scaling plots confirmed that the biggest source of variation between all analysed samples was the respective cell line (Figure 6.11). Probes were then filtered to remove poor performing probes, probes affected by common SNPs, probes binding to the sex chromosomes and known cross-reactive probes (Pidsley et al., 2016). Beta and M values were calculated (Figure 6.12), and multiple dimensional scaling plots confirmed that the biggest source of variation between all analysed samples was the still respective cell line (Figure 6.13) before probe-wise differential methylation analysis was carried out using the limma pipeline (Ritchie et al., 2015). Beta values are calculated from the ratio of array intensities of the methylated and unmethylated alleles of each probe and correspond to the level of methylation. Although they are easier to interpret, they are not suitable for statistical analysis. Beta values are therefore transformed into M values, which are used for statistical testing. These results were then further examined to reveal differentially methylated

regions using *DMRcate* (Peters et al., 2015). Visualisation of differentially methylated probes and regions was performed using *Gviz* (Hahne and Ivanek, 2016).

The resulting data indicated that of the 690594 analysed probes, 42146 appeared to be demethylated and 62562 hypermethylated with a difference in DNA methylation bigger than ± 0.15 beta (equivalent to > ± 15 % methylation difference) and adjusted *P*-value < 0.05. This number of CpGs found to be differentially methylated was unexpectedly high (15.2 % of all analysed probes). In total, these CpGs were annotated 19694 unique genes. When the differentially methylated sites (probes, DMPs) were summarised to differentially methylated regions (DMRs), 48383 regions corresponding to 16839 distinct genes were identified (*P*-value < 0.01, Fisher) containing at least two differentially methylated CpG sites.

Gene set analysis on genes corresponding to DMPs was performed using the gometh tool in missMethyl (Phipson et al., 2016) and 295 GO terms identified (FDR < 0.01), which were further summarised using REViGO (Table 6.4, 6.5 and 6.6). Each term produced a score of uniqueness (similarity of each term to the overall group) and dispensability (score of redundancy). GO terms similar to KEGG pathways identified after RNA sequencing are highlighted in light yellow, terms relating to the ECM are highlighted in dark yellow. Most cellular component GO terms were linked to the plasma membrane, extracellular space or related terms (Table 6.4). Biological process GO terms described mainly different types of signalling, transports and cellular movement (Table 6.5). The top molecular function GO terms included extracellular matrix constituent, phospholipase activity and transporter activity (Table 6.6).

742 genes with at least one DMPs were also differentially expressed. Of the genes connected to significantly altered regions containing differentially methylated probes (15382), 636 annotated genes were also found to be differentially expressed (Figure 6.14). The vast majority of differentially methylated probes and regions did not translate into changes in expression.

When the location of DMPs was considered, it revealed a total of 16505 genes were annotated for DMPs in a promoter region (1st Exon, TSS200, TSS1500), of which 5962 genes were also expressed in HT1080 cells as detected by RNA sequencing.

675/988 (68.3 %) genes that were differentially expressed had at least one DMP within a region annotated as a promoter (Figure 6.15 A, 6.17 A). Of these genes, 590 (59.7 % of DEGs) were found to also be associated with a DMR (Figure 6.15 A, 6.17 A). In contrast, when genes of DMPs and DMRs were compared to genes displaying no difference in expression (Figure 6.15 B, 6.17 A), 5287 (46 %) of genes that were not differentially expressed had at least one DMP located in promoter regions, and 4339 (37.9 %) of these were annotated for at least one DMR.

A total of 15872 different genes were annotated for DMPs outside promoter regions (Figure 6.16, 6.17 B), of which 6126 genes were also found to be expressed by HT1080 cells. 677 genes that exhibited changes in expression level were also annotated for at least one DMP outside a promoter region (Figure 6.16 A, 6.17 B). Therefore, 68.5 % of differentially expressed genes exhibited changes in DNA methylation outside a promoter region. Of these 677 genes, 583 genes (59 % of all DEGs) were also associated with a DMR. 5449 genes that were annotated for DMPs did not change in expression (Figure 6.16 B, 6.17 B), meaning 47.5 % of genes that were not differentially expressed displayed changes in DNA methylation outside promoter regions.

When specific genes of interest were analysed, *COMP* for example, indeed one region containing 25 CpG sites was identified to be differentially methylated and located in close proximity to the human *COMP* promoter region (Deere et al., 2001). None of the individual CpGs displayed a methylation change of more than 15 %, but six CpG sites exhibited changes in DNA methylation greater than 10 % (Figure 6.18, Table 6.7). For *MMP9* one region containing seven CpG sites appeared differentially methylated. More than 10 % difference in methylation was observed for three individual CpG sites, of which two displayed a difference of more than 15 % (Figure 6.19, Table 6.7). Only one differentially methylated region containing 17 CpG sites was associated with *PRDX2*. For eight individual CpGs within this region, the difference in methylation was greater than 15 % (Figure 6.20, Table 6.7). For *GALNT18,* 15 regions were identified as differentially methylated, with a total of 36 individual probes exhibiting a difference in DNA methylation greater than 15 % (Table 6.7, regions visualised in *Gviz* are highlighted in orange). The region with the highest number of individual CpGs contained 15 CpG sites of which six CpGs exhibited more than 15 % change in DNA methylation (Figure 6.21). Six differentially methylated

regions were found to be associated with *SMAD3*, which contained 14 CpGs with a change in DNA methylation greater than 10 % (Table 6.7). Of these, 10 displayed more than 15 % difference in methylation levels. One DMR associated with *SMAD3,* containing six individual CpG sites and a mean beta difference of -0.12, was found close to the start of *SMAD3* transcript variant 2 (Figure 6.22).

In addition to a *P*-value threshold, a threshold can be applied to the maximum or mean beta difference of a DMR. When a threshold of 0.15 mean beta difference was applied, 8644 DMRs were identified that mapped to 3932 different genes. 294 differentially expressed genes (29.9 % of all differentially expressed genes) were annotated at least one DMR with a mean beta difference > 0.15 and at least one DMP in a promoter region (Figure 6.23 A). In contrast, 940 genes that did not change expression (8.2 % of all unchanged genes) were associated with at least one DMR with a mean beta difference > 0.15 and at least one DMP in a promoter region (Figure 6.23 B). When DMPs outside promoter regions were analysed, 300 differentially expressed genes (30.5 %) were associated with a DMR with a mean beta difference < 0.15 and at least one DMP outside a promoter region (Figure 6.24 A), whereas 1070 genes that did not change expression (9.3 % of all unchanged genes) were associated to a DMR and at least one DMP (Figure 6.24 B).
DMRs associated with *COMP, PRDX2* and *MMP9* did not exhibit a mean beta value difference bigger than 0.15, but all 15 regions annotated for *GALNT18* and three regions associated with *SMAD3* displayed mean beta value changes bigger than 0.15 (Table 6.7). All regions associated with *GALNT18* displayed an increase in mean beta value difference in D469del COMP cells whilst one *SMAD3*-annotated regions exhibited an increase and two regions displayed a reduction in mean beta value difference (Table 6.7). Nevertheless, expression of both *GALNT18* and *SMAD3* was elevated in D469del COMP cells.

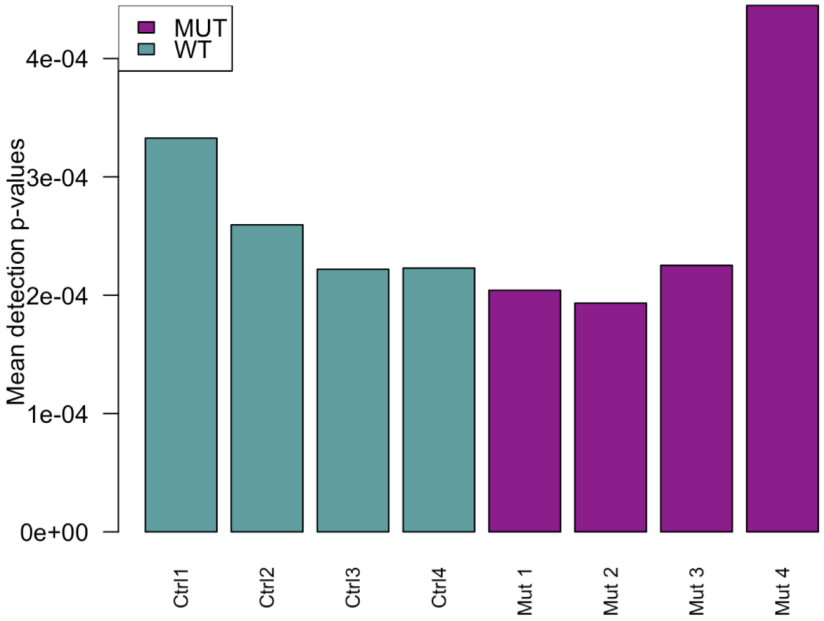

Figure 6.9 – Quality of Illumina Infinium MethylationEPIC data. Mean detection *P*-value per for each sample. Large *P*-values indicate failed probes, whilst small *P*-values suggest reliable signal.

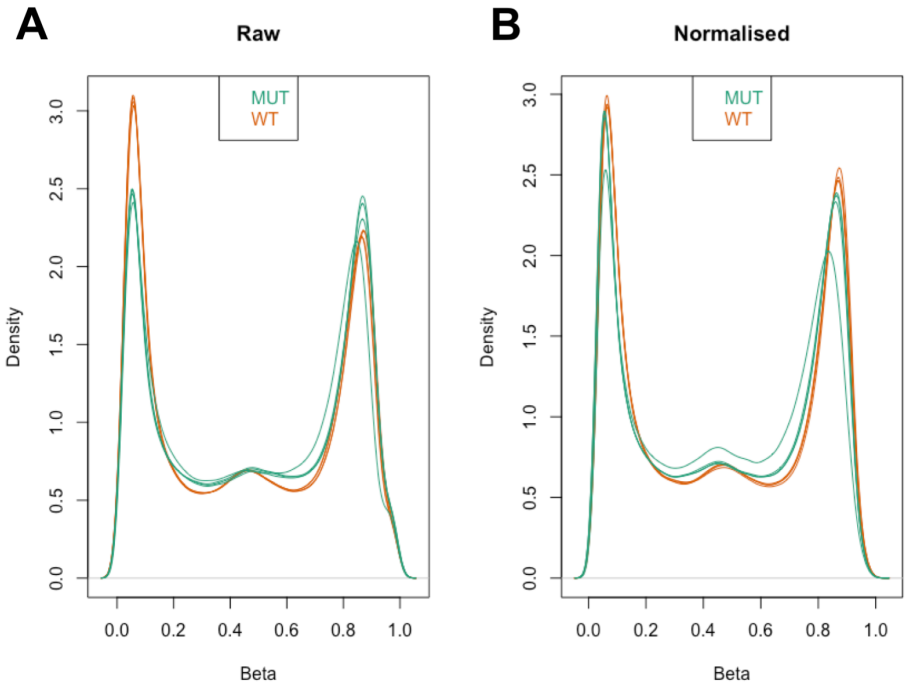

Figure 6.10 – Distribution of beta values for each sample before (A) and after (B) normalisation using preprocessQuantile.

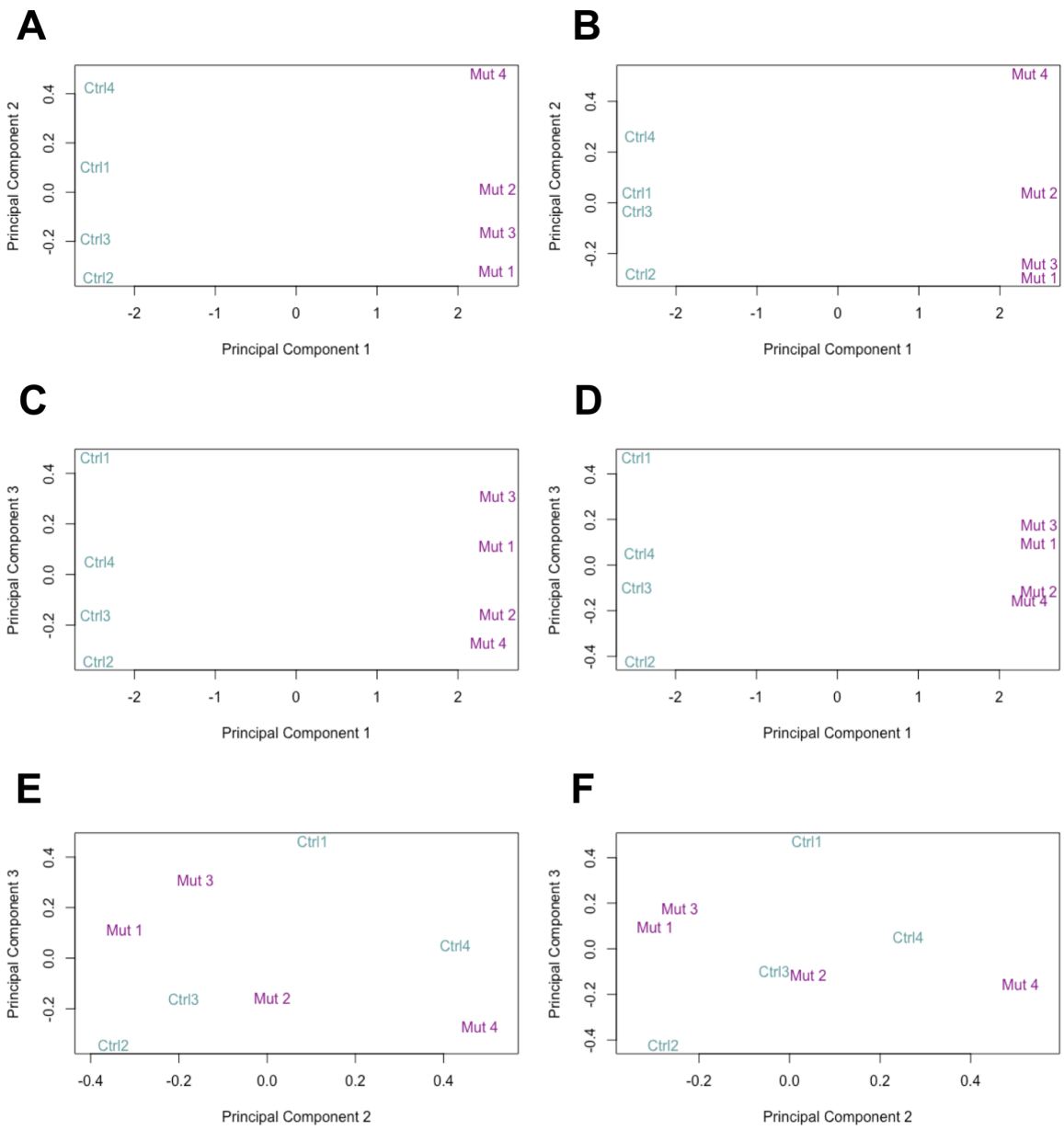

6.11 – Multiple dimensional scaling plots before (A, C, E) and after (B, D, F) normalisation. Dimensions (or components) capture different sources of variation between groups of samples. Similar samples group together, whereas samples that are different to each other are separated by greater distance. WT and MUT samples are clearly separated by principal component (PC) one (A, B, C, D) but not PC2 or PC3 (E, F).

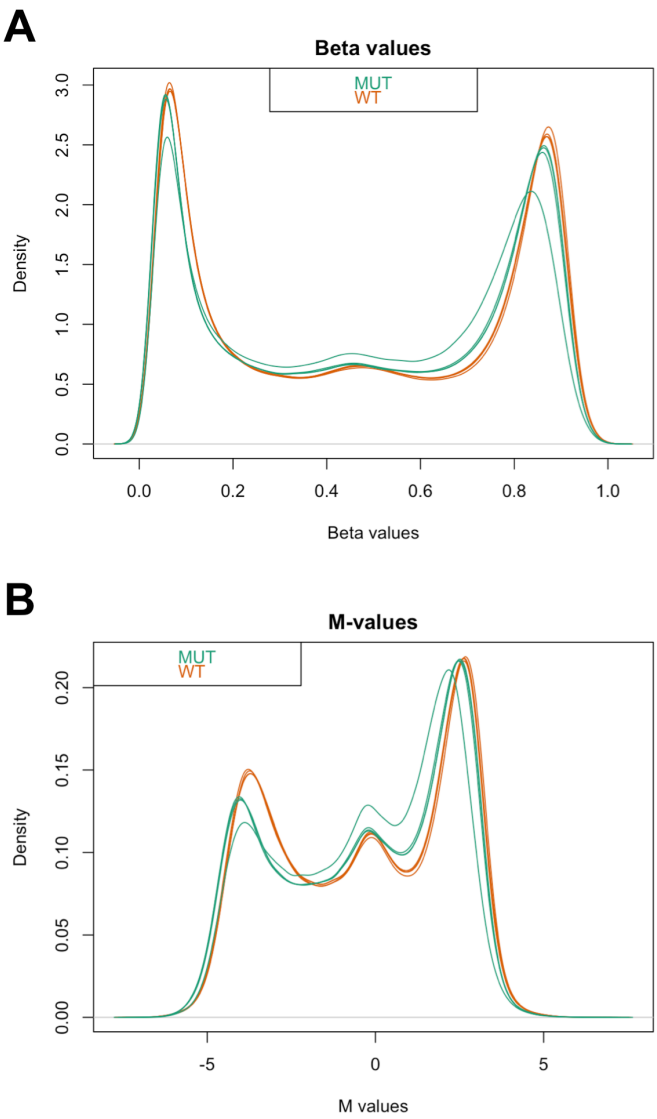

Figure 6.12 – Distribution of beta (A) and M values (B) in wild type (WT) and D469del (MUT) COMP expressing cells after filtering of poor performing probes. Beta values are easier to interpret as they describe the percentage of methylation, whilst M values are more appropriate for statistical analysis.

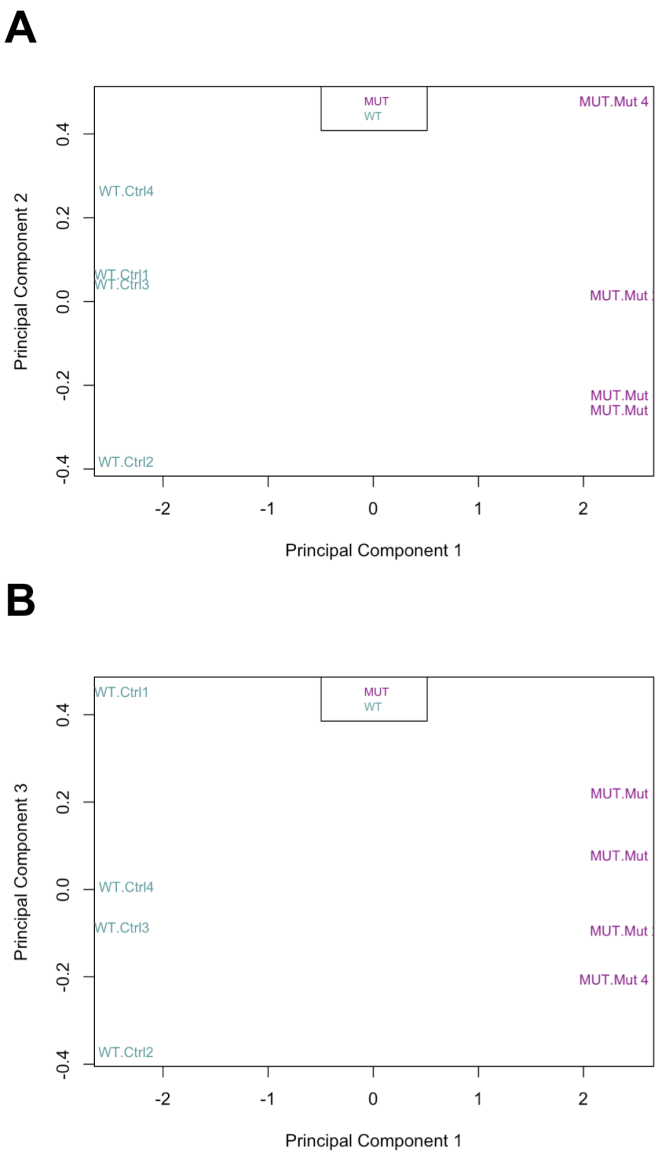

Figure 6.13 – Multiple dimensional scaling plots after filtering of poor performing probes for (A) principal component 1 and 2 and (B) principal component 1 and 3. Removing poor performing probes did not affect the separation of the samples into two groups according to cell line.

Term ID	Description	Uniqueness	Dispensability
GO:0045177	Apical part of cell	1.00	0.00
GO:0036477	Somatodendritic compartment	1.00	0.00
GO:0009986	Cell surface	1.00	0.00
GO:0030054	Cell junction	1.00	0.00
GO:0042995	Cell projection	1.00	0.00
GO:0071944	Cell periphery	1.00	0.00
GO:0016020	Membrane	1.00	0.00
GO:0005615	Extracellular space	1.00	0.00
GO:0005576	Extracellular region	1.00	0.00
GO:0015629	Actin cytoskeleton	0.94	0.00
GO:0043025	Neuronal cell body	0.93	0.00
GO:0043235	Receptor complex	0.92	0.00
GO:0120025	Plasma membrane bounded cell projection	0.89	0.00
GO:0005887	Integral component of plasma membrane	0.73	0.00
GO:0045202	Synapse	0.73	0.00
GO:0098552	Side of membrane	0.97	0.03
GO:0031225	Anchored component of membrane	0.97	0.05
GO:0031224	Intrinsic component of membrane	0.94	0.07
GO:0005581	Collagen trimer	0.92	0.27
GO:0009897	External side of plasma membrane	0.84	0.27
GO:0031012	Extracellular matrix	0.83	0.28
GO:0016021	Apical plasma membrane	0.71	0.28
GO:0016021	Integral component of membrane	0.93	0.30
GO:0098590	Plasma membrane region	0.81	0.33
GO:0030017	Sarcomere	0.87	0.35
GO:0031226	Intrinsic component of plasma membrane	0.78	0.38
GO:0098797	Plasma membrane protein complex	0.68	0.38

Table 6.4 REViGO GO Cellular component terms with differentially methylated regions. GO terms similar to KEGG pathways identified after RNA sequencing are highlighted in light yellow, terms relating to the ECM are highlighted in dark yellow.

Term ID	Description	Uniqueness	Dispensability
GO:0007610	Behaviour	1.00	0.00
GO:0016042	Lipid catabolic process	1.00	0.00
GO:0032501	Multicellular organismal process	1.00	0.00
GO:0032502	Developmental process	1.00	0.00
GO:0040011	Locomotion	1.00	0.00
GO:0022610	Biological adhesion	1.00	0.00
GO:0023052	Signalling	1.00	0.00
GO:0007631	Feeding behaviour	0.99	0.00
GO:0009611	Response to wounding	0.96	0.00
GO:0006812	Cation transport	0.86	0.00
GO:0043269	Regulation of ion transport	0.78	0.00
GO:0003008	System process	0.70	0.00
GO:0030154	Cell differentiation	0.64	0.00
GO:0006928	Movement of cell or subcellular component	0.99	0.01
GO:0007155	Cell adhesion	0.98	0.01
GO:0030198	Extracellular matrix organisation	0.96	0.01
GO:0007267	Cell-cell signalling	0.94	0.01
GO:0007154	Cell communication	0.99	0.02
GO:0050804	Modulation of chemical synaptic transmission	0.86	0.18
GO:0044057	Regulation of system process	0.84	0.18
GO:0051094	Positive regulation of developmental process	0.80	0.20
GO:0043279	Response to alkaloid	0.96	0.21
GO:0065008	Regulation of biological quality	0.85	0.23

Table 6.5 - REViGO Go Biological process terms associated with differentially methylated regions.

Term ID	Description	Uniqueness	Dispensability
GO:0005215	Transporter activity	1.00	0.00
GO:0005201	Extracellular matrix structural constituent	1.00	0.00
GO:0004620	Phospholipase activity	0.98	0.00
GO:0005102	Signalling receptor binding	0.97	0.00
GO:0030545	Signalling receptor regulator activity	0.94	0.00
GO:0015318	Inorganic molecular entity transmembrane transporter activity	0.51	0.00
GO:0008528	G protein-coupled peptide receptor activity	0.84	0.01
GO:0005539	Glycosaminnoglycan binding	0.98	0.05
GO:0005509	Calcium ion binding	0.99	0.06
GO:0008289	Lipid binding	0.99	0.06
GO:0008201	Heparin binding	0.98	0.21
GO:0003700	DNA-binding transcription factor activity	0.93	0.26
GO:0016298	Lipase activity	0.98	0.46

Table 6.6 – REViGO GO Molecular Function terms associated with differentially methylated regions.

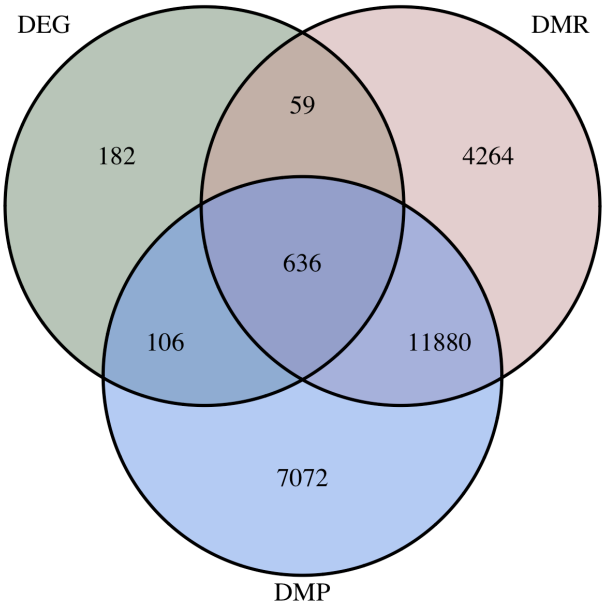

Figure 6.14 – Venn diagram of differentially expressed genes (DEG), differentially methylated regions (DMR) and differentially methylated probes (DMP). In 636 DMRs, one or more individual CpGs displayed a change in methylation greater than 15 % whilst gene expression was significantly altered.

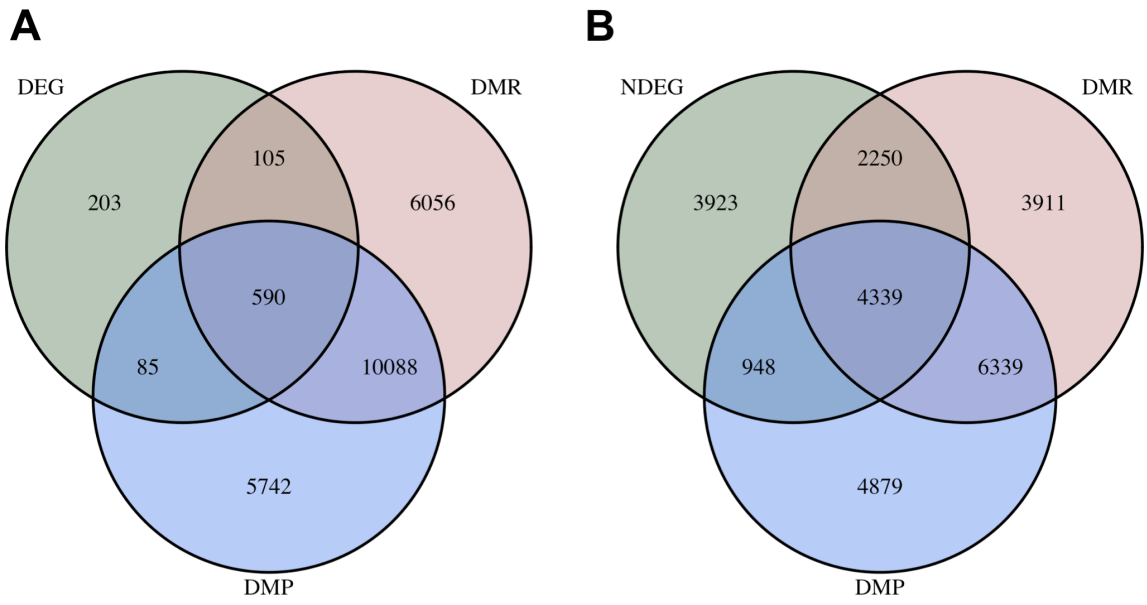

Figure 6.15 - Venn diagram of (A) differentially expressed genes (DEG) and (B) not differentially expressed genes (NDEG), differentially methylated regions (DMR) and differentially methylated probes (DMP) located in promoter regions. (A) For 590 genes (59.7 % of DEG) associated with a DMR, one or more individual probes displayed a change in methylation greater than 0.15 whilst gene expression was significantly altered. (B) 4339 genes (37.9 % of all NDEG) that did not change expression were still annotated to a DMR and at least one DMP.

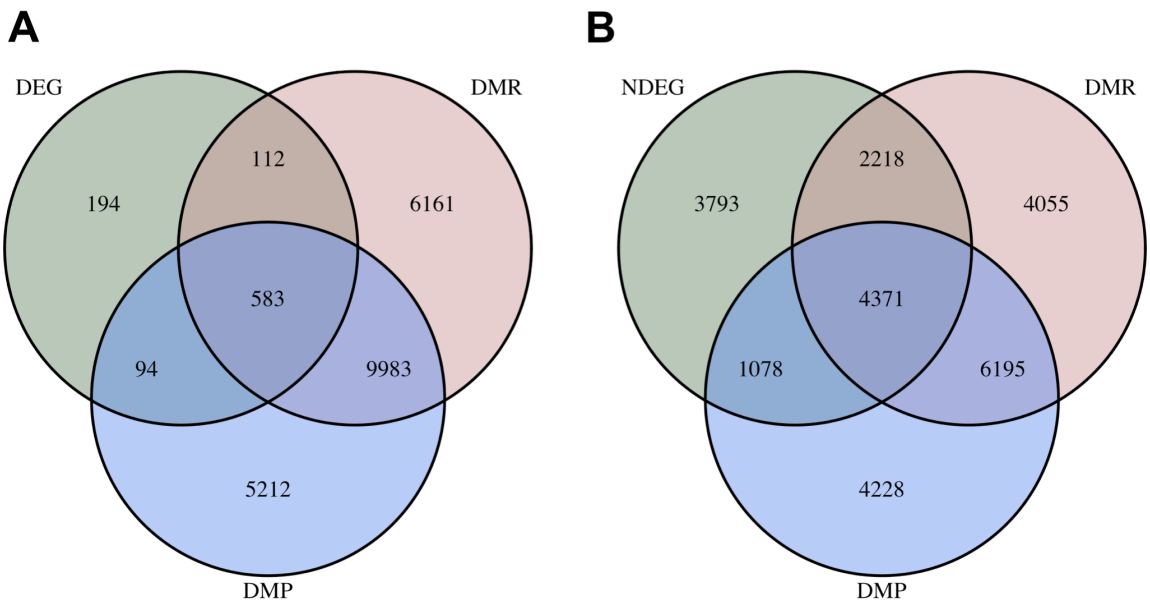

Figure 6.16 - Venn diagram of (A) differentially expressed genes (DEG), and (B) not differentially expressed genes (NDEG), differentially methylated regions (DMR) and differentially methylated probes (DMP) located outside promoter regions. (A) For 583 genes (59.0 % of DEG) associated with a DMR, one or more individual probes displayed a change in methylation greater than 0.15 whilst gene expression was significantly altered. (B) 4371 genes (38.1 % of NDEG) that did not change expression were still annotated to a DMR and at least one DMP.

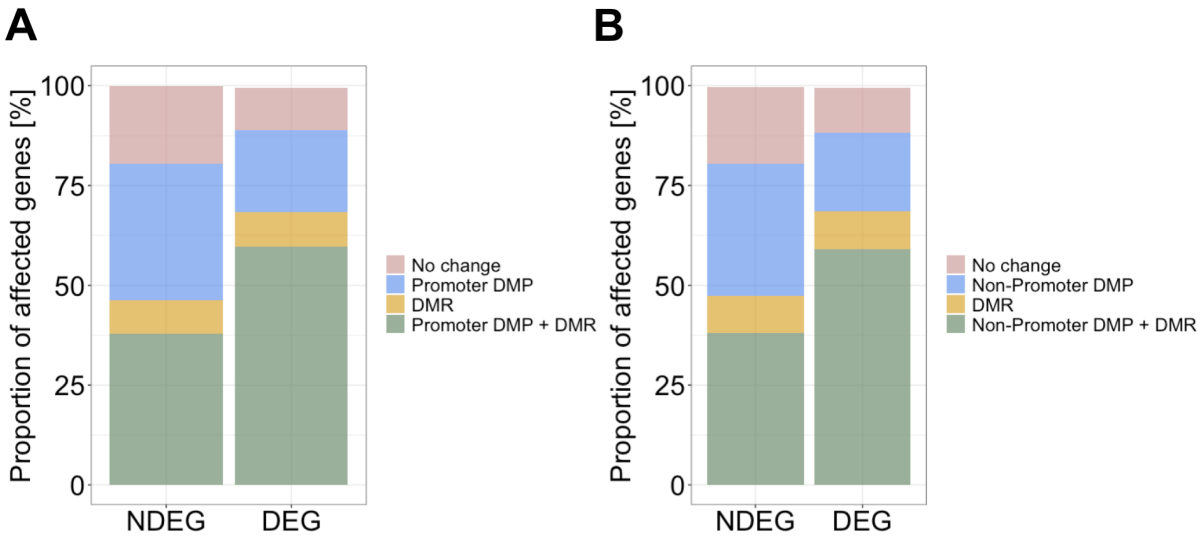

Figure 6.17 – Proportion of genes associated with (A) changes in DNA methylation in promoter regions and (B) changes in DNA methylation in other regions. No change: No differentially methylated probes or region was observed. DEG: Differentially expressed genes. NDEG: genes that did not change in expression. Promoter DMPs: Genes annotated with at least one individual probe in a promoter region that exhibited a difference in methylation of more than 0.15 between wild type and D469del COMP. DMR: Genes annotated with at least one differentially methylated region. Promoter DMP + DMR: Genes annotated with at least one differentially methylated region and a at least one individual probe in a promoter region that displayed a difference in methylation of more than 0.15 between wild type and D469del COMP. Non-promoter DMPs: Genes annotated with a least one individual probe outside a promoter region that exhibited a difference in methylation of more than 0.15 between wild type and D469del COMP. Non-promoter DMP + DMR: Genes annotated with at least one differentially methylated region and a at least one individual probe outside a promoter region that displayed a difference in methylation of more than 0.15 between wild type and D469del COMP.

Gene	Number of CpGs	Mean beta difference	HMFDR
COMP	25	0.056	2.77E-05
MMP9	7	0.12	1.72E-07
PRDX2	17	-0.014	3.72E-07
GALNT18	15	0.16	1.24E-07
GALNT18	8	0.47	3.60E-08
GALNT18	7	0.64	5.63E-08
GALNT18	5	0.48	3.79E-08
GALNT18	4	0.40	9.22E-08
GALNT18	3	0.58	3.53E-08
GALNT18	3	0.39	4.48E-08
GALNT18	3	0.40	5.41E-08
GALNT18	2	0.55	2.19E-08
GALNT18	2	0.72	2.51E-08
GALNT18	2	0.48	3.66E-08
GALNT18	2	0.33	4.64E-08
GALNT18	2	0.40	5.12E-08
GALNT18	2	0.36	5.06E-08
GALNT18	2	-0.30	5.54E-08
SMAD3	6	0.16	1.84E-06
SMAD3	6	-0.12	2.97E-07
SMAD3	5	0.012	0.0001
SMAD3	4	-0.06	7.70E-05
SMAD3	3	-0.16	6.38E-07
SMAD3	2	-0.25	7.72E-08

Table 6.7 – Number of individual CpGs and their mean difference of beta value in DMRs associated with *COMP, MMP9, PRDX2, GALNT18* and *SMAD3*. Regions visualised in Gviz are highlighted. HMFDR: **H**armonic **M**ean of the individual CpG **F**alse **D**iscovery **R**ates.

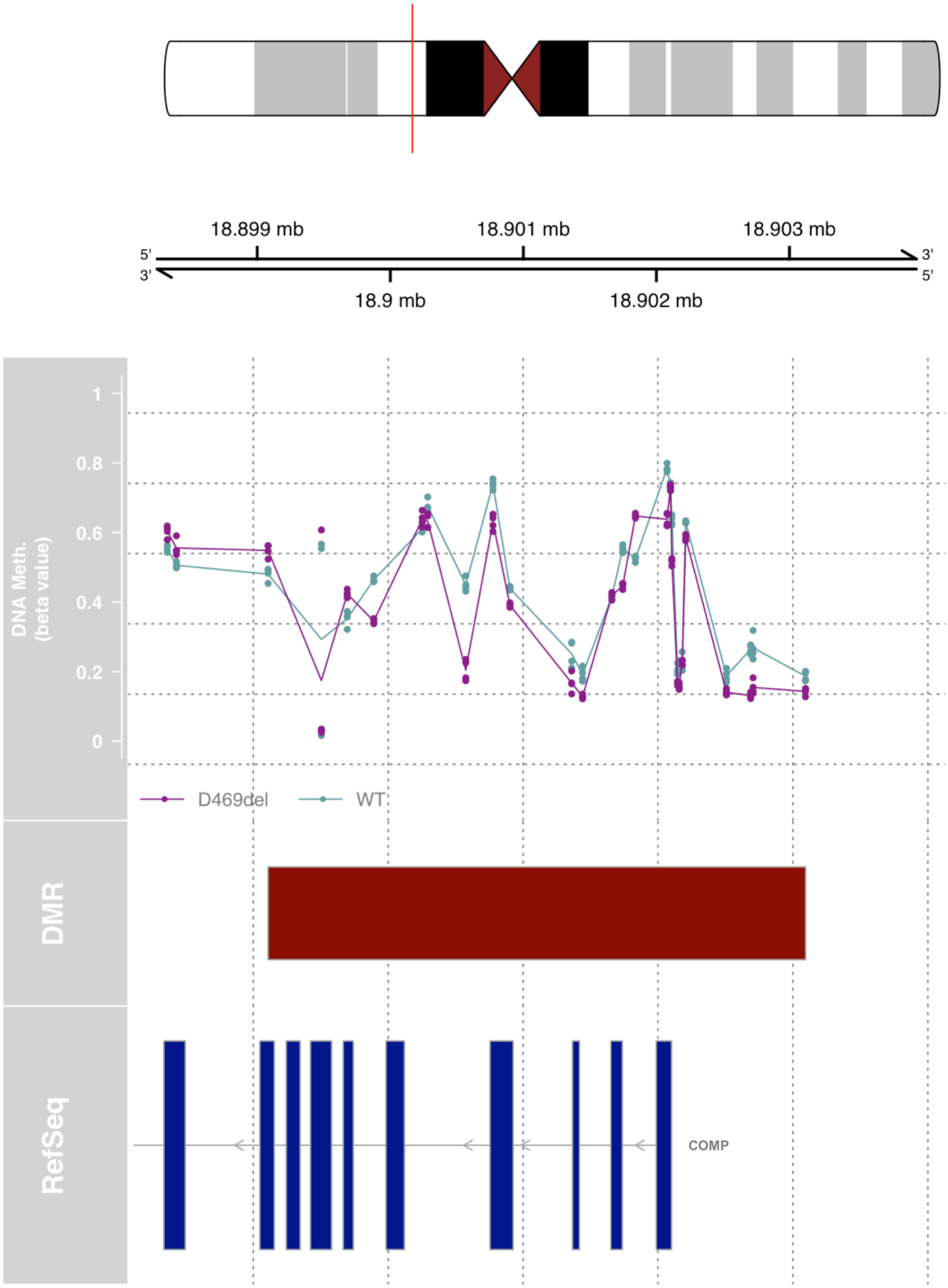

Figure 6.18 – Differentially methylated sites within the differentially methylated region associated with *COMP*. Visualisation was performed using the *Gviz* package in R studio.

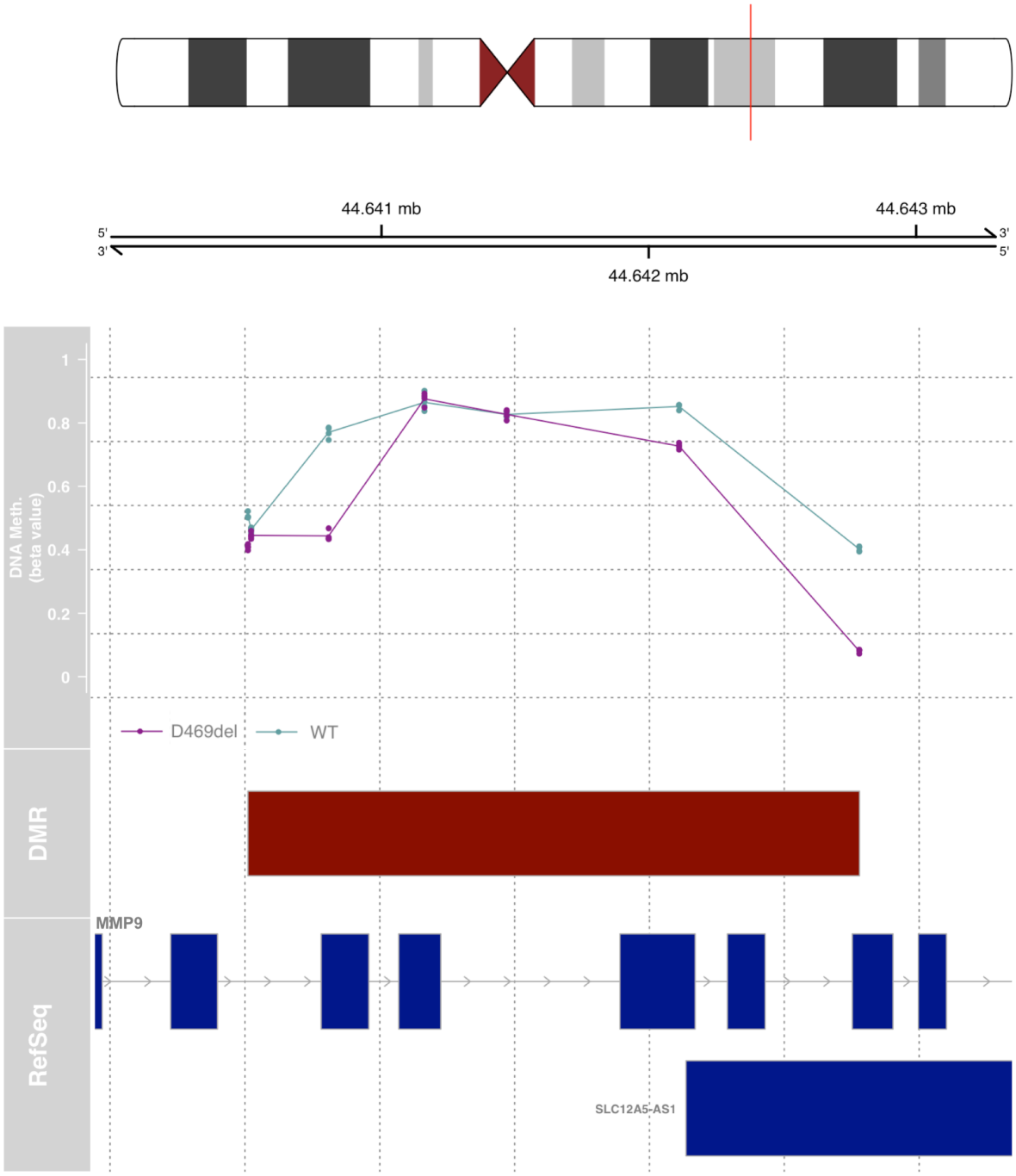

Figure 6.19 – Differentially methylated sites within the differentially methylated region associated with *MMP9.*

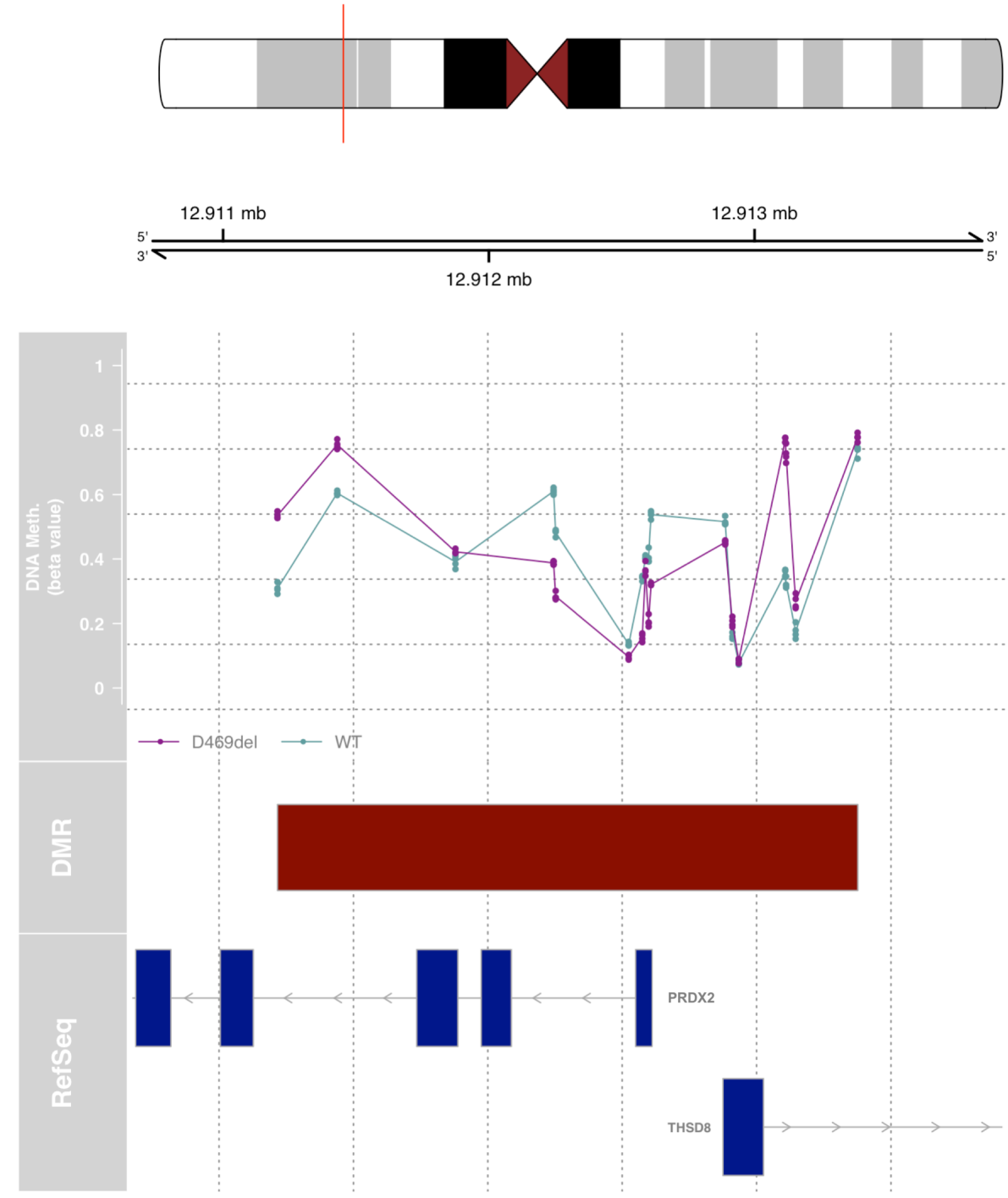

Figure 6.20 - Differentially methylated sites within the differentially methylated region associated with *PRDX2*.

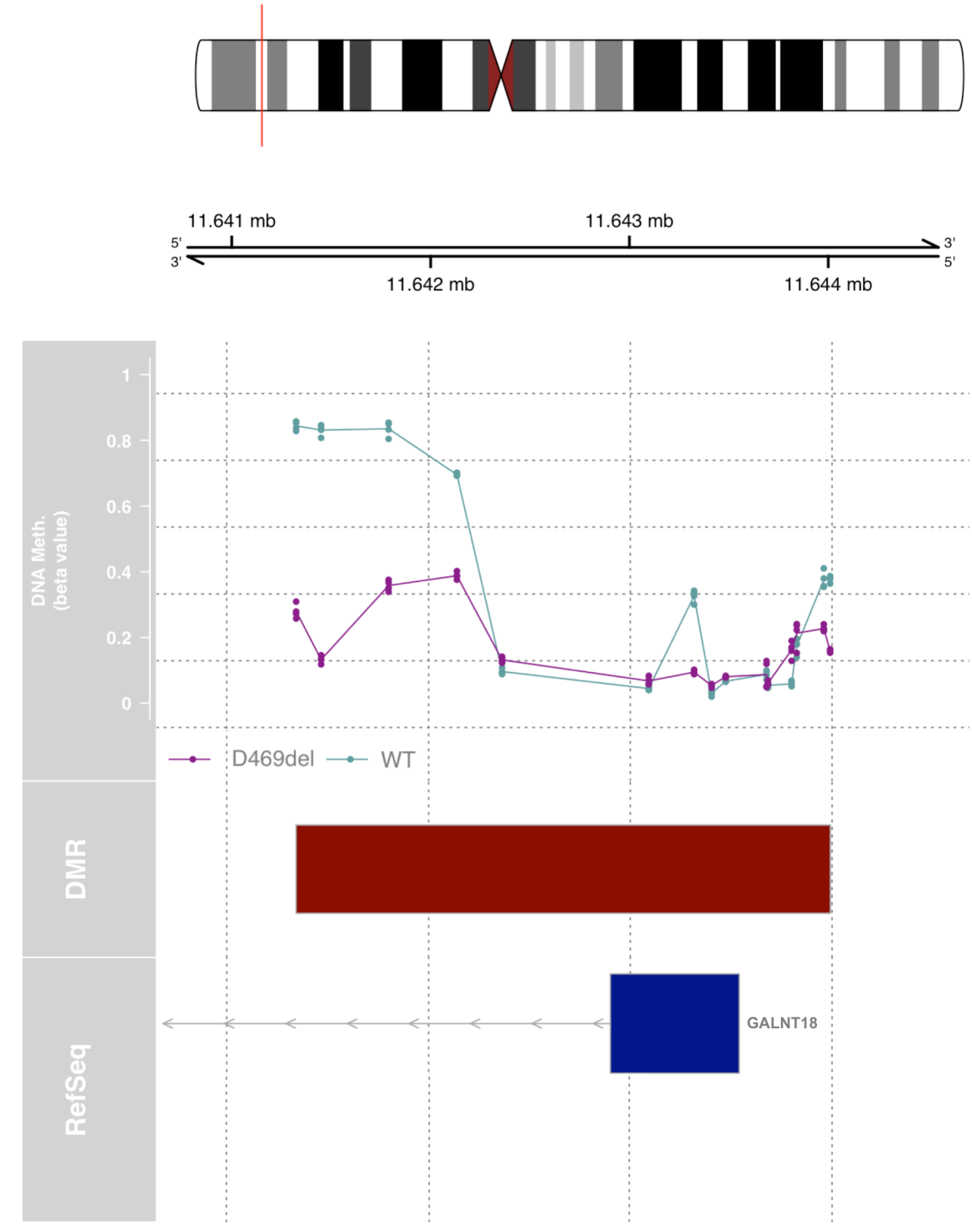

Figure 6.21 – Differentially methylated sites within the differentially methylated region associated with *GALNT18* with the highest number of individual CpGs.

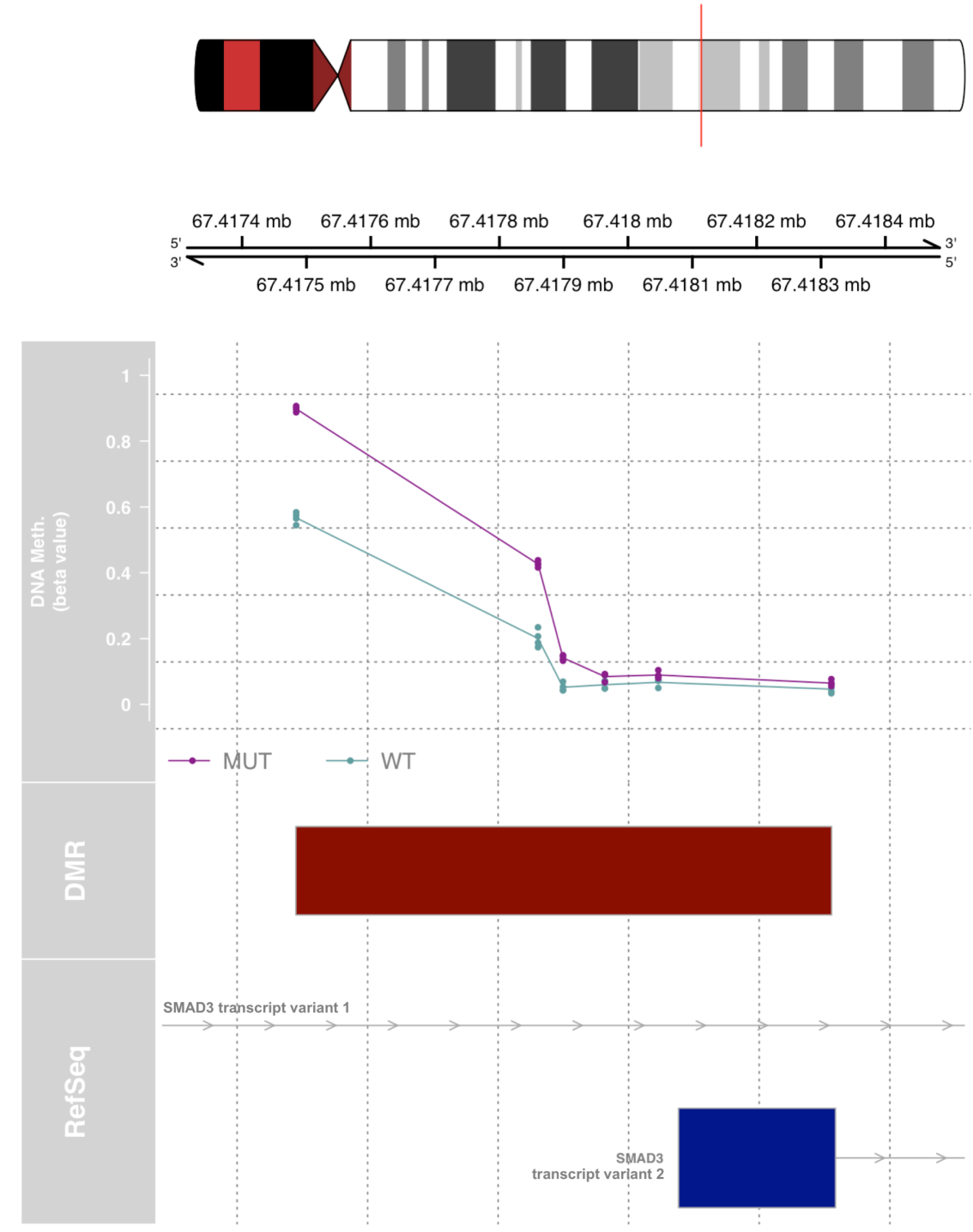

Figure 6.22 – Differentially methylated sites within the differentially methylated region located at the start of *SMAD3* transcript variant 2.

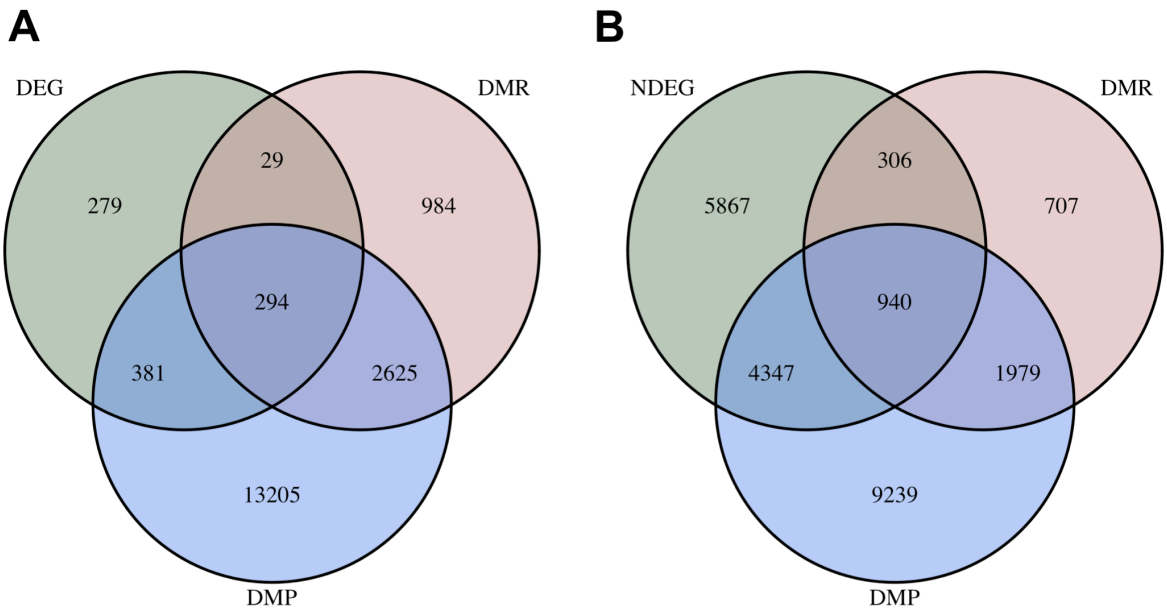

Figure 6.23 – Venn diagram of (A) differentially expressed genes (DEG) and (B) not differentially expressed genes (NDEG), differentially methylated regions (DMR) with a mean beta difference > 0.15 and differentially methylated probes (DMP) located in promoter regions. (A) For 294 genes (29.9 %) associated with a DMR, one or more individual probes displayed a change in methylation greater than 0.15 whilst gene expression was significantly altered. (B) 940 genes (8.2 %) that did not change expression were still annotated to a DMR and at least one DMP.

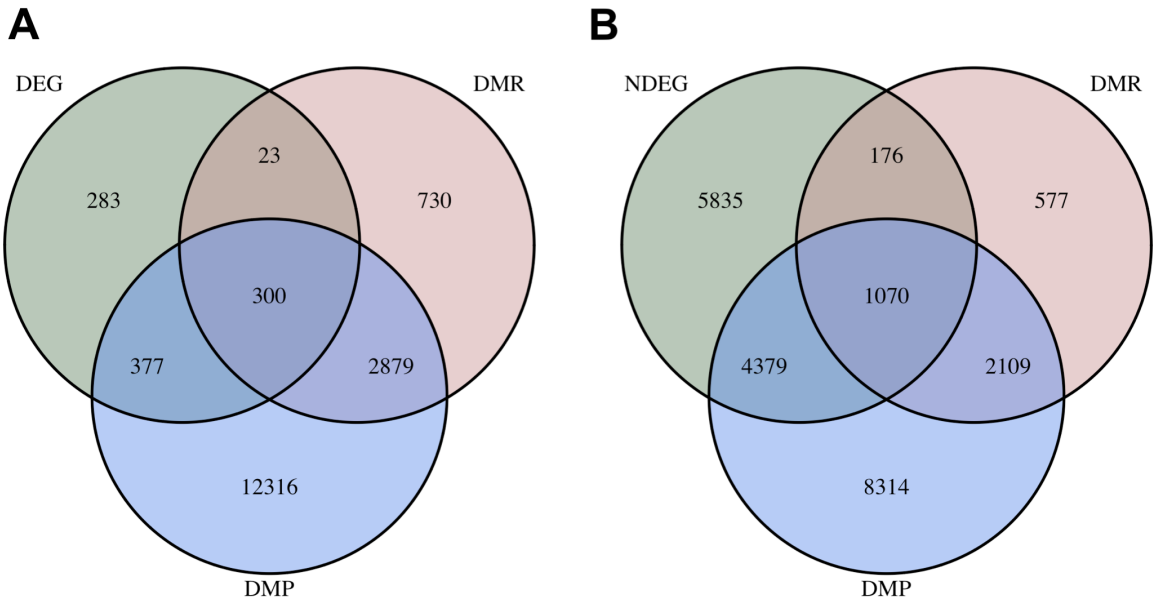

Figure 6.24 – Venn diagram of (A) differentially expressed genes (DEG), and (B) not differentially expressed genes (NDEG), differentially methylated regions (DMR) with a mean beta difference > 0.15 and differentially methylated probes (DMP) located outside promoter regions. (A) For 300 genes (30.5 %) associated with a DMR, one or more individual probes displayed a change in methylation greater than 0.15 whilst gene expression was significantly altered. (B) 1070 genes (9.3 %) that did not change expression were still annotated to a DMR and at least one DMP.

6.7 Discussion

The aims of this chapter were to investigate the consequences of COMP-induced stress in PSACH using the D469del COMP cell model by analysing pathways that were previously implicated in PSACH, but also by using an unbiased, transcriptomic approach. Additionally, it was investigated whether DNA methylation is altered in the D469del COMP cell model.

Instead of activating the UPR, p.D469del COMP-induced ER stress appears to cause oxidative stress resulting in elevated levels of superoxide. However, no difference was observed by RNA sequencing in the expression of *SOD1* and *SOD2* (superoxide dismutase 1 and 2, respectively), encoding enzymes responsible for the conversion of superoxide to the less volatile hydrogen peroxide. Furthermore, no striking difference in mitochondrial integrity was observed when mitochondria were visualised by microscopy, suggesting that instead of a rise in superoxide production, D469del COMP cells may experience decreased availability of anti-oxidative factors. Both *TXNRD1* and *TXNRD2,* encoding thioredoxin reductase 1 and 2 respectively, displayed elevated expression in D469del COMP cells as observed by RNA sequencing. Thioredoxin reductases regenerate thioredoxin, which itself reduces peroxiredoxins after oxidation by ROS (Cunniff et al., 2014). In contrast, three members of the glutathione-s-transferase enzyme family (*GSTM1, GSTM3* and *GSTO2*) exhibited reduced expression. This suggests an imbalance of redox factors in D469del COMP cells.

Surprisingly, and despite the increase in superoxide, mtDNA content was found to be comparable between wild type and D469del COMP-overexpressing cells. Nevertheless, a key regulatory enzyme of glycolysis, *PFKFB2*, was strongly downregulated in D469del COMP cells as revealed by RNA sequencing. The enzymes of the 6-phosphofructose-2-kinase/fructose-2,6-bisphosphatase family synthesise (and degrade) the potent allosteric activator of the phosphofructosekinase enzyme family, thereby strongly inducing glycolysis (Heine-Suñer et al., 1998). A downregulation of *PFKFB2* could therefore imply a decrease in glycolytic activity. In future studies to investigate this in more detail, a SeahorseAnalyzer extracellular flux experiment could be performed. This method directly measures extracellular acidification and oxygen consumption, allowing the determination of relative contribution of mitochondrial and glycolytic activity in intact cells. To confirm the

results obtained in the cell model, primary chondrocytes from wild type or D469del mice could also be used.

The expression of p.D469del COMP may alter cellular metabolism by affecting oxygen-sensing. The α subunits of HIF are protected from proteasomal degradation under hypoxic conditions; thus, the activity is controlled by controlling protein stability. In contrast to that, the β subunits of HIF, encoded by *ARNT* and *ARNT2,* are typically constitutively expressed and are not degraded in an oxygen-dependent fashion. The phosphorylation of AMPK and HIF1α protein levels were unaffected by D469del COMP expression, but RNA sequencing revealed decreased expression of both *EPAS1*, which encodes for HIF2α and *ARNT2* which binds to HIF1α or HIF2α under hypoxic conditions, before the heterodimer of ARNT2 and HIF1α (or HIF2α) can act as transcription factor. These changes suggest that the ability of D469del COMP cells to respond to low oxygen may be impaired. To determine what effect hypoxia has on D469del COMP cells, both wild type and D469del COMP-overexpressing cells could be cultured in a hypoxic environment prior to analysis. Apart from HIF1α protein levels, cell viability and superoxide levels could be examined to evaluate whether D469del COMP cells behave similar to wild type COMP cells under hypoxia. In humans, reduction of *EPAS1* expression was demonstrated to be responsible for the adaption of high-altitude Tibetans to lower oxygen levels, avoiding hypoxia-induced signalling and polycythemia (Peng et al., 2017). The reduction of *EPAS1* expression therefore has a beneficial effect under low oxygen conditions. However, when *Epas1* was inactivated in limb bud mesenchyme, only the final step of chondrocyte hypertrophy marked by the expression of *Vegf, Spp1* and *Mmp13* appeared to be impaired with no significant difference in body size observed (Araldi et al., 2011). Intriguingly, *VEGFA* and *SPP1* also exhibited reduced expression in the D469del COMP cell model. In contrast, in *Epas1*$^{+/-}$ mice the reduction in Epas1 levels resulted in mild proportional dwarfism as well as an elongation of the hypertrophic zone and simultaneously delayed ossification (Saito et al., 2010).

EPAS1 expression was shown to be regulated by IGF1R and INSR via PI3K-signalling in an mTORC2-dependent manner in neuroblastoma (Mohlin et al., 2015). The phosphorylation of AKT on Ser473 is often used as a marker of mTORC2 activity, and as this was reduced in D469del COMP cells, this suggests that mTORC2 activity may be highly impaired by p.D469del COMP expression. Activated

AKT promotes mTORC1 activity via multiple effectors, including PRAS40, TSC2 and the NFκB signalling pathway (Dan et al., 2014). Subsequently, active mTORC1 is able to inhibit mTORC2 mediated phosphorylation of AKT on Ser473 (Julien et al., 2010). The activation of mTORC1 also inhibits autophagy by regulating the phosphorylation of ULK1/2 (J. Kim et al., 2011). Importantly, ULK1 has been found to modulate the formation of ER exit sites, resulting in decreased protein secretion when autophagy activity is high (Gan et al., 2017). Whilst no significant difference was detected in D469del COMP cells, LC3B-II levels tended to be lower in these cells compared to wild type COMP cells, consistent with a reduction in autophagy. Conversely, *ULK2* expression was strongly induced, and so was expression of *E2F1*, a transcription factor known to regulate genes involved in autophagy (Di Malta et al., 2019). Importantly, areas of the ER containing accumulated mutant COMP may be degraded using ER-phagy when the mutant protein cannot be folded or removed otherwise. Protein aggregates could also be removed using ER-to-lysosome-associated degradation (ERLAD). Indeed, recent work has identified ER-phagy mediated by calnexin and FAM143B as an important pathway in misfolded procollagen clearance (Forrester et al., 2019), whilst the importance of ERLAD was demonstrated for successful degradation of aggregates of α1 antitrypsin Z (Fregno et al., 2018). To assess autophagic flux in more detail, levels of p62/SQSTM1 should be analysed. Inhibition of the autophagy machinery and subsequent analysis of the autophagic flux may reveal if mutant COMP is at least partly degraded via autophagy. Furthermore, colocalization of LC3B-II and LAMP1 with mutant COMP could also be examined by confocal microscopy to determine whether mutant COMP is degraded via autophagy and lysosomes. Treatment of D469del COMP cells with chloroquine and bafilomycin A, which inhibit autophagy via different mechanisms (Mauthe et al., 2018), could deliver a more detailed insight into how mutant COMP may be degraded and how its clearance from the ER might be stimulated pharmacologically.

Since COMP is a member of the thrombospondin protein family and the loss of *Comp* expression in a COMP knock-out mouse model did not lead to a striking phenotype, it has been speculated in the past whether a loss of COMP would be compensated by upregulation of other thrombospondins. Although no obvious upregulation of other thrombospondins was observed in cartilage of COMP-deficient mice (Svensson et al., 2002), in PSACH knock-in mouse model *Thbs4* and *Thbs2* were found to be

upregulated (Suleman et al., 2012). In HT1080 D469del COMP cells, both *THBS1* and *THBS2* (encoding TSP-1 and TSP-2 respectively) were found to be upregulated at the mRNA level, but not *THBS4*. Both proteins have been shown to be important for bone development. Whilst VEGFA is seen as a major driver of angiogenesis, TSP-1 and TSP-2 have been suggested to have anti-angiogenic properties (Lawler and Lawler, 2012), implying that p.D469del COMP expression may compromise factors involved in angiogenesis. Loss of TSP-1 results in decreased osteoclast activity and thus affects bone quality in mice (Amend et al., 2015), whilst loss of TSP-2 delays osteoblastogenesis and mineralisation (Delany and Hankenson, 2009; Hankenson et al., 2000). The consequences of elevated levels of both TSP-1 and TSP-2 in D469del COMP cells are not entirely clear, as TSP-1 is able to inhibit matrix mineralisation and osteoblast differentiation (DuBose et al., 2012), whilst TSP-2 has been demonstrated to promote matrix mineralisation *in vitro* (Alford et al., 2010).

Various thrombospondins have also been implicated as regulators of TGFβ-signalling (Crawford et al., 1998; Muppala et al., 2017). Whilst *TGFBR2* expression was significantly decreased, expression of *TGFB2* and *SMAD3* was increased on transcript level. Furthermore, a reduction in SMAD2 phosphorylation was detected by western blotting, whilst the increase in SMAD3 protein failed to reach statistical significance. Interestingly, COMP has been shown to interact directly with TGFβ1 (Haudenschild et al., 2011; Maly et al., 2021) as well as BMP2 (Ishida et al., 2013) and alter its activity *in vitro.* Notably, *BMP2* expression was found to be increased by RNA sequencing. It has also been demonstrated that the addition of recombinant COMP induces phosphorylation of ERK1/2, but this effect of COMP is impaired in the presence of TGFβ1 (Maly et al., 2021). Since COMP was identified as a direct interaction partner of TGFβ as well as BMPs, it would be interesting to investigate whether this modification of TGFβ-signalling is driven directly by the loss of extracellular COMP.

Addition of recombinant COMP to cell culture medium of D469del COMP followed by evaluation of SMAD2/3 phosphorylation could allow us to uncover whether the lack of extracellular COMP or the intracellular retention of mutant COMP are responsible for the change in TGFβ-signalling. It is currently not known whether mutations like the p.D469del mutation affect the ability of COMP to bind to TGFβ; however, since mutant COMP is retained intracellularly the direct modulation of signalling due to

reduced binding ability would most likely be limited. Instead, differences in TGFβ-signalling may be secondary to alterations in other intracellular signalling pathways, affecting expression levels of pathway components or may be driven by changes in ECM composition and thus TGFβ activation. It is also possible that secreted COMP, as a component of the ECM, is involved in regulating local concentrations of growth factors and cytokines. Indeed, it has been demonstrated recently that secreted COMP is able to directly stimulate NOTCH3-JAGGED1 signalling (Papadakos et al., 2019). Whilst both NOTCH3 and JAGGED1 are transmembrane proteins, extracellular COMP appears to function as adaptor protein by binding to both. In breast cancer cells, this was observed to lead to enhanced JAGGED1 internalisation and NOTCH3 activation. A change in the ability of COMP to bind to both JAGGED1 and NOTCH3, potentially caused by mutations, may impair downstream signalling. Notably, both *JAG1* and *NOTCH3* are downregulated in D469del COMP cells. What drives this reduction, and whether this change in expression translates to the protein levels are yet to be determined.

The absence of COMP may also drive changes in ECM integrity and architecture, which become detrimental in combination with a rise in inflammatory signalling caused by the mutation protein retention. For example, the absence of COMP from the ECM could affect collagen fibrillogenesis and crosslinking, making it more accessible for proteases. Combined with an increased expression of *MMP1* and *MMP9* driven by inflammation, this could lead to enhanced ECM degradation and potentially growth factor release (or degradation). This would also explain why some C-terminal mutations, albeit secreted, cause disease and why the genetic ablation of COMP in mice did not recapitulate the PSACH phenotype: Whilst they may not exhibit the inflammatory signalling observed upon protein retention, mutant COMP may still impair ECM assembly and render it susceptible to aberrant degradation.

RNA sequencing confirmed the involvement of inflammatory cascades in D469del COMP-caused stress, uncovering an increase in *IL-1B* expression as well as NFκB- and TNF-signalling. *IL1B*, Interleukin-1β (IL-1β) is often used to model the cellular processes of conditions like osteoarthritis *in vitro* (Vincent, 2019), whilst TNFα is often used in the study of RA and TNFα inhibitors are amongst the biological treatments of RA (Johnson et al., 2019). Additionally, several ECM degrading enzymes, including some MMPs, were found to be differentially regulated. It is

noteworthy that in models of α1 antitrypsin deficiency, accumulation of the misfolding protein leads to the activation of NFκB-signalling without activation of the UPR, which is marked by a downregulation of *Egr1* and increased expression of MMPs (Mukherjee et al., 2019). A downregulation of *EGR1* was also observed following D469del COMP expression, resulting in elevated expression of *MMP1* and *MMP9* as well as enhanced MMP9 activity.

MMP1, also called fibroblast collagenase, preferentially cleaves fibrillar type I, II and III collagens. In contrast to MMP9, a gelatinase that cleaves denatured parts of the collagen triple helix, MMP1 cleaves collagen into characteristic fragments (Löffek et al., 2011; Pardo and Selman, 2005). Within the joint, high levels of MMP1 are mostly associated with inflammation of the synovium, for example during RA (Goldring and Otero, 2011), whereas MMP9 is expressed by osteoclasts and has been demonstrated to play a role in endochondral ossification alongside MMP13 (Ortega et al., 2003; Stickens et al., 2004). Alongside MMP1 and other MMPs, MMP9 has also been found to be upregulated in RA (Ahrens et al., 1996), most likely also in association with inflammation of the synovium (Xue et al., 2014). MMP9 is known to facilitate cell migration and thus invasion of immune cells when secreted during inflammation (Di Girolamo et al., 2006). Fibroblast-like synoviocytes play an important role in the secretion of inflammatory cytokines, as well as the production of MMPs during RA (Nygaard and Firestein, 2020), and whilst it is known that COMP is expressed by synovial fibroblasts from unaffected as well as RA and OA patients (Dodge et al., 1998), the effects of mutant COMP on synovial fibroblasts remain to be studied. The inflammatory response that D469del COMP appears to provoke in both chondrocytes and HT1080 cells raises the question, whether and to what extent the synovium is involved in the cartilage phenotype of PSACH.

In agreement with increased inflammatory signalling, *PDGFB* expression was observed to be strongly induced by D469del COMP. Intriguingly, *PDGFB* expression was found to be significantly elevated in fibroblast-like synoviocytes from patients with rheumatoid arthritis (Charbonneau et al., 2016) and excessive levels of PDGF-B secretion have been linked to the induction of angiogenesis in the subchondral bone in the early stages of osteoarthritis (Su et al., 2020). Early-onset osteoarthritis (OA) has been described inpatients suffering with PSACH (Briggs et al., 1995); however, it is difficult to dissect whether this is due to similarity in the molecular mechanisms of

both diseases (especially since OA is heterogenous and several sub types exist) or due to impaired joint development and altered joint loading. Still, ER stress has been described as a possible factor in development of OA (Kung et al., 2019; Li et al., 2016; Uehara et al., 2014) and deciphering the pathways underlying COMP-induced ER stress may contribute to further the understanding of the disease mechanism of not only PSACH, but also OA. Intriguingly, when the transcriptome of OA synoviocytes and chondrocytes was dissected using single-cell sequencing, *PDGFB* was found to be expressed exclusively by synoviocytes, but not chondrocytes (Chou et al., 2020), again implicating a role of the synovium in inflammation during PSACH.

In RA, inflammatory cascades also involve the complement system, which COMP itself is known to interact with (Happonen et al., 2012, 2010; Otteby et al., 2013). It was shown that COMP has the ability to inhibit both the classical and lectin pathway of the complement by interacting with MBL and with C1q via its collagenous stalk. COMP therefore interferes with the next step of the complement cascade, the activation of C4. Surprisingly, COMP also acts as an activator of the alternative complement pathway by binding to properdin and C3 directly, and circulating levels of COMP-C3b were significantly higher in serum, but not synovial fluid, from RA patients compared to OA patients (Happonen et al., 2012). In D469del COMP cells, *C1R* was significantly downregulated alongside *ITGAX*, whilst *ITGB2* was upregulated. C1r together with C1q and C1s forms part of the major complement complex C1. *ITGAX* and *ITGB2* encode integrins that are regarded as complement receptors, and together form the inactivated C3b receptor 4 (CR4) (Gjelstrup et al., 2010).

Apart from cartilage, COMP is expressed in several other tissues, including skin, tendon and synovium. In fact, previous work has demonstrated that disease-causing mutations of COMP affect tendon and muscle integrity in mice (Piróg et al., 2013, 2010). However, a considerable amount of research has focused on the effect that mutant COMP exerts on chondrocytes. The fact that expression of D469del COMP in HT1080 fibrosarcoma cells leads to a pronounced inflammatory stress response suggests that in addition to chondrocytes, other cell types of the joint may be involved in PSACH pathology. Indeed, chondrodysplasias caused by mutations in other genes with a more restrictive expression profile, such as *MATN3* (matrilin-3), appear to cause a similar, but milder phenotype via different stress pathways. Whilst

mutant matrilin-3 is – similarly to COMP - retained intracellularly, it has been shown to activate the UPR (Nundlall et al., 2010).
Similar to matrilin-3, COMP forms disulphide linked oligomers within the ER. COMP is a much larger protein than matrilin-3, thus it is possible that both proteins interact with a different subset of factors of the secretory pathway. Recent work has characterised GRASP55-dependent unconventional protein secretion via secretory autophagosomes and multi-vesicular bodies, identifying not only parts of the pathway but also its cargo (Nüchel et al., 2021). In brief, activation of mTORC1 prevents GRASP55-dependent unconventional protein secretion. Intriguingly, proteins identified as potential clients of unconventional protein secretion included matrilin-3, but also peroxiredoxin-2. Strikingly, when mTORC1 was inactivated by several forms of stress (e.g. nutrient depletion, hypoxia), GRASP55-dependent unconventional protein secretion was induced and amino acid depletion in the absence of GRASP55 prompted a reduction in extracellular levels of matrilin-3 and peroxiredoxin-2. Importantly, unconventional protein secretion has been suggested to allow protein secretion when the conventional secretory pathway is disrupted (Rabouille, 2017) which, in PSACH, could be driven by the accumulation of mutant COMP. The aberrant activation of mTORC1 could further disrupt protein secretion in PSACH, including the trafficking of growth factors and receptors. Unfortunately, COMP was not detected in this study and it therefore remains unclear, whether COMP secretion could depend on autophagosomes during periods of cellular stress. It is currently thought however that unconventional protein secretion via autophagosomes originates in the vicinity of ER exit sites, bypassing the Golgi compartment (Rabouille, 2017), whereas the posttranslational modifications of native COMP are consistent with its passage through the Golgi apparatus. It appears more likely that the persistent activation of mTORC1 prevents the degradation of COMP via autophagy (or ER-phagy), whilst additionally interfering with unconventional protein secretion.

A previous study has used rapamycin to inhibit mTORC1 in a mouse model of PSACH and has found a reduction in intracellular D469del COMP accumulation (Posey et al., 2019). It would be interesting to treat D469del COMP cells with rapamycin and examine the consequences for AKT phosphorylation, PRDX2 levels and e.g. *EPAS1* expression alongside COMP secretion and MMP activity. It would also be interesting to use an inhibitor of PI3K-signalling in wild type COMP cells and

compare the activity of some signalling pathways to D469del COMP cells to see to which extent a dysregulation of PI3K-signalling resembles the cellular phenotype caused by D469del COMP expression and to determine whether certain aspects of PSACH are independent of PI3K-AKT-signalling.

In addition to transcriptome analysis using RNA sequencing, DNA methylation was examined in D469del COMP cells using the Illumina Infinium EPIC array. Thus far, DNA methylation has not been studied in the context of pseudoachondroplasia (or multiple epiphyseal dysplasia). Impaired DNA methylation is typically linked to imprinting disorders, including those that present with short stature, such as Silver-Russell syndrome (Begemann et al., 2015; Wit et al., 2016). It remained therefore unknown, whether DNA methylation is altered in PSACH, if it could act as a potential disease modifier, and if DNA methylation could eventually be used as a methylation biomarker. Although expression of p.D469del COMP was associated with a high number of statistically significant changes in DNA methylation, the functional relevance is yet to be determined. Some of these differences will most likely result from random mutations that occurred during the culture of the different cell lines. Nevertheless, it is highly probable that some of the changes in DNA methylation are linked to the expression of D469del COMP. Indeed, when DNA methylation of specific genes of interest was analysed, methylation was changed significantly for most. Interestingly, DNA methylation of 36 individual CpGs located in differentially methylated regions associated with *GALNT18* was changed more than 15 %.

A differentially methylated region associated with *COMP* was of particular interest, especially as a reduction of *Comp* expression was also observed in later developmental stages of a PSACH mouse model. Future studies will have to examine these differences in methylation more closely, and evaluate their functional relevance. Targeted methylation and demethylation using Cas9-fused enzymes could be used to specifically modify CpGs of interest followed by evaluation of *COMP* expression.

To investigate the relationship between DNA methylation and COMP-induced ER stress in more detail, methylation could also be analysed in cell lines expressing other MED- and PSACH-causing COMP mutants. This could allow to identify differences in DNA methylation between wild type, MED and PSACH COMP-

overexpressing cells. Overexpression of other proteins linked to skeletal dysplasia, such as wild type and p.V194D matrilin-3 may allow to eliminate loci that are differentially methylated in response to other types of stresses and not specifically to COMP-induced stress.

Investigating DNA methylation in other species is still more complicated and requires more sophisticated analysis. To examine DNA methylation in cartilage from a PSACH mouse model, whole genome sequencing (WGS) could be performed. The development of assays similar to the Infinium MethylationEPIC array for mouse tissue has led to the availability of the Infinium Mouse Methylation array; however, with more than 285 000 probes, the genomic coverage of this assay is currently limited. In this case, a better approach could be to select some loci of interest. This would allow the use of pyrosequencing to interrogate DNA methylation specifically at these sites.

Apart from a possible role in modifying disease severity, studies have also suggested that DNA methylation changes within specific regions of DNA from serum samples could serve as biomarkers for some diseases (Horvath and Raj, 2018; Kobayashi et al., 2020, 2016; Willmer et al., 2018). Whilst extracting DNA from serum samples can be automated and is therefore convenient, it is questionable if and to what extent DNA methylation in DNA from serum would be affected by mutations of *COMP*. Still, changes in DNA methylation may offer one explanation for a diverse spectrum of phenotypes, and varying degrees of symptom severity even in individuals carrying the same mutation. The role of epigenetics in skeletal dysplasia therefore remains to be studied in more detail.

Transcriptomic analysis uncovered new aspects of COMP-induced stress and also raised further, exciting questions. It also allowed the identification of several potential markers for COMP-induced stress, including *GALNT18*, *MMP1* and *MMP9*. The function of GALNT18 is so far only poorly characterised. Whilst named polypeptide N-acetylgalactosaminyltransferase 18, it exhibits very limited catalytic activity. Still, its genetic ablation appears to drive a reduction in protein O-glycosylation and induction of ER stress (Li et al., 2012; Shan et al., 2019). Conversely, it was found to be downregulated following treatment with tunicamycin and thapsigargin (Shan et al.,

2019). Furthermore, GALNT18 expression, although apparently an ER-resident protein, was elevated following mucin-type Golgi stress (Jamaludin et al., 2019). Recently, it was also reported that the localisation of GALNT18 to the ER depends on its interaction with PLOD3, also known as lysyl hydroxylase (LH) 3, which is known to modify collagens post-translationally (Jia et al., 2021).

MMP9, but also MMP1, are of particular interest as potential biomarkers for COMP-induced stress. In contrast to GALNT18, a hardly characterised, intracellular enzyme, both MMP1 and MMP9 are secreted and have been studied extensively. Activity-based assays as well as ELISA-based approaches are available to determine the level of MMP1 and MMP9 in conditioned media from D469del COMP cells and primary murine chondrocytes or serum samples from the PSACH knock-in mouse model. Still, mutations of COMP do not only cause PSACH, but also MED and previous reports have shown that retention of mutant COMP may vary between mutations (Chen et al., 2004). Specifically, MED-causing mutations may be secreted to a much larger extent than PSACH-causing mutations within the type 3 repeats. Whilst MMP9 activity was increased on expression levels as well as in conditioned media of D469del COMP cells and therefore a strong candidate for a COMP-induced stress biomarker, previous work has not examined MMP1/MMP9 expression in the context of other COMP mutations. Extensive analysis is needed as to whether the findings presented in this chapter apply to other PSACH-causing mutations within the type 3 repeats as well, and whether there are differences between MED- and PSACH-causing mutations within the type 3 repeats. Importantly, the activation of the UPR has to be evaluated in other disease-causing COMP mutations, since most studies have focused on the common p.D469del mutation or compared mutations within the type 3 repeats with mutations located in the C-terminal domain of COMP. Furthermore, it needs to be addressed whether MED-causing mutations exhibit less pronounced protein retention and whether this results in a different type of stress response than the PSACH-causing mutation p.D469del. The identification of a common marker for COMP-induced pathology *in vitro* would facilitate future *in vitro* research and drug development.

To establish if their expression is specifically upregulated as a result of COMP-induced stress or if this is a common occurrence in skeletal dysplasia, *MMP1* and

MMP9 expression should be examined in models of other skeletal disorders, most importantly matrilin-3 MED.

6.8 Summary

- D469del COMP cells show a complex molecular phenotype with several dysregulated signalling pathways, including AKT and TGFβ signalling.

- Although increased superoxide levels were observed, no differences were detected in markers of mitochondrial integrity.

- D469del COMP cells do not display significant changes in common markers for hypoxia, nutrient deprivation or autophagy.

- DNA methylation was excessively altered in D469del COMP cells, with several genes of interest exhibiting changes in DNA methylation.

- MMP9 was induced transcriptionally by D469del COMP expression, resulting in increased extracellular MMP9 activity and therefore may be a biomarker of COMP-induced stress.

Chapter 7. Investigation of a potential common disease mechanism and biomarker for COMPopathies

7.1 Introduction

The previous chapters confirmed that overexpressing p.D469del COMP in HT1080 cells replicated important features of PSACH *in vitro*. Using this cell model, the complex molecular pathways underlying PSACH were then investigated *in vitro* and potential genes of interest identified. Although many studies have focused on the p.D469del COMP mutation, it is not fully understood whether all disease-causing *COMP* mutations share a common disease mechanism, or whether characteristics are specific to individual mutations. Therefore, HT1080 cells expressing different, disease-causing *COMP* mutations were analysed and the results compared to observations made in p.D469del COMP cells.

7.11 Chapter aims

- Examine mutant protein retention in HT1080 cells overexpressing MED- and PSACH-causing mutant COMP.
- Investigate whether MED and PSACH-causing mutations of COMP trigger the UPR.
- Analyse genes of interest selected from RNA sequencing.
- Investigate whether these genes of interest could be specific for COMP mutations or are common targets in chondrodysplasia.

7.2 Disease-causing COMP mutations display varying degrees of protein retention when overexpressed in HT1080 cells

Previous studies were able to show that mutations in some regions of COMP are more likely to result in MED, whilst mutations in others result in PSACH (Briggs et al., 2014). This indicates that some regions in COMP are less sensitive to mutation, perhaps because they are less important for the function of COMP or because their amino acid composition is less restricted. So far, most research has focused on a few, specific mutations, and only limited research has been undertaken to compare mutations within the same region of COMP. It is so far unknown whether the p.D469del mutation exerts its effect via the same or distinct pathways as other disease-causing mutations. Therefore, HT1080 cells overexpressing MED- or

PSACH-causing mutant COMP were examined and the findings compared to the findings from p.D469del COMP cells. Notably, these cell lines were not FACS sorted.

Firstly, the effect of several disease-causing COMP mutations on intracellular retention was examined (Figure 7.1). In total, cell lysates and conditioned media from HT1080 cells overexpressing three MED-causing mutations (p.C312Y, p.D385N and p.N489K) and three PSACH-causing mutations (p.D473H, p.G440R and p.D511Y) were analysed alongside wild type COMP-overexpressing cells. Unfortunately, no protein was detected in either cell lysate or conditioned media of p.N489K COMP cells (Figure 7.1 A, B, indicated by *), implying that these cells express no or only very small amounts of this COMP variant. This cell line was therefore not used for further studies.

Whilst wild type COMP was readily detected in both cell lysates and conditioned media (Figure 7.1, A, B), the amount of secreted COMP appeared decreased in MED-causing mutations and below detection limits in PSACH-causing mutations. Apart from p.N489K COMP, all mutant COMP proteins were successfully detected in samples from cell lysates. Interestingly, whilst the amount of intracellular COMP relative to GAPDH was not significantly different between wild type- and mutant COMP-overexpressing cell lines (Figure 7.1, C, D), the ratio between intracellular and secreted COMP was significantly changed in all but one (p.C312Y) mutation (Figure 7.1 E, F, G, H). A similar observation had been made for cells overexpressing p.D469del COMP (see Chapter 5). Furthermore, there appeared to be a difference between the p.C312Y MED-causing mutation and the p.D473H PSACH-causing mutation, indicating that a milder effect on protein secretion may be associated with a milder phenotype. This demonstrated that disease-causing mutations within the type 3 repeats of COMP affect COMP secretion, and that PSACH-causing mutations of the type 3 repeats may impact secretion more severely than MED-causing mutations. Since retained p.D469del COMP does not appear to trigger the activation of the UPR, the levels of several UPR markers (BiP, calnexin, phosphorylation of eiF2α and *XBP1* splicing) were assessed in p.C312Y, p.D385N, p.D473H, p.G440R and p.D511Y COMP-overexpressing cells to investigate whether this is a common occurrence in COMPopathies.

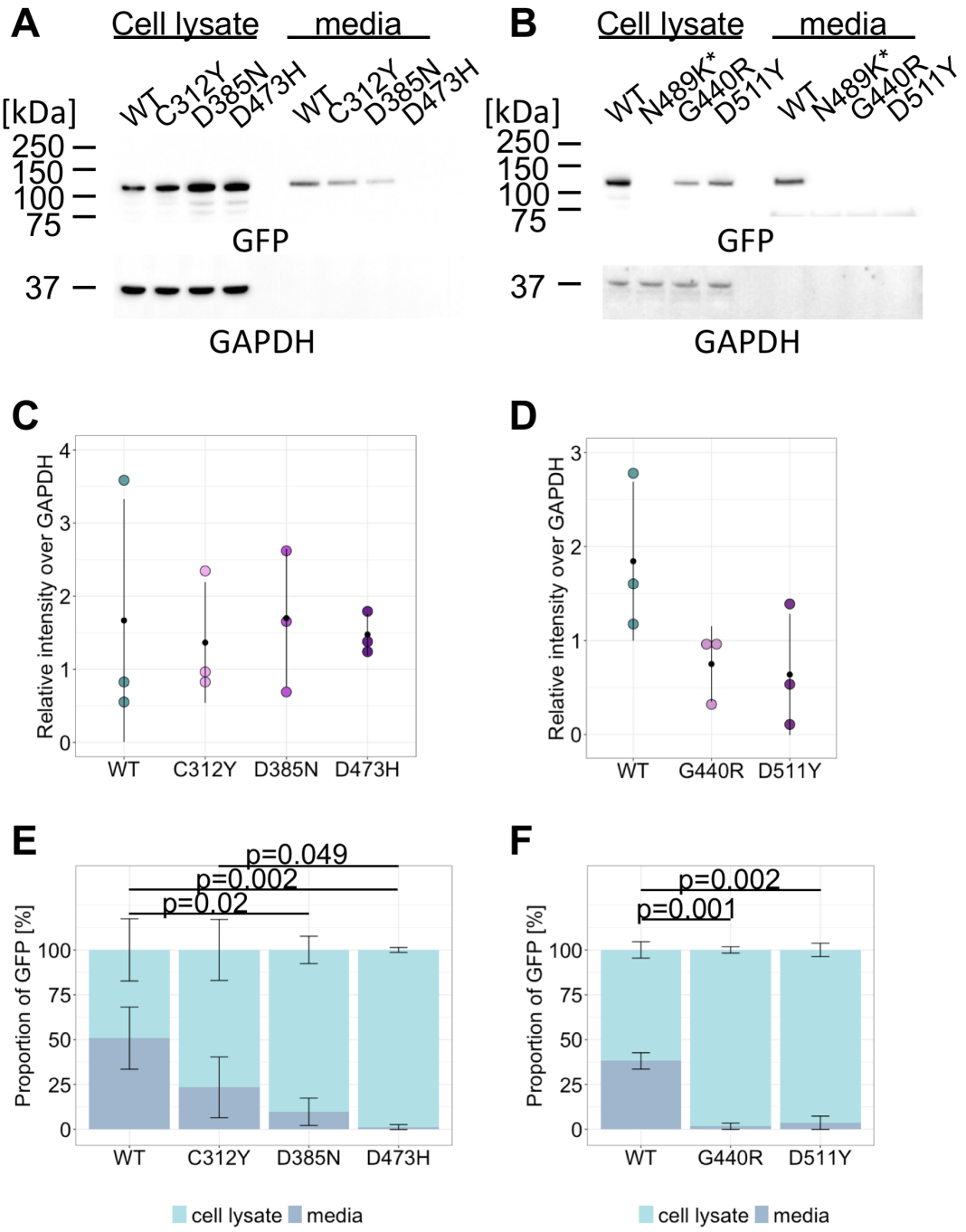

Figure 7.1 – Intracellular retention of disease-causing COMP proteins in HT1080 cells. (A, B) Western Blot of cell lysates and media from HT1080 cells overexpressing wild type COMP (WT) or mutant COMP. COMP proteins were detected via the C-terminal GFP tag. GAPDH was used as a loading control for cell lysates. (C, D) Densitometric quantification of total intracellular GFP-COMP protein levels. Black dots represent mean values, bars show standard deviation. (E, F) Quantification of relative proportion of GFP-COMP protein in cell lysates and conditioned media. N = 3 experiments. Bars represent standard deviation, *P*-values were determined using ANOVA and Tukey post-hoc.

7.3 Disease-causing COMP mutations do not trigger the UPR

Protein levels of BiP were examined by western blotting (Figure 7.2 A, B). Whilst BiP was successfully detected in samples from all cell lines, no significant increase in BiP protein was observed in mutant COMP cell lines compared to wild type COMP cells (Figure 7.2 C, D). Only cells overexpressing p.D473H COMP tended to have slightly higher BiP level; however, this was not statistically significant. In contrast to that, protein levels of BiP in cells overexpressing p.D511Y COMP appeared reduced, although this too failed to reach statistical significance. These cells also displayed a relative low amount of intracellular GFP-COMP (Figure 7.1 D). This could indicate that these cells express less recombinant COMP compared to wild type COMP-overexpressing cells, potentially due to the stress caused by retention of the mutant protein.

When calnexin levels were evaluated, again no significant difference was observed between wild type and mutant COMP cells (Figure 7.3). This demonstrated that whilst mutations within the type 3 repeats of COMP inhibited efficient protein secretion, they did not appear to cause an increase in chaperone levels.

Next, phosphorylation of eiF2α was analysed. A downstream effector of the PERK branch of the UPR, phosphorylation of eiF2α could affect general protein translation as well as expression of pro-apoptotic genes, such as *DDIT3.* When examined (Figure 7.4), some phosphorylation of eiF2α was observed in all cell lines. Similar to p.D469del COMP cells, none of the cell lines expressing MED- or PSACH-causing COMP mutations exhibited significantly elevated phosphorylation of eiF2α suggesting that the PERK branch is not activated in response to overexpression of mutant COMP.

Lastly, splicing of *XBP1* was evaluated by RT-PCR (Figure 7.5). No difference in spliced *XBP1* was observed between wild type, p.C312Y, p.D385N and p.D473H COMP-overexpressing cells (Figure 7.5, A, C). There appeared to be a small, but significant difference between p.D385N COMP and p.D473H COMP-overexpressing cells, although *XBP1* splicing in both cell lines was not significantly different from *XBP1* splicing in wild type COMP cells. Compared to wild type COMP cells, p.G440R and p.D511Y COMP-overexpressing cells displayed reduced *XBP1* splicing levels (Figure 7.5 B, D), similar to p.D469del COMP-overexpressing cells.

Together, these findings demonstrate that mutations within the type 3 repeats of COMP do not cause the activation of the UPR, despite impairing the secretion of COMP.

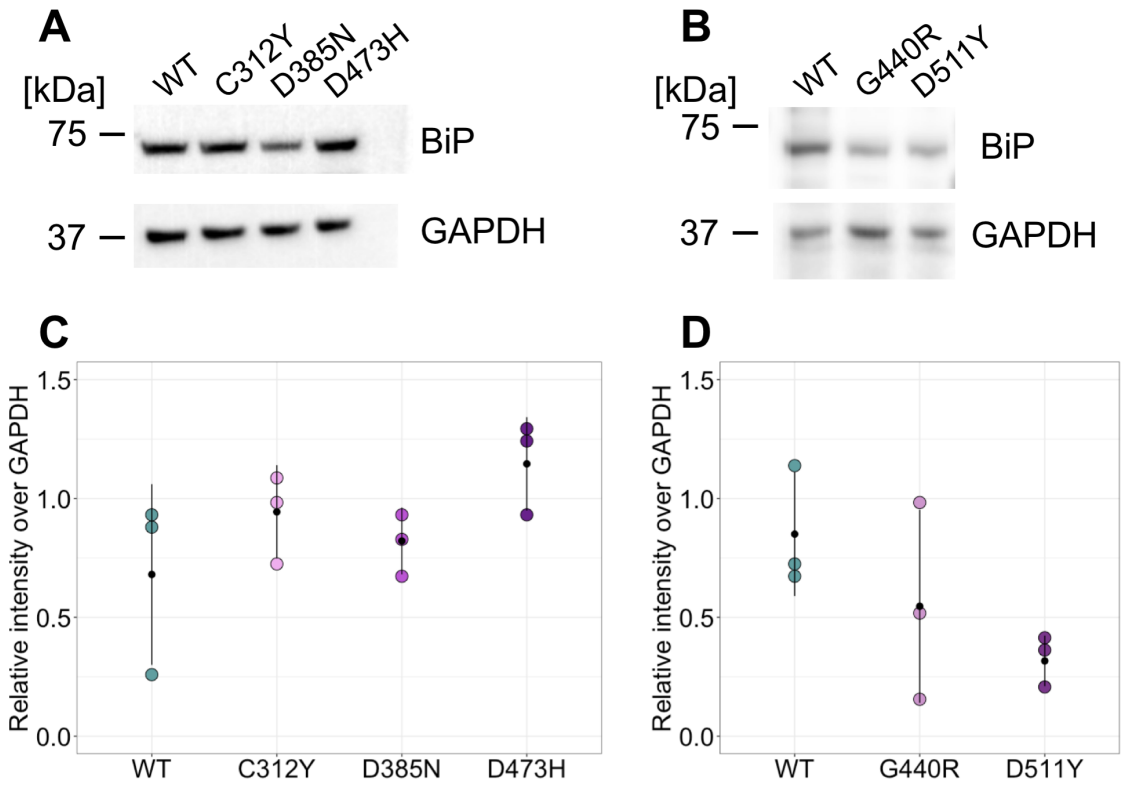

Figure 7.2 – BiP protein levels of HT1080 cells expressing disease-causing COMP mutants. (A, B) Western Blot and (C, D) quantification of BiP levels in wild type COMP (WT) or mutant COMP cells. GAPDH was used as loading control. Black dots represent mean values, bars show standard deviation, n = 3 experiments, *P*-values were determined using ANOVA and Tukey post-hoc.

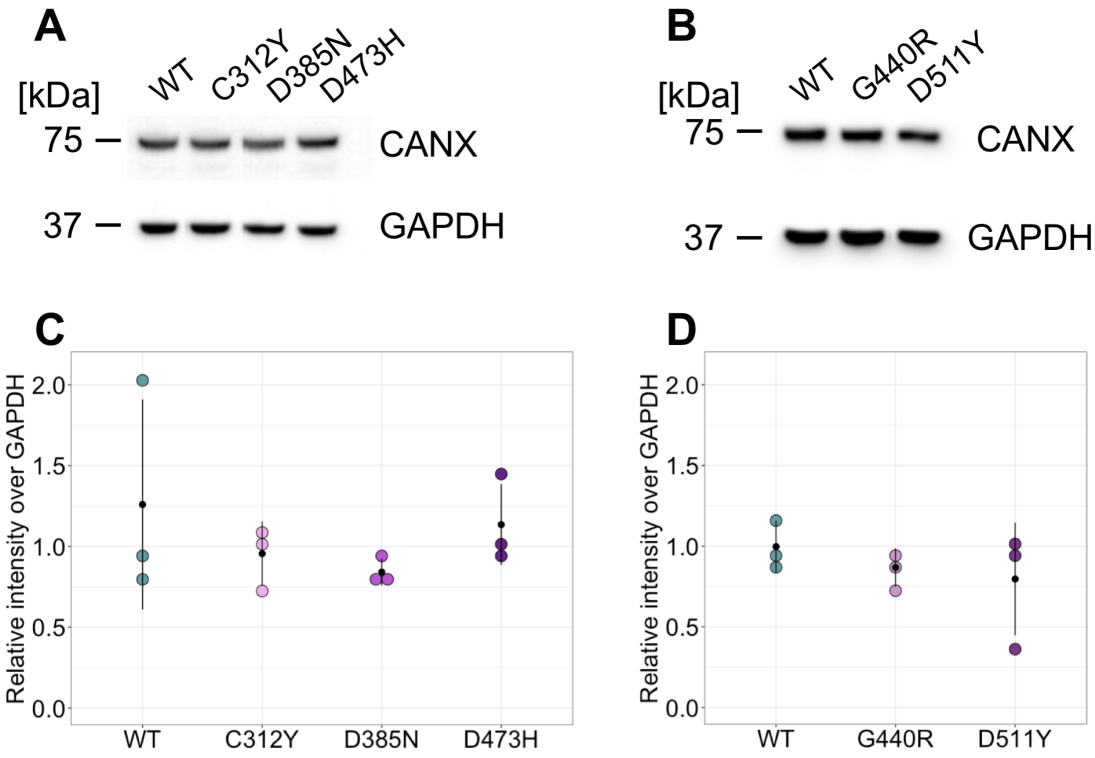

Figure 7.3 – Calnexin protein levels of cells expressing disease-causing COMP mutants. (A, B) Western Blot and (C, D) quantification of calnexin (CANX) levels in wild type COMP (WT) or mutant COMP HT1080 cells. GAPDH was used as loading control. Black dots represent mean values, bars show standard deviation, n = 3 experiments, *P*-values were determined using ANOVA and Tukey post-hoc.

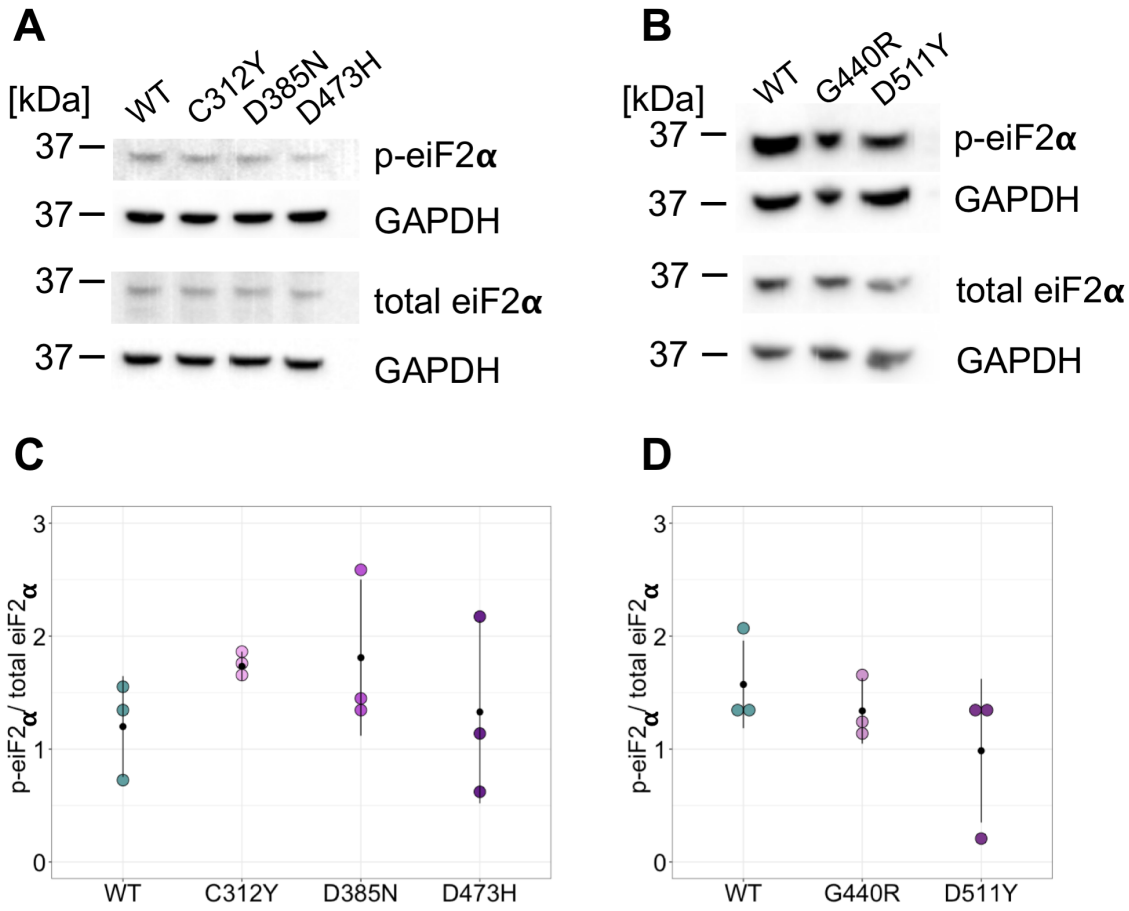

Figure 7.4 - Phosphorylation of eiF2α in mutant COMP cells. (A, B) Western blot and (C, D) quantification of phosphorylated (p-eiF2α) and total eiF2α in wild type (WT) and mutant COMP-overexpressing cells, n = 3 experiments. GAPDH was used as loading control. Black dots represent mean values, bars show standard deviation, *P*-values were determined using ANOVA and Tukey post-hoc. The membrane used in Figure 7.1 A was re-incubated with p-eiF2α antibody, thus the same GAPDH is shown as loading control.

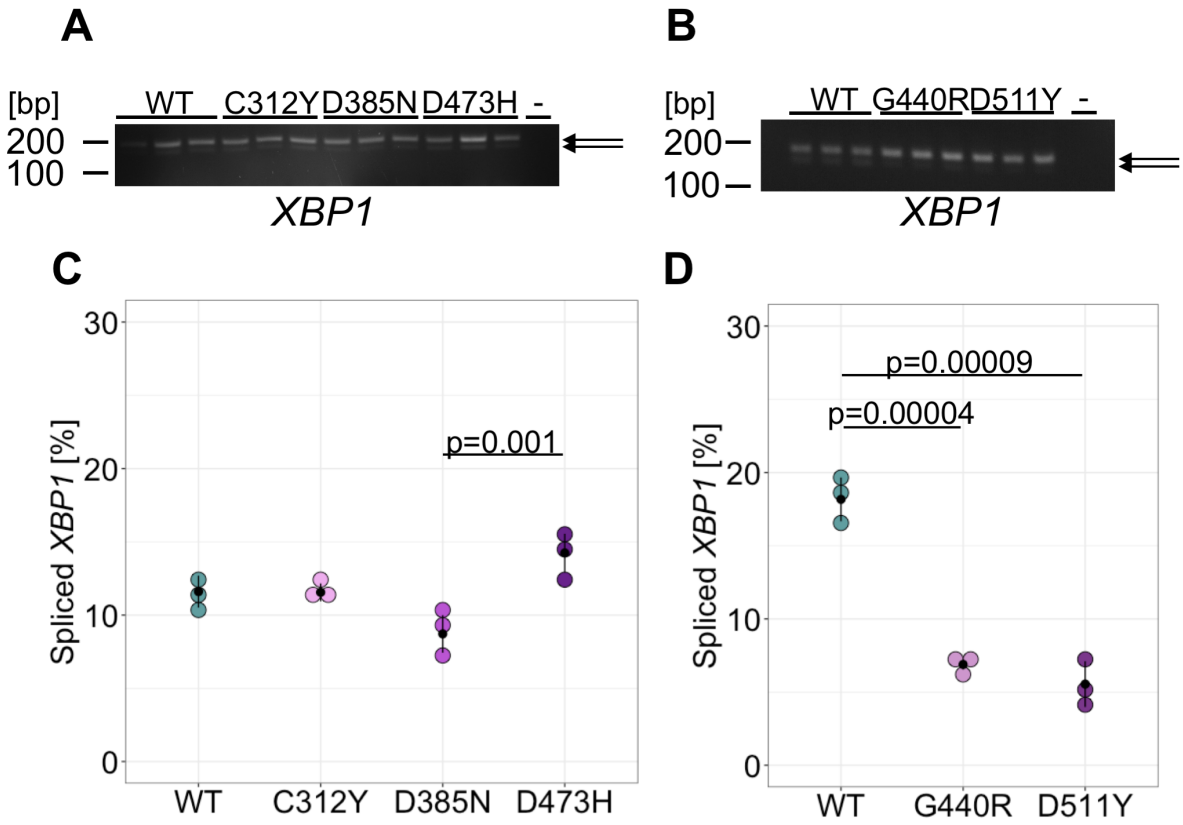

Figure 7.5 – *XBP1* splicing in cells overexpressing wild type and mutant COMP. (A, B) RT-PCR and subsequent agarose gelelectrophoresis were used to visualise spliced and unspliced *XBP1* (arrows). Brightness of both images was adjusted equally after quantification. (C, D) Quantification of spliced *XBP1*. Black dots represent mean values, bars show standard deviation, *P*-values were determined using ANOVA and Tukey post-hoc.

7.4 Disease-causing COMP mutations do not affect cell proliferation or oxidative stress

Since peroxiredoxin-2 (PRDX2) levels are reduced in p.D469del COMP cells, PRDX2 levels were analysed by western blotting. Surprisingly, PRDX2 levels remained unchanged in all cell lines studied (Figure 7.6).
In p.D469del COMP cells, reduced levels of PRDX2 were accompanied by a reduction in AKT phosphorylation. When phosphorylation of AKT was examined in p.C312Y, p.D385N, p.D473H, p.G440R and p.D511Y COMP cells (Figure 7.7), no significant changes to wild type COMP cells were detected, consistent with normal levels of PRDX2.

Because AKT is closely linked to pro-survival signalling, and a reduction in cell proliferation was identified in p.D469del COMP cells, cell proliferation was analysed in p.C312Y, p.D385N, p.D473H, p.G440R and p.D511Y COMP-overexpressing cells by BrdU-labelling (Figure 7.8). Surprisingly, cell proliferation appeared unaffected by the expression of p.C312Y, p.D385N, p.D473H, p.G440R and p.D511Y COMP.

This raised the question as to whether these cells would display other features previously identified in p.D469del COMP cells, such as an increase in superoxide levels. Therefore, superoxide levels were analysed using a modified NBT-assay and mitochondrial integrity was examined using MitoTracker staining (Figure 7.9). No difference in mitochondrial staining was observed between wild type and p.D473H COMP-overexpressing HT1080 cells (Figure 7.9 A). This is in agreement with findings from p.D469del COMP-overexpressing cells, which also did not display a prominent change in MitoTracker staining pattern or intensity. Surprisingly, the MitoTracker staining was visibly reduced in both p.C312Y and p.D385N COMP-overexpressing HT1080 cells. Since this experiment was performed only once, further repeats will be necessary to make meaningful conclusions.

Surprisingly, when levels of superoxide were examined, no significant differences were observed under basal conditions as well as after additional challenge with menadione between wild type and mutant COMP-overexpressing HT1080 cells. Nevertheless, cells overexpressing p.D385N and p.D473H COMP tended to have slightly increased superoxide levels after menadione treatment compared to wild type COMP cells.

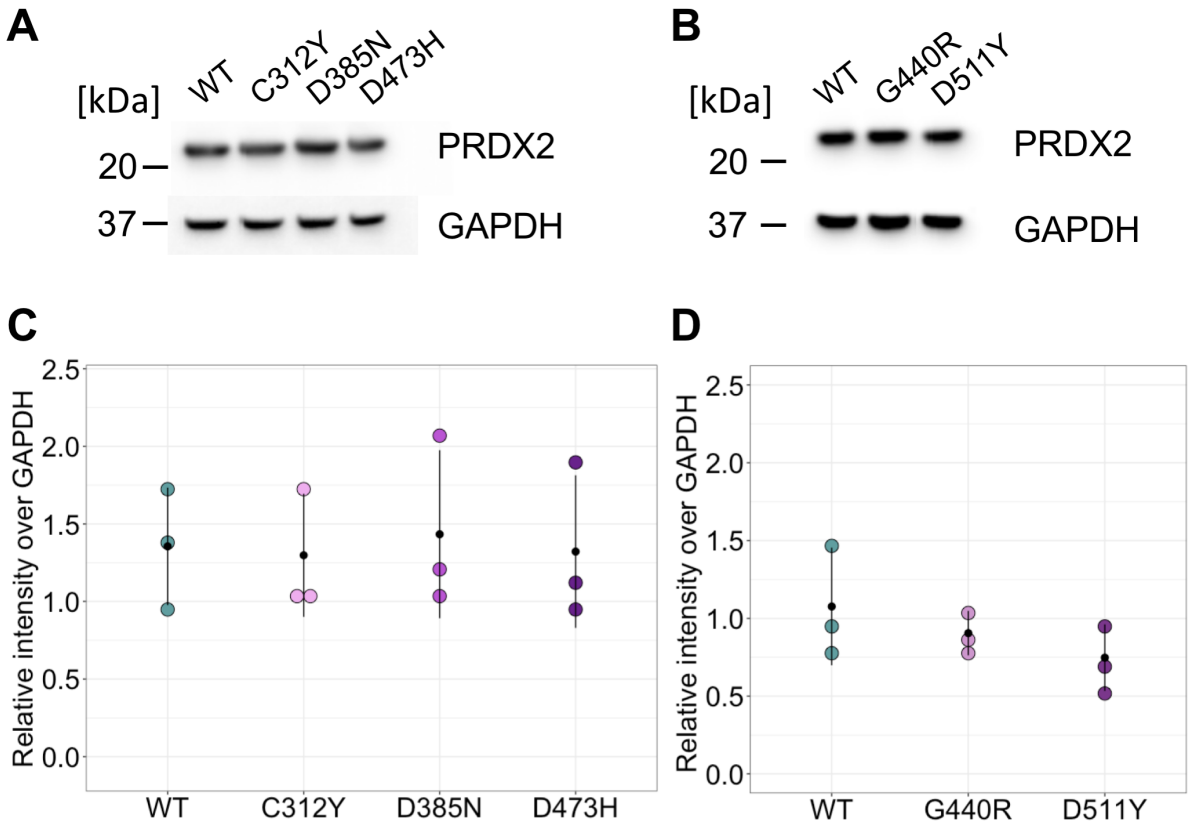

Figure 7.6 – Peroxiredoxin-2 protein levels in mutant COMP cells. (A, B) Western blot and (C, D) quantification of peroxiredoxin-2 (PRDX2) in wild type (WT) and mutant COMP-overexpressing cells, n = 3 experiments. GAPDH was used as loading control. Black dots represent mean values, bars show standard deviation, *P*-values were determined using ANOVA and Tukey post-hoc.

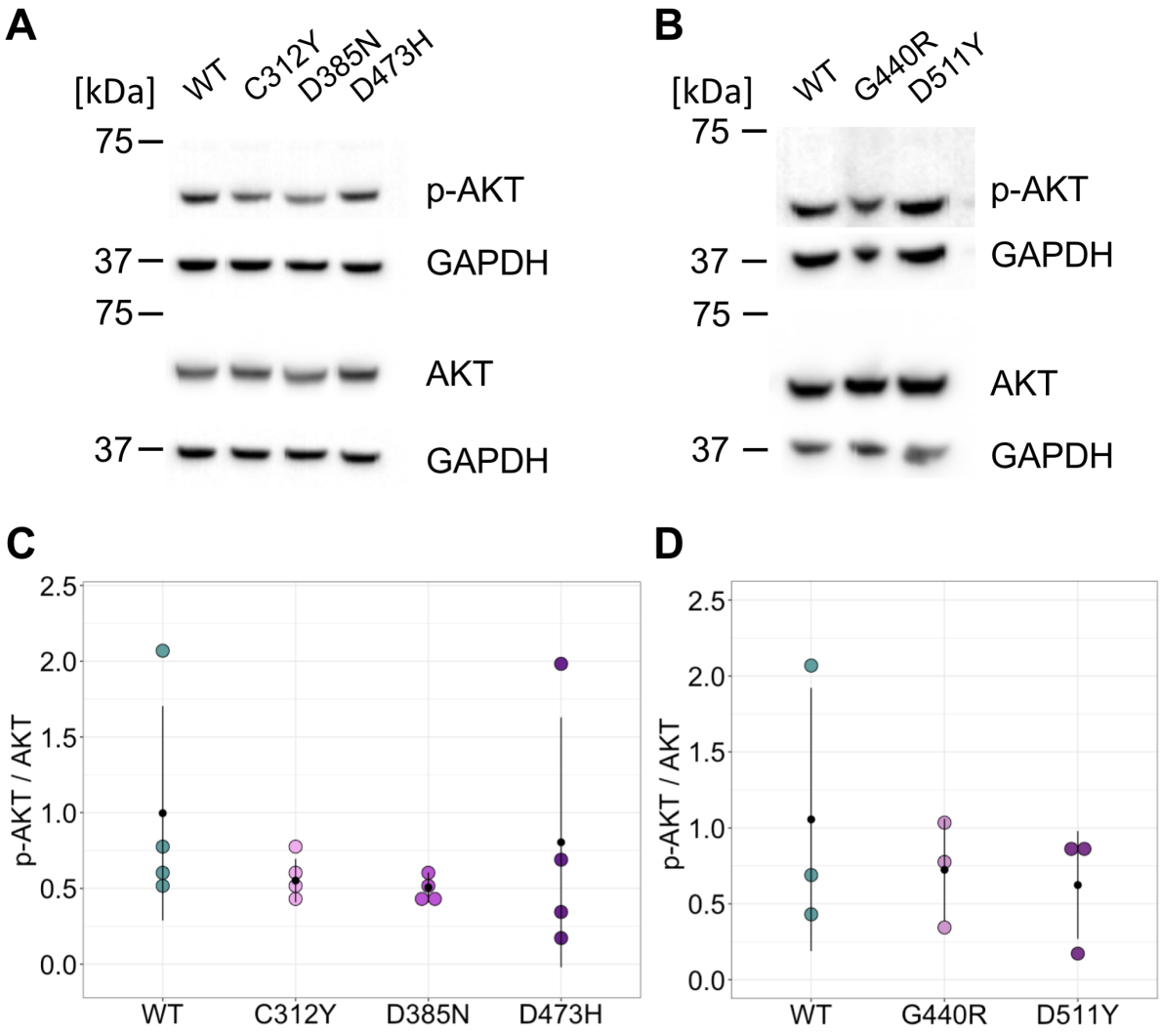

Figure 7.7 - Phosphorylation of AKT in mutant COMP cells. (A, B) Western blot of phosphorylated AKT (p-AKT) and total AKT (AKT) and (C, D) quantification of AKT phosphorylation in wild type (WT) and mutant COMP-overexpressing cells, n = 3-4 experiments. GAPDH was used as loading control. Black dots represent mean values, bars show standard deviation, *P*-values were determined using ANOVA and Tukey post-hoc. (A) The membranes shown in Figure 7.1 A and Figure 7.4 A (bottom) were re-incubated with (p-)AKT-specific antibodies, respectively, thus the same GAPDH is shown as loading control. (B) The membranes used in Figure 7.4 (p-/total eiF2α) were re-incubated with (p-)AKT-specific antibodies, therefore the same GAPDH is shown as loading control.

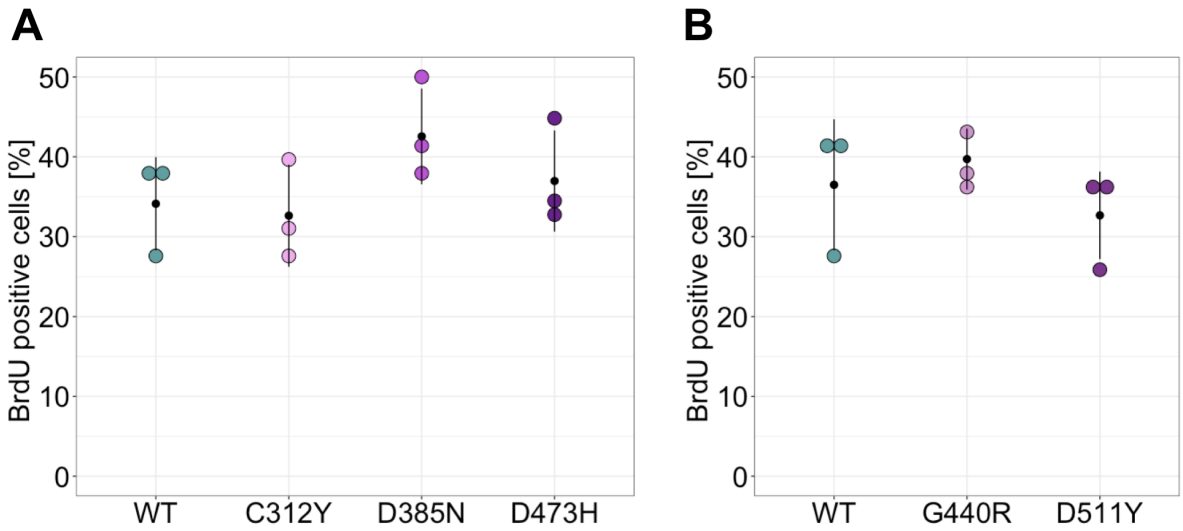

Figure 7.8 – Analysis of cell proliferation in HT1080 cells overexpressing mutant COMP. (A) Quantification of BrdU positive nuclei relative to total number of nuclei in cells overexpressing wild type, C312Y, D385N or D473H COMP. (B) Quantification of BrdU positive nuclei relative to total number of nuclei in cells overexpressing wild type, G440R or D511Y COMP. N = 3 experiments, *P*-value calculated using ANOVA and Tukey post-hoc. Black dots represent mean value, black bars display standard deviation.

A

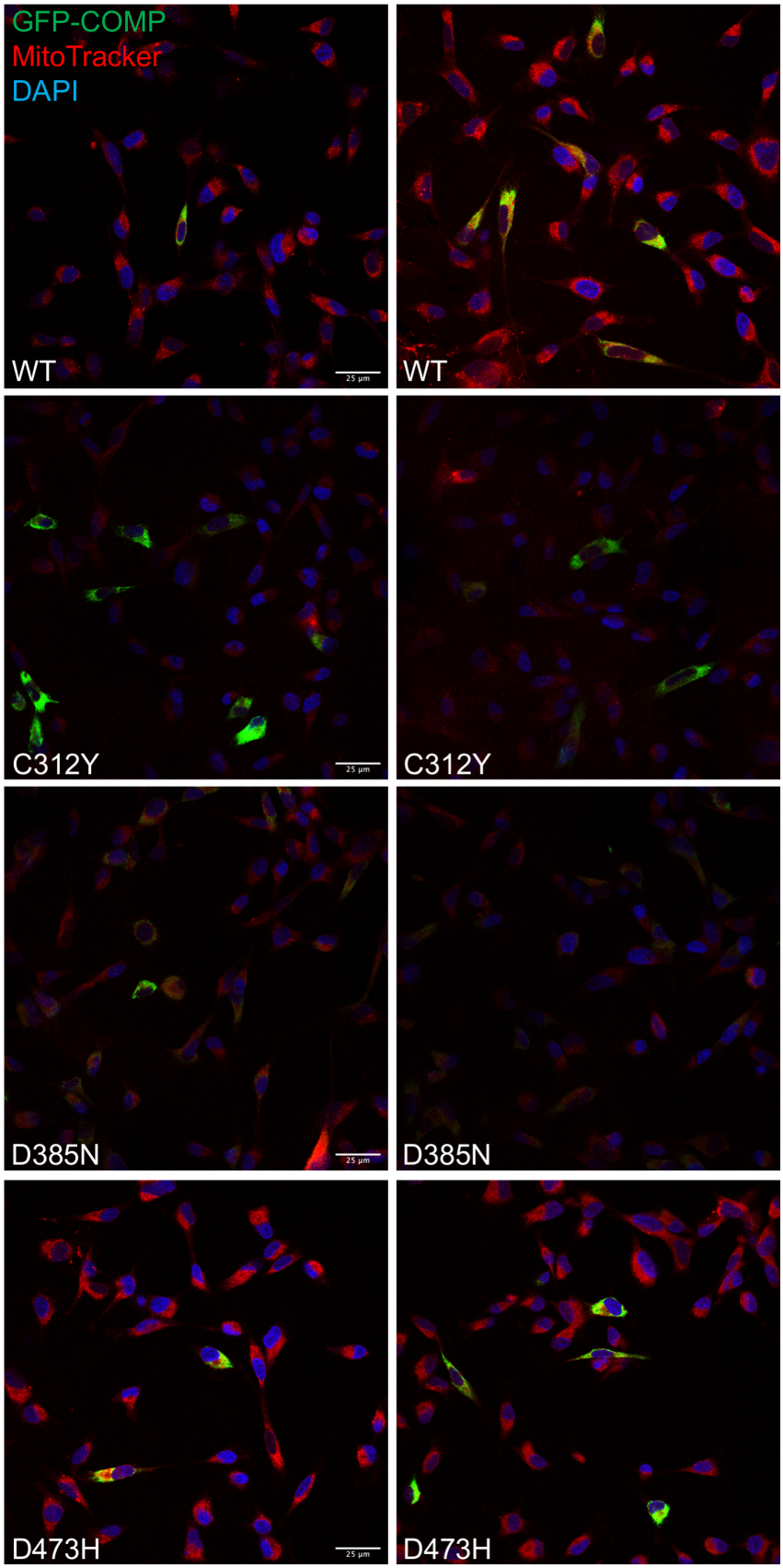
GFP-COMP
MitoTracker
DAPI
WT
WT
C312Y
C312Y
D385N
D385N
D473H
D473H

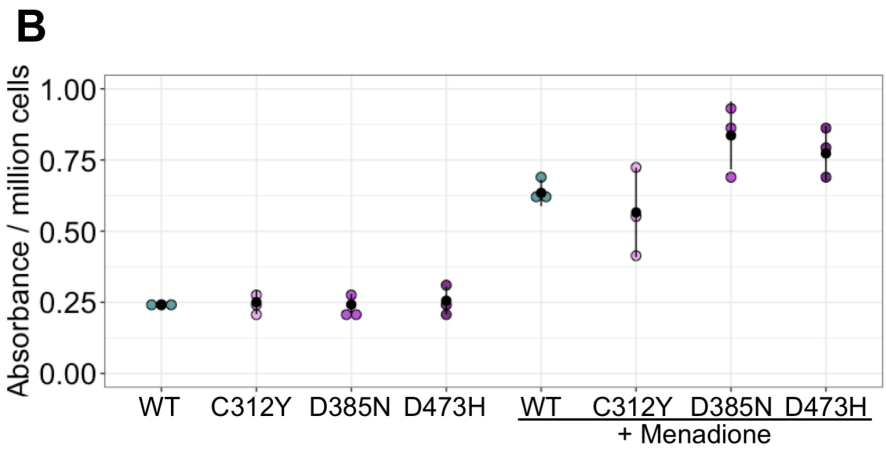

Figure 7.9 – Mitochondrial integrity and superoxide levels in cells overexpressing mutant COMP. (A) Mitochondria were visualised using MitoTrackerRed-CM-H_2Xros. The reduced dye becomes visible (red) upon oxidation in the mitochondria. Accumulation is dependent on intact membrane potential, n = 1 experiment. (B) Modified NBT-assay revealed no differences in superoxide levels between wild type (WT) and mutant COMP cells under basal conditions as well as after additional challenge with menadione, n = 3 experiments. Black dots represent mean values, bars show standard deviation *P*-values were determined using ANOVA and Tukey post-hoc

7.5 Disease-causing COMP mutations exhibit a genotype-dependent increase in *MMP9* expression

Although p.D473H, p.G440R and p.D511Y and – to a lesser extent – p.C312Y and p.D385N impaired COMP secretion and did not trigger the UPR, similar to p.D469del COMP expression, neither a reduction in cell proliferation nor signs of oxidative stress were observed. This raised the question, whether cells overexpressing p.C312Y, p.D385N, p.D473H, p.G440R and p.D511Y express less of these mutant proteins compared to wild type COMP-overexpressing cells, perhaps even too little to drive significant changes in cellular behaviour. A decrease in expression of the mutant transcript had previously been observed in p.D469del COMP cells. Nevertheless, in the case of p.D469del COMP cells, the mutant protein appeared to be present in sufficient quantities to stress the cells despite the reduced expression.

When *GFP* expression was examined as a proxy for recombinant COMP expression (Figure 7.10), no significant difference was detected between wild type COMP- and p.C312Y as well as p.D385N COMP-overexpressing cells (Figure 7.10 A). For p.D473H COMP-overexpressing cells, expression appeared very variable, but consistently increased compared to wild type, p.C312Y and p.D385N COMP-overexpressing cells. The PSACH-causing mutations p.G440R and p.D511Y appeared to result in significantly lower expression of recombinant COMP compared to wild type COMP cells (Figure 7.10 B).

Apart from differences in expression, different mutations may also exert their effect via different pathways. It was therefore important to determine whether some of the DEGs identified by RNA sequencing of p.D469del COMP cells would also be differentially expressed in these other mutant COMP cells. Expression of *MMP9*, *GALNT18*, and *MMP1* was therefore assessed by qRT-PCR (Figure 7.11). Intriguingly, *MMP9* expression was consistently elevated in cell lines overexpressing mutant COMP compared to wild type (Figure 7.11 A, B). Notably, the increase in *MMP9* expression in p.C312Y and p.D385N COMP-overexpressing cells - both of which cause MED – was considerably less than in cells overexpressing the PSACH-causing mutations p.D473H (Figure 7.11 A). Importantly, this difference was found to be statistically significant (Figure 7.11 A). Despite expressing less recombinant COMP than the wild type COMP-overexpressing cells, p.G440R and p.D511Y COMP cells both displayed substantial increases in *MMP9* expression when compared to

wild type COMP-overexpressing cells (Figure 7.11 B), with p.D511 COMP cells also exhibiting significantly higher *MMP9* expression compared to p.G440R COMP cells.

When *GALNT18* expression was examined, p.C312Y, p.D385N, p.D473H and p.D511Y COMP cells exhibited elevated expression levels. Only p.G440R COMP-overexpressing cells displayed a reduction in *GALNT18* expression. No statistically significant differences were identified between cell lines overexpressing different mutations of COMP.

Lastly, *MMP1* expression was analysed. Although *MMP1* expression tended to be slightly higher in p.G440R and p.D511Y COMP-overexpressing HT1080 cells, no significant alterations in *MMP1* expression were identified in p.C312Y, p.D385N, p.G440R and p.D511Y COMP cells. Only p.D473H COMP cells demonstrated an increase in *MMP1* expression level, although the expression of *MMP1* in these cells was found to vary considerably.

When gelatinase activity was assessed by gelatin zymography (Figure 7.12), concentrated conditioned media of p.C312Y, p.D385N and p.D473H COMP-overexpressing cells exhibited a pronounced increase in active MMP9 as well as MMP2 compared to concentrated conditioned media of wild type COMP-overexpressing cells (Figure 7.12 A). As a loading control, samples that were used for zymography were also subjected to SDS-PAGE and subsequent Coomassie staining (Figure 7.12 B). When normalised to the protein amount, only conditioned media from p.D473H COMP cells displayed significantly enhanced MMP9 activity, despite the increase in conditioned media from p.C312Y and p.D385N COMP cells being clearly visible. When concentrated conditioned media of p.G440R and p.D511Y COMP-overexpressing cells were examined, the difference was less pronounced. Nevertheless, p.D511Y COMP cells displayed significantly elevated levels of active MMP9 compared to wild type COMP cells (Figure 7.12 C).

To summarise, expression of recombinant COMP of the milder mutations p.C312Y and p.D385N COMP was not significantly different compared to wild type COMP and induced significant elevations of both *MMP9* and *GALNT18* expression. The mutation causing a more severe phenotype (p.D473H COMP) displayed a highly variable, but potentially increased, expression of recombinant COMP. In p.D473H COMP cells,

MMP9 and *GALNT18* expression was found to be significantly higher than in wild type COMP as well as p.C312Y and p.D385N COMP cells. Cells overexpressing p.G440R and p.D511Y COMP showed a significant reduction in recombinant protein expression, but nevertheless exhibited elevated levels of *MMP9* expression. Interestingly, *GALNT18* expression was only increased in p.D511Y COMP cells. *MMP1* expression was only affected by p.D473H COMP expression, but displayed a high variability. A rise in *MMP9* expression caused significantly higher MMP9 activity in p.D473H and p.D511Y COMP cells compared to wild type COMP cells. In p.C312Y and p.D385N COMP cells, MMP9 activity was consistently elevated although this failed to reach statistical significance.

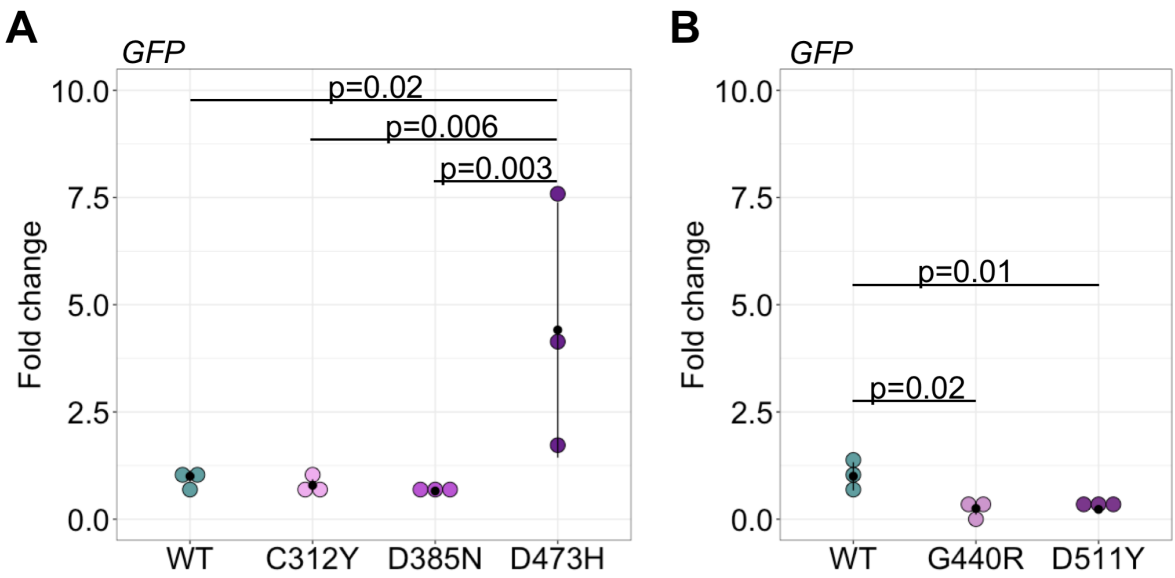

Figure 7.10 – *GFP* expression in cell lines overexpressing wild type and mutant COMP. (A, B) *GFP* expression was evaluated by qRT-PCR in wild type (WT) and mutant COMP-overexpressing HT1080 cells. 18S was used as housekeeping gene. Black dots represent mean values, bars show standard deviation, *P*-values were determined using ANOVA and Tukey post-hoc.

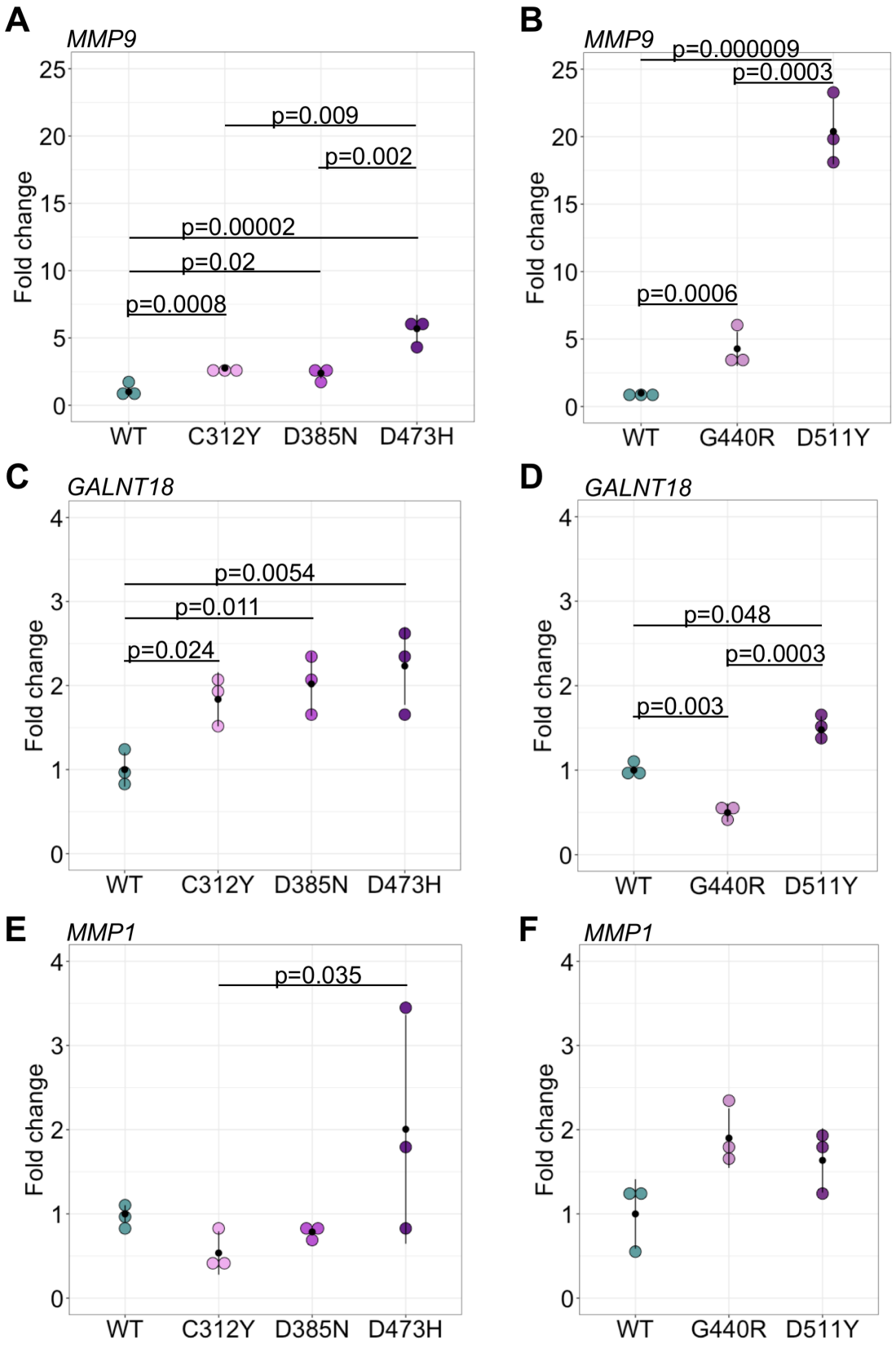

Figure 7.11 – Expression of (A, B) *MMP9,* (C, D) *GALNT18* and (E, F) *MMP1* in wild type and mutant COMP-overexpressing HT1080 cell lines. Expression was analysed by qRT-PCR, using 18S as housekeeping gene. Black dots represent mean values, bars show standard deviation, *P*-values were determined using ANOVA and Tukey post-hoc.

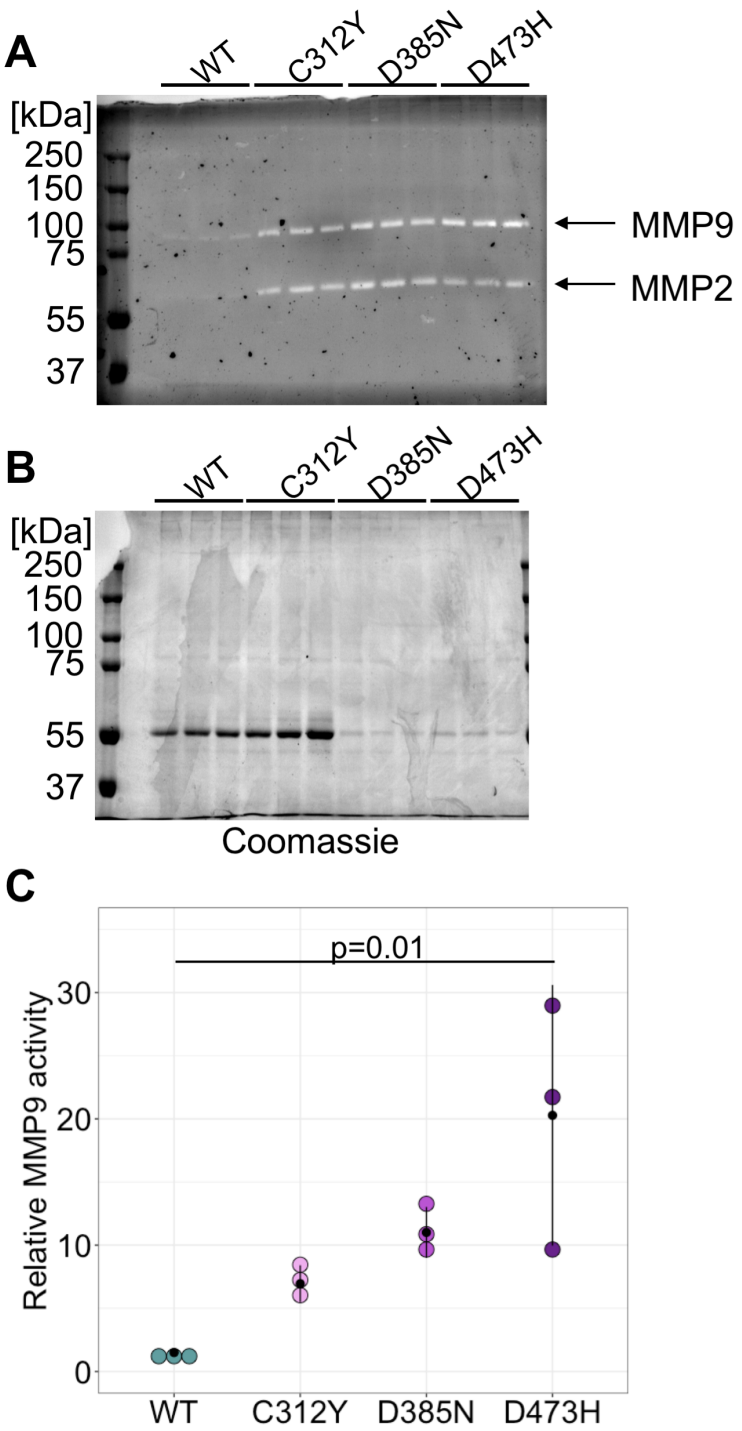

Figure 7.12 – Gelatinase activity in cells overexpressing wild type and p.C312Y, p.D385N or p.D473H mutant COMP. (A) Gelatin zymogram of concentrated, conditioned media of wild type, p.C312Y, p.D385N and p.D473H COMP-overexpressing cells. (B) Coomassie stained SDS-PAGE of samples used in (A). (C) Quantification of MMP9 activity relative to intensity of Coomassie staining. Black dots represent mean values, bars show standard deviation, *P*-values were determined using ANOVA and Tukey post-hoc.

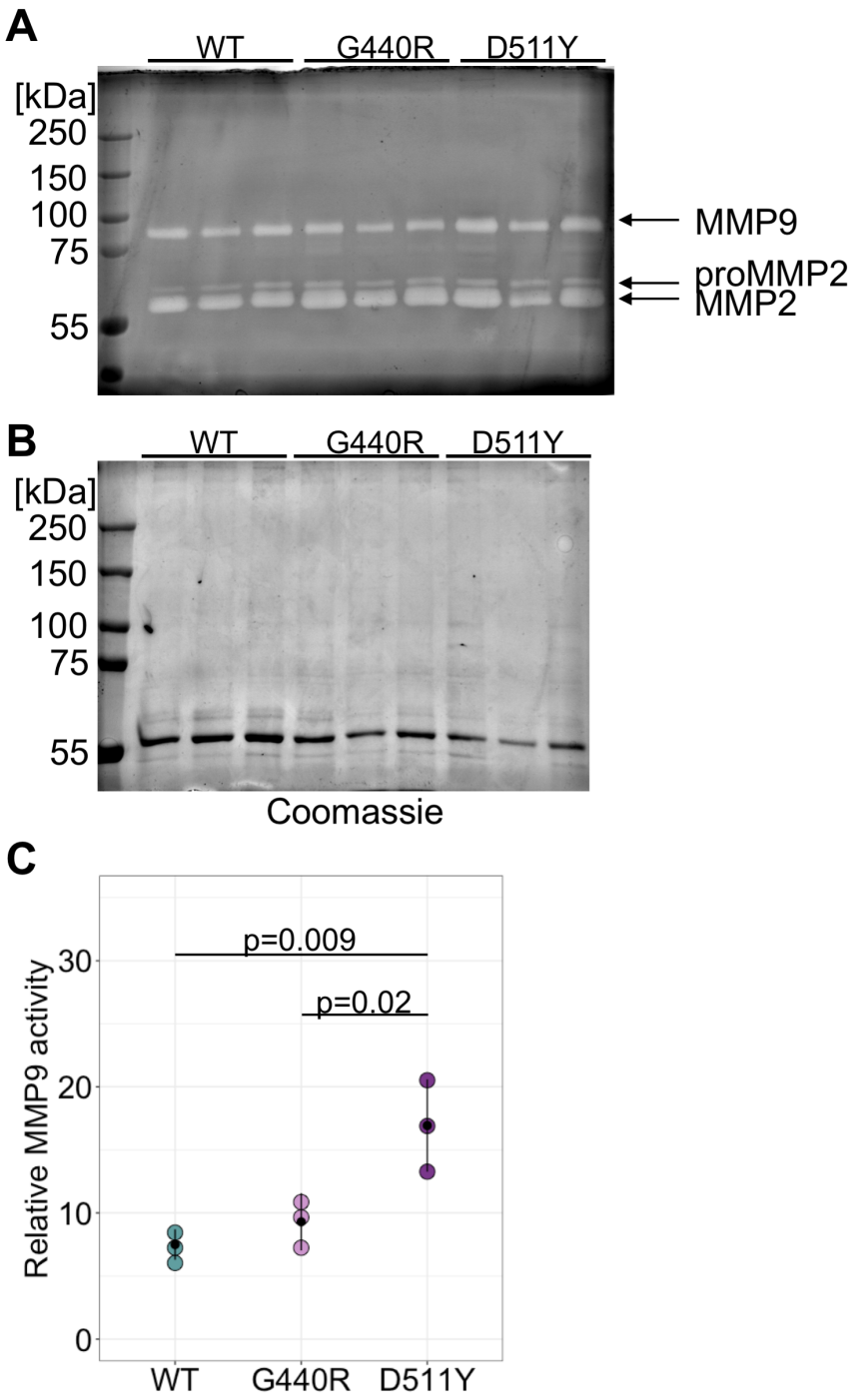

Figure 7.13 - Gelatinase activity in cells overexpressing wild type and p.G440R or p.D511Y mutant COMP. (A) Gelatin zymogram of concentrated, conditioned media of wild type, p.G440R and p.D511Y COMP-overexpressing cells. (B) Coomassie stained SDS-PAGE of samples used in (A). (C) Quantification of MMP9 activity relative to intensity of Coomassie staining. Black dots represent mean values, bars show standard deviation, *P*-values were determined using ANOVA and Tukey post-hoc

7.6 *MMP9* expression is not triggered by the expression of the MED-causing matrilin-3 p.V194D mutation

Although p.C312Y, p.D385N, p.D473H, p.G440R and p.D511Y COMP cells did not display any reductions in PRDX2 protein level, AKT phosphorylation or cell proliferation, *MMP9* and *GALNT18* expression was significantly elevated in these cell lines. This raised the question whether *MMP9* and *GALNT18* were specifically upregulated in response to mutant COMP, or whether accumulation of other disease-causing mutant proteins could induce the same effect. Mutations of matrilin-3 (*MATN3)* can lead – like some mutations of *COMP* – to MED; however, in contrast to mutant COMP, the intracellular accumulation of p.V194D matrilin-3 triggers the activation of the UPR (Leighton et al., 2007).

Therefore, flag-tagged wild type and the MED-causing (p.V194D) matrilin-3 were overexpressed transiently in HT1080 cells. After the confirmation of protein retention and induction of the UPR, expression of *MMP9* and *GALNT18* was examined (Figure 7.14). As expected, wild type matrilin-3 was detected in both cell lysates and conditioned media of transfected cells whilst p.V194D matrilin-3 was only present in the cell lysate (Figure 7.14 A). This led to increased levels of BiP protein in p.V194D matrilin-3-overexpressing cells compared to wild type matrilin-3-overexpressing as well as non-transfected cells. (Figure 7.14 A, B). Levels of spliced *XBP1* were also elevated in p.V194D matrilin-3 compared to wild type matrilin-3 cells (Figure 7.14 C, D). A rise in BiP protein levels as well as increased *XBP1* splicing clearly demonstrated the expected activation of the UPR by the expression of p.V194D matrilin-3.

When gene expression was examined by qRT-PCR, no differences in *GALNT18* and *MMP9* expression were detected, whilst expression levels of *HSPA5* were increased as expected in p.V194D matrilin-3 cells (Figure 7.14 E).These findings clearly demonstrate that *MMP9* and - at least to some extent - *GALNT18* expression is induced specifically by mutations of *COMP* but not *MATN3.* To further confirm this finding, *GALNT18* and *MMP9* expression was analysed in wild type and p.D469del COMP-overexpressing cells treated with tunicamycin or thapsigargin to induce ER stress and the activation of the UPR (Figure 7.15). When *MMP9* expression was evaluated, DMSO-treated p.D469del COMP cells exhibited increased *MMP9* expression compared to wild type COMP cells as expected. There appeared to be a

tendency for reduced *MMP9* expression after treatment with both tunicamycin and thapsigargin in both cell lines, although this was not found to be significant (Figure 7.15 A). When *GALNT18* expression was investigated, again, p.D469del COMP cells treated with DMSO exhibited elevated *GALNT18* expression compared to DMSO-treated wild type COMP-overexpressing cells. Interestingly, treatment with thapsigargin caused a substantial reduction in *GALNT18* expression in p.D469del COMP cells. Whilst a similar trend was observed in thapsigargin-treated wild type COMP-overexpressing cells, this was not statistically significant (Figure 7.15 B).

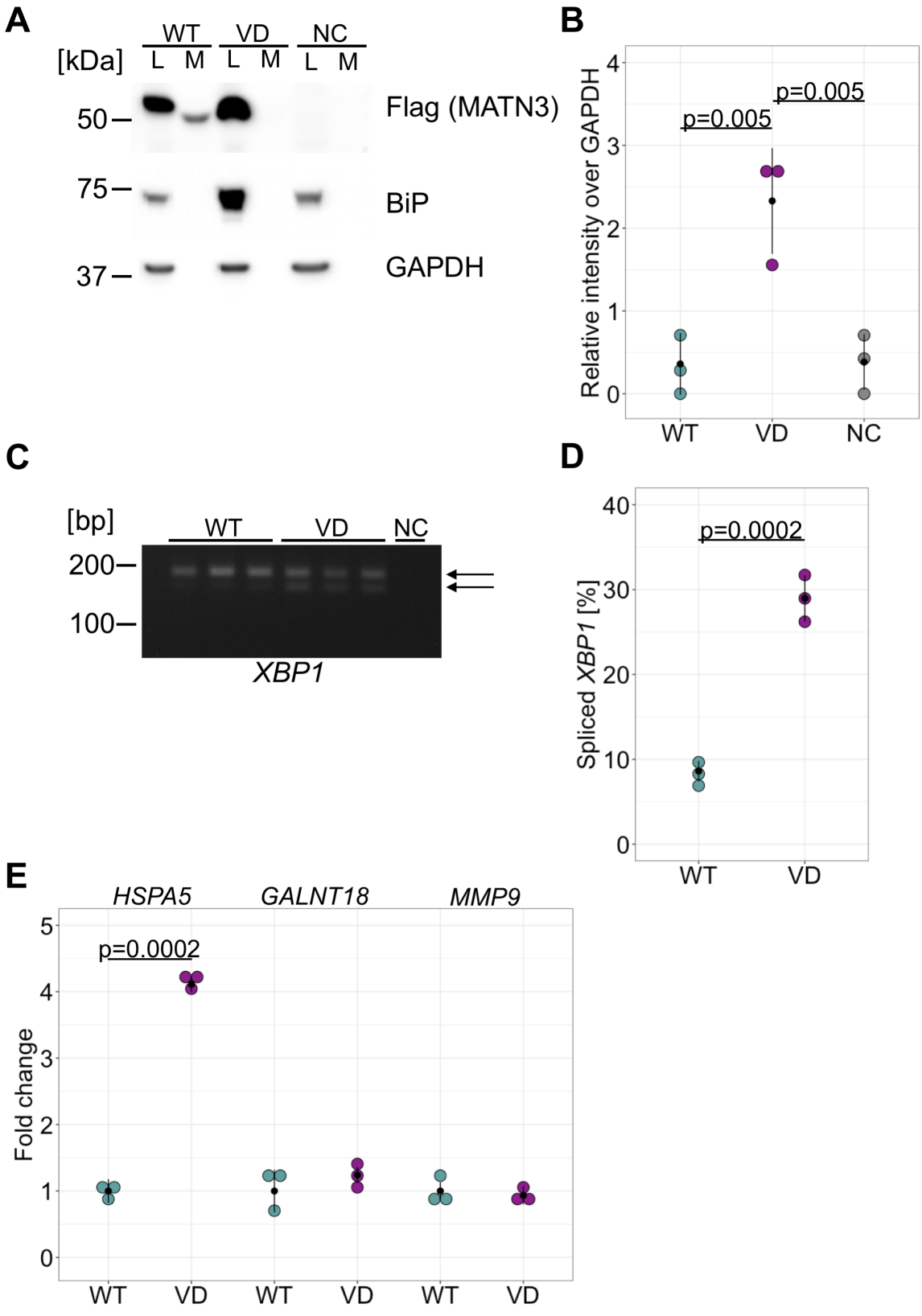

Figure 7.14 – Transient overexpression of p.V194D matrilin-3 does not trigger changes in *GALNT18* or *MMP9* expression. (A Western blot of cell transiently transfected with plasmid DNA encoding flag-tagged wild type (WT) or p.V194D (VD) matrilin-3 probed for flag-tag (recombinant matrilin-3), BiP and GAPDH (loading control). NC: non-transfected cells (negative control). L: cell lysate, m: conditioned media. (B) Quantification of BiP protein levels in cells transiently overexpressing wild type (WT) or p.V194D (VD) matrilin-3. NC: non-transfected cells (negative

control). (C) *XBP1* splicing was analysed by RT-PCR and subsequent agarose gelelectrophoresis. NC: No cDNA (negative control). (D) Densitometric quantification of *XBP1* splicing in cells transiently overexpressing wild type (WT) or p.V194D (VD) matrilin-3.
(E) Expression of *HSPA5, GALNT18* and *MMP9* was evaluated using qRT-PCR. (B, D, E) Black dots represent mean values, bars show standard deviation, *P*-values were determined using student's t-test (paired).

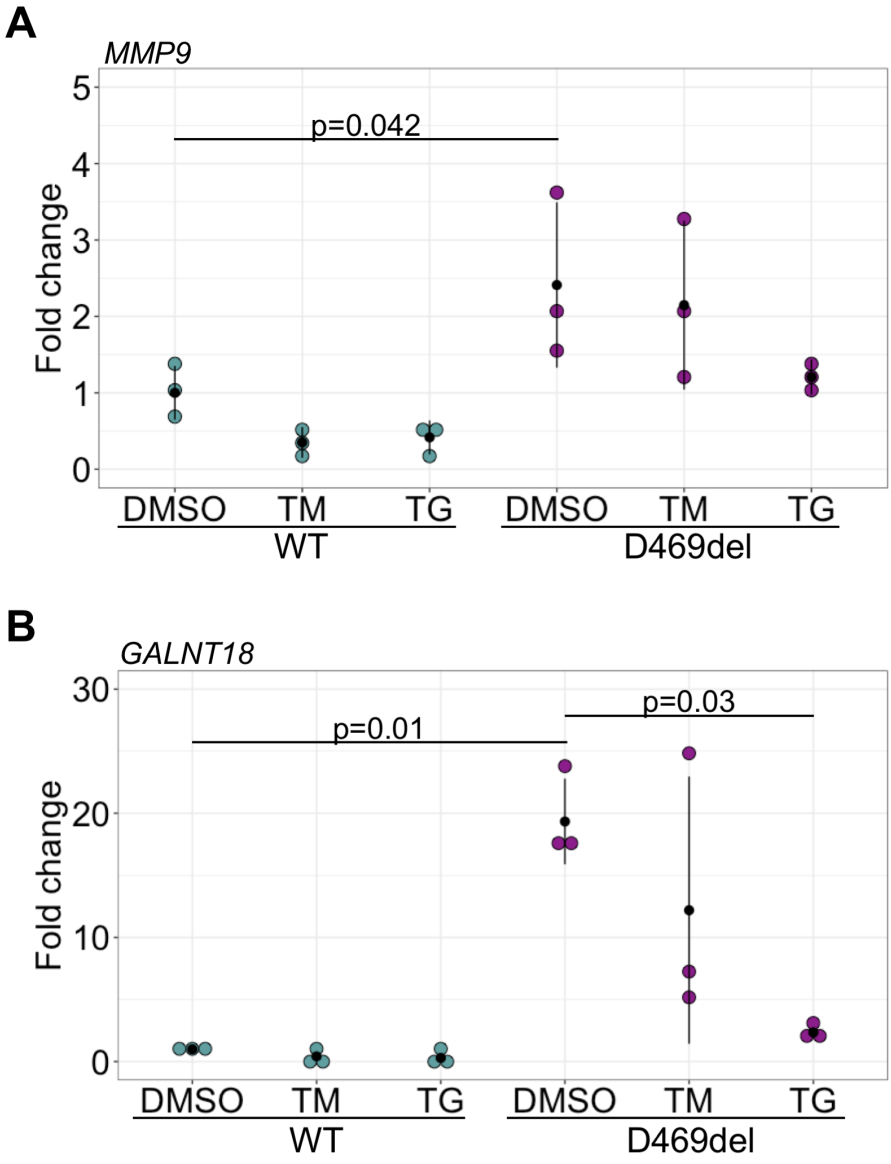

Figure 7.15 – *MMP9* and *GALNT18* expression in response to treatment with tunicamycin or thapsigargin. After treating either wild type (WT) or p.D469del COMP-overexpressing HT1080 cells with DMSO, tunicamycin (TM) or thapsigargin (TG) (A) *MMP9* and (B) *GALNT18* expression was measured by qRT-PCR. Black dots represent mean values, bars show standard deviation, *P*-values were determined using student's t-test (paired) and Bonferroni multiple test correction.

7.7 Discussion

The aims of this chapter were to systematically characterise the consequences of disease-causing point mutations within the type 3 repeats of COMP on its secretion, and to determine whether missense mutations within the type 3 repeats of COMP drive similar molecular changes to p.D469del, including gene expression.

This chapter provides evidence that missense mutations of COMP that are located within the type 3 repeats impact COMP secretion with varying severity. Mutations causing the milder MED phenotype displayed more residual secretion than mutations causing the more severe PSACH phenotype. This is in agreement with results of previous studies that analysed the retention of COMP proteins carrying mutations in various regions of COMP including the type 3 repeats (Chen et al., 2008; Schmitz et al., 2006). These studies concluded that MED-causing mutations were typically associated with less pronounced COMP retention in rat chondrosarcoma chondrocytic cells (RCS) and primary bovine chondrocytes compared to PSACH-causing mutations. Nevertheless, both studies included mutations located within the C-terminal domain. Since mutations in this region do not typically appear to interfere with COMP secretion, the comparison of PSACH causing mutations in the type 3 repeats with MED-causing mutations in the C-terminal domain is problematic. The work of this chapter was therefore restricted to mutations within the same domain of the protein.

Intriguingly, none of the mutations analysed here appeared to lead to the activation of the UPR despite the observed retention of mutant protein. This strongly suggests that the underlying mechanism is – at least – partly shared by different mutations within the same region of COMP. Whilst previous studies have suggested that mutations of *COMP* that are located within the C-terminal domain drive a transient upregulation of components of the UPR, even in the absence of intracellular protein retention (Piróg-Garcia et al., 2007), conflicting results have been described as to whether mutations within the type 3 repeats of COMP prevent efficient secretion and induce the activation of the UPR (Suleman et al., 2012; Posey et al., 2009; Chen et al., 2008; Dinser et al., 2002). Earlier work has also raised the question whether the degree of protein retention and subsequent ER stress is dependent on the cell type expressing the mutant protein (Maddox et al., 1997). This is particularly relevant because *COMP* is not only present in cartilage, and indeed expressed by a variety of cell types (Di Cesare et al., 2000, 1997; Dodge et al., 1998; Riessen et al., 2001; Södersten et al.,

2006). The direct consequences and cellular responses to mutant COMP may therefore vary between individual cell types, but may also influence each other *in vivo*, for example in the context of the joint.

Some of the features observed in D469del COMP cells, such as reduced cell proliferation, reduced PRDX2 protein levels and increased superoxide levels, were not displayed by cells overexpressing other mutant COMP constructs. This could indicate that these features are more specific to the mutation, or that these events are tied more closely to the expression level of the recombinant protein. The FACS sorting of D469del and its wild type COMP control cell line selected for cells with high intracellular or pericellular levels of GFP. Whilst this ensured the robust expression of D469del COMP and thus the analysis of a comparatively homogenous cell population, this may also have selected for cells that were more resistant to high levels of stress. Furthermore, cells with a particularly high level of COMP expression may have undergone apoptosis in response to the mutant protein accumulation, resulting in an advantage for cells with a high but tolerable expression level. With regards to the wild type COMP cell line, the sorting by intracellular and pericellular GFP fluorescence may have selected not only for high COMP secretion, but also for cells with a slow secretory pathway and high intracellular levels of COMP, which would result in a high intracellular GFP signal. In contrast to that, the p.C312Y, p.D385N, p.D473H, p.G440R, p.D511Y and wild type COMP cell lines were not sorted by GFP fluorescence, resulting in a more heterogenous cell population. The combination of both approaches allowed me to exclude, at least to some degree, that changes in gene expression were in fact artefacts caused by the sorting process. In future experiments, single cell sequencing approaches could be employed to distinguish between cell populations with different expression levels and to correlate *COMP* expression with changes in other genes of interest. Alternatively, expressing wild type and mutant COMP under the control of an inducible promoter could avoid some of the consequences of cytotoxic mutant protein accumulation and result in a more comparable amount of protein between cell lines.

In a pilot experiment, cells overexpressing the MED-causing p.C312Y and p.D385N COMP and the PSACH-causing p.D473H COMP were stained with MitoTracker dye. Only cells expressing MED-causing mutant COMP exhibited a reduction in MitoTracker staining intensity. Whilst this experiment will have to be repeated in the

future, it presents an interesting finding, since cells overexpressing the PSACH-causing p.D469del and p.D473H COMP did not exhibit any changes in staining intensity or pattern. In the future, these cell lines need to be examined in more detail to investigate whether mitochondrial function is in fact impaired by the expression of MED-causing COMP proteins. Because mitochondria are the primary source of ATP for the ER, and ER stress results in higher demand for ATP and thus, increased mitochondrial activity (Yong et al., 2019), elevated mitochondrial activity in MED and PSACH appears plausible. However, a potential decrease in MitoTracker staining in p.C312Y and p.D385N COMP cells indicates a reduction in mitochondrial membrane potential, mitochondrial activity and thus a decrease in ATP production (Camara et al., 2017). A reduction in mitochondrial membrane potential also occurs during the intrinsic pathway of apoptosis initiation (Wang and Youle, 2009). In D469del COMP cells, increased apoptosis has been observed alongside a reduction in cell proliferation. Whilst no defect in cell proliferation was observed in cells expressing p.C312Y, p.D385N, p.D473H, p.G440R or p.D511Y COMP, future experiments should address apoptosis and could also investigate whether apoptosis is driven by the same pathways in these cell lines.

Similarly to D469del COMP cells, the cells overexpressing the PSACH-causing p.G440R and p.D511Y COMP mutations displayed a reduction in *GFP* expression when compared to wild type COMP-overexpressing cells. Surprisingly, p.D473H COMP expression appeared increased; however, large variation was observed between replicates. Interestingly, expression of MED-causing p.C312Y and p.D385N COMP was not changed. This raises the question whether cells have a higher tolerance for MED-causing COMP than for PSACH-causing COMP. It is also possible that high expression of PSACH-causing p.D469del, p.G440R and p.D511Y COMP leads to apoptosis, and these cell lines therefore contain a higher proportion of cells that express a moderate amount of COMP. Whilst differential expression is an important factor to take into consideration, this finding does not invalidate the cell model, since a similar observation was made in a mouse model of PSACH (see chapter 5).

Although cells overexpressing p.C312Y, p.D385N, p.D473H, p.G440R and p.D511Y COMP did not display any significant changes in cell proliferation, superoxide levels, phosphorylation of AKT or PRDX2 protein levels, all cell lines exhibited elevated

levels of *MMP9* expression. Intriguingly, expression was elevated in a genotype-dependent manner, with cells expressing PSACH-causing mutations exhibiting more pronounced increases in *MMP9* expression. Furthermore, *GALNT18* expression was increased in all cell lines apart from the p.G440R COMP-overexpressing cells, whereas *MMP1* expression was only significantly changed in p.D473H COMP-overexpressing cells. It was surprising to find that p.G440R COMP-overexpressing cells did not display elevated *GALNT18* expression. Since little is known about the transcriptional regulation of *GALNT18*, the reason for this is difficult to determine.

The signalling pathway mediating the effect of p.G440R COMP could be distinct from other mutations; however, because cells expressing p.G440R COMP do not appear to differ significantly from cells expressing other disease-causing mutations, this appears unlikely. Indeed, p.G440R COMP and p.D511Y COMP-overexpressing cells display a high similarity: Both exhibited reduced *XBP1* splicing levels, similar to p.D469del COMP cells, as well as reduced expression of recombinant COMP, but did not show any significant defect in cell proliferation, superoxide and PRDX2 levels or AKT phosphorylation. It is also possible that a lower expression of *GALNT18* presented an advantage for p.G440R COMP cells. Whilst it is unclear why the upregulation of *GALNT18* would be a disadvantage for p.G440R COMP cells, ER stress driven by treatment with tunicamycin or thapsigargin does appear to cause a downregulation of *GALNT18* and conversely, silencing of *GALNT18* induces ER stress (Shan et al., 2019). It has been speculated that GALNT18 may act as a chaperone for other UDP-N-acetyl-α-D-galactosamine:polypeptide N-acetylgalactosaminyltransferases (GalNAc-Ts) (Li et al., 2012), since it is able to modulate the activity of other GalNAc-Ts and is located in the ER and not – as most others – in the Golgi. Perhaps some mutations of COMP exhibit a more pronounced effect on protein glycosylation compared to p.G440R COMP, thus limiting the need for elevated *GALNT18* expression in these cells. Whilst enzymes of the GalNAc-Ts family typically catalyse the first step or O-linked protein glycosylation, namely the transfer of a N-acteyl-D-galactosamine residue to a serine or threonine residue of the receptor protein, COMP itself does not appear to carry O-linked glycosylation (Zaia et al., 1997). This implies that COMP-induced stress may have broader consequences for ER homeostasis, in which GALNT18 may play a role rather than GALNT18 function being directly linked to COMP. Interestingly, a single nucleotide polymorphism (SNP) in *GALNT18* was reported to be a potential predictor of

successful treatment of RA with the IL-6 receptor inhibitor TCZ (Maldonado-Montoro et al., 2016). The consequences of this SNP for GALNT18 expression and/or splicing have not yet been investigated, and therefore, it is currently unknown whether this relationship is at all linked to the gene product. Similarly, a decrease in DNA methylation of Cg16204559 has been observed in Lupus patients during active nephritis (Coit et al., 2020); however, if the change in DNA methylation at this site affects *GALNT18* itself is currently unknown. Nevertheless, it implicates *GALNT18* to two inflammatory diseases.

The elevated expression of *MMP9* also translated into increased extracellular activity of MMP9. Whilst this was not technically significant for p.C312Y, p.D385N as well as p.G440R COMP, a trend for increased activity was clearly visible. To confirm this, a more accurate and precise method of quantification may be necessary, for example an ELISA-based method. Another way to improve the accuracy of activity-based detection could be the use of a fluorogenic substrate; however, fluorogenic substrates may be cleaved by multiple, similar enzymes. A combination of ELISA- and activity-based assays would be preferable to ascertain the genotype-dependent increase in MMP9 in cell models of COMPopathies in the future.

To investigate whether *MMP9* expression is specifically induced by mutations of *COMP*, an *in vitro* model of the closely related but milder MED was employed. After overexpressing both wild type and disease-causing p.V194D matrilin-3, the mutant p.V194D matrilin-3 was retained intracellularly and induced ER stress as expected. Remarkably, neither *MMP9* nor *GALNT18* expression was affected by the expression of mutant matrilin-3. This was particularly surprising with regards to *GALNT18*, which was shown to be differentially regulated in response to tunicamycin and thapsigargin-driven ER stress. When *MMP9* and *GALNT18* expression was examined in D469del and wild type COMP cells after treatment with DMSO, tunicamycin or thapsigargin, *MMP9* expression was not significantly changed in response to tunicamycin or thapsigargin treatment. *GALNT18* expression was also not affected in wild type COMP cells. A reduction of *GALNT18* expression occurred only in D469del COMP cells after treatment with thapsigargin, but not after treatment with tunicamycin. This questions whether the transcriptional regulation of *GALNT18* is more complex than previously assumed, but also whether GALNT18 function is linked to inflammation and/or oxidative stress.

The fact that *MMP9* was not upregulated in response to either p.V194D matrilin-3, or treatment with tunicamycin or thapsigargin demonstrates that MMP9 levels are elevated specifically in response to the expression of mutant COMP, but not 'conventional' ER stress. This confirms that MMP9 could be a potential biomarker for COMPopathies. Once again, it calls into question to which extent the expression of COMP by other cells of the joint influence the cartilage phenotype. Although early-onset OA is common in patients with PSACH and other skeletal dysplasias, elevated MMP9 levels are more often associated with synovial inflammation as it occurs during RA, and not OA (Xue et al., 2014). This may have important implications for the repurposing of drug treatments, but also for the development of novel treatments. Because COMP is expressed substantially in the synovium (Di Cesare et al., 1997; Dodge et al., 1998), it cannot be excluded that COMP retention in synovial cells causes RA-like inflammation. Simultaneously, retention in chondrocytes may drive changes more similar to those observed in OA.

Nevertheless, the increase in *MMP9* expression and MMP9 activity has so far only been observed in HT1080 cells. Future studies have to investigate whether other human cell lines and tissue from murine disease models exhibit the same response to mutations of *COMP.* Indeed, mild myopathy and irregularities of the tendon structure have previously been reported in mouse models of PSACH (Piróg et al., 2013, 2010), indicating that chondrocytes are not the only cell type to exhibit COMP-induced ER stress. Due to the fact that inflammation has been described as an important factor in PSACH (Posey et al., 2015; Suleman et al., 2012), it is also possible that secreted factors, such as cytokines, that are produced by one type of cell alter the behaviour of a different cell type, even if this cell type does not express mutant COMP itself.

Research on the effects of mutant COMP retention have predominantly focused on the underlying disease mechanism, and potential treatments have often been evaluated based on cellular markers, for example the rate of apoptosis or restoring cell proliferation within the cartilage growth plate (Hecht et al., 2021a, 2021b; Posey et al., 2015).
Obtaining cartilage samples from patients is invasive, painful and assessment of a potential treatment therefore complicated. The success and efficacy of a drug

treatment must therefore be evaluated using a biomarker. There is currently one clinical trial (ClinicalTrials.gov Identifier: NCT03866200), investigating whether the treatment with resveratrol can reduce pain in adults with PSACH. Nevertheless, resveratrol is not suitable for treatment of pregnant women and children, indicating the need for other treatment options and relevant biomarkers.

One potential primary outcome measure in clinical trials involving skeletal dysplasias could be final bone length or velocity of growth (and therefore restoration of growth); however, the use of bone length (or growth) as measure may create several problems. Firstly, human growth is a comparatively lengthy process, therefore any effects of the treatment, positive or negative, would only become evident after a relatively long time. Secondly, and most importantly, positive effects such as a reduction in inflammation and/or oxidative stress may not necessarily be reflected in absolute bone growth although they may influence the amount of pain experienced by the patient.

A clinical trial currently assessing the safety and suitability of carbamazepine to treat MCDS in children is therefore using bone growth alongside changes in pain and bone alignment as measured by x-ray imaging as outcome measures (EudraCT number 2018-002633-38). Nevertheless, samples collected during this trial may facilitate discovery of a suitable biomarker for treatment of MCDS.
For PSACH, a biomarker that could be detected in serum or urine samples would greatly facilitate future drug and clinical trials. Because MMP9 is secreted into the extracellular space, there is a chance that elevated expression of *MMP9* could translate into increased MMP9 protein levels in serum. Furthermore, MMP9 has been implicated in other diseases involving inflammation. This could suggest that a significant reduction of inflammation upon treatment, which could potentially improve quality of life for PSACH patients, could be reflected in decreased MMP9 levels.

Future studies should firstly ascertain the increase in MMP9 activity by using a more quantitative approach. Then, other human cell lines and murine disease models should be examined for enhanced MMP9 activity in response to mutant COMP expression. Analysis of mouse models should not be restricted to cartilage, but also investigate other tissues known to contain COMP as well as serum. Secondly, the

specificity for COMPopathies should be systematically investigated by analysing models of several other skeletal dysplasias.

7.8 Summary

- MED-causing p.C312Y and p.D385N COMP and the PSACH-causing p.D473H, p.G440R and p.D511Y COMP display a genotype-dependent degree of protein retention when overexpressed in HT1080 cells.

- Mutations located within the type 3 repeats of *COMP* do not drive the activation of the UPR.

- No changes relating to oxidative stress or decreased cell proliferation were observed in the p.C312Y, p.D385N, p.D473H, p.G440R and p.D511Y COMP cell lines.

- *GALNT18* expression was consistently increased in cells overexpressing mutant COMP with the exception of the p.G440R COMP.

- *MMP9* expression was elevated in a genotype-dependent fashion, and this resulted in enhanced extracellular MMP9 activity.

Chapter 8. Discussion

The aims of this work were to investigate DNA methylation changes in ER-stress related skeletal dysplasia, to study in more detail why p.D469del COMP appears to elicit a distinct stress response compared to other related chondrodysplasias, if this novel stress response is a common feature of COMPopathies and whether there is a common marker for COMP-induced stress in MED and PSACH.

To study DNA methylation in skeletal dysplasia, a suitable model system had to be identified. The genome-wide analysis of DNA methylation is commonly conducted using the Illumina Infinium EPIC Methylation array, a probe-based approach that was limited to human samples until very recently. During the course of this work, hiPSCs were therefore explored as a suitable model systems for MCDS and OI. Whilst hiPSCs offer exciting opportunities to study skeletal disorders *in vitro*, it became apparent that the lengthy, complex protocol for hypertrophic differentiation required to study MCDS introduced too many variations and thus was considered not suitable to reproducibly study DNA methylation in this model system at this time. Future work will be required to optimise the differentiation protocol for induction of hypertrophy and investigate the consequences of mutations in *COL10A1* in this model system before any changes in DNA methylation can be investigated.

In contrast to this, the protocol for osteogenic differentiation of hiPSCs was much briefer and thus potentially introduced fewer variations. Despite this, the success of differentiation as indicated by mineralisation varied considerably even between gene-corrected ‘control’ cell lines. This finding indicates that the osteogenic potential may be distinct between hiPSC cell lines – perhaps depending on the parental tissue, the culture method (feeder-dependent or feeder-free) or even the reprogramming method. The success of osteogenic differentiation as measured by alizarin red staining also varied depending on the culture substrate used; however, to conclusively demonstrate this, gene expression analysis of *COL1A1* and *BGLAP* would be required. The current lack of gene expression data is therefore a major limitation of the work presented here. Future work will have to investigate the expression level of *COL1A1* and *BGLAP* during the course of osteogenic differentiation of RM3.5c cells and whether there are differences in gene expression between cell lines and culture/differentiation substrates. After the selection of one substrate, the differentiation of isogenic OI hiPSCs and RM3.5c hiPSCs should be compared. ER stress and the UPR have been implicated in the disease mechanism

of some *COL1A1* and *COL1A2* mutations, and studying this in hiPSC-derived osteoblast-like cells could complement previous research conducted using mouse models and patient-derived fibroblasts. In addition to using patient-derived and gene-corrected control cell lines, disease-causing mutations could also be introduced into other available ('wild type') hiPS cell lines. Potential changes in DNA methylation could also be analysed after differentiation, investigating if and to what extent methylation of DNA is affected in OI.

To reduce the complexity of the model system, the suitability of HT1080 fibrosarcoma cells overexpressing wild type and p.D469del COMP to study DNA methylation, but also the disease mechanism of PSACH in more detail, was assessed. This eliminated the need for a multi-step differentiation protocol; however, it also presents a major limitation of this work as some cell-type specific aspects are not replicated by this model. For example, a possible co-retention of matrilin-3 and type IX collagen could not be investigated in HT1080 cells, as these proteins are not expressed by this cell type. A detailed characterisation of the HT1080 cell model was performed prior to transcriptomic and DNA methylation analysis. In agreement with a previous report (Suleman et al., 2012), the results of this work indicate that HT1080 cells, despite being a fibrosarcoma cell line, replicate the response of PSACH chondrocytes from the D469del *Comp* knock-in mouse model. Compellingly, D469del COMP cells appeared to reflect features of juvenile (six weeks), but not younger (one week) PSACH cartilage. This implies that the HT1080 cell model is a model of more persistent COMP-induced ER stress and this may also limit the possibility to study events that occur very early on in PSACH pathology. Nevertheless, the analysis of the HT1080 cell model was continued, because affected individuals are typically only diagnosed with the onset of symptoms, which likely occur considerably after the onset of chondrocyte pathology.

Furthermore, whilst D469del and the corresponding wild type COMP cell line were sorted by GFP fluorescence, all other PSACH and MED cell lines (and corresponding wild type controls) were analysed without being sorted. The reason for this decision was the possibility that by sorting cells for strong GFP signal, the sorting process would be biased to select for cells that retain even wild type COMP. However, the p.C312Y, p.D385N, p.D473H, p.G440R and p.D511Y COMP cell lines are therefore potentially very heterogenous. The expression of the PSACH mutations p.D469del

(albeit GFP-sorted), p.G440R and p.D511Y lead to significantly decreased *GFP-COMP* expression, indicating that high levels of these proteins cause severe stress and are likely incompatible with cell survival. Although a similar observation was made *in vivo* using a knock-in mouse model of PSACH, the low expression level may have contributed to the absence of significant effects on superoxide levels and proliferation in the p.G440R and p.D511Y COMP cells (Table 8.1).
Future work could employ CRISPR/Cas9 to introduce mutations into *COMP* in chondrocyte-like and fibroblast-like cell lines after confirming that they express sufficient levels of endogenous *COMP*. Additionally, in chondrocyte-like cells, *in vitro* loading experiments could be considered. COMP was shown to be responsive to biomechanical loading *in vivo* and *in vitro* (Bleuel et al., 2015; Smith et al., 1997), and incorporation of biomechanical stimulation into the experimental approach may result in a more physiologically relevant model system for cartilage.

When DNA methylation levels were compared between D469del and wild type COMP cells, a surprisingly large number of significant changes was observed. The interpretation of these changes is however complicated by the experimental design. At this point, it cannot be excluded that at least some, or even most of the observed DNA methylation changes arose due to genetic drift of D469del or wild type COMP cell lines. Since DNA methylation had never before been analysed in a skeletal dysplasia cell model, the experimental design was aimed at reducing variation, and thus false-negative results and discovering as many significant changes as possible. This was achieved by using a plasmid overexpression cell model instead of hiPSC-derived samples. However, in light of the large number of significantly changed probes/sites, the experimental design should also have included additional samples to reduce the number of potentially false-positive results. For example, including samples from other COMPopathy cell models could have helped to identify changes in DNA methylation that are common in multiple cell models and thus likely to be related to mutant COMP accumulation. Future work should take advantage of the availability of multiple PSACH cell models, and compare DNA methylation between multiple PSACH and wild type COMP cell lines to exclude potential differences that were introduced by chance during culture. Cell models of various COMP-MED mutations could also be included to address potential differences between MED and PSACH. The analysis of different overexpression models (for example stable cells and transiently transfected cells) could also be considered; however, acute and

persistent COMP-induced stress may have distinct consequences. CRISPR/Cas9 mediated gene-editing could also be employed to generate additional PSACH cell models without the need for plasmid overexpression. Furthermore, the recently launched Illumina Infinium Mouse Methylation array presents a novel tool to explore DNA methylation in cartilage (or other tissues) from a PSACH mouse model. Whilst the coverage is not as extensive as the Infinium EPIC methylation array, this could serve as further validation after analysis of multiple PSACH cell models. To investigate whether the downregulation of *Comp* in femoral head cartilage chondrocytes at the age of 6 weeks is mediated by DNA methylation, a more targeted approach could also be considered, for example bisulfite conversion of methylated cytosine residues within the *Comp* promoter region, followed by pyrosequencing.

Whilst future studies regarding DNA methylation should also be carried out in chondrocytes or chondrocyte-like cells, using HT1080 cells in this study also raised some important questions. Indeed, COMP has been shown to be expressed by dermal fibroblasts and to support type I collagen secretion (Schulz et al., 2016), but the consequences of mutant COMP accumulation for primary dermal fibroblasts have not yet been characterised. The effects of mutant COMP on other cell types of the joint, including synovial fibroblasts, have also not yet been explored in great detail, since it was presumed that chondrocytes are the primarily affected cells. Interestingly, joint laxity is observed in individuals with PSACH as well as in mouse models (Délot et al., 1999; Piróg et al., 2013), and retention of COMP in tendon cells was indeed observed by some studies (Weirich et al., 2007). However, others have reportedly not observed COMP retention in tendon cells (Chen et al., 2004; Maddox et al., 1997). Whilst chondrocytes are certainly most affected, other cell types of the joint might contribute to the disease mechanism of COMPopathies. In some cases, retention of mutant COMP in tendon cells, for example, may alter tendon integrity and result in altered loading of the cartilage which may directly alter *COMP* expression and its integration into the extracellular matrix if any COMP is secreted (Bleuel et al., 2015; Smith et al., 1997). Furthermore, synovial fibroblasts might contribute to inflammatory processes as a result of mutant COMP accumulation itself, or as a reaction to the oxidative/inflammatory stress signalling from chondrocytes (Figure 8.1). Thus, synovial fibroblasts may play a role in degeneration of cartilage and ultimately facilitate early-onset osteoarthritis that is observed in PSACH.

Future work could address this by isolating different types of primary cells from the knock-in PSACH mouse model, or by employing CRISPR/Cas9 to introduce *COMP* mutations into various cell types. Analysis of primary fibroblasts from individuals with PSACH may also help to address whether mutant COMP is retained in primary cells. Additionally, as PSACH is an autosomal dominant disease, primary fibroblasts may be a more physiologically relevant model to investigate some aspects of PSACH, for example the consequences of mixed wild type and mutant oligomers. To investigate whether the synovium is at all affected by oxidative/inflammatory stress signalling of PSACH chondrocytes *in vivo*, histological analysis of the PSACH mouse model could be performed. Furthermore, levels of inflammatory signalling could be examined following stimulation of normal fibroblasts with conditioned media from primary PSACH chondrocytes.

Why accumulation of COMP induces this inflammatory response in contrast to the UPR is not yet entirely understood, however, the results of this study suggest that at least some features of inflammation are present in other PSACH and MED cell models, as evidenced by the absence of UPR activation and increased *MMP9* expression. RNA sequencing of D469del COMP cells has confirmed a potential involvement of TNFα as well as NFκB signalling observed by previous studies (Hecht et al., 2021b; Suleman et al., 2012). Furthermore, a potential dysregulation of TGFβ signalling was observed by RNA sequencing and confirmed by western blotting. Indeed, a proteomic study using cartilage from a knock-in mouse model of PSACH reported decreased levels of transforming growth factor β induced protein ig-h3 (Tgfbi) (Bell et al., 2013), suggesting that D469del COMP disturbs TGFβ signalling independent of the affected cell type. Recombinant COMP has also been shown to modify TGFβ signalling in chondrocytes, prompting the question as to whether inflammation caused by COMP retention might be exacerbated by a lack of signalling regulation by extracellular COMP (Figure 8.2). Although the absence of *Comp* did not result in an obvious skeletal phenotype in mice (Svensson et al., 2002), crossing of a transgenic p.D469del *Comp* mouse line with a *Comp*-deficient mouse line resulted in a more severe phenotype (Schmitz et al., 2008). Chondrocytes may be able to compensate for the loss of Comp alone, but not for the loss of Comp whilst experiencing severe ER stress. To dissect intracellular and extracellular aspects of PSACH, future work could examine, for example, TGFβ signalling and *MMP9* expression after culturing D469del COMP cells in the presence of recombinant wild

type COMP. Additionally, it should be determined whether dysregulation of TNFα, NFκB and TGFβ signalling also occurs in other cell models of COMPopathy. In addition to western blotting of phospho-SMAD2/3, TGFβ activity in conditioned media of mutant and wild type COMP cells could be assessed using a Mink lung epithelial cell (MLEC)-based activity assay (Abe et al., 1994; Khan et al., 2012).

Whilst the exact underlying mechanism prompting inflammatory signalling in response to mutant COMP remains to be elucidated, this study has demonstrated that the upregulation of *MMP9* is a common feature in both COMP-MED and PSACH. Regulation of *MMP9* is controlled by several cytokines and their downstream transcription factors (Di Girolamo et al., 2006; Ray et al., 2005; Steenport et al., 2009; Xie et al., 2004), some of which are themselves de-regulated in PSACH, for example Interleukin-1β (*IL1B).* This offers the exciting opportunity to exploit *MMP9* as a biomarker to discover drugs that could mitigate inflammation in COMPopathies.

Although densitometric quantification of in-gel zymography clearly demonstrated higher MMP9 activity in p.D473H and p.D511Y PSACH cell models, this was not significant in MED cell models. However, in-gel zymography is an end point reaction, and also not suitable for high throughput screening. MMP9 activity could be measured using fluorogenic substrates, which carry a fluorophore as well as a quencher-molecule, which is released upon cleavage by MMP so that fluorescence can be detected. Since it allows determination of enzyme kinetic parameters, this method may present a more accurate way to quantify MMP9 activity, and could also be employed in high throughput screening. However, currently available substrates are often not specific to MMP9 (Fields, 2010), and thus, the activity of other MMPs in the HT1080 cell model would have to be examined first.
Another approach could be the expression of a luciferase enzyme driven by the *MMP9* promoter (Figure 8.3). A similar approach has been adopted to monitor 'classical' ER stress in HeLa cells transfected with MED-causing p.V194D matrilin-3 and MCDS-causing p.N617K type X collagen (Dennis et al., 2021). Using a *MMP9*-promoter driven luciferase construct could enable high throughout screenings of large compound libraries and could thus greatly facilitate drug repurposing for COMPopathies. A smaller selection of candidate compounds could then be examined in more detail. This would represent a significant advancement of drug

development for PSACH, which so far relied heavily on testing candidate drugs with known anti-inflammatory properties. To confirm the suitability of *MMP9* as a biomarker for COMPopathies *in vitro*, the impact of TNFα, NFκB and TGFβ modulation on *MMP9* expression levels should be assessed by luciferase-based assays as well as qRT-PCR in the D469del COMP cell model. Confirmation that regulation of these pathways results in both changed *MMP9* expression as well as altered luciferase activity, would validate the luciferase-based approach.

With regards to MMP9, one limitation of this study is that the levels of *MMP9* expression and MMP9 activity were not investigated in the knock-in mouse model of PSACH. This was out of scope of the presented work for several reasons. Firstly, *Mmp9* is not typically expressed by growth plate chondrocytes, but by osteoclasts and inflammatory cells (Reponen et al., 1994; Vu et al., 1998; Wucherpfennig et al., 1994). It is therefore unclear, whether mutant Comp accumulation would induce *Mmp9* expression in cartilage. However, as previously described, there are a number of other tissues that express COMP and could act as a source of MMMP9, including the synovium. For this reason, several tissues will have to be collected from D469del *Comp* knock-in mice and wild type controls for RNA and protein extraction as well as histological analysis. *Mmp9* expression could then be examined alongside Mmp9 activity, whilst *Comp* expression and potential COMP retention should also be evaluated. Analysis of Comp and Mmp9 levels in the synovial fluid could also be considered; however, the amount of synovial fluid would be very limited due to the small size of the mouse joint. Instead, MMP9 levels could be examined in serum from D469del *Comp* and wild type mice. A second parameter that is currently unknown is the required age to detect potential differences in MMP9 levels. The D469del COMP cell model appeared to represent cartilage from a juvenile mouse more accurately than cartilage from a younger mouse. This raises the question how advanced inflammation has to be *in vivo* to influence MMP9 levels, and whether there is a specific time point after which differences in MMP9 become detectable. Samples would therefore have to be collected at various ages, for example at least at three weeks, six weeks and nine weeks. If changes in MMP9 are detected as early as three weeks, samples from younger animals could also be analysed.

Finally, there is also a possibility that mutant COMP already accumulates during embryonic stages and so progressively impairs chondrocyte function. Whilst

individuals with PSACH are typically diagnosed in early childhood, it is not known exactly when mutant COMP starts to accumulate within the chondrocyte ER. In the p.N617K *Col10a1* knock-in mouse model of MCDS, expression of *Col10a1* was detected from E14.5 by in situ hybridisation. Delayed type X collagen secretion and concomitant upregulation of *BiP/Grp78* was also observed already at this very early stage (Kung et al., 2012). Electron microscopy of chondrocytes from the p.D469del *Comp* mouse model has revealed the characteristically enlarged ER as early as five days after birth. Nevertheless, gene expression changes were observed in cartilage from new born animals by microarray (Suleman et al., 2012). The presence of COMP in skeletal (and extra-skeletal) tissues during embryonic development has been revealed by several studies (Di Cesare et al., 2000; Fang et al., 2000; Murphy et al., 1999); however, whether mutant Comp accumulates during embryonic development in a similar fashion as mutant type X collagen (Kung et al., 2012) has not yet been investigated.

Nevertheless, this work has important implications for the development of potential drug treatments for individuals affected by COMPopathies. In absence of a consistent activation of the UPR, evaluating drug treatments has relied heavily on growth plate organisation, bone length measurements, levels of apoptosis and cell proliferation (Posey et al., 2015). This approach limits the number of potential treatments that can be assessed, and also hinders timely identification of unsuccessful treatments, resulting in the loss of time and resources. Using a *MMP9*-promoter driven luciferase construct could accelerate drug development for COMPopathies by specifically identifying compounds that ameliorate inflammation in a cell model of PSACH. By screening libraries of already FDA-approved drugs, drug development for COMPopathies could be accelerated even more. The repurposing of CBZ for the treatment of MCDS caused by mutations in *COL10A1* has clearly demonstrated the benefits of drug repurposing for rare skeletal diseases, with the recruitment for a clinical trial opening only three years after orphan drug designation for treatment of MCDS with CBZ was received (“MCDS-Therapy Project,” 2022; mcds-therapy.eu, 2022). Using *MMP9* expression as a biomarker for COMP-induced ER stress may therefore have a substantial translational impact in identifying treatments for COMPopathies.

In summary, the work presented in this thesis has validated an existing cell model of PSACH, characterised further cell models of COMPopathy, and demonstrated their suitability to study various aspects of MED and PSACH pathology *in vitro*. This work has identified a potential common biomarker for COMPopathies that could facilitate *in vitro* drug screenings. Furthermore, several questions arise from the work presented here that should be addressed in future studies.

- Is DNA methylation affected in other cell models of COMPopathy?
    - Is there a difference in DNA methylation between MED and PSACH?

- What is the reason for the inflammatory signalling in COMPopathies?
    - Calcium signalling? Mitochondria? Lack of extracellular COMP?

- How does mutant Comp retention affect the synovium *in vivo*? Does the synovium play a role in inflammatory signalling?

- How is embryonic skeletal development affected by mutant Comp retention?

- Is MMP9 a biomarker for COMPopathies *in vivo*?

	p.D469del	p.C312Y	p.D385N	p.D473H	p.G440R	p.D511Y
Reduced secretion	++	-/+	+	++	++	++
GFP	++	-	-	-	++	++
BiP	+	-	-	-	-	-
Calnexin	+	-	-	-	-	-
p-eiF2a	-	-	-	-	-	-
XBP1s	+	-	-	-	+	+
Cell proliferation	+	-	-	-	-	-
Superoxide	+	-	-	-	-	-
PRDX2	++	-	-	-	-	-
p-AKT	++	-	-	-	-	-
MMP9	++	+	+	++	++	++
MMP9 activity	++	+	+	++	+	++
MMP1	+	-	-	+	-	-
GALNT18	+	+	+	+	-	+
DNA methylation	+/++?	?	?	?	?	?

++ strongly affected + affected – does not affect

Table 8.2 - Comparison of COMPopathy cell models examined in this work. This table provides an overview over part of the analysis performed on cell models of COMPopathies in this thesis and whether there was a significant change detected in one or more of the cell models. Some observations are made only in p.D469del COMP, p.G440R and p.D511Y COMP cells (all PSACH), for example a significant effect on *XBP1s*, whilst others like *MMP9* and *GALNT18* expression, were changed in all or most cell models, respectively.

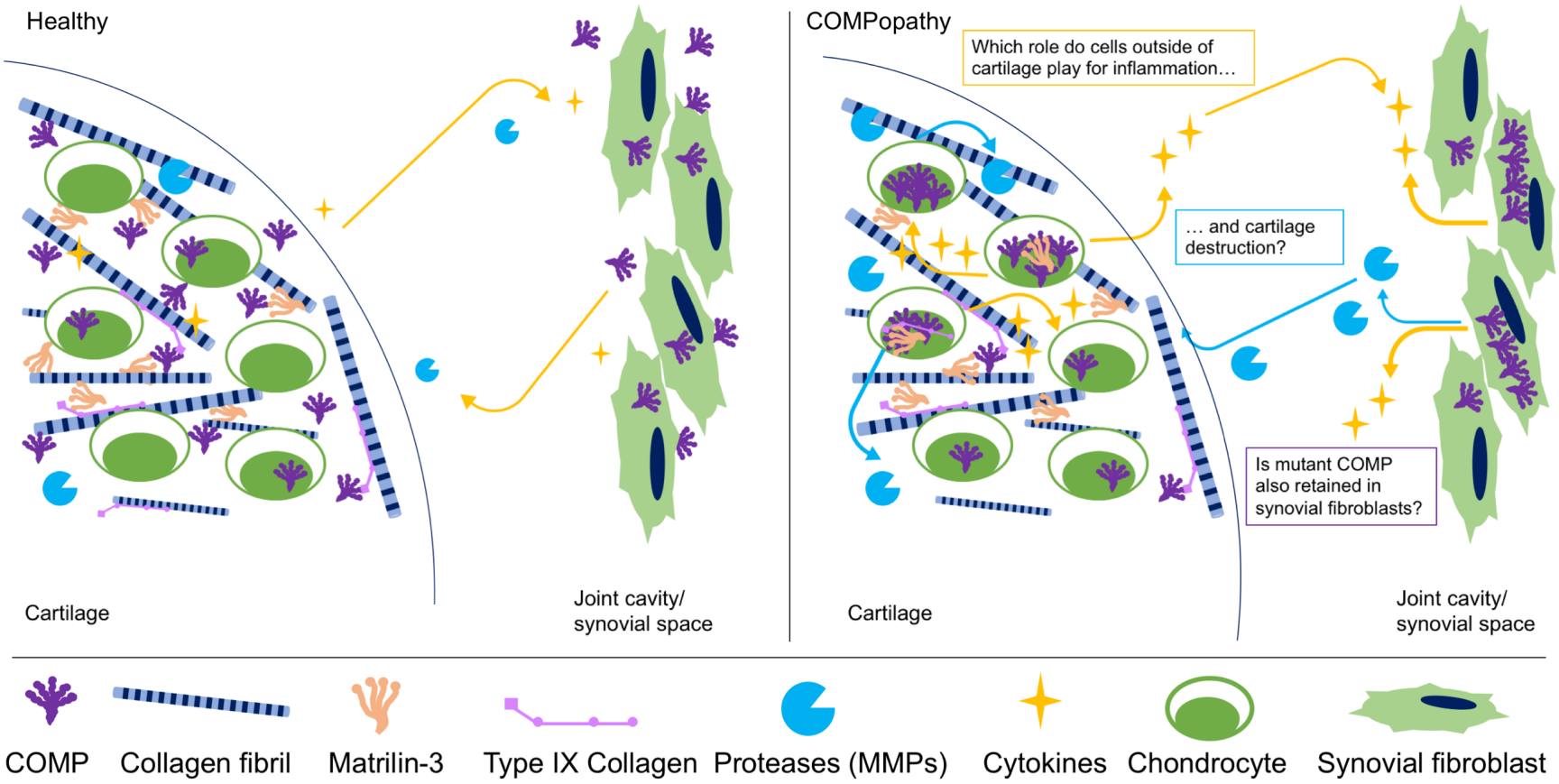

Figure 8.1 – Under normal conditions (left), COMP is secreted into the extracellular matrix and cartilage and synovial tissues communicate via secreted factors, such as enzymes and cytokines. What role does the synovium play for the inflammation observed in PSACH (right)? Is mutant COMP also retained in synovial fibroblasts? Do synovial fibroblasts secrete inflammatory cytokines and proteases that impact on cartilage integrity, perhaps in response to mutant COMP retention? Do mutant COMP-retaining chondrocytes secrete pro-inflammatory cytokines that cause inflammatory responses by synovial fibroblasts? Do chondrocytes and synovial fibroblasts enter a vicious cycle of ever-increasing inflammation?

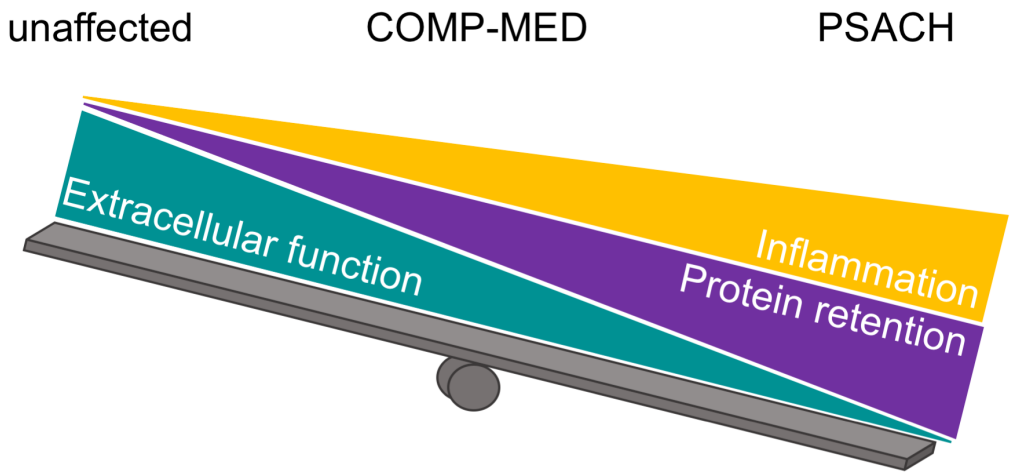

Figure 8.2 – Cellular homeostasis is disturbed in COMPopathies by a combination of protein retention, inflammation and potentially a lack of extracellular COMP.

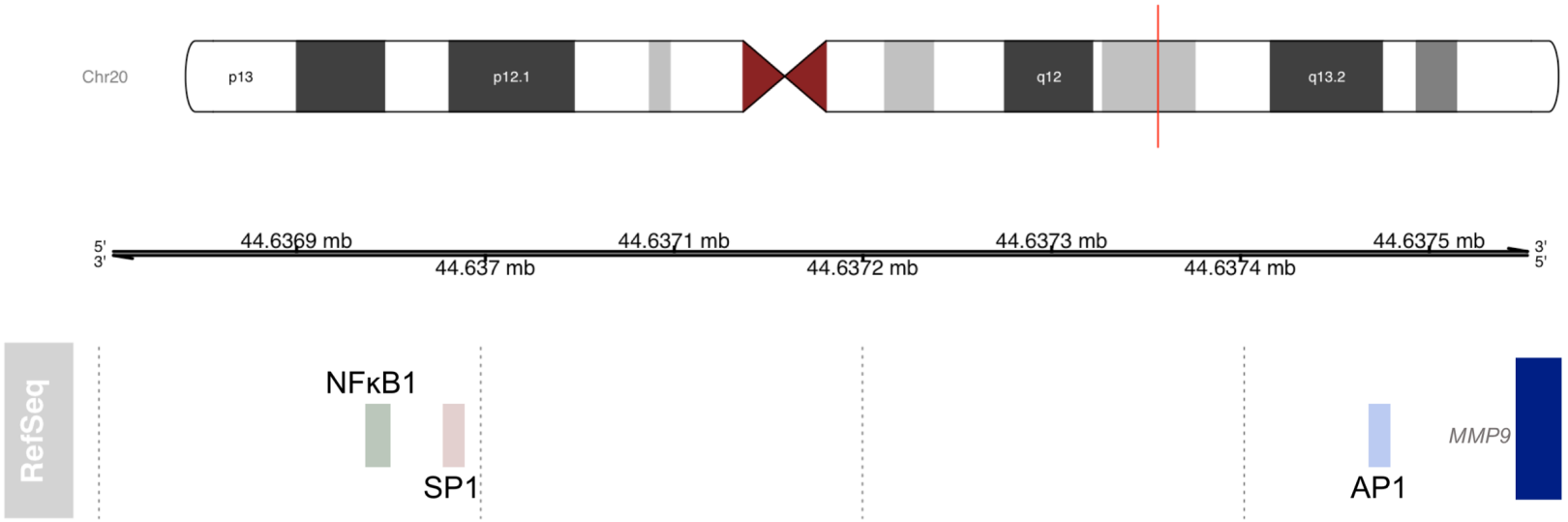

Figure 8.3 – Schematic depiction of the upstream genomic region of *MMP9.* The region contains several transcription factor binding sites, with NFκB and AP1 both directly implicated in COMP-induced stress. Positions of transcription factor binding sites from (Ray et al., 2005; Roupakia et al., 2018).

References

Abe, M., Harpel, J.G., Metz, C.N., Nunes, I., Loskutoff, D.J., Rifkin, D.B., 1994. An assay for transforming growth factor-beta using cells transfected with a plasminogen activator inhibitor-1 promoter-luciferase construct. Anal Biochem 216, 276–284. https://doi.org/10.1006/abio.1994.1042

Abisambra, J.F., Jinwal, U.K., Blair, L.J., O'Leary, J.C., Li, Q., Brady, S., Wang, L., Guidi, C.E., Zhang, B., Nordhues, B.A., Cockman, M., Suntharalingham, A., Li, P., Jin, Y., Atkins, C.A., Dickey, C.A., 2013. Tau Accumulation Activates the Unfolded Protein Response by Impairing Endoplasmic Reticulum-Associated Degradation. J Neurosci 33, 9498–9507. https://doi.org/10.1523/JNEUROSCI.5397-12.2013

Acharya, C., Yik, J.H.N., Kishore, A., Van Dinh, V., Di Cesare, P.E., Haudenschild, D.R., 2014. Cartilage oligomeric matrix protein and its binding partners in the cartilage extracellular matrix: interaction, regulation and role in chondrogenesis. Matrix Biol. 37, 102–111. https://doi.org/10.1016/j.matbio.2014.06.001

Adams, J.C., Lawler, J., 2011. The thrombospondins. Cold Spring Harb Perspect Biol 3, a009712. https://doi.org/10.1101/cshperspect.a009712

Adkar, S.S., Wu, C.-L., Willard, V.P., Dicks, A., Ettyreddy, A., Steward, N., Bhutani, N., Gersbach, C.A., Guilak, F., 2019. Step-Wise Chondrogenesis of Human Induced Pluripotent Stem Cells and Purification Via a Reporter Allele Generated by CRISPR-Cas9 Genome Editing. Stem Cells 37, 65–76. https://doi.org/10.1002/stem.2931

Afgan, E., Baker, D., Batut, B., van den Beek, M., Bouvier, D., Čech, M., Chilton, J., Clements, D., Coraor, N., Grüning, B.A., Guerler, A., Hillman-Jackson, J., Hiltemann, S., Jalili, V., Rasche, H., Soranzo, N., Goecks, J., Taylor, J., Nekrutenko, A., Blankenberg, D., 2018. The Galaxy platform for accessible, reproducible and collaborative biomedical analyses: 2018 update. Nucleic Acids Research 46, W537–W544. https://doi.org/10.1093/nar/gky379

Afzal, A.R., Jeffery, S., 2003. One gene, two phenotypes: ROR2 mutations in autosomal recessive Robinow syndrome and autosomal dominant brachydactyly type B. Hum Mutat 22, 1–11. https://doi.org/10.1002/humu.10233

Ahrens, D., Koch, A.E., Pope, R.M., Stein-Picarella, M., Niedbala, M.J., 1996. Expression of matrix metalloproteinase 9 (96-kd gelatinase B) in human rheumatoid arthritis. Arthritis Rheum 39, 1576–1587. https://doi.org/10.1002/art.1780390919

Akiyama, H., Chaboissier, M.-C., Martin, J.F., Schedl, A., de Crombrugghe, B., 2002. The transcription factor Sox9 has essential roles in successive steps of the chondrocyte differentiation pathway and is required for expression of Sox5 and Sox6. Genes Dev 16, 2813–2828. https://doi.org/10.1101/gad.1017802

Akiyama, H., Lyons, J.P., Mori-Akiyama, Y., Yang, X., Zhang, R., Zhang, Z., Deng, J.M., Taketo, M.M., Nakamura, T., Behringer, R.R., McCrea, P.D., de Crombrugghe, B., 2004. Interactions between Sox9 and β-catenin control chondrocyte differentiation. Genes Dev 18, 1072–1087. https://doi.org/10.1101/gad.1171104

Alford, A.I., Terkhorn, S.P., Reddy, A.B., Hankenson, K.D., 2010. Thrombospondin-2 regulates matrix mineralization in MC3T3-E1 pre-osteoblasts. Bone 46, 464. https://doi.org/10.1016/j.bone.2009.08.058

Amend, S.R., Uluckan, O., Hurchla, M., Leib, D., Novack, D.V., Silva, M., Frazier, W., Weilbaecher, K.N., 2015. Thrombospondin-1 regulates bone homeostasis

through effects on bone matrix integrity and nitric oxide signaling in osteoclasts. J Bone Miner Res 30, 106–115. https://doi.org/10.1002/jbmr.2308
Andrews, S., 2019. Babraham Bioinformatics - FastQC A Quality Control tool for High Throughput Sequence Data [WWW Document]. URL https://www.bioinformatics.babraham.ac.uk/projects/fastqc/ (accessed 1.21.22).
Angeloni, A., Bogdanovic, O., 2019. Enhancer DNA methylation: implications for gene regulation. Essays Biochem 63, 707–715. https://doi.org/10.1042/EBC20190030
Apte, S., Mattei, M.G., Olsen, B.R., 1991. Cloning of human alpha 1(X) collagen DNA and localization of the COL10A1 gene to the q21-q22 region of human chromosome 6. FEBS Lett. 282, 393–396.
Araldi, E., Khatri, R., Giaccia, A.J., Simon, M.C., Schipani, E., 2011. Lack of HIF-2α in limb bud mesenchyme causes a modest and transient delay of endochondral bone development. Nat Med 17, 25–29. https://doi.org/10.1038/nm0111-25
Aryee, M.J., Jaffe, A.E., Corrada-Bravo, H., Ladd-Acosta, C., Feinberg, A.P., Hansen, K.D., Irizarry, R.A., 2014. Minfi: a flexible and comprehensive Bioconductor package for the analysis of Infinium DNA methylation microarrays. Bioinformatics 30, 1363–1369. https://doi.org/10.1093/bioinformatics/btu049
Aszódi, A., Bateman, J.F., Hirsch, E., Baranyi, M., Hunziker, E.B., Hauser, N., Bösze, Z., Fässler, R., 1999. Normal skeletal development of mice lacking matrilin 1: redundant function of matrilins in cartilage? Mol Cell Biol 19, 7841–7845. https://doi.org/10.1128/MCB.19.11.7841
Baker, S., Booth, C., Fillman, C., Shapiro, M., Blair, M.P., Hyland, J.C., Ala-Kokko, L., 2011. A loss of function mutation in the COL9A2 gene causes autosomal recessive Stickler syndrome. Am J Med Genet A 155A, 1668–1672. https://doi.org/10.1002/ajmg.a.34071
Balasubramanian, K., Li, B., Krakow, D., Nevarez, L., Ho, P.J., Ainsworth, J.A., Nickerson, D.A., Bamshad, M.J., Immken, L., Lachman, R.S., Cohn, D.H., 2017. MED resulting from recessively inherited mutations in the gene encoding calcium-activated nucleotidase CANT1. Am J Med Genet A 173, 2415–2421. https://doi.org/10.1002/ajmg.a.38349
Baratela, W.A.R., Bober, M.B., Tiller, G.E., Okenfuss, E., Ditro, C., Duker, A., Krakow, D., Stabley, D.L., Sol-Church, K., Mackenzie, W., Lachman, R., Scott Jr, C.I., 2012. A newly recognized syndrome with characteristic facial features, skeletal dysplasia, and developmental delay. American Journal of Medical Genetics Part A 158A, 1815–1822. https://doi.org/10.1002/ajmg.a.35445
Barnes, A.M., Ashok, A., Makareeva, E.N., Brusel, M., Cabral, W.A., Weis, M., Moali, C., Bettler, E., Eyre, D.R., Cassella, J.P., Leikin, S., Hulmes, D.J.S., Kessler, E., Marini, J.C., 2019. COL1A1 C-propeptide mutations cause ER mislocalization of procollagen and impair C-terminal procollagen processing. Biochim Biophys Acta Mol Basis Dis 1865, 2210–2223. https://doi.org/10.1016/j.bbadis.2019.04.018
Bartoszewski, R., Rab, A., Jurkuvenaite, A., Mazur, M., Wakefield, J., Collawn, J.F., Bebők, Z., 2008a. Activation of the Unfolded Protein Response by ΔF508 CFTR. Am J Respir Cell Mol Biol 39, 448–457. https://doi.org/10.1165/rcmb.2008-0065OC

Bartoszewski, R., Rab, A., Twitty, G., Stevenson, L., Fortenberry, J., Piotrowski, A., Dumanski, J.P., Bebok, Z., 2008b. The mechanism of cystic fibrosis transmembrane conductance regulator transcriptional repression during the unfolded protein response. J. Biol. Chem. 283, 12154–12165. https://doi.org/10.1074/jbc.M707610200

Bateman, J.F., Boot-Handford, R.P., Lamandé, S.R., 2009. Genetic diseases of connective tissues: cellular and extracellular effects of ECM mutations. Nat Rev Genet 10, 173–183. https://doi.org/10.1038/nrg2520

Bateman, J.F., Freddi, S., McNeil, R., Thompson, E., Hermanns, P., Savarirayan, R., Lamandé, S.R., 2004. Identification of four novel COL10A1 missense mutations in schmid metaphyseal chondrodysplasia: Further evidence that collagen X NC1 mutations impair trimer assembly. Human Mutation 23, 396–396. https://doi.org/10.1002/humu.9222

Bateman, J.F., Freddi, S., Nattrass, G., Savarirayan, R., 2003. Tissue-specific RNA surveillance? Nonsense-mediated mRNA decay causes collagen X haploinsufficiency in Schmid metaphyseal chondrodysplasia cartilage. Hum Mol Genet 12, 217–225. https://doi.org/10.1093/hmg/ddg054

Bateman, J.F., Wilson, R., Freddi, S., Lamandé, S.R., Savarirayan, R., 2005. Mutations of COL10A1 in Schmid metaphyseal chondrodysplasia. Human Mutation 25, 525–534. https://doi.org/10.1002/humu.20183

Begemann, M., Zirn, B., Santen, G., Wirthgen, E., Soellner, L., Büttel, H.-M., Schweizer, R., van Workum, W., Binder, G., Eggermann, T., 2015. Paternally Inherited IGF2 Mutation and Growth Restriction [WWW Document]. http://dx.doi.org/10.1056/NEJMoa1415227. https://doi.org/10.1056/NEJMoa1415227

Bell, M.C., Meier, S.E., Ingram, A.L., Abisambra, J.F., 2016. PERK-Opathies: An Endoplasmic Reticulum Stress Mechanism Underlying Neurodegeneration. Curr Alzheimer Res 13, 150–163.

Bell, P.A., Wagener, R., Zaucke, F., Koch, M., Selley, J., Warwood, S., Knight, D., Boot-Handford, R.P., Thornton, D.J., Briggs, M.D., 2013. Analysis of the cartilage proteome from three different mouse models of genetic skeletal diseases reveals common and discrete disease signatures. Biol Open 2, 802–811. https://doi.org/10.1242/bio.20135280

Bellucci, A., Navarria, L., Zaltieri, M., Falarti, E., Bodei, S., Sigala, S., Battistin, L., Spillantini, M., Missale, C., Spano, P., 2011. Induction of the unfolded protein response by α-synuclein in experimental models of Parkinson's disease. Journal of Neurochemistry 116, 588–605. https://doi.org/10.1111/j.1471-4159.2010.07143.x

Besio, R., Iula, G., Garibaldi, N., Cipolla, L., Sabbioneda, S., Biggiogera, M., Marini, J.C., Rossi, A., Forlino, A., 2018. 4-PBA ameliorates cellular homeostasis in fibroblasts from osteogenesis imperfecta patients by enhancing autophagy and stimulating protein secretion. Biochim Biophys Acta 1864, 1642–1652. https://doi.org/10.1016/j.bbadis.2018.02.002

Bi, W., Deng, J.M., Zhang, Z., Behringer, R.R., de Crombrugghe, B., 1999. Sox9 is required for cartilage formation. Nat. Genet. 22, 85–89. https://doi.org/10.1038/8792

Bi, X., Grafe, I., Ding, H., Flores, R., Munivez, E., Jiang, M.M., Dawson, B., Lee, B., Ambrose, C.G., 2017. Correlations Between Bone Mechanical Properties and Bone Composition Parameters in Mouse Models of Dominant and Recessive

Osteogenesis Imperfecta and the Response to Anti-TGF-β Treatment. J Bone Miner Res 32, 347–359. https://doi.org/10.1002/jbmr.2997
Bleuel, J., Zaucke, F., Brüggemann, G.-P., Heilig, J., Wolter, M.-L., Hamann, N., Firner, S., Niehoff, A., 2015. Moderate cyclic tensile strain alters the assembly of cartilage extracellular matrix proteins in vitro. J Biomech Eng 137, 061009. https://doi.org/10.1115/1.4030053
Blighe, K., Rana, S., Turkes, E., Ostendorf, B., Grioni, A., Lewis, M., 2022. EnhancedVolcano: Publication-ready volcano plots with enhanced colouring and labeling. Bioconductor version: Release (3.14). https://doi.org/10.18129/B9.bioc.EnhancedVolcano
Blumbach, K., Niehoff, A., Paulsson, M., Zaucke, F., 2008. Ablation of collagen IX and COMP disrupts epiphyseal cartilage architecture. Matrix Biology 27, 306–318. https://doi.org/10.1016/j.matbio.2007.11.007
Bogin, O., Kvansakul, M., Rom, E., Singer, J., Yayon, A., Hohenester, E., 2002. Insight into Schmid metaphyseal chondrodysplasia from the crystal structure of the collagen X NC1 domain trimer. Structure 10, 165–173.
Bolduc, V., Zou, Y., Ko, D., Bönnemann, C.G., 2014. siRNA-mediated Allele-specific Silencing of a COL6A3 Mutation in a Cellular Model of Dominant Ullrich Muscular Dystrophy. Mol Ther Nucleic Acids 3, e147. https://doi.org/10.1038/mtna.2013.74
Bönnemann, C.G., Cox, G.F., Shapiro, F., Wu, J.-J., Feener, C.A., Thompson, T.G., Anthony, D.C., Eyre, D.R., Darras, B.T., Kunkel, L.M., 2000. A mutation in the alpha 3 chain of type IX collagen causes autosomal dominant multiple epiphyseal dysplasia with mild myopathy. Proc Natl Acad Sci U S A 97, 1212–1217.
Borochowitz, Z.U., Scheffer, D., Adir, V., Dagoneau, N., Munnich, A., Cormier-Daire, V., 2004. Spondylo-epi-metaphyseal dysplasia (SEMD) matrilin 3 type: homozygote matrilin 3 mutation in a novel form of SEMD. Journal of Medical Genetics 41, 366–372. https://doi.org/10.1136/jmg.2003.013342
Briggs, M.D., Bell, P.A., Wright, M.J., Pirog, K.A., 2015. New therapeutic targets in rare genetic skeletal diseases. Expert Opin Orphan Drugs 3, 1137–1154. https://doi.org/10.1517/21678707.2015.1083853
Briggs, M.D., Brock, J., Ramsden, S.C., Bell, P.A., 2014. Genotype to phenotype correlations in cartilage oligomeric matrix protein associated chondrodysplasias. Eur J Hum Genet 22, 1278–1282. https://doi.org/10.1038/ejhg.2014.30
Briggs, M.D., Hoffman, S.M., King, L.M., Olsen, A.S., Mohrenweiser, H., Leroy, J.G., Mortier, G.R., Rimoin, D.L., Lachman, R.S., Gaines, E.S., 1995. Pseudoachondroplasia and multiple epiphyseal dysplasia due to mutations in the cartilage oligomeric matrix protein gene. Nat. Genet. 10, 330–336. https://doi.org/10.1038/ng0795-330
Budde, B., Blumbach, K., Ylöstalo, J., Zaucke, F., Ehlen, H.W.A., Wagener, R., Ala-Kokko, L., Paulsson, M., Bruckner, P., Grässel, S., 2005. Altered integration of matrilin-3 into cartilage extracellular matrix in the absence of collagen IX. Mol Cell Biol 25, 10465–10478. https://doi.org/10.1128/MCB.25.23.10465-10478.2005
Bui, C., Huber, C., Tuysuz, B., Alanay, Y., Bole-Feysot, C., Leroy, J.G., Mortier, G., Nitschke, P., Munnich, A., Cormier-Daire, V., 2014. XYLT1 Mutations in Desbuquois Dysplasia Type 2. The American Journal of Human Genetics 94, 405–414. https://doi.org/10.1016/j.ajhg.2014.01.020

Bulman, M.P., Kusumi, K., Frayling, T.M., McKeown, C., Garrett, C., Lander, E.S., Krumlauf, R., Hattersley, A.T., Ellard, S., Turnpenny, P.D., 2000. Mutations in the human delta homologue, DLL3, cause axial skeletal defects in spondylocostal dysostosis. Nat Genet 24, 438–441. https://doi.org/10.1038/74307

Buscemi, L., Ramonet, D., Klingberg, F., Formey, A., Smith-Clerc, J., Meister, J.-J., Hinz, B., 2011. The single-molecule mechanics of the latent TGF-β1 complex. Curr Biol 21, 2046–2054. https://doi.org/10.1016/j.cub.2011.11.037

Butterfield, R.J., Foley, A.R., Dastgir, J., Asman, S., Dunn, D.M., Zou, Y., Hu, Y., Donkervoort, S., Flanigan, K.M., Swoboda, K.J., Winder, T.L., Weiss, R.B., Bönnemann, C.G., 2013. Position of Glycine Substitutions in the Triple Helix of COL6A1, COL6A2, and COL6A3 is Correlated with Severity and Mode of Inheritance in Collagen VI Myopathies. Human Mutation 34, 1558–1567. https://doi.org/10.1002/humu.22429

Califf, R.M., 2018. Biomarker definitions and their applications. Exp Biol Med (Maywood) 243, 213–221. https://doi.org/10.1177/1535370217750088

Camara, A.K.S., Zhou, Y., Wen, P.-C., Tajkhorshid, E., Kwok, W.-M., 2017. Mitochondrial VDAC1: A Key Gatekeeper as Potential Therapeutic Target. Frontiers in Physiology 8, 460. https://doi.org/10.3389/fphys.2017.00460

Cameron, T.L., Bell, K.M., Gresshoff, I.L., Sampurno, L., Mullan, L., Ermann, J., Glimcher, L.H., Boot-Handford, R.P., Bateman, J.F., 2015a. XBP1-Independent UPR Pathways Suppress C/EBP-β Mediated Chondrocyte Differentiation in ER-Stress Related Skeletal Disease. PLoS Genet. 11, e1005505. https://doi.org/10.1371/journal.pgen.1005505

Cameron, T.L., Bell, K.M., Tatarczuch, L., Mackie, E.J., Rajpar, M.H., McDermott, B.T., Boot-Handford, R.P., Bateman, J.F., 2011. Transcriptional Profiling of Chondrodysplasia Growth Plate Cartilage Reveals Adaptive ER-Stress Networks That Allow Survival but Disrupt Hypertrophy. PLoS One 6. https://doi.org/10.1371/journal.pone.0024600

Cameron, T.L., Gresshoff, I.L., Bell, K.M., Piróg, K.A., Sampurno, L., Hartley, C.L., Sanford, E.M., Wilson, R., Ermann, J., Boot-Handford, R.P., Glimcher, L.H., Briggs, M.D., Bateman, J.F., 2015b. Cartilage-specific ablation of XBP1 signaling in mouse results in a chondrodysplasia characterized by reduced chondrocyte proliferation and delayed cartilage maturation and mineralization. Osteoarthr. Cartil. 23, 661–670. https://doi.org/10.1016/j.joca.2015.01.001

Caterson, B., Melrose, J., 2018. Keratan sulfate, a complex glycosaminoglycan with unique functional capability. Glycobiology 28, 182–206. https://doi.org/10.1093/glycob/cwy003

Cha, H.-N., Park, S., Dan, Y., Kim, J.-R., Park, S.-Y., 2019. Peroxiredoxin2 Deficiency Aggravates Aging-Induced Insulin Resistance and Declines Muscle Strength. The Journals of Gerontology: Series A 74, 147–154. https://doi.org/10.1093/gerona/gly113

Chakkalakal, S.A., Heilig, J., Baumann, U., Paulsson, M., Zaucke, F., 2018. Impact of Arginine to Cysteine Mutations in Collagen II on Protein Secretion and Cell Survival. Int J Mol Sci 19, E541. https://doi.org/10.3390/ijms19020541

Chang, J., Garva, R., Pickard, A., Yeung, C.-Y.C., Mallikarjun, V., Swift, J., Holmes, D.F., Calverley, B., Lu, Y., Adamson, A., Raymond-Hayling, H., Jensen, O., Shearer, T., Meng, Q.J., Kadler, K.E., 2020. Circadian control of the secretory pathway maintains collagen homeostasis. Nat Cell Biol 22, 74–86. https://doi.org/10.1038/s41556-019-0441-z

Chapman, K.L., Mortier, G.R., Chapman, K., Loughlin, J., Grant, M.E., Briggs, M.D., 2001. Mutations in the region encoding the von Willebrand factor A domain of matrilin-3 are associated with multiple epiphyseal dysplasia. Nat. Genet. 28, 393–396. https://doi.org/10.1038/ng573

Charbonneau, M., Lavoie, R.R., Lauzier, A., Harper, K., McDonald, P.P., Dubois, C.M., 2016. Platelet-Derived Growth Factor Receptor Activation Promotes the Prodestructive Invadosome-Forming Phenotype of Synoviocytes from Patients with Rheumatoid Arthritis. J.I. 196, 3264–3275. https://doi.org/10.4049/jimmunol.1500502

Chen, S., Tao, J., Bae, Y., Jiang, M.-M., Bertin, T., Chen, Y., Yang, T., Lee, B., 2013. Notch gain of function inhibits chondrocyte differentiation via Rbpj-dependent suppression of Sox9. J Bone Miner Res 28, 649–659. https://doi.org/10.1002/jbmr.1770

Chen, T.-L.L., Posey, K.L., Hecht, J.T., Vertel, B.M., 2008. COMP mutations: domain-dependent relationship between abnormal chondrocyte trafficking and clinical PSACH and MED phenotypes. J Cell Biochem 103, 778–787. https://doi.org/10.1002/jcb.21445

Chen, T.-L.L., Stevens, J.W., Cole, W.G., Hecht, J.T., Vertel, B.M., 2004. Cell-type specific trafficking of expressed mutant COMP in a cell culture model for PSACH. Matrix Biol 23, 433–444. https://doi.org/10.1016/j.matbio.2004.09.005

Chessler, S.D., Byers, P.H., 1993. BiP binds type I procollagen pro alpha chains with mutations in the carboxyl-terminal propeptide synthesized by cells from patients with osteogenesis imperfecta. J. Biol. Chem. 268, 18226–18233.

Chou, C.-H., Jain, V., Gibson, J., Attarian, D.E., Haraden, C.A., Yohn, C.B., Laberge, R.-M., Gregory, S., Kraus, V.B., 2020. Synovial cell cross-talk with cartilage plays a major role in the pathogenesis of osteoarthritis. Sci Rep 10, 10868. https://doi.org/10.1038/s41598-020-67730-y

Chung, H.J., Jensen, D.A., Gawron, K., Steplewski, A., Fertala, A., 2009. R992C (p.R1192C) Substitution in collagen II alters the structure of mutant molecules and induces the unfolded protein response. J Mol Biol 390, 306–318. https://doi.org/10.1016/j.jmb.2009.05.004

Coit, P., Ortiz-Fernandez, L., Lewis, E.E., McCune, W.J., Maksimowicz-McKinnon, K., Sawalha, A.H., 2020. A longitudinal and transancestral analysis of DNA methylation patterns and disease activity in lupus patients. JCI Insight 5, e143654. https://doi.org/10.1172/jci.insight.143654

Cotterill, S.L., Jackson, G.C., Leighton, M.P., Wagener, R., Mäkitie, O., Cole, W.G., Briggs, M.D., 2005. Multiple epiphyseal dysplasia mutations in MATN3 cause misfolding of the A-domain and prevent secretion of mutant matrilin-3. Hum. Mutat. 26, 557–565. https://doi.org/10.1002/humu.20263

Couchman, J.R., Pataki, C.A., 2012. An Introduction to Proteoglycans and Their Localization. J Histochem Cytochem 60, 885–897. https://doi.org/10.1369/0022155412464638

Coustry, F., Posey, K.L., Liu, P., Alcorn, J.L., Hecht, J.T., 2012. D469del-COMP retention in chondrocytes stimulates caspase-independent necroptosis. Am J Pathol 180, 738–748. https://doi.org/10.1016/j.ajpath.2011.10.033

Crawford, S.E., Stellmach, V., Murphy-Ullrich, J.E., Ribeiro, S.M., Lawler, J., Hynes, R.O., Boivin, G.P., Bouck, N., 1998. Thrombospondin-1 is a major activator of TGF-beta1 in vivo. Cell 93, 1159–1170. https://doi.org/10.1016/s0092-8674(00)81460-9

Credle, J.J., Forcelli, P.A., Delannoy, M., Oaks, A.W., Permaul, E., Berry, D.L., Duka, V., Wills, J., Sidhu, A., 2015. α-Synuclein-mediated inhibition of ATF6 processing into COPII vesicles disrupts UPR signaling in Parkinson's disease. Neurobiol Dis 76, 112–125. https://doi.org/10.1016/j.nbd.2015.02.005

Crevenna, A.H., Blank, B., Maiser, A., Emin, D., Prescher, J., Beck, G., Kienzle, C., Bartnik, K., Habermann, B., Pakdel, M., Leonhardt, H., Lamb, D.C., von Blume, J., 2016. Secretory cargo sorting by Ca2+-dependent Cab45 oligomerization at the trans-Golgi network. J Cell Biol 213, 305–314. https://doi.org/10.1083/jcb.201601089

Criddle, D.N., Gillies, S., Baumgartner-Wilson, H.K., Jaffar, M., Chinje, E.C., Passmore, S., Chvanov, M., Barrow, S., Gerasimenko, O.V., Tepikin, A.V., Sutton, R., Petersen, O.H., 2006. Menadione-induced reactive oxygen species generation via redox cycling promotes apoptosis of murine pancreatic acinar cells. J Biol Chem 281, 40485–40492. https://doi.org/10.1074/jbc.M607704200

Csobonyeiova, M., Polak, S., Zamborsky, R., Danisovic, L., 2017. iPS cell technologies and their prospect for bone regeneration and disease modeling: A mini review. Journal of Advanced Research 8, 321–327. https://doi.org/10.1016/j.jare.2017.02.004

Cunniff, B., Snider, G.W., Fredette, N., Stumpff, J., Hondal, R.J., Heintz, N.H., 2014. Resolution of oxidative stress by thioredoxin reductase: Cysteine versus selenocysteine. Redox Biology 2, 475–484. https://doi.org/10.1016/j.redox.2014.01.021

Czarny-Ratajczak, M., Lohiniva, J., Rogala, P., Kozlowski, K., Perälä, M., Carter, L., Spector, T.D., Kolodziej, L., Seppänen, U., Glazar, R., Królewski, J., Latos-Bielenska, A., Ala-Kokko, L., 2001. A mutation in COL9A1 causes multiple epiphyseal dysplasia: further evidence for locus heterogeneity. Am. J. Hum. Genet. 69, 969–980. https://doi.org/10.1086/324023

Dan, H.C., Ebbs, A., Pasparakis, M., Dyke, T.V., Basseres, D.S., Baldwin, A.S., 2014. Akt-dependent Activation of mTORC1 Complex Involves Phosphorylation of mTOR (Mammalian Target of Rapamycin) by IκB Kinase α (IKKα) *. Journal of Biological Chemistry 289, 25227–25240. https://doi.org/10.1074/jbc.M114.554881

Das, L., Dhiman, V., Van Hul, W., Bhansali, A., Gogate, Y., Steenackers, E., Mortier, G., Bhadada, S.K., 2020. Spondylo-epi-metaphyseal dysplasia due to a homozygous missense mutation in the gene encoding Matrilin-3 (T120M). Bone Reports 12, 100245. https://doi.org/10.1016/j.bonr.2020.100245

Davegårdh, C., García-Calzón, S., Bacos, K., Ling, C., 2018. DNA methylation in the pathogenesis of type 2 diabetes in humans. Mol Metab 14, 12–25. https://doi.org/10.1016/j.molmet.2018.01.022

Day, T.F., Guo, X., Garrett-Beal, L., Yang, Y., 2005. Wnt/beta-catenin signaling in mesenchymal progenitors controls osteoblast and chondrocyte differentiation during vertebrate skeletogenesis. Dev Cell 8, 739–750. https://doi.org/10.1016/j.devcel.2005.03.016

De Jager, P., Srivastava, G., Lunnon, K., Burgess, J., Schalkwyk, L., Yu, L., Eaton, M., Keenan, B., Ernst, J., McCabe, C., Tang, A., Raj, T., Replogle, J., Brodeur, W., Gabriel, S., Chai, H., Younkin, C., Younkin, S., Zou, F., Szyf, M., Epstein, C., Schneider, J., Bernstein, B., Meissner, A., Ertekin-Taner, N., Chibnik, L., Kellis, M., Mill, J., Bennett, D., 2014. Alzheimery's disease pathology is associated with early alterations in brain DNA methylation at

ANK1, BIN1, RHBDF2 and other loci. Nat Neurosci 17, 1156–1163. https://doi.org/10.1038/nn.3786
Decker, R.S., 2017. Articular cartilage and joint development from embryogenesis to adulthood. Semin Cell Dev Biol 62, 50–56. https://doi.org/10.1016/j.semcdb.2016.10.005
Deere, M., Rhoades Hall, C., Gunning, K.B., LeFebvre, V., Ridall, A.L., Hecht, J.T., 2001. Analysis of the promoter region of human cartilage oligomeric matrix protein (COMP). Matrix Biology 19, 783–792. https://doi.org/10.1016/S0945-053X(00)00127-X
Delany, A.M., Hankenson, K.D., 2009. Thrombospondin-2 and SPARC/osteonectin are critical regulators of bone remodeling. J. Cell Commun. Signal. 3, 227–238. https://doi.org/10.1007/s12079-009-0076-0
Delépine, M., Nicolino, M., Barrett, T., Golamaully, M., Mark Lathrop, G., Julier, C., 2000. *EIF2AK3*, encoding translation initiation factor 2-α kinase 3, is mutated in patients with Wolcott-Rallison syndrome. Nature Genetics 25, 406–409. https://doi.org/10.1038/78085
Délot, E., Brodie, S.G., King, L.M., Wilcox, W.R., Cohn, D.H., 1998. Physiological and pathological secretion of cartilage oligomeric matrix protein by cells in culture. J. Biol. Chem. 273, 26692–26697. https://doi.org/10.1074/jbc.273.41.26692
Délot, E., King, L.M., Briggs, M.D., Wilcox, W.R., Cohn, D.H., 1999. Trinucleotide expansion mutations in the cartilage oligomeric matrix protein (COMP) gene. Hum. Mol. Genet. 8, 123–128. https://doi.org/10.1093/hmg/8.1.123
Deng, C., Wynshaw-Boris, A., Zhou, F., Kuo, A., Leder, P., 1996. Fibroblast growth factor receptor 3 is a negative regulator of bone growth. Cell 84, 911–921. https://doi.org/10.1016/s0092-8674(00)81069-7
Dennis, E.P., Greenhalgh-Maychell, P.L., Briggs, M.D., 2021. Multiple epiphyseal dysplasia and related disorders: Molecular genetics, disease mechanisms, and therapeutic avenues. Developmental Dynamics 250, 345–359. https://doi.org/10.1002/dvdy.221
Dhounchak, S., Popp, S.K., Brown, D.J., Laybutt, D.R., Biden, T.J., Bornstein, S.R., Parish, C.R., Simeonovic, C.J., 2021. Heparan sulfate proteoglycans in beta cells provide a critical link between endoplasmic reticulum stress, oxidative stress and type 2 diabetes. PLoS One 16, e0252607. https://doi.org/10.1371/journal.pone.0252607
Di Cesare, P.E., Carlson, C.S., Stollerman, E.S., Chen, F.S., Leslie, M., Perris, R., 1997. Expression of cartilage oligomeric matrix protein by human synovium. FEBS Lett 412, 249–252. https://doi.org/10.1016/s0014-5793(97)00789-8
Di Cesare, P.E., Chen, F.S., Moergelin, M., Carlson, C.S., Leslie, M.P., Perris, R., Fang, C., 2002. Matrix-matrix interaction of cartilage oligomeric matrix protein and fibronectin. Matrix Biol. 21, 461–470.
Di Cesare, P.E., Fang, C., Leslie, M.P., Tulli, H., Perris, R., Carlson, C.S., 2000. Expression of cartilage oligomeric matrix protein (COMP) by embryonic and adult osteoblasts. J Orthop Res 18, 713–720. https://doi.org/10.1002/jor.1100180506
Di Girolamo, N., Indoh, I., Jackson, N., Wakefield, D., McNeil, H.P., Yan, W., Geczy, C., Arm, J.P., Tedla, N., 2006. Human mast cell-derived gelatinase B (matrix metalloproteinase-9) is regulated by inflammatory cytokines: role in cell migration. J Immunol 177, 2638–2650. https://doi.org/10.4049/jimmunol.177.4.2638

Di Malta, C., Cinque, L., Settembre, C., 2019. Transcriptional Regulation of Autophagy: Mechanisms and Diseases. Frontiers in Cell and Developmental Biology 7, 114. https://doi.org/10.3389/fcell.2019.00114
Dicks, A., Wu, C.-L., Steward, N., Adkar, S.S., Gersbach, C.A., Guilak, F., 2020. Prospective isolation of chondroprogenitors from human iPSCs based on cell surface markers identified using a CRISPR-Cas9-generated reporter. Stem Cell Res Ther 11. https://doi.org/10.1186/s13287-020-01597-8
Diederichs, S., Klampfleuthner, F.A.M., Moradi, B., Richter, W., 2019. Chondral Differentiation of Induced Pluripotent Stem Cells Without Progression Into the Endochondral Pathway. Front Cell Dev Biol 7, 270. https://doi.org/10.3389/fcell.2019.00270
Diekman, B.O., Christoforou, N., Willard, V.P., Sun, H., Sanchez-Adams, J., Leong, K.W., Guilak, F., 2012. Cartilage tissue engineering using differentiated and purified induced pluripotent stem cells. Proc. Natl. Acad. Sci. U.S.A. 109, 19172–19177. https://doi.org/10.1073/pnas.1210422109
Diekman, B.O., Thakore, P.I., O'Connor, S.K., Willard, V.P., Brunger, J.M., Christoforou, N., Leong, K.W., Gersbach, C.A., Guilak, F., 2015. Knockdown of the Cell Cycle Inhibitor p21 Enhances Cartilage Formation by Induced Pluripotent Stem Cells. Tissue Eng Part A 21, 1261–1274. https://doi.org/10.1089/ten.tea.2014.0240
Dieterle, M.P., Husari, A., Rolauffs, B., Steinberg, T., Tomakidi, P., 2021. Integrins, cadherins and channels in cartilage mechanotransduction: perspectives for future regeneration strategies. Expert Rev Mol Med 23, e14. https://doi.org/10.1017/erm.2021.16
Dinser, R., Zaucke, F., Kreppel, F., Hultenby, K., Kochanek, S., Paulsson, M., Maurer, P., 2002. Pseudoachondroplasia is caused through both intra- and extracellular pathogenic pathways. J. Clin. Invest. 110, 505–513. https://doi.org/10.1172/JCI14386
Dodge, G.R., Hawkins, D., Boesler, E., Sakai, L., Jimenez, S.A., 1998. Production of cartilage oligomeric matrix protein (COMP) by cultured human dermal and synovial fibroblasts. Osteoarthritis Cartilage 6, 435–440. https://doi.org/10.1053/joca.1998.0147
Dor, Y., Cedar, H., 2018. Principles of DNA methylation and their implications for biology and medicine. The Lancet 392, 777–786. https://doi.org/10.1016/S0140-6736(18)31268-6
DuBose, K.B., Zayzafoon, M., Murphy-Ullrich, J.E., 2012. Thrombospondin-1 inhibits osteogenic differentiation of human mesenchymal stem cells through latent TGF-β activation. Biochem Biophys Res Commun 422, 488–493. https://doi.org/10.1016/j.bbrc.2012.05.020
Duennwald, M.L., Lindquist, S., 2008. Impaired ERAD and ER stress are early and specific events in polyglutamine toxicity. Genes Dev 22, 3308–3319. https://doi.org/10.1101/gad.1673408
Duksin, D., Bornstein, P., 1977. Impaired conversion of procollagen to collagen by fibroblasts and bone treated with tunicamycin, an inhibitor of protein glycosylation. J Biol Chem 252, 955–962.
Duran, I., Zieba, J., Csukasi, F., Martin, J.H., Wachtell, D., Barad, M., Dawson, B., Fafilek, B., Jacobson, C.M., Ambrose, C.G., Cohn, D.H., Krejci, P., Lee, B.H., Krakow, D., 2022. 4-PBA treatment improves bone phenotypes in the Aga2 mouse model of osteogenesis imperfecta. Journal of Bone and Mineral Research n/a. https://doi.org/10.1002/jbmr.4501

Duran-Aniotz, C., Cornejo, V.H., Espinoza, S., Ardiles, Á.O., Medinas, D.B., Salazar, C., Foley, A., Gajardo, I., Thielen, P., Iwawaki, T., Scheper, W., Soto, C., Palacios, A.G., Hoozemans, J.J.M., Hetz, C., 2017. IRE1 signaling exacerbates Alzheimer's disease pathogenesis. Acta Neuropathol 134, 489–506. https://doi.org/10.1007/s00401-017-1694-x

Dwan, K., Phillipi, C.A., Steiner, R.D., Basel, D., 2016. Bisphosphonate therapy for osteogenesis imperfecta. Cochrane Database Syst Rev 2016, CD005088. https://doi.org/10.1002/14651858.CD005088.pub4

Dy, P., Wang, W., Bhattaram, P., Wang, Q., Wang, L., Ballock, R.T., Lefebvre, V., 2012. Sox9 Directs Hypertrophic Maturation and Blocks Osteoblast Differentiation of Growth Plate Chondrocytes. Dev Cell 22, 597–609. https://doi.org/10.1016/j.devcel.2011.12.024

Engin, F., Yao, Z., Yang, T., Zhou, G., Bertin, T., Jiang, M.M., Chen, Y., Wang, L., Zheng, H., Sutton, R.E., Boyce, B.F., Lee, B., 2008. Dimorphic effects of Notch signaling in bone homeostasis. Nat Med 14, 299–305. https://doi.org/10.1038/nm1712

Esfandiari, N., Sharma, R.K., Saleh, R.A., Thomas, A.J., Agarwal, A., 2003. Utility of the Nitroblue Tetrazolium Reduction Test for Assessment of Reactive Oxygen Species Production by Seminal Leukocytes and Spermatozoa. Journal of Andrology 24, 862–870. https://doi.org/10.1002/j.1939-4640.2003.tb03137.x

Ewels, P., Magnusson, M., Lundin, S., Käller, M., 2016. MultiQC: summarize analysis results for multiple tools and samples in a single report. Bioinformatics 32, 3047–3048. https://doi.org/10.1093/bioinformatics/btw354

Faletra, F., D'Adamo, A.P., Bruno, I., Athanasakis, E., Biskup, S., Esposito, L., Gasparini, P., 2014. Autosomal recessive Stickler syndrome due to a loss of function mutation in the COL9A3 gene. Am J Med Genet A 164A, 42–47. https://doi.org/10.1002/ajmg.a.36165

Fang, C., Carlson, C.S., Leslie, M.P., Tulli, H., Stolerman, E., Perris, R., Ni, L., Di Cesare, P.E., 2000. Molecular cloning, sequencing, and tissue and developmental expression of mouse cartilage oligomeric matrix protein (COMP). Journal of Orthopaedic Research 18, 593–603. https://doi.org/10.1002/jor.1100180412

Fields, G.B., 2010. Using fluorogenic peptide substrates to assay matrix metalloproteinases. Methods Mol Biol 622, 393–433. https://doi.org/10.1007/978-1-60327-299-5_24

Finch, P.W., Cunha, G.R., Rubin, J.S., Wong, J., Ron, D., 1995. Pattern of keratinocyte growth factor and keratinocyte growth factor receptor expression during mouse fetal development suggests a role in mediating morphogenetic mesenchymal-epithelial interactions. Dev Dyn 203, 223–240. https://doi.org/10.1002/aja.1002030210

Forlino, A., Marini, J.C., 2016. Osteogenesis imperfecta. The Lancet 387, 1657–1671. https://doi.org/10.1016/S0140-6736(15)00728-X

Forouhan, M., Mori, K., Boot-Handford, R.P., 2018a. Paradoxical roles of ATF6α and ATF6β in modulating disease severity caused by mutations in collagen X. Matrix Biol 70, 50–71. https://doi.org/10.1016/j.matbio.2018.03.004

Forouhan, M., Sonntag, S., Boot-Handford, R.P., 2018b. Carbamazepine reduces disease severity in a mouse model of metaphyseal chondrodysplasia type Schmid caused by a premature stop codon (Y632X) in the Col10a1 gene. Hum. Mol. Genet. 27, 3840–3853. https://doi.org/10.1093/hmg/ddy253

Forrester, A., De Leonibus, C., Grumati, P., Fasana, E., Piemontese, M., Staiano, L., Fregno, I., Raimondi, A., Marazza, A., Bruno, G., Iavazzo, M., Intartaglia, D., Seczynska, M., van Anken, E., Conte, I., De Matteis, M.A., Dikic, I., Molinari, M., Settembre, C., 2019. A selective ER-phagy exerts procollagen quality control via a Calnexin-FAM134B complex. EMBO J 38, e99847. https://doi.org/10.15252/embj.201899847

Foster, J.W., Dominguez-Steglich, M.A., Guioli, S., Kwok, C., Weller, P.A., Stevanović, M., Weissenbach, J., Mansour, S., Young, I.D., Goodfellow, P.N., 1994. Campomelic dysplasia and autosomal sex reversal caused by mutations in an SRY-related gene. Nature 372, 525–530. https://doi.org/10.1038/372525a0

Fregno, I., Fasana, E., Bergmann, T.J., Raimondi, A., Loi, M., Soldà, T., Galli, C., D'Antuono, R., Morone, D., Danieli, A., Paganetti, P., van Anken, E., Molinari, M., 2018. ER-to-lysosome-associated degradation of proteasome-resistant ATZ polymers occurs via receptor-mediated vesicular transport. EMBO J 37, e99259. https://doi.org/10.15252/embj.201899259

Fresquet, M., Jackson, G.C., Loughlin, J., Briggs, M.D., 2008. Novel mutations in exon 2 of MATN3 affect residues within the alpha-helices of the A-domain and can result in the intracellular retention of mutant matrilin-3. Hum. Mutat. 29, 330. https://doi.org/10.1002/humu.9518

Fresquet, M., Jowitt, T.A., Ylöstalo, J., Coffey, P., Meadows, R.S., Ala-Kokko, L., Thornton, D.J., Briggs, M.D., 2007. Structural and functional characterisation of recombinant matrilin-3 A domain and implications for human genetic bone diseases. J Biol Chem 282, 34634–34643. https://doi.org/10.1074/jbc.M705301200

Fukui, M., Choi, H.J., Zhu, B.T., 2012. Rapid generation of mitochondrial superoxide induces mitochondrion-dependent but caspase-independent cell death in hippocampal neuronal cells that morphologically resembles necroptosis. Toxicol Appl Pharmacol 262, 156–166. https://doi.org/10.1016/j.taap.2012.04.030

Furlan, A.G., Spanou, C.E.S., Godwin, A.R.F., Wohl, A.P., Zimmermann, L.-M.A., Imhof, T., Koch, M., Baldock, C., Sengle, G., 2021. A new MMP-mediated prodomain cleavage mechanism to activate bone morphogenetic proteins from the extracellular matrix. The FASEB Journal 35, e21353. https://doi.org/10.1096/fj.202001264R

Furumatsu, T., Tsuda, M., Taniguchi, N., Tajima, Y., Asahara, H., 2005. Smad3 induces chondrogenesis through the activation of SOX9 via CREB-binding protein/p300 recruitment. J Biol Chem 280, 8343–8350. https://doi.org/10.1074/jbc.M413913200

Gallegos-Gómez, M.-L., Greotti, E., López-Méndez, M.-C., Sánchez-Vázquez, V.-H., Arias, J.-M., Guerrero-Hernández, A., 2018. The Trans Golgi Region is a Labile Intracellular Ca2+ Store Sensitive to Emetine. Sci Rep 8, 17143. https://doi.org/10.1038/s41598-018-35280-z

Gan, W., Zhang, C., Siu, K.Y., Satoh, A., Tanner, J.A., Yu, S., 2017. ULK1 phosphorylates Sec23A and mediates autophagy-induced inhibition of ER-to-Golgi traffic. BMC Cell Biology 18, 22. https://doi.org/10.1186/s12860-017-0138-8

Garcia, S., Dirat, B., Tognacci, T., Rochet, N., Mouska, X., Bonnafous, S., Patouraux, S., Tran, A., Gual, P., Le Marchand-Brustel, Y., Gennero, I., Gouze, E., 2013. Postnatal soluble FGFR3 therapy rescues achondroplasia

symptoms and restores bone growth in mice. Sci Transl Med 5, 203ra124. https://doi.org/10.1126/scitranslmed.3006247
Garibaldi, N., Contento, B.M., Babini, G., Morini, J., Siciliani, S., Biggiogera, M., Raspanti, M., Marini, J.C., Rossi, A., Forlino, A., Besio, R., 2021. Targeting cellular stress in vitro improves osteoblast homeostasis, matrix collagen content and mineralization in two murine models of osteogenesis imperfecta. Matrix Biol 98, 1–20. https://doi.org/10.1016/j.matbio.2021.03.001
Garofalo, S., Kliger-Spatz, M., Cooke, J.L., Wolstin, O., Lunstrum, G.P., Moshkovitz, S.M., Horton, W.A., Yayon, A., 1999. Skeletal dysplasia and defective chondrocyte differentiation by targeted overexpression of fibroblast growth factor 9 in transgenic mice. J Bone Miner Res 14, 1909–1915. https://doi.org/10.1359/jbmr.1999.14.11.1909
Gasparoni, G., Bultmann, S., Lutsik, P., Kraus, T.F.J., Sordon, S., Vlcek, J., Dietinger, V., Steinmaurer, M., Haider, M., Mulholland, C.B., Arzberger, T., Roeber, S., Riemenschneider, M., Kretzschmar, H.A., Giese, A., Leonhardt, H., Walter, J., 2018. DNA methylation analysis on purified neurons and glia dissects age and Alzheimer's disease-specific changes in the human cortex. Epigenetics Chromatin 11, 41. https://doi.org/10.1186/s13072-018-0211-3
Gelse, K., Pöschl, E., Aigner, T., 2003. Collagens—structure, function, and biosynthesis. Advanced Drug Delivery Reviews, Collagen in drug delivery and tissue engineering 55, 1531–1546. https://doi.org/10.1016/j.addr.2003.08.002
Gerakis, Y., Hetz, C., 2018. Emerging roles of ER stress in the etiology and pathogenesis of Alzheimer's disease. The FEBS Journal 285, 995–1011. https://doi.org/10.1111/febs.14332
Gerber, H.P., Vu, T.H., Ryan, A.M., Kowalski, J., Werb, Z., Ferrara, N., 1999. VEGF couples hypertrophic cartilage remodeling, ossification and angiogenesis during endochondral bone formation. Nat. Med. 5, 623–628. https://doi.org/10.1038/9467
Gibson, B.G., Briggs, M.D., 2016. The aggrecanopathies; an evolving phenotypic spectrum of human genetic skeletal diseases. Orphanet J Rare Dis 11, 86. https://doi.org/10.1186/s13023-016-0459-2
Gjelstrup, L.C., Boesen, T., Kragstrup, T.W., Jørgensen, A., Klein, N.J., Thiel, S., Deleuran, B.W., Vorup-Jensen, T., 2010. Shedding of Large Functionally Active CD11/CD18 Integrin Complexes from Leukocyte Membranes during Synovial Inflammation Distinguishes Three Types of Arthritis through Differential Epitope Exposure. The Journal of Immunology 185, 4154–4168. https://doi.org/10.4049/jimmunol.1000952
Glorieux, F.H., Devogelaer, J.-P., Durigova, M., Goemaere, S., Hemsley, S., Jakob, F., Junker, U., Ruckle, J., Seefried, L., Winkle, P.J., 2017. BPS804 Anti-Sclerostin Antibody in Adults With Moderate Osteogenesis Imperfecta: Results of a Randomized Phase 2a Trial. J Bone Miner Res 32, 1496–1504. https://doi.org/10.1002/jbmr.3143
Goldring, M.B., Otero, M., 2011. Inflammation in osteoarthritis. Curr Opin Rheumatol 23, 471–478. https://doi.org/10.1097/BOR.0b013e328349c2b1
Gossage, D.L., Cieslarová, B., Ap, S., Zheng, H., Xin, Y., Lal, P., Chen, G., Smith, V., Sundy, J.S., 2018. Phase 1b Study of the Safety, Pharmacokinetics, and Disease-related Outcomes of the Matrix Metalloproteinase-9 Inhibitor Andecaliximab in Patients With Rheumatoid Arthritis. Clin Ther 40, 156-165.e5. https://doi.org/10.1016/j.clinthera.2017.11.011

Gray, A., Schloss, R.S., Yarmush, M., 2016. Donor variability among anti-inflammatory pre-activated mesenchymal stromal cells. Technology (Singap World Sci) 4, 201–215. https://doi.org/10.1142/S2339547816500084

Green, A.C., Kocovski, P., Jovic, T., Walia, M.K., Chandraratna, R. a. S., Martin, T.J., Baker, E.K., Purton, L.E., 2017. Retinoic acid receptor signalling directly regulates osteoblast and adipocyte differentiation from mesenchymal progenitor cells. Exp Cell Res 350, 284–297. https://doi.org/10.1016/j.yexcr.2016.12.007

Greenberg, M.V.C., Bourc'his, D., 2019. The diverse roles of DNA methylation in mammalian development and disease. Nat Rev Mol Cell Biol 20, 590–607. https://doi.org/10.1038/s41580-019-0159-6

Greene, B., Russo, R.J., Dwyer, S., Malley, K., Roberts, E., Serrielo, J., Piepenhagen, P., Cummings, S., Ryan, S., Zarazinski, C., Uppuganti, S., Bukanov, N., Nyman, J.S., Cox, M.K., Liu, S., Ibraghimov-Beskrovnaya, O., Sabbagh, Y., 2021. Inhibition of TGF-β Increases Bone Volume and Strength in a Mouse Model of Osteogenesis Imperfecta. JBMR Plus 5, e10530. https://doi.org/10.1002/jbm4.10530

Gripp, K.W., Robbins, K.M., Sobreira, N.L., Witmer, P.D., Bird, L.M., Avela, K., Makitie, O., Alves, D., Hogue, J.S., Zackai, E.H., Doheny, K.F., Stabley, D.L., Sol-Church, K., 2015. Truncating mutations in the last exon of NOTCH3 cause lateral meningocele syndrome. Am J Med Genet A 167A, 271–281. https://doi.org/10.1002/ajmg.a.36863

Groma, G., Xin, W., Grskovic, I., Niehoff, A., Brachvogel, B., Paulsson, M., Zaucke, F., 2012. Abnormal bone quality in cartilage oligomeric matrix protein and matrilin 3 double-deficient mice caused by increased tissue inhibitor of metalloproteinases 3 deposition and delayed aggrecan degradation. Arthritis Rheum. 64, 2644–2654. https://doi.org/10.1002/art.34435

Gualeni, B., Rajpar, M.H., Kellogg, A., Bell, P.A., Arvan, P., Boot-Handford, R.P., Briggs, M.D., 2013. A novel transgenic mouse model of growth plate dysplasia reveals that decreased chondrocyte proliferation due to chronic ER stress is a key factor in reduced bone growth. Dis Model Mech 6, 1414–1425. https://doi.org/10.1242/dmm.013342

Guo, J., Chung, U.-I., Yang, D., Karsenty, G., Bringhurst, F.R., Kronenberg, H.M., 2006. PTH/PTHrP receptor delays chondrocyte hypertrophy via both Runx2-dependent and -independent pathways. Dev. Biol. 292, 116–128. https://doi.org/10.1016/j.ydbio.2005.12.044

Guo, X., Mak, K.K., Taketo, M.M., Yang, Y., 2009. The Wnt/β-Catenin Pathway Interacts Differentially with PTHrP Signaling to Control Chondrocyte Hypertrophy and Final Maturation. PLOS ONE 4, e6067. https://doi.org/10.1371/journal.pone.0006067

Hahne, F., Ivanek, R., 2016. Visualizing Genomic Data Using Gviz and Bioconductor. Methods Mol Biol 1418, 335–351. https://doi.org/10.1007/978-1-4939-3578-9_16

Han, B., Li, Q., Wang, C., Patel, P., Adams, S.M., Doyran, B., Nia, H.T., Oftadeh, R., Zhou, S., Li, C.Y., Liu, X.S., Lu, X.L., Enomoto-Iwamoto, M., Qin, L., Mauck, R.L., Iozzo, R.V., Birk, D.E., Han, L., 2019. Decorin Regulates the Aggrecan Network Integrity and Biomechanical Functions of Cartilage Extracellular Matrix. ACS Nano 13, 11320–11333. https://doi.org/10.1021/acsnano.9b04477

Hankenson, K.D., Bain, S.D., Kyriakides, T.R., Smith, E.A., Goldstein, S.A., Bornstein, P., 2000. Increased marrow-derived osteoprogenitor cells and endosteal bone formation in mice lacking thrombospondin 2. J Bone Miner Res 15, 851–862. https://doi.org/10.1359/jbmr.2000.15.5.851
Hansen, U., Platz, N., Becker, A., Bruckner, P., Paulsson, M., Zaucke, F., 2011. A secreted variant of cartilage oligomeric matrix protein carrying a chondrodysplasia-causing mutation (p.H587R) disrupts collagen fibrillogenesis. Arthritis Rheum 63, 159–167. https://doi.org/10.1002/art.30073
Happonen, K.E., Saxne, T., Aspberg, A., Mörgelin, M., Heinegård, D., Blom, A.M., 2010. Regulation of complement by cartilage oligomeric matrix protein allows for a novel molecular diagnostic principle in rheumatoid arthritis. Arthritis Rheum 62, 3574–3583. https://doi.org/10.1002/art.27720
Happonen, K.E., Saxne, T., Geborek, P., Andersson, M., Bengtsson, A.A., Hesselstrand, R., Heinegård, D., Blom, A.M., 2012. Serum COMP-C3b complexes in rheumatic diseases and relation to anti-TNF-α treatment. Arthritis Res Ther 14, R15. https://doi.org/10.1186/ar3694
Hartley, C.L., Edwards, S., Mullan, L., Bell, P.A., Fresquet, M., Boot-Handford, R.P., Briggs, M.D., 2013. Armet/Manf and Creld2 are components of a specialized ER stress response provoked by inappropriate formation of disulphide bonds: implications for genetic skeletal diseases. Hum Mol Genet 22, 5262–5275. https://doi.org/10.1093/hmg/ddt383
Haudenschild, D.R., Hong, E., Yik, J.H.N., Chromy, B., Mörgelin, M., Snow, K.D., Acharya, C., Takada, Y., Di Cesare, P.E., 2011. Enhanced activity of transforming growth factor β1 (TGF-β1) bound to cartilage oligomeric matrix protein. J. Biol. Chem. 286, 43250–43258. https://doi.org/10.1074/jbc.M111.234716
Hayashi, T., 2019. The Sigma-1 Receptor in Cellular Stress Signaling. Front Neurosci 13, 733. https://doi.org/10.3389/fnins.2019.00733
Hayden, M.S., Ghosh, S., 2012. NF-κB, the first quarter-century: remarkable progress and outstanding questions. Genes Dev 26, 203–234. https://doi.org/10.1101/gad.183434.111
Hecht, J.T., Coustry, F., Veerisetty, A.C., Hossain, M.G., Posey, K.L., 2021a. Resveratrol Reduces COMPopathy in Mice Through Activation of Autophagy. JBMR Plus 5, e10456. https://doi.org/10.1002/jbm4.10456
Hecht, J.T., Nelson, L.D., Crowder, E., Wang, Y., Elder, F.F., Harrison, W.R., Francomano, C.A., Prange, C.K., Lennon, G.G., Deere, M., 1995. Mutations in exon 17B of cartilage oligomeric matrix protein (COMP) cause pseudoachondroplasia. Nat. Genet. 10, 325–329. https://doi.org/10.1038/ng0795-325
Hecht, J.T., Veerisetty, A.C., Hossain, M.G., Patra, D., Chiu, F., Coustry, F., Posey, K.L., 2021b. Joint Degeneration in a Mouse Model of Pseudoachondroplasia: ER Stress, Inflammation, and Block of Autophagy. Int J Mol Sci 22, 9239. https://doi.org/10.3390/ijms22179239
Hedbom, E., Antonsson, P., Hjerpe, A., Aeschlimann, D., Paulsson, M., Rosa-Pimentel, E., Sommarin, Y., Wendel, M., Oldberg, A., Heinegård, D., 1992. Cartilage matrix proteins. An acidic oligomeric protein (COMP) detected only in cartilage. J Biol Chem 267, 6132–6136.
Heilig, J., Dietmar, H.F., Brachvogel, B., Paulsson, M., Zaucke, F., Niehoff, A., 2020. Collagen IX deficiency leads to premature vascularization and ossification of murine femoral heads through an imbalance of pro- and antiangiogenic

factors. Osteoarthritis Cartilage 28, 988–999. https://doi.org/10.1016/j.joca.2020.03.015
Heinegård, D., 2009. Proteoglycans and more – from molecules to biology. Int J Exp Pathol 90, 575–586. https://doi.org/10.1111/j.1365-2613.2009.00695.x
Heine-Suñer, D., Díaz-Guillén, M.A., Lange, A.J., Rodríguez de Córdoba, S., 1998. Sequence and structure of the human 6-phosphofructo-2-kinase/fructose-2,6-bisphosphatase heart isoform gene (PFKFB2). Eur J Biochem 254, 103–110. https://doi.org/10.1046/j.1432-1327.1998.2540103.x
Hetz, C., Papa, F.R., 2018. The Unfolded Protein Response and Cell Fate Control. Molecular Cell 69, 169–181. https://doi.org/10.1016/j.molcel.2017.06.017
Hetz, C., Thielen, P., Matus, S., Nassif, M., Court, F., Kiffin, R., Martinez, G., Cuervo, A.M., Brown, R.H., Glimcher, L.H., 2009. XBP-1 deficiency in the nervous system protects against amyotrophic lateral sclerosis by increasing autophagy. Genes Dev 23, 2294–2306. https://doi.org/10.1101/gad.1830709
Hilton, M.J., Tu, X., Wu, X., Bai, S., Zhao, H., Kobayashi, T., Kronenberg, H.M., Teitelbaum, S.L., Ross, F.P., Kopan, R., Long, F., 2008. Notch signaling maintains bone marrow mesenchymal progenitors by suppressing osteoblast differentiation. Nat Med 14, 306–314. https://doi.org/10.1038/nm1716
Ho, M.S.P., Tsang, K.Y., Lo, R.L.K., Susic, M., Mäkitie, O., Chan, T.W.Y., Ng, V.C.W., Sillence, D.O., Boot-Handford, R.P., Gibson, G., Cheung, K.M.C., Cole, W.G., Cheah, K.S.E., Chan, D., 2007. COL10A1 nonsense and frame-shift mutations have a gain-of-function effect on the growth plate in human and mouse metaphyseal chondrodysplasia type Schmid. Hum Mol Genet 16, 1201–1215. https://doi.org/10.1093/hmg/ddm067
Holden, P., Keene, D.R., Lunstrum, G.P., Bächinger, H.P., Horton, W.A., 2005. Secretion of cartilage oligomeric matrix protein is affected by the signal peptide. J Biol Chem 280, 17172–17179. https://doi.org/10.1074/jbc.M411716200
Hollien, J., Lin, J.H., Li, H., Stevens, N., Walter, P., Weissman, J.S., 2009. Regulated Ire1-dependent decay of messenger RNAs in mammalian cells. J Cell Biol 186, 323–331. https://doi.org/10.1083/jcb.200903014
Horiuchi, K., Tohmonda, T., Morioka, H., 2016. The unfolded protein response in skeletal development and homeostasis. Cell Mol Life Sci 73, 2851–2869. https://doi.org/10.1007/s00018-016-2178-1
Horkay, F., Basser, P.J., Hecht, A.-M., Geissler, E., 2017. Structure and Properties of Cartilage Proteoglycans. Macromol Symp 372, 43–50. https://doi.org/10.1002/masy.201700014
Horvath, S., Raj, K., 2018. DNA methylation-based biomarkers and the epigenetic clock theory of ageing. Nature Reviews Genetics 19, 371. https://doi.org/10.1038/s41576-018-0004-3
Hosseini Far, H., Patria, Y.N., Motazedian, A., Elefanty, A.G., Stanley, E.G., Lamandé, S.R., Bateman, J.F., 2019. Generation of a heterozygous COL1A1 (c.3969_3970insT) osteogenesis imperfecta mutation human iPSC line, MCRIi001-A-1, using CRISPR/Cas9 editing. Stem Cell Research 37, 101449. https://doi.org/10.1016/j.scr.2019.101449
Howden, S., Hosseini Far, H., Motazedian, A., Elefanty, A.G., Stanley, E.G., Lamandé, S.R., Bateman, J.F., 2019. The use of simultaneous reprogramming and gene correction to generate an osteogenesis imperfecta patient COL1A1 c. 3936 G>T iPSC line and an isogenic control iPSC line. Stem Cell Research 38, 101453. https://doi.org/10.1016/j.scr.2019.101453

Hu, K., Olsen, B.R., 2017. Vascular endothelial growth factor control mechanisms in skeletal growth and repair. Developmental Dynamics 246, 227–234. https://doi.org/10.1002/dvdy.24463
Hughes, A., Oxford, A.E., Tawara, K., Jorcyk, C.L., Oxford, J.T., 2017. Endoplasmic Reticulum Stress and Unfolded Protein Response in Cartilage Pathophysiology; Contributing Factors to Apoptosis and Osteoarthritis. Int J Mol Sci 18. https://doi.org/10.3390/ijms18030665
Huybrechts, Y., Mortier, G., Boudin, E., Van Hul, W., 2020. WNT Signaling and Bone: Lessons From Skeletal Dysplasias and Disorders. Front Endocrinol (Lausanne) 11, 165. https://doi.org/10.3389/fendo.2020.00165
Hwang, C.T., Halper, J., 2021. Proteoglycans and Diseases of Soft Tissues, in: Halper, J. (Ed.), Progress in Heritable Soft Connective Tissue Diseases, Advances in Experimental Medicine and Biology. Springer International Publishing, Cham, pp. 127–138. https://doi.org/10.1007/978-3-030-80614-9_5
Ikegawa, S., Nakamura, K., Nagano, A., Haga, N., Nakamura, Y., 1997. Mutations in the N-terminal globular domain of the type X collagen gene (COL10A1) in patients with Schmid metaphyseal chondrodysplasia. Hum. Mutat. 9, 131–135. https://doi.org/10.1002/(SICI)1098-1004(1997)9:2<131::AID-HUMU5>3.0.CO;2-C
Ishida, K., Acharya, C., Christiansen, B.A., Yik, J.H.N., DiCesare, P.E., Haudenschild, D.R., 2013. Cartilage oligomeric matrix protein enhances osteogenesis by directly binding and activating bone morphogenetic protein-2. Bone 55, 23–35. https://doi.org/10.1016/j.bone.2013.03.007
Ishikawa, T., Kashima, M., Nagano, A.J., Ishikawa-Fujiwara, T., Kamei, Y., Todo, T., Mori, K., 2017. Unfolded protein response transducer IRE1-mediated signaling independent of XBP1 mRNA splicing is not required for growth and development of medaka fish. eLife 6, e26845. https://doi.org/10.7554/eLife.26845
Ishikawa, T., Okada, T., Ishikawa-Fujiwara, T., Todo, T., Kamei, Y., Shigenobu, S., Tanaka, M., Saito, T.L., Yoshimura, J., Morishita, S., Toyoda, A., Sakaki, Y., Taniguchi, Y., Takeda, S., Mori, K., 2013. ATF6α/β-mediated adjustment of ER chaperone levels is essential for development of the notochord in medaka fish. Mol Biol Cell 24, 1387–1395. https://doi.org/10.1091/mbc.E12-11-0830
Isidor, B., Lindenbaum, P., Pichon, O., Bézieau, S., Dina, C., Jacquemont, S., Martin-Coignard, D., Thauvin-Robinet, C., Le Merrer, M., Mandel, J.-L., David, A., Faivre, L., Cormier-Daire, V., Redon, R., Le Caignec, C., 2011. Truncating mutations in the last exon of NOTCH2 cause a rare skeletal disorder with osteoporosis. Nat Genet 43, 306–308. https://doi.org/10.1038/ng.778
Iwawaki, T., Akai, R., Kohno, K., 2010. IRE1α Disruption Causes Histological Abnormality of Exocrine Tissues, Increase of Blood Glucose Level, and Decrease of Serum Immunoglobulin Level. PLoS One 5, e13052. https://doi.org/10.1371/journal.pone.0013052
Jackson, G.C., Barker, F.S., Jakkula, E., Czarny-Ratajczak, M., Mäkitie, O., Cole, W.G., Wright, M.J., Smithson, S.F., Suri, M., Rogala, P., Mortier, G.R., Baldock, C., Wallace, A., Elles, R., Ala-Kokko, L., Briggs, M.D., 2004. Missense mutations in the beta strands of the single A-domain of matrilin-3 result in multiple epiphyseal dysplasia. J. Med. Genet. 41, 52–59.
Jackson, G.C., Mittaz-Crettol, L., Taylor, J.A., Mortier, G.R., Spranger, J., Zabel, B., Merrer, M.L., Cormier-Daire, V., Hall, C.M., Offiah, A., Wright, M.J., Savarirayan, R., Nishimura, G., Ramsden, S.C., Elles, R., Bonafe, L., Superti-

Furga, A., Unger, S., Zankl, A., Briggs, M.D., 2012. Pseudoachondroplasia and multiple epiphyseal dysplasia: A 7-year comprehensive analysis of the known disease genes identify novel and recurrent mutations and provides an accurate assessment of their relative contribution. Human Mutation 33, 144–157. https://doi.org/10.1002/humu.21611

Jacob, A.L., Smith, C., Partanen, J., Ornitz, D.M., 2006. Fibroblast growth factor receptor 1 signaling in the osteo-chondrogenic cell lineage regulates sequential steps of osteoblast maturation. Dev Biol 296, 315–328. https://doi.org/10.1016/j.ydbio.2006.05.031

Jamaludin, M.I., Wakabayashi, S., Taniguchi, M., Sasaki, K., Komori, R., Kawamura, H., Takase, H., Sakamoto, M., Yoshida, H., 2019. MGSE Regulates Crosstalk from the Mucin Pathway to the TFE3 Pathway of the Golgi Stress Response. Cell Struct Funct 44, 137–151. https://doi.org/10.1247/csf.19009

Jeradi, S., Hammerschmidt, M., 2016. Retinoic acid-induced premature osteoblast-to-preosteocyte transitioning has multiple effects on calvarial development. Development 143, 1205–1216. https://doi.org/10.1242/dev.129189

Jerram, S.T., Dang, M.N., Leslie, R.D., 2017. The Role of Epigenetics in Type 1 Diabetes. Curr. Diab. Rep. 17, 89. https://doi.org/10.1007/s11892-017-0916-x

Jia, W., Zou, X., Xu, Z., Bai, L., Shan, A., Li, Y., Shi, J., Yang, F., Ding, C., Narimatsu, H., Zhang, Y., 2021. Polypeptide N-acetylgalactosaminyltransferase 18 retains in endoplasmic reticulum depending on its luminal regions interacting with ER resident UGGT1, PLOD3 and LPCAT1. Glycobiology 31, 947–958. https://doi.org/10.1093/glycob/cwab031

Jin, L., Nonaka, Y., Miyakawa, S., Fujiwara, M., Nakamura, Y., 2016. Dual Therapeutic Action of a Neutralizing Anti-FGF2 Aptamer in Bone Disease and Bone Cancer Pain. Mol Ther 24, 1974–1986. https://doi.org/10.1038/mt.2016.158

Jobert, A.S., Zhang, P., Couvineau, A., Bonaventure, J., Roume, J., Le Merrer, M., Silve, C., 1998. Absence of functional receptors for parathyroid hormone and parathyroid hormone-related peptide in Blomstrand chondrodysplasia. J Clin Invest 102, 34–40. https://doi.org/10.1172/JCI2918

Johnson, K.J., Sanchez, H.N., Schoenbrunner, N., 2019. Defining response to TNF-inhibitors in rheumatoid arthritis: the negative impact of anti-TNF cycling and the need for a personalized medicine approach to identify primary non-responders. Clin Rheumatol 38, 2967–2976. https://doi.org/10.1007/s10067-019-04684-1

Jones, P.A., 2012. Functions of DNA methylation: islands, start sites, gene bodies and beyond. Nat Rev Genet 13, 484–492. https://doi.org/10.1038/nrg3230

Julien, L.-A., Carriere, A., Moreau, J., Roux, P.P., 2010. mTORC1-activated S6K1 phosphorylates Rictor on threonine 1135 and regulates mTORC2 signaling. Mol Cell Biol 30, 908–921. https://doi.org/10.1128/MCB.00601-09

Kannu, P., Bateman, J., Savarirayan, R., 2012. Clinical phenotypes associated with type II collagen mutations. J Paediatr Child Health 48, E38-43. https://doi.org/10.1111/j.1440-1754.2010.01979.x

Karaplis, A.C., Luz, A., Glowacki, J., Bronson, R.T., Tybulewicz, V.L., Kronenberg, H.M., Mulligan, R.C., 1994. Lethal skeletal dysplasia from targeted disruption of the parathyroid hormone-related peptide gene. Genes Dev 8, 277–289. https://doi.org/10.1101/gad.8.3.277

Kars, M., Yang, L., Gregor, M.F., Mohammed, B.S., Pietka, T.A., Finck, B.N., Patterson, B.W., Horton, J.D., Mittendorfer, B., Hotamisligil, G.S., Klein, S., 2010. Tauroursodeoxycholic Acid May Improve Liver and Muscle but Not Adipose Tissue Insulin Sensitivity in Obese Men and Women. Diabetes 59, 1899–1905. https://doi.org/10.2337/db10-0308

Karsenty, G., Kronenberg, H.M., Settembre, C., 2009. Genetic Control of Bone Formation. Annual Review of Cell and Developmental Biology 25, 629–648. https://doi.org/10.1146/annurev.cellbio.042308.113308

Kawai, S., Yoshitomi, H., Sunaga, J., Alev, C., Nagata, S., Nishio, M., Hada, M., Koyama, Y., Uemura, M., Sekiguchi, K., Maekawa, H., Ikeya, M., Tamaki, S., Jin, Y., Harada, Y., Fukiage, K., Adachi, T., Matsuda, S., Toguchida, J., 2019. In vitro bone-like nodules generated from patient-derived iPSCs recapitulate pathological bone phenotypes. Nat Biomed Eng 3, 558–570. https://doi.org/10.1038/s41551-019-0410-7

Khan, S.A., Joyce, J., Tsuda, T., 2012. Quantification of active and total transforming growth factor-β levels in serum and solid organ tissues by bioassay. BMC Research Notes 5, 636. https://doi.org/10.1186/1756-0500-5-636

Kim, D., Paggi, J.M., Park, C., Bennett, C., Salzberg, S.L., 2019. Graph-based genome alignment and genotyping with HISAT2 and HISAT-genotype. Nat Biotechnol 37, 907–915. https://doi.org/10.1038/s41587-019-0201-4

Kim, J., Kundu, M., Viollet, B., Guan, K.-L., 2011. AMPK and mTOR regulate autophagy through direct phosphorylation of Ulk1. Nat Cell Biol 13, 132–141. https://doi.org/10.1038/ncb2152

Kim, M., Erickson, I.E., Huang, A.H., Garrity, S.T., Mauck, R.L., Steinberg, D.R., 2018. Donor Variation and Optimization of Human Mesenchymal Stem Cell Chondrogenesis in Hyaluronic Acid. Tissue Eng Part A 24, 1693–1703. https://doi.org/10.1089/ten.tea.2017.0520

Kim, M.-J., Son, M.J., Son, M.-Y., Seol, B., Kim, J., Park, J., Kim, J.H., Kim, Y.-H., Park, S.A., Lee, C.-H., Lee, K.-S., Han, Y.-M., Chang, J.-S., Cho, Y.S., 2011. Generation of human induced pluripotent stem cells from osteoarthritis patient-derived synovial cells. Arthritis Rheum. 63, 3010–3021. https://doi.org/10.1002/art.30488

Kim, S.-H., Turnbull, J., Guimond, S., 2011. Extracellular matrix and cell signalling: the dynamic cooperation of integrin, proteoglycan and growth factor receptor. J. Endocrinol. 209, 139–151. https://doi.org/10.1530/JOE-10-0377

Klatt, A.R., Becker, A.-K.A., Neacsu, C.D., Paulsson, M., Wagener, R., 2011. The matrilins: modulators of extracellular matrix assembly. Int. J. Biochem. Cell Biol. 43, 320–330. https://doi.org/10.1016/j.biocel.2010.12.010

Knudson, C.B., Knudson, W., 2001. Cartilage proteoglycans. Semin. Cell Dev. Biol. 12, 69–78. https://doi.org/10.1006/scdb.2000.0243

Ko, Y., Kobbe, B., Nicolae, C., Miosge, N., Paulsson, M., Wagener, R., Aszódi, A., 2004. Matrilin-3 is dispensable for mouse skeletal growth and development. Mol. Cell. Biol. 24, 1691–1699.

Kobayashi, N., Shinagawa, S., Nagata, T., Shimada, K., Shibata, N., Ohnuma, T., Kasanuki, K., Arai, H., Yamada, H., Nakayama, K., Kondo, K., 2016. Development of Biomarkers Based on DNA Methylation in the NCAPH2/LMF2 Promoter Region for Diagnosis of Alzheimer's Disease and Amnesic Mild Cognitive Impairment. PLOS ONE 11, e0146449. https://doi.org/10.1371/journal.pone.0146449

Kobayashi, N., Shinagawa, S., Niimura, H., Kida, H., Nagata, T., Tagai, K., Shimada, K., Oka, N., Shikimoto, R., Noda, Y., Nakajima, S., Mimura, M., Shigeta, M., Kondo, K., 2020. Increased blood COASY DNA methylation levels a potential biomarker for early pathology of Alzheimer's disease. Sci Rep 10, 12217. https://doi.org/10.1038/s41598-020-69248-9

Kokame, K., Kato, H., Miyata, T., 2001. Identification of ERSE-II, a new cis-acting element responsible for the ATF6-dependent mammalian unfolded protein response. J. Biol. Chem. 276, 9199–9205. https://doi.org/10.1074/jbc.M010486200

Komla-Ebri, D., Dambroise, E., Kramer, I., Benoist-Lasselin, C., Kaci, N., Le Gall, C., Martin, L., Busca, P., Barbault, F., Graus-Porta, D., Munnich, A., Kneissel, M., Di Rocco, F., Biosse-Duplan, M., Legeai-Mallet, L., 2016. Tyrosine kinase inhibitor NVP-BGJ398 functionally improves FGFR3-related dwarfism in mouse model. J Clin Invest 126, 1871–1884. https://doi.org/10.1172/JCI83926

Komori, T., Yagi, H., Nomura, S., Yamaguchi, A., Sasaki, K., Deguchi, K., Shimizu, Y., Bronson, R.T., Gao, Y.H., Inada, M., Sato, M., Okamoto, R., Kitamura, Y., Yoshiki, S., Kishimoto, T., 1997. Targeted disruption of Cbfa1 results in a complete lack of bone formation owing to maturational arrest of osteoblasts. Cell 89, 755–764. https://doi.org/10.1016/s0092-8674(00)80258-5

Korvala, J., Jüppner, H., Mäkitie, O., Sochett, E., Schnabel, D., Mora, S., Bartels, C.F., Warman, M.L., Deraska, D., Cole, W.G., Hartikka, H., Ala-Kokko, L., Männikkö, M., 2012. Mutations in LRP5 cause primary osteoporosis without features of OI by reducing Wnt signaling activity. BMC Med Genet 13, 26. https://doi.org/10.1186/1471-2350-13-26

Kracht, M., Müller-Ladner, U., Schmitz, M.L., 2020. Mutual regulation of metabolic processes and proinflammatory NF-κB signaling. Journal of Allergy and Clinical Immunology 146, 694–705. https://doi.org/10.1016/j.jaci.2020.07.027

Krakow, D., Rimoin, D.L., 2010. The skeletal dysplasias. Genetics in Medicine 12, 327–341. https://doi.org/10.1097/GIM.0b013e3181daae9b

Krejci, P., Krakow, D., Mekikian, P.B., Wilcox, W.R., 2007. Fibroblast growth factors 1, 2, 17, and 19 are the predominant FGF ligands expressed in human fetal growth plate cartilage. Pediatr Res 61, 267–272. https://doi.org/10.1203/pdr.0b013e318030d157

Krishnan, Y., Grodzinsky, A.J., 2018. Cartilage diseases. Matrix Biology, Extracellular Matrix-Driven Diseases 71–72, 51–69. https://doi.org/10.1016/j.matbio.2018.05.005

Kronenberg, H.M., Chung, U., 2001. The parathyroid hormone-related protein and Indian hedgehog feedback loop in the growth plate. Novartis Found. Symp. 232, 144–152; discussion 152-157.

Kuleshov, M.V., Jones, M.R., Rouillard, A.D., Fernandez, N.F., Duan, Q., Wang, Z., Koplev, S., Jenkins, S.L., Jagodnik, K.M., Lachmann, A., McDermott, M.G., Monteiro, C.D., Gundersen, G.W., Ma'ayan, A., 2016. Enrichr: a comprehensive gene set enrichment analysis web server 2016 update. Nucleic Acids Res 44, W90–W97. https://doi.org/10.1093/nar/gkw377

Kung, L.H.W., Mullan, L., Soul, J., Wang, P., Mori, K., Bateman, J.F., Briggs, M.D., Boot-Handford, R.P., 2019. Cartilage endoplasmic reticulum stress may influence the onset but not the progression of experimental osteoarthritis. Arthritis Res Ther 21. https://doi.org/10.1186/s13075-019-1988-6

Kung, L.H.W., Rajpar, M.H., Briggs, M.D., Boot-Handford, R.P., 2012. Hypertrophic chondrocytes have a limited capacity to cope with increases in endoplasmic

reticulum stress without triggering the unfolded protein response. J. Histochem. Cytochem. 60, 734–748. https://doi.org/10.1369/0022155412458436
Kung, L.H.W., Rajpar, M.H., Preziosi, R., Briggs, M.D., Boot-Handford, R.P., 2015. Increased classical endoplasmic reticulum stress is sufficient to reduce chondrocyte proliferation rate in the growth plate and decrease bone growth. PLoS ONE 10, e0117016. https://doi.org/10.1371/journal.pone.0117016
Kunova Bosakova, M., Nita, A., Gregor, T., Varecha, M., Gudernova, I., Fafilek, B., Barta, T., Basheer, N., Abraham, S.P., Balek, L., Tomanova, M., Fialova Kucerova, J., Bosak, J., Potesil, D., Zieba, J., Song, J., Konik, P., Park, S., Duran, I., Zdrahal, Z., Smajs, D., Jansen, G., Fu, Z., Ko, H.W., Hampl, A., Trantirek, L., Krakow, D., Krejci, P., 2019. Fibroblast growth factor receptor influences primary cilium length through an interaction with intestinal cell kinase. Proceedings of the National Academy of Sciences 116, 4316–4325. https://doi.org/10.1073/pnas.1800338116
Kurtishi, A., Rosen, B., Patil, K.S., Alves, G.W., Møller, S.G., 2019. Cellular Proteostasis in Neurodegeneration. Mol Neurobiol 56, 3676–3689. https://doi.org/10.1007/s12035-018-1334-z
Kwan, K.M., Pang, M.K.M., Zhou, S., Cowan, S.K., Kong, R.Y.C., Pfordte, T., Olsen, B.R., Sillence, D.O., Tam, P.P.L., Cheah, K.S.E., 1997. Abnormal Compartmentalization of Cartilage Matrix Components in Mice Lacking Collagen X: Implications for Function. J Cell Biol 136, 459–471.
Kwee, M.L., Balemans, W., Cleiren, E., Gille, J.J.P., Van Der Blij, F., Sepers, J.M., Van Hul, W., 2005. An autosomal dominant high bone mass phenotype in association with craniosynostosis in an extended family is caused by an LRP5 missense mutation. J Bone Miner Res 20, 1254–1260. https://doi.org/10.1359/JBMR.050303
LaCroix, A.J., Stabley, D., Sahraoui, R., Adam, M.P., Mehaffey, M., Kernan, K., Myers, C.T., Fagerstrom, C., Anadiotis, G., Akkari, Y.M., Robbins, K.M., Gripp, K.W., Baratela, W.A.R., Bober, M.B., Duker, A.L., Doherty, D., Dempsey, J.C., Miller, D.G., Kircher, M., Bamshad, M.J., Nickerson, D.A., University of Washington Center for Mendelian Genomics, Mefford, H.C., Sol-Church, K., 2019. GGC Repeat Expansion and Exon 1 Methylation of XYLT1 Is a Common Pathogenic Variant in Baratela-Scott Syndrome. Am J Hum Genet 104, 35–44. https://doi.org/10.1016/j.ajhg.2018.11.005
Lanske, B., Karaplis, A.C., Lee, K., Luz, A., Vortkamp, A., Pirro, A., Karperien, M., Defize, L.H., Ho, C., Mulligan, R.C., Abou-Samra, A.B., Jüppner, H., Segre, G.V., Kronenberg, H.M., 1996. PTH/PTHrP receptor in early development and Indian hedgehog-regulated bone growth. Science 273, 663–666.
Law, C.W., Chen, Y., Shi, W., Smyth, G.K., 2014. voom: precision weights unlock linear model analysis tools for RNA-seq read counts. Genome Biol 15, R29. https://doi.org/10.1186/gb-2014-15-2-r29
Lawler, P.R., Lawler, J., 2012. Molecular basis for the regulation of angiogenesis by thrombospondin-1 and -2. Cold Spring Harb Perspect Med 2, a006627. https://doi.org/10.1101/cshperspect.a006627
Lebeaupin, C., Yong, J., Kaufman, R.J., 2020. The Impact of the ER Unfolded Protein Response on Cancer Initiation and Progression: Therapeutic Implications. Adv Exp Med Biol 1243, 113–131. https://doi.org/10.1007/978-3-030-40204-4_8

Legeai-Mallet, L., Savarirayan, R., 2020. Novel therapeutic approaches for the treatment of achondroplasia. Bone 141, 115579. https://doi.org/10.1016/j.bone.2020.115579

Lehmann-Werman, R., Neiman, D., Zemmour, H., Moss, J., Magenheim, J., Vaknin-Dembinsky, A., Rubertsson, S., Nellgård, B., Blennow, K., Zetterberg, H., Spalding, K., Haller, M.J., Wasserfall, C.H., Schatz, D.A., Greenbaum, C.J., Dorrell, C., Grompe, M., Zick, A., Hubert, A., Maoz, M., Fendrich, V., Bartsch, D.K., Golan, T., Ben Sasson, S.A., Zamir, G., Razin, A., Cedar, H., Shapiro, A.M.J., Glaser, B., Shemer, R., Dor, Y., 2016. Identification of tissue-specific cell death using methylation patterns of circulating DNA. Proc Natl Acad Sci U S A 113, E1826–E1834. https://doi.org/10.1073/pnas.1519286113

Leighton, M.P., Nundlall, S., Starborg, T., Meadows, R.S., Suleman, F., Knowles, L., Wagener, R., Thornton, D.J., Kadler, K.E., Boot-Handford, R.P., Briggs, M.D., 2007. Decreased chondrocyte proliferation and dysregulated apoptosis in the cartilage growth plate are key features of a murine model of epiphyseal dysplasia caused by a matn3 mutation. Hum Mol Genet 16, 1728–1741. https://doi.org/10.1093/hmg/ddm121

Li, M., Baumeister, P., Roy, B., Phan, T., Foti, D., Luo, S., Lee, A.S., 2000. ATF6 as a transcription activator of the endoplasmic reticulum stress element: thapsigargin stress-induced changes and synergistic interactions with NF-Y and YY1. Mol Cell Biol 20, 5096–5106. https://doi.org/10.1128/MCB.20.14.5096-5106.2000

Li, P., Fleischhauer, L., Nicolae, C., Prein, C., Farkas, Z., Saller, M.M., Prall, W.C., Wagener, R., Heilig, J., Niehoff, A., Clausen-Schaumann, H., Alberton, P., Aszodi, A., 2020. Mice Lacking the Matrilin Family of Extracellular Matrix Proteins Develop Mild Skeletal Abnormalities and Are Susceptible to Age-Associated Osteoarthritis. Int J Mol Sci 21, E666. https://doi.org/10.3390/ijms21020666

Li, R.C., Wong, M.Y., DiChiara, A.S., Hosseini, A.S., Shoulders, M.D., 2021. Collagen's enigmatic, highly conserved N-glycan has an essential proteostatic function. Proc Natl Acad Sci U S A 118, e2026608118. https://doi.org/10.1073/pnas.2026608118

Li, X., Wang, J., Li, W., Xu, Y., Shao, D., Xie, Y., Xie, W., Kubota, T., Narimatsu, H., Zhang, Y., 2012. Characterization of ppGalNAc-T18, a member of the vertebrate-specific Y subfamily of UDP-N-acetyl-α-D-galactosamine:polypeptide N-acetylgalactosaminyltransferases. Glycobiology 22, 602–615. https://doi.org/10.1093/glycob/cwr179

Li, Y.-H., Tardif, G., Hum, D., Kapoor, M., Fahmi, H., Pelletier, J.-P., Martel-Pelletier, J., 2016. The unfolded protein response genes in human osteoarthritic chondrocytes: PERK emerges as a potential therapeutic target. Arthritis Res Ther 18. https://doi.org/10.1186/s13075-016-1070-6

Liang, G., Lian, C., Huang, Di, Gao, W., Liang, A., Peng, Y., Ye, W., Wu, Z., Su, P., Huang, Dongsheng, 2014. Endoplasmic reticulum stress-unfolding protein response-apoptosis cascade causes chondrodysplasia in a col2a1 p.Gly1170Ser mutated mouse model. PLoS One 9, e86894. https://doi.org/10.1371/journal.pone.0086894

Liao, Y., Smyth, G.K., Shi, W., 2014. featureCounts: an efficient general purpose program for assigning sequence reads to genomic features. Bioinformatics 30, 923–930. https://doi.org/10.1093/bioinformatics/btt656

Liu, Z., Xu, J., Colvin, J.S., Ornitz, D.M., 2002. Coordination of chondrogenesis and osteogenesis by fibroblast growth factor 18. Genes Dev 16, 859–869. https://doi.org/10.1101/gad.965602

Livak, K.J., Schmittgen, T.D., 2001. Analysis of Relative Gene Expression Data Using Real-Time Quantitative PCR and the 2−ΔΔCT Method. Methods 25, 402–408. https://doi.org/10.1006/meth.2001.1262

Loeser, R.F., 2014. Integrins and chondrocyte-matrix interactions in articular cartilage. Matrix Biol. 39, 11–16. https://doi.org/10.1016/j.matbio.2014.08.007

Loeys, B.L., Chen, J., Neptune, E.R., Judge, D.P., Podowski, M., Holm, T., Meyers, J., Leitch, C.C., Katsanis, N., Sharifi, N., Xu, F.L., Myers, L.A., Spevak, P.J., Cameron, D.E., De Backer, J., Hellemans, J., Chen, Y., Davis, E.C., Webb, C.L., Kress, W., Coucke, P., Rifkin, D.B., De Paepe, A.M., Dietz, H.C., 2005. A syndrome of altered cardiovascular, craniofacial, neurocognitive and skeletal development caused by mutations in TGFBR1 or TGFBR2. Nat Genet 37, 275–281. https://doi.org/10.1038/ng1511

Löffek, S., Schilling, O., Franzke, C.-W., 2011. Biological role of matrix metalloproteinases: a critical balance. European Respiratory Journal 38, 191–208. https://doi.org/10.1183/09031936.00146510

Lohiniva, J., Paassilta, P., Seppänen, U., Vierimaa, O., Kivirikko, S., Ala-Kokko, L., 2000. Splicing mutations in the COL3 domain of collagen IX cause multiple epiphyseal dysplasia. Am. J. Med. Genet. 90, 216–222.

Long, F., Ornitz, D.M., 2013. Development of the Endochondral Skeleton. Cold Spring Harb Perspect Biol 5. https://doi.org/10.1101/cshperspect.a008334

Lorget, F., Kaci, N., Peng, J., Benoist-Lasselin, C., Mugniery, E., Oppeneer, T., Wendt, D.J., Bell, S.M., Bullens, S., Bunting, S., Tsuruda, L.S., O'Neill, C.A., Di Rocco, F., Munnich, A., Legeai-Mallet, L., 2012. Evaluation of the therapeutic potential of a CNP analog in a Fgfr3 mouse model recapitulating achondroplasia. Am J Hum Genet 91, 1108–1114. https://doi.org/10.1016/j.ajhg.2012.10.014

Lu, Y., Ren, X., Wang, Y., Bardai, G., Sturm, M., Dai, Y., Riess, O., Zhang, Y., Li, H., Li, T., Zhai, N., Zhang, J., Rauch, F., Han, J., 2018. Novel WNT1 mutations in children with osteogenesis imperfecta: Clinical and functional characterization. Bone 114, 144–149. https://doi.org/10.1016/j.bone.2018.06.018

Lu, Z., Chiu, J., Lee, L.R., Schindeler, A., Jackson, M., Ramaswamy, Y., Dunstan, C.R., Hogg, P.J., Zreiqat, H., 2020. Reprogramming of human fibroblasts into osteoblasts by insulin-like growth factor-binding protein 7. Stem Cells Transl Med 9, 403–415. https://doi.org/10.1002/sctm.19-0281

Mackie, E.J., Ahmed, Y.A., Tatarczuch, L., Chen, K.-S., Mirams, M., 2008. Endochondral ossification: How cartilage is converted into bone in the developing skeleton. The International Journal of Biochemistry & Cell Biology 40, 46–62. https://doi.org/10.1016/j.biocel.2007.06.009

Mackie, E.J., Tatarczuch, L., Mirams, M., 2011. The skeleton: a multi-functional complex organ: the growth plate chondrocyte and endochondral ossification. J. Endocrinol. 211, 109–121. https://doi.org/10.1530/JOE-11-0048

Maddox, B.K., Keene, D.R., Sakai, L.Y., Charbonneau, N.L., Morris, N.P., Ridgway, C.C., Boswell, B.A., Sussman, M.D., Horton, W.A., Bächinger, H.P., Hecht, J.T., 1997. The Fate of Cartilage Oligomeric Matrix Protein Is Determined by the Cell Type in the Case of a Novel Mutation in Pseudoachondroplasia *. Journal of Biological Chemistry 272, 30993–30997. https://doi.org/10.1074/jbc.272.49.30993

Maeda, K., Kobayashi, Y., Koide, M., Uehara, S., Okamoto, M., Ishihara, A., Kayama, T., Saito, M., Marumo, K., 2019. The Regulation of Bone Metabolism and Disorders by Wnt Signaling. Int J Mol Sci 20, 5525. https://doi.org/10.3390/ijms20225525

Makareeva, E., Sun, G., Mirigian, L.S., Mertz, E.L., Vera, J.C., Espinoza, N.A., Yang, K., Chen, D., Klein, T.E., Byers, P.H., Leikin, S., 2018. Substitutions for arginine at position 780 in triple helical domain of the α1(I) chain alter folding of the type I procollagen molecule and cause osteogenesis imperfecta. PLoS One 13, e0200264. https://doi.org/10.1371/journal.pone.0200264

Mäkitie, O., Mortier, G.R., Czarny-Ratajczak, M., Wright, M.J., Suri, M., Rogala, P., Freund, M., Jackson, G.C., Jakkula, E., Ala-Kokko, L., Briggs, M.D., Cole, W.G., 2004. Clinical and radiographic findings in multiple epiphyseal dysplasia caused by MATN3 mutations: Description of 12 patients. American Journal of Medical Genetics Part A 125A, 278–284. https://doi.org/10.1002/ajmg.a.20486

Makrythanasis, P., Temtamy, S., Aglan, M.S., Otaify, G.A., Hamamy, H., Antonarakis, S.E., 2014. A novel homozygous mutation in FGFR3 causes tall stature, severe lateral tibial deviation, scoliosis, hearing impairment, camptodactyly, and arachnodactyly. Hum Mutat 35, 959–963. https://doi.org/10.1002/humu.22597

Maksimovic, J., Phipson, B., Oshlack, A., 2016. A cross-package Bioconductor workflow for analysing methylation array data. F1000Res 5, 1281. https://doi.org/10.12688/f1000research.8839.3

Maldonado-Montoro, M., Cañadas-Garre, M., González-Utrilla, A., Plaza-Plaza, J.C., Calleja-Hernández, M.Ÿ., 2016. Genetic and clinical biomarkers of tocilizumab response in patients with rheumatoid arthritis. Pharmacol Res 111, 264–271. https://doi.org/10.1016/j.phrs.2016.06.016

Maly, K., Andres Sastre, E., Farrell, E., Meurer, A., Zaucke, F., 2021. COMP and TSP-4: Functional Roles in Articular Cartilage and Relevance in Osteoarthritis. Int J Mol Sci 22, 2242. https://doi.org/10.3390/ijms22052242

Mann, H.H., Ozbek, S., Engel, J., Paulsson, M., Wagener, R., 2004. Interactions between the cartilage oligomeric matrix protein and matrilins. Implications for matrix assembly and the pathogenesis of chondrodysplasias. J. Biol. Chem. 279, 25294–25298. https://doi.org/10.1074/jbc.M403778200

Marciniak, S.J., Yun, C.Y., Oyadomari, S., Novoa, I., Zhang, Y., Jungreis, R., Nagata, K., Harding, H.P., Ron, D., 2004. CHOP induces death by promoting protein synthesis and oxidation in the stressed endoplasmic reticulum. Genes Dev 18, 3066–3077. https://doi.org/10.1101/gad.1250704

Marini, J.C., Forlino, A., Cabral, W.A., Barnes, A.M., San Antonio, J.D., Milgrom, S., Hyland, J.C., Körkkö, J., Prockop, D.J., De Paepe, A., Coucke, P., Symoens, S., Glorieux, F.H., Roughley, P.J., Lund, A.M., Kuurila-Svahn, K., Hartikka, H., Cohn, D.H., Krakow, D., Mottes, M., Schwarze, U., Chen, D., Yang, K., Kuslich, C., Troendle, J., Dalgleish, R., Byers, P.H., 2007. Consortium for osteogenesis imperfecta mutations in the helical domain of type I collagen: regions rich in lethal mutations align with collagen binding sites for integrins and proteoglycans. Hum. Mutat. 28, 209–221. https://doi.org/10.1002/humu.20429

Marshall, D.C., Lyman, S.K., McCauley, S., Kovalenko, M., Spangler, R., Liu, C., Lee, M., O'Sullivan, C., Barry-Hamilton, V., Ghermazien, H., Mikels-Vigdal, A., Garcia, C.A., Jorgensen, B., Velayo, A.C., Wang, R., Adamkewicz, J.I., Smith,

V., 2015. Selective Allosteric Inhibition of MMP9 Is Efficacious in Preclinical Models of Ulcerative Colitis and Colorectal Cancer. PLoS One 10, e0127063. https://doi.org/10.1371/journal.pone.0127063
Martin, L., Kaci, N., Benoist-Lasselin, C., Mondoloni, M., Decaudaveine, S., Estibals, V., Cornille, M., Loisay, L., Flipo, J., Demuynck, B., de la Luz Cádiz-Gurrea, M., Barbault, F., Fernández-Arroyo, S., Schibler, L., Segura-Carretero, A., Dambroise, E., Legeai-Mallet, L., 2022. Theobroma cacao improves bone growth by modulating defective ciliogenesis in a mouse model of achondroplasia. Bone Res 10, 1–13. https://doi.org/10.1038/s41413-021-00177-7
Martin, M., 2011. Cutadapt removes adapter sequences from high-throughput sequencing reads. EMBnet.journal 17, 10–12. https://doi.org/10.14806/ej.17.1.200
Martinez-Garcia, M., Garcia-Canto, E., Fenollar-Cortes, M., Aytes, A.P., Trujillo-Tiebas, M.J., 2016. Characterization of an acromesomelic dysplasia, Grebe type case: novel mutation affecting the recognition motif at the processing site of GDF5. J Bone Miner Metab 34, 599–603. https://doi.org/10.1007/s00774-015-0693-z
Mátés, L., Nicolae, C., Mörgelin, M., Deák, F., Kiss, I., Aszódi, A., 2004. Mice lacking the extracellular matrix adaptor protein matrilin-2 develop without obvious abnormalities. Matrix Biol 23, 195–204. https://doi.org/10.1016/j.matbio.2004.05.003
Matsuzaki, S., Hiratsuka, T., Taniguchi, M., Shingaki, K., Kubo, T., Kiya, K., Fujiwara, T., Kanazawa, S., Kanematsu, R., Maeda, T., Takamura, H., Yamada, K., Miyoshi, K., Hosokawa, K., Tohyama, M., Katayama, T., 2015. Physiological ER Stress Mediates the Differentiation of Fibroblasts. PLoS One 10, e0123578. https://doi.org/10.1371/journal.pone.0123578
Mauthe, M., Orhon, I., Rocchi, C., Zhou, X., Luhr, M., Hijlkema, K.-J., Coppes, R.P., Engedal, N., Mari, M., Reggiori, F., 2018. Chloroquine inhibits autophagic flux by decreasing autophagosome-lysosome fusion. Autophagy 14, 1435–1455. https://doi.org/10.1080/15548627.2018.1474314
MCDS-Therapy Project [WWW Document], 2022. . MCDS-Therapy Project | Fact Sheet. URL https://cordis.europa.eu/project/id/754825 (accessed 2.21.22).
mcds-therapy.eu, 2022. mcds-therapy.eu. MCDS Therapy. URL https://mcds-therapy.eu/mcds-therapy-project/ (accessed 2.21.22).
McGarry, A., Leinonen, M., Kieburtz, K., Geva, M., Olanow, C.W., Hayden, M., 2020. Effects of Pridopidine on Functional Capacity in Early-Stage Participants from the PRIDE-HD Study. J Huntingtons Dis 9, 371–380. https://doi.org/10.3233/JHD-200440
McLeod, C.M., Mauck, R.L., 2017. On the origin and impact of mesenchymal stem cell heterogeneity: New insights and emerging tools for single cell analysis. Eur Cell Mater 34, 217–231. https://doi.org/10.22203/eCM.v034a14
Mellgren, A.E.C., Bruland, O., Vedeler, A., Saraste, J., Schönheit, J., Bredrup, C., Knappskog, P.M., Rødahl, E., 2015. Development of Congenital Stromal Corneal Dystrophy Is Dependent on Export and Extracellular Deposition of Truncated Decorin. Investigative Ophthalmology & Visual Science 56, 2909–2915. https://doi.org/10.1167/iovs.14-16014
Melrose, J., Shu, C., Whitelock, J.M., Lord, M.S., 2016. The cartilage extracellular matrix as a transient developmental scaffold for growth plate maturation. Matrix Biology 52–54, 363–383. https://doi.org/10.1016/j.matbio.2016.01.008

Mirigian, L.S., Makareeva, E., Mertz, E.L., Omari, S., Roberts-Pilgrim, A.M., Oestreich, A.K., Phillips, C.L., Leikin, S., 2016. Osteoblast malfunction caused by cell stress response to procollagen misfolding in α2(I)-G610C mouse model of osteogenesis imperfecta. J Bone Miner Res 31, 1608–1616. https://doi.org/10.1002/jbmr.2824

Mohlin, S., Hamidian, A., von Stedingk, K., Bridges, E., Wigerup, C., Bexell, D., Påhlman, S., 2015. PI3K-mTORC2 but not PI3K-mTORC1 regulates transcription of HIF2A/EPAS1 and vascularization in neuroblastoma. Cancer Res 75, 4617–4628. https://doi.org/10.1158/0008-5472.CAN-15-0708

Montibeller, L., de Belleroche, J., 2018. Amyotrophic lateral sclerosis (ALS) and Alzheimer's disease (AD) are characterised by differential activation of ER stress pathways: focus on UPR target genes. Cell Stress Chaperones 23, 897–912. https://doi.org/10.1007/s12192-018-0897-y

Morgan, M.A.J., Shilatifard, A., 2020. Reevaluating the roles of histone-modifying enzymes and their associated chromatin modifications in transcriptional regulation. Nat Genet 52, 1271–1281. https://doi.org/10.1038/s41588-020-00736-4

Mori, K., Sant, A., Kohno, K., Normington, K., Gething, M.J., Sambrook, J.F., 1992. A 22 bp cis-acting element is necessary and sufficient for the induction of the yeast KAR2 (BiP) gene by unfolded proteins. EMBO J. 11, 2583–2593.

Mori, T., Hayashi, T., Hayashi, E., Su, T.-P., 2013. Sigma-1 Receptor Chaperone at the ER-Mitochondrion Interface Mediates the Mitochondrion-ER-Nucleus Signaling for Cellular Survival. PLoS One 8, e76941. https://doi.org/10.1371/journal.pone.0076941

Morishima, N., Nakanishi, K., Takenouchi, H., Shibata, T., Yasuhiko, Y., 2002. An endoplasmic reticulum stress-specific caspase cascade in apoptosis. Cytochrome c-independent activation of caspase-9 by caspase-12. J. Biol. Chem. 277, 34287–34294. https://doi.org/10.1074/jbc.M204973200

Mortier, G.R., Chapman, K., Leroy, J.L., Briggs, M.D., 2001. Clinical and radiographic features of multiple epiphyseal dysplasia not linked to the COMP or type IX collagen genes. Eur. J. Hum. Genet. 9, 606–612. https://doi.org/10.1038/sj.ejhg.5200690

Mortier, G.R., Cohn, D.H., Cormier-Daire, V., Hall, C., Krakow, D., Mundlos, S., Nishimura, G., Robertson, S., Sangiorgi, L., Savarirayan, R., Sillence, D., Superti-Furga, A., Unger, S., Warman, M.L., 2019. Nosology and classification of genetic skeletal disorders: 2019 revision. American Journal of Medical Genetics Part A 179, 2393–2419. https://doi.org/10.1002/ajmg.a.61366

Mukherjee, A., Hidvegi, T., Araya, P., Ewing, M., Stolz, D.B., Perlmutter, D.H., 2019. NFκB mitigates the pathological effects of misfolded α1-antitrypsin by activating autophagy and an integrated program of proteostasis mechanisms. Cell Death Differ 26, 455–469. https://doi.org/10.1038/s41418-018-0130-7

Mullan, L.A., Mularczyk, E.J., Kung, L.H., Forouhan, M., Wragg, J.M., Goodacre, R., Bateman, J.F., Swanton, E., Briggs, M.D., Boot-Handford, R.P., 2017. Increased intracellular proteolysis reduces disease severity in an ER stress-associated dwarfism. J. Clin. Invest. 127, 3861–3865. https://doi.org/10.1172/JCI93094

Multhaupt, H.A.B., Couchman, J.R., 2012. Heparan Sulfate Biosynthesis. J Histochem Cytochem 60, 908–915. https://doi.org/10.1369/0022155412460056

Mundlos, S., Otto, F., Mundlos, C., Mulliken, J.B., Aylsworth, A.S., Albright, S., Lindhout, D., Cole, W.G., Henn, W., Knoll, J.H., Owen, M.J., Mertelsmann, R., Zabel, B.U., Olsen, B.R., 1997. Mutations involving the transcription factor CBFA1 cause cleidocranial dysplasia. Cell 89, 773–779. https://doi.org/10.1016/s0092-8674(00)80260-3

Muppala, S., Xiao, R., Krukovets, I., Verbovetsky, D., Yendamuri, R., Habib, N., Raman, P., Plow, E., Stenina-Adognravi, O., 2017. Thrombospondin-4 mediates TGF-β-induced angiogenesis. Oncogene 36, 5189–5198. https://doi.org/10.1038/onc.2017.140

Muragaki, Y., Mariman, E.C., van Beersum, S.E., Perälä, M., van Mourik, J.B., Warman, M.L., Olsen, B.R., Hamel, B.C., 1996. A mutation in the gene encoding the alpha 2 chain of the fibril-associated collagen IX, COL9A2, causes multiple epiphyseal dysplasia (EDM2). Nat. Genet. 12, 103–105. https://doi.org/10.1038/ng0196-103

Murphy, J.M., Heinegård, D., McIntosh, A., Sterchi, D., Barry, F.P., 1999. Distribution of cartilage molecules in the developing mouse joint. Matrix Biology 18, 487–497. https://doi.org/10.1016/S0945-053X(99)00042-6

Newton, G., Weremowicz, S., Morton, C.C., Copeland, N.G., Gilbert, D.J., Jenkins, N.A., Lawler, J., 1994. Characterization of human and mouse cartilage oligomeric matrix protein. Genomics 24, 435–439. https://doi.org/10.1006/geno.1994.1649

Nilsson, E., Ling, C., 2017. DNA methylation links genetics, fetal environment, and an unhealthy lifestyle to the development of type 2 diabetes. Clin Epigenetics 9, 105. https://doi.org/10.1186/s13148-017-0399-2

Nishimori, S., Lai, F., Shiraishi, M., Kobayashi, T., Kozhemyakina, E., Yao, T.-P., Lassar, A.B., Kronenberg, H.M., 2019. PTHrP targets HDAC4 and HDAC5 to repress chondrocyte hypertrophy. JCI Insight 4. https://doi.org/10.1172/jci.insight.97903

Nixon, T.R.W., Alexander, P., Richards, A., McNinch, A., Bearcroft, P.W.P., Cobben, J., Snead, M.P., 2019. Homozygous Type IX collagen variants (COL9A1, COL9A2, and COL9A3) causing recessive Stickler syndrome-Expanding the phenotype. Am J Med Genet A 179, 1498–1506. https://doi.org/10.1002/ajmg.a.61191

Noonan, K.J., Hunziker, E.B., Nessler, J., Buckwalter, J.A., 1998. Changes in cell, matrix compartment, and fibrillar collagen volumes between growth-plate zones. J. Orthop. Res. 16, 500–508. https://doi.org/10.1002/jor.1100160416

Nüchel, J., Tauber, M., Nolte, J.L., Mörgelin, M., Türk, C., Eckes, B., Demetriades, C., Plomann, M., 2021. An mTORC1-GRASP55 signaling axis controls unconventional secretion to reshape the extracellular proteome upon stress. Molecular Cell 81, 3275-3293.e12. https://doi.org/10.1016/j.molcel.2021.06.017

Nundlall, S., Rajpar, M.H., Bell, P.A., Clowes, C., Zeeff, L.A.H., Gardner, B., Thornton, D.J., Boot-Handford, R.P., Briggs, M.D., 2010. An unfolded protein response is the initial cellular response to the expression of mutant matrilin-3 in a mouse model of multiple epiphyseal dysplasia. Cell Stress Chaperones 15, 835–849. https://doi.org/10.1007/s12192-010-0193-y

Nygaard, G., Firestein, G.S., 2020. Restoring synovial homeostasis in rheumatoid arthritis by targeting fibroblast-like synoviocytes. Nat Rev Rheumatol 16, 316–333. https://doi.org/10.1038/s41584-020-0413-5

Oda, T., Elkahloun, A.G., Pike, B.L., Okajima, K., Krantz, I.D., Genin, A., Piccoli, D.A., Meltzer, P.S., Spinner, N.B., Collins, F.S., Chandrasekharappa, S.C., 1997. Mutations in the human Jagged1 gene are responsible for Alagille syndrome. Nat Genet 16, 235–242. https://doi.org/10.1038/ng0797-235

Oláhová, M., Veal, E.A., 2015. A peroxiredoxin, PRDX -2, is required for insulin secretion and insulin/ IIS -dependent regulation of stress resistance and longevity. Aging Cell 14, 558–568. https://doi.org/10.1111/acel.12321

Oldberg, A., Antonsson, P., Lindblom, K., Heinegård, D., 1992. COMP (cartilage oligomeric matrix protein) is structurally related to the thrombospondins. J Biol Chem 267, 22346–22350.

Omar, R., Malfait, F., Van Agtmael, T., 2021. Four decades in the making: Collagen III and mechanisms of vascular Ehlers Danlos Syndrome. Matrix Biol Plus 12, 100090. https://doi.org/10.1016/j.mbplus.2021.100090

Ornitz, D.M., Marie, P.J., 2019. Fibroblast growth factors in skeletal development. Curr Top Dev Biol 133, 195–234. https://doi.org/10.1016/bs.ctdb.2018.11.020

Ortega, N., Behonick, D., Stickens, D., Werb, Z., 2003. How Proteases Regulate Bone Morphogenesis. Annals of the New York Academy of Sciences 995, 109–116. https://doi.org/10.1111/j.1749-6632.2003.tb03214.x

Ortega, N., Behonick, D.J., Werb, Z., 2004. Matrix remodeling during endochondral ossification. Trends Cell Biol 14, 86–93. https://doi.org/10.1016/j.tcb.2003.12.003

Otteby, K.E., Holmquist, E., Saxne, T., Heinegård, D., Hesselstrand, R., Blom, A.M., 2013. Cartilage oligomeric matrix protein-induced complement activation in systemic sclerosis. Arthritis Research & Therapy 15, R215. https://doi.org/10.1186/ar4410

Otten, C., Hansen, U., Talke, A., Wagener, R., Paulsson, M., Zaucke, F., 2010. A matrilin-3 mutation associated with osteoarthritis does not affect collagen affinity but promotes the formation of wider cartilage collagen fibrils. Hum. Mutat. 31, 254–263. https://doi.org/10.1002/humu.21182

Paassilta, P., Lohiniva, J., Annunen, S., Bonaventure, J., Le Merrer, M., Pai, L., Ala-Kokko, L., 1999. COL9A3: A third locus for multiple epiphyseal dysplasia. Am. J. Hum. Genet. 64, 1036–1044. https://doi.org/10.1086/302328

Paganini, C., Gramegna Tota, C., Monti, L., Monti, I., Maurizi, A., Capulli, M., Bourmaud, M., Teti, A., Cohen-Solal, M., Villani, S., Forlino, A., Superti-Furga, A., Rossi, A., 2021. Improvement of the skeletal phenotype in a mouse model of diastrophic dysplasia after postnatal treatment with N-acetylcysteine. Biochemical Pharmacology 185, 114452. https://doi.org/10.1016/j.bcp.2021.114452

Paganoni, S., Hendrix, S., Dickson, S.P., Knowlton, N., Macklin, E.A., Berry, J.D., Elliott, M.A., Maiser, S., Karam, C., Caress, J.B., Owegi, M.A., Quick, A., Wymer, J., Goutman, S.A., Heitzman, D., Heiman-Patterson, T.D., Jackson, C.E., Quinn, C., Rothstein, J.D., Kasarskis, E.J., Katz, J., Jenkins, L., Ladha, S., Miller, T.M., Scelsa, S.N., Vu, T.H., Fournier, C.N., Glass, J.D., Johnson, K.M., Swenson, A., Goyal, N.A., Pattee, G.L., Andres, P.L., Babu, S., Chase, M., Dagostino, D., Hall, M., Kittle, G., Eydinov, M., McGovern, M., Ostrow, J., Pothier, L., Randall, R., Shefner, J.M., Sherman, A.V., St Pierre, M.E., Tustison, E., Vigneswaran, P., Walker, J., Yu, H., Chan, J., Wittes, J., Yu, Z., Cohen, J., Klee, J., Leslie, K., Tanzi, R.E., Gilbert, W., Yeramian, P.D., Schoenfeld, D., Cudkowicz, M.E., 2021. Long-term survival of participants in

the CENTAUR trial of sodium phenylbutyrate-taurursodiol in amyotrophic lateral sclerosis. Muscle Nerve 63, 31–39. https://doi.org/10.1002/mus.27091
Pakos-Zebrucka, K., Koryga, I., Mnich, K., Ljujic, M., Samali, A., Gorman, A.M., 2016. The integrated stress response. EMBO Rep 17, 1374–1395. https://doi.org/10.15252/embr.201642195
Panda, A., Gamanagatti, S., Jana, M., Gupta, A.K., 2014. Skeletal dysplasias: A radiographic approach and review of common non-lethal skeletal dysplasias. World J Radiol 6, 808–825. https://doi.org/10.4329/wjr.v6.i10.808
Panicker, L.M., Miller, D., Awad, O., Bose, V., Lun, Y., Park, T.S., Zambidis, E.T., Sgambato, J.A., Feldman, R.A., 2014. Gaucher iPSC-derived macrophages produce elevated levels of inflammatory mediators and serve as a new platform for therapeutic development. Stem Cells 32, 2338–2349. https://doi.org/10.1002/stem.1732
Panicker, L.M., Srikanth, M.P., Castro-Gomes, T., Miller, D., Andrews, N.W., Feldman, R.A., 2018. Gaucher disease iPSC-derived osteoblasts have developmental and lysosomal defects that impair bone matrix deposition. Hum Mol Genet 27, 811–822. https://doi.org/10.1093/hmg/ddx442
Papadakos, K.S., Bartoschek, M., Rodriguez, C., Gialeli, C., Jin, S.-B., Lendahl, U., Pietras, K., Blom, A.M., 2019. Cartilage Oligomeric Matrix Protein initiates cancer stem cells through activation of Jagged1-Notch3 signaling. Matrix Biol 81, 107–121. https://doi.org/10.1016/j.matbio.2018.11.007
Pardo, A., Selman, M., 2005. MMP-1: the elder of the family. Int J Biochem Cell Biol 37, 283–288. https://doi.org/10.1016/j.biocel.2004.06.017
Peng, Y., Cui, C., He, Yaoxi, Ouzhuluobu, Zhang, H., Yang, D., Zhang, Q., Bianbazhuoma, Yang, L., He, Yibo, Xiang, K., Zhang, X., Bhandari, S., Shi, P., Yangla, Dejiquzong, Baimakangzhuo, Duojizhuoma, Pan, Y., Cirenyangji, Baimayangji, Gonggalanzi, Bai, C., Bianba, Basang, Ciwangsangbu, Xu, S., Chen, H., Liu, S., Wu, T., Qi, X., Su, B., 2017. Down-Regulation of EPAS1 Transcription and Genetic Adaptation of Tibetans to High-Altitude Hypoxia. Molecular Biology and Evolution 34, 818–830. https://doi.org/10.1093/molbev/msw280
Pepin, M.G., Schwarze, U., Rice, K.M., Liu, M., Leistritz, D., Byers, P.H., 2014. Survival is affected by mutation type and molecular mechanism in vascular Ehlers–Danlos syndrome (EDS type IV). Genetics in Medicine 16, 881–888. https://doi.org/10.1038/gim.2014.72
Percival, C.J., Richtsmeier, J.T., 2013. Angiogenesis and Intramembranous Osteogenesis. Dev Dyn 242, 909–922. https://doi.org/10.1002/dvdy.23992
Person, A.D., Beiraghi, S., Sieben, C.M., Hermanson, S., Neumann, A.N., Robu, M.E., Schleiffarth, J.R., Billington, C.J., van Bokhoven, H., Hoogeboom, J.M., Mazzeu, J.F., Petryk, A., Schimmenti, L.A., Brunner, H.G., Ekker, S.C., Lohr, J.L., 2010. WNT5A mutations in patients with autosomal dominant Robinow syndrome. Dev Dyn 239, 327–337. https://doi.org/10.1002/dvdy.22156
Peters, T.J., Buckley, M.J., Statham, A.L., Pidsley, R., Samaras, K., V Lord, R., Clark, S.J., Molloy, P.L., 2015. De novo identification of differentially methylated regions in the human genome. Epigenetics & Chromatin 8, 6. https://doi.org/10.1186/1756-8935-8-6
Phipson, B., Maksimovic, J., Oshlack, A., 2016. missMethyl: an R package for analyzing data from Illumina's HumanMethylation450 platform. Bioinformatics 32, 286–288. https://doi.org/10.1093/bioinformatics/btv560

Pickard, A., Chang, J., Alachkar, N., Calverley, B., Garva, R., Arvan, P., Meng, Q.-J., Kadler, K.E., 2019. Preservation of circadian rhythms by the protein folding chaperone, BiP. FASEB J 33, 7479–7489. https://doi.org/10.1096/fj.201802366RR

Pickard, A., Garva, R., Adamson, A., Calverley, B., Hoyle, A., Hayward, C., Spiller, D., Lu, Y., Hodson, N., Swift, J., Bigger, B., Kadler, K., 2022. ER-Golgi and lysosomal pathways together drive fibrous tissue formation. https://doi.org/10.21203/rs.3.rs-1336021/v1

Pidsley, R., Zotenko, E., Peters, T.J., Lawrence, M.G., Risbridger, G.P., Molloy, P., Van Djik, S., Muhlhausler, B., Stirzaker, C., Clark, S.J., 2016. Critical evaluation of the Illumina MethylationEPIC BeadChip microarray for whole-genome DNA methylation profiling. Genome Biology 17, 208. https://doi.org/10.1186/s13059-016-1066-1

Pihlajamaa, T., Lankinen, H., Ylöstalo, J., Valmu, L., Jäälinoja, J., Zaucke, F., Spitznagel, L., Gösling, S., Puustinen, A., Mörgelin, M., Peränen, J., Maurer, P., Ala-Kokko, L., Kilpelaïnen, I., 2004. Characterization of recombinant amino-terminal NC4 domain of human collagen IX: interaction with glycosaminoglycans and cartilage oligomeric matrix protein. J. Biol. Chem. 279, 24265–24273. https://doi.org/10.1074/jbc.M402865200

Piróg, K.A., Dennis, E.P., Hartley, C.L., Jackson, R.M., Soul, J., Schwartz, J.-M., Bateman, J.F., Boot-Handford, R.P., Briggs, M.D., 2019. XBP1 signalling is essential for alleviating mutant protein aggregation in ER-stress related skeletal disease. PLoS Genet. 15, e1008215. https://doi.org/10.1371/journal.pgen.1008215

Piróg, K.A., Irman, A., Young, S., Halai, P., Bell, P.A., Boot-Handford, R.P., Briggs, M.D., 2014. Abnormal Chondrocyte Apoptosis in the Cartilage Growth Plate is Influenced by Genetic Background and Deletion of CHOP in a Targeted Mouse Model of Pseudoachondroplasia. PLoS One 9. https://doi.org/10.1371/journal.pone.0085145

Piróg, K.A., Jaka, O., Katakura, Y., Meadows, R.S., Kadler, K.E., Boot-Handford, R.P., Briggs, M.D., 2010. A mouse model offers novel insights into the myopathy and tendinopathy often associated with pseudoachondroplasia and multiple epiphyseal dysplasia. Hum Mol Genet 19, 52–64. https://doi.org/10.1093/hmg/ddp466

Piróg, K.A., Katakura, Y., Mironov, A., Briggs, M.D., 2013. Mild Myopathy Is Associated with COMP but Not MATN3 Mutations in Mouse Models of Genetic Skeletal Diseases. PLoS One 8, e82412. https://doi.org/10.1371/journal.pone.0082412

Piróg-Garcia, K.A., Meadows, R.S., Knowles, L., Heinegård, D., Thornton, D.J., Kadler, K.E., Boot-Handford, R.P., Briggs, M.D., 2007. Reduced cell proliferation and increased apoptosis are significant pathological mechanisms in a murine model of mild pseudoachondroplasia resulting from a mutation in the C-terminal domain of COMP. Hum Mol Genet 16, 2072–2088. https://doi.org/10.1093/hmg/ddm155

Posey, K.L., Coustry, F., Veerisetty, A.C., Hossain, M., Alcorn, J.L., Hecht, J.T., 2015. Antioxidant and anti-inflammatory agents mitigate pathology in a mouse model of pseudoachondroplasia. Hum Mol Genet 24, 3918–3928. https://doi.org/10.1093/hmg/ddv122

Posey, K.L., Coustry, F., Veerisetty, A.C., Hossain, M., Gattis, D., Booten, S., Alcorn, J.L., Seth, P.P., Hecht, J.T., 2017. Antisense Reduction of Mutant COMP

Reduces Growth Plate Chondrocyte Pathology. Molecular Therapy 25, 705–714. https://doi.org/10.1016/j.ymthe.2016.12.024
Posey, K.L., Coustry, F., Veerisetty, A.C., Hossain, M.G., Gambello, M.J., Hecht, J.T., 2019. Novel mTORC1 Mechanism Suggests Therapeutic Targets for COMPopathies. The American Journal of Pathology 189, 132–146. https://doi.org/10.1016/j.ajpath.2018.09.008
Posey, K.L., Coustry, F., Veerisetty, A.C., Liu, P., Alcorn, J.L., Hecht, J.T., 2012. Chop (Ddit3) Is Essential for D469del-COMP Retention and Cell Death in Chondrocytes in an Inducible Transgenic Mouse Model of Pseudoachondroplasia. Am J Pathol 180, 727–737. https://doi.org/10.1016/j.ajpath.2011.10.035
Posey, K.L., Veerisetty, A.C., Liu, P., Wang, H.R., Poindexter, B.J., Bick, R., Alcorn, J.L., Hecht, J.T., 2009. An Inducible Cartilage Oligomeric Matrix Protein Mouse Model Recapitulates Human Pseudoachondroplasia Phenotype. Am J Pathol 175, 1555–1563. https://doi.org/10.2353/ajpath.2009.090184
Prakash, K., Fournier, D., 2018. Evidence for the implication of the histone code in building the genome structure. Biosystems 164, 49–59. https://doi.org/10.1016/j.biosystems.2017.11.005
Pretemer, Y., Kawai, S., Nagata, S., Nishio, M., Watanabe, M., Tamaki, S., Alev, C., Yamanaka, Y., Xue, J.-Y., Wang, Z., Fukiage, K., Tsukanaka, M., Futami, T., Ikegawa, S., Toguchida, J., 2021. Differentiation of Hypertrophic Chondrocytes from Human iPSCs for the In Vitro Modeling of Chondrodysplasias. Stem Cell Reports 16, 610–625. https://doi.org/10.1016/j.stemcr.2021.01.014
Rabouille, C., 2017. Pathways of Unconventional Protein Secretion. Trends in Cell Biology, Special Issue: Membrane Biology 27, 230–240. https://doi.org/10.1016/j.tcb.2016.11.007
Rajpar, M.H., McDermott, B., Kung, L., Eardley, R., Knowles, L., Heeran, M., Thornton, D.J., Wilson, R., Bateman, J.F., Poulsom, R., Arvan, P., Kadler, K.E., Briggs, M.D., Boot-Handford, R.P., 2009. Targeted induction of endoplasmic reticulum stress induces cartilage pathology. PLoS Genet. 5, e1000691. https://doi.org/10.1371/journal.pgen.1000691
Rasheed, S., Nelson-Rees, W.A., Toth, E.M., Arnstein, P., Gardner, M.B., 1974. Characterization of a newly derived human sarcoma cell line (HT-1080). Cancer 33, 1027–1033. https://doi.org/10.1002/1097-0142(197404)33:4<1027::AID-CNCR2820330419>3.0.CO;2-Z
Ray, A., Bal, B.S., Ray, B.K., 2005. Transcriptional Induction of Matrix Metalloproteinase-9 in the Chondrocyte and Synoviocyte Cells Is Regulated via a Novel Mechanism: Evidence for Functional Cooperation between Serum Amyloid A-Activating Factor-1 and AP-1. The Journal of Immunology 175, 4039–4048. https://doi.org/10.4049/jimmunol.175.6.4039
Refinetti, P., Warren, D., Morgenthaler, S., Ekstrøm, P.O., 2017. Quantifying mitochondrial DNA copy number using robust regression to interpret real time PCR results. BMC Res Notes 10, 1–7. https://doi.org/10.1186/s13104-017-2913-1
Reilmann, R., McGarry, A., Grachev, I.D., Savola, J.-M., Borowsky, B., Eyal, E., Gross, N., Langbehn, D., Schubert, R., Wickenberg, A.T., Papapetropoulos, S., Hayden, M., Squitieri, F., Kieburtz, K., Landwehrmeyer, G.B., European Huntington's Disease Network, Huntington Study Group investigators, 2019. Safety and efficacy of pridopidine in patients with Huntington's disease

(PRIDE-HD): a phase 2, randomised, placebo-controlled, multicentre, dose-ranging study. Lancet Neurol 18, 165–176. https://doi.org/10.1016/S1474-4422(18)30391-0
Reponen, P., Sahlberg, C., Munaut, C., Thesleff, I., Tryggvason, K., 1994. High expression of 92-kD type IV collagenase (gelatinase B) in the osteoclast lineage during mouse development. J Cell Biol 124, 1091–1102. https://doi.org/10.1083/jcb.124.6.1091
Reynard, L.N., Bui, C., Canty-Laird, E.G., Young, D.A., Loughlin, J., 2011. Expression of the osteoarthritis-associated gene GDF5 is modulated epigenetically by DNA methylation. Hum Mol Genet 20, 3450–3460. https://doi.org/10.1093/hmg/ddr253
Reynard, L.N., Bui, C., Syddall, C.M., Loughlin, J., 2014. CpG methylation regulates allelic expression of GDF5 by modulating binding of SP1 and SP3 repressor proteins to the osteoarthritis susceptibility SNP rs143383. Hum Genet 133, 1059–1073. https://doi.org/10.1007/s00439-014-1447-z
Ricard-Blum, S., 2011. The Collagen Family. Cold Spring Harb Perspect Biol 3. https://doi.org/10.1101/cshperspect.a004978
Riessen, R., Fenchel, M., Chen, H., Axel, D.I., Karsch, K.R., Lawler, J., 2001. Cartilage oligomeric matrix protein (thrombospondin-5) is expressed by human vascular smooth muscle cells. Arterioscler Thromb Vasc Biol 21, 47–54. https://doi.org/10.1161/01.atv.21.1.47
Ritchie, M.E., Phipson, B., Wu, D., Hu, Y., Law, C.W., Shi, W., Smyth, G.K., 2015. limma powers differential expression analyses for RNA-sequencing and microarray studies. Nucleic Acids Research 43, e47. https://doi.org/10.1093/nar/gkv007
Roa, L.A., Bloemen, M., Carels, C.E.L., Wagener, F.A.D.T.G., Von den Hoff, J.W., 2019. Retinoic acid disrupts osteogenesis in pre-osteoblasts by down-regulating WNT signaling. The International Journal of Biochemistry & Cell Biology 116, 105597. https://doi.org/10.1016/j.biocel.2019.105597
Rohmann, E., Brunner, H.G., Kayserili, H., Uyguner, O., Nürnberg, G., Lew, E.D., Dobbie, A., Eswarakumar, V.P., Uzumcu, A., Ulubil-Emeroglu, M., Leroy, J.G., Li, Y., Becker, C., Lehnerdt, K., Cremers, C.W.R.J., Yüksel-Apak, M., Nürnberg, P., Kubisch, Christian, Kubisch, Chriütian, Schlessinger, J., van Bokhoven, H., Wollnik, B., 2006. Mutations in different components of FGF signaling in LADD syndrome. Nat Genet 38, 414–417. https://doi.org/10.1038/ng1757
Rosati, R., Horan, G.S., Pinero, G.J., Garofalo, S., Keene, D.R., Horton, W.A., Vuorio, E., de Crombrugghe, B., Behringer, R.R., 1994. Normal long bone growth and development in type X collagen-null mice. Nat. Genet. 8, 129–135. https://doi.org/10.1038/ng1094-129
Rosenberg, K., Olsson, H., Mörgelin, M., Heinegård, D., 1998. Cartilage oligomeric matrix protein shows high affinity zinc-dependent interaction with triple helical collagen. J. Biol. Chem. 273, 20397–20403.
Rossi, A., Superti-Furga, A., 2001. Mutations in the diastrophic dysplasia sulfate transporter (DTDST) gene (SLC26A2): 22 novel mutations, mutation review, associated skeletal phenotypes, and diagnostic relevance. Human Mutation 17, 159–171. https://doi.org/10.1002/humu.1
Roupakia, E., Markopoulos, G.S., Kolettas, E., 2018. IL-12-mediated transcriptional regulation of matrix metalloproteinases. Biosci Rep 38, BSR20171420. https://doi.org/10.1042/BSR20171420

Rousseau, F., Bonaventure, J., Legeai-Mallet, L., Pelet, A., Rozet, J.M., Maroteaux, P., Le Merrer, M., Munnich, A., 1994. Mutations in the gene encoding fibroblast growth factor receptor-3 in achondroplasia. Nature 371, 252–254. https://doi.org/10.1038/371252a0
RStudio Team, 2016. RStudio: Integrated Development for R. RStudio, Inc., Boston, MA.
Rys, J.P., Monteiro, D.A., Alliston, T., 2016. Mechanobiology of TGFβ signaling in the skeleton. Matrix Biol 52–54, 413–425. https://doi.org/10.1016/j.matbio.2016.02.002
Saal, H.M., Prows, C.A., Guerreiro, I., Donlin, M., Knudson, L., Sund, K.L., Chang, C.-F., Brugmann, S.A., Stottmann, R.W., 2015. A mutation in FRIZZLED2 impairs Wnt signaling and causes autosomal dominant omodysplasia. Hum Mol Genet 24, 3399–3409. https://doi.org/10.1093/hmg/ddv088
Safina, A., Ren, M.-Q., Vandette, E., Bakin, A.V., 2008. TAK1 is required for TGF-β1-mediated regulation of matrix metalloproteinase-9 and metastasis. Oncogene 27, 1198–1207. https://doi.org/10.1038/sj.onc.1210768
Sagara, Y., Inesi, G., 1991. Inhibition of the sarcoplasmic reticulum Ca2+ transport ATPase by thapsigargin at subnanomolar concentrations. J Biol Chem 266, 13503–13506.
Saito, A., Ochiai, K., Kondo, S., Tsumagari, K., Murakami, T., Cavener, D.R., Imaizumi, K., 2011. Endoplasmic Reticulum Stress Response Mediated by the PERK-eIF2α-ATF4 Pathway Is Involved in Osteoblast Differentiation Induced by BMP2. J Biol Chem 286, 4809–4818. https://doi.org/10.1074/jbc.M110.152900
Saito, T., Fukai, A., Mabuchi, A., Ikeda, T., Yano, F., Ohba, S., Nishida, N., Akune, T., Yoshimura, N., Nakagawa, T., Nakamura, K., Tokunaga, K., Chung, U., Kawaguchi, H., 2010. Transcriptional regulation of endochondral ossification by HIF-2α during skeletal growth and osteoarthritis development. Nat Med 16, 678–686. https://doi.org/10.1038/nm.2146
Sanchez-Mut, J.V., Heyn, H., Vidal, E., Moran, S., Sayols, S., Delgado-Morales, R., Schultz, M.D., Ansoleaga, B., Garcia-Esparcia, P., Pons-Espinal, M., de Lagran, M.M., Dopazo, J., Rabano, A., Avila, J., Dierssen, M., Lott, I., Ferrer, I., Ecker, J.R., Esteller, M., 2016. Human DNA methylomes of neurodegenerative diseases show common epigenomic patterns. Transl Psychiatry 6, e718. https://doi.org/10.1038/tp.2015.214
Santos, L.E., Ferreira, S.T., 2018. Crosstalk between endoplasmic reticulum stress and brain inflammation in Alzheimer's disease. Neuropharmacology, Metabolic Impairment as Risk Factors for Neurodegenerative Disorders 136, 350–360. https://doi.org/10.1016/j.neuropharm.2017.11.016
Sasarman, F., Maftei, C., Campeau, P.M., Brunel-Guitton, C., Mitchell, G.A., Allard, P., 2016. Biosynthesis of glycosaminoglycans: associated disorders and biochemical tests. J Inherit Metab Dis 39, 173–188. https://doi.org/10.1007/s10545-015-9903-z
Saxena, S., Cabuy, E., Caroni, P., 2009. A role for motoneuron subtype–selective ER stress in disease manifestations of FALS mice. Nat Neurosci 12, 627–636. https://doi.org/10.1038/nn.2297
Scheiber, A.L., Wilkinson, K.J., Suzuki, A., Enomoto-Iwamoto, M., Kaito, T., Cheah, K.S., Iwamoto, M., Leikin, S., Otsuru, S., 2022. 4PBA reduces growth deficiency in osteogenesis imperfecta by enhancing transition of hypertrophic

chondrocytes to osteoblasts. JCI Insight 7, e149636. https://doi.org/10.1172/jci.insight.149636
Scheuner, D., Kaufman, R.J., 2008. The unfolded protein response: a pathway that links insulin demand with beta-cell failure and diabetes. Endocr. Rev. 29, 317–333. https://doi.org/10.1210/er.2007-0039
Schindelin, J., Arganda-Carreras, I., Frise, E., Kaynig, V., Longair, M., Pietzsch, T., Preibisch, S., Rueden, C., Saalfeld, S., Schmid, B., Tinevez, J.-Y., White, D.J., Hartenstein, V., Eliceiri, K., Tomancak, P., Cardona, A., 2012. Fiji: an open-source platform for biological-image analysis. Nat Methods 9, 676–682. https://doi.org/10.1038/nmeth.2019
Schipani, E., Lanske, B., Hunzelman, J., Luz, A., Kovacs, C.S., Lee, K., Pirro, A., Kronenberg, H.M., Jüppner, H., 1997. Targeted expression of constitutively active receptors for parathyroid hormone and parathyroid hormone-related peptide delays endochondral bone formation and rescues mice that lack parathyroid hormone-related peptide. Proc Natl Acad Sci U S A 94, 13689–13694.
Schipani, E., Ryan, H.E., Didrickson, S., Kobayashi, T., Knight, M., Johnson, R.S., 2001. Hypoxia in cartilage: HIF-1α is essential for chondrocyte growth arrest and survival. Genes Dev 15, 2865–2876. https://doi.org/10.1101/gad.934301
Schmid, T.M., Linsenmayer, T.F., 1983. A short chain (pro)collagen from aged endochondral chondrocytes. Biochemical characterization. J. Biol. Chem. 258, 9504–9509.
Schmitz, M., Becker, A., Schmitz, A., Weirich, C., Paulsson, M., Zaucke, F., Dinser, R., 2006. Disruption of extracellular matrix structure may cause pseudoachondroplasia phenotypes in the absence of impaired cartilage oligomeric matrix protein secretion. J Biol Chem 281, 32587–32595. https://doi.org/10.1074/jbc.M601976200
Schmitz, M., Niehoff, A., Miosge, N., Smyth, N., Paulsson, M., Zaucke, F., 2008. Transgenic mice expressing D469Delta mutated cartilage oligomeric matrix protein (COMP) show growth plate abnormalities and sternal malformations. Matrix Biol 27, 67–85. https://doi.org/10.1016/j.matbio.2007.08.001
Schreml, J., Durmaz, B., Cogulu, O., Keupp, K., Beleggia, F., Pohl, E., Milz, E., Coker, M., Ucar, S.K., Nürnberg, G., Nürnberg, P., Kuhn, J., Ozkinay, F., 2014. The missing “link”: an autosomal recessive short stature syndrome caused by a hypofunctional XYLT1 mutation. Hum Genet 133, 29–39. https://doi.org/10.1007/s00439-013-1351-y
Schulz, J.-N., Nüchel, J., Niehoff, A., Bloch, W., Schönborn, K., Hayashi, S., Kamper, M., Brinckmann, J., Plomann, M., Paulsson, M., Krieg, T., Zaucke, F., Eckes, B., 2016. COMP-assisted collagen secretion--a novel intracellular function required for fibrosis. J. Cell. Sci. 129, 706–716. https://doi.org/10.1242/jcs.180216
Shaheen, A., 2018. Effect of the unfolded protein response on ER protein export: a potential new mechanism to relieve ER stress. Cell Stress Chaperones 23, 797–806. https://doi.org/10.1007/s12192-018-0905-2
Shan, A., Lu, J., Xu, Z., Li, X., Xu, Y., Li, W., Liu, F., Yang, F., Sato, T., Narimatsu, H., Zhang, Y., 2019. Polypeptide N-acetylgalactosaminyltransferase 18 non-catalytically regulates the ER homeostasis and O-glycosylation. Biochim Biophys Acta Gen Subj 1863, 870–882. https://doi.org/10.1016/j.bbagen.2019.01.009

Sharma, R.B., Landa-Galván, H.V., Alonso, L.C., 2021. Living Dangerously: Protective and Harmful ER Stress Responses in Pancreatic β-Cells. Diabetes 70, 2431–2443. https://doi.org/10.2337/dbi20-0033
Shi, Y., Vattem, K.M., Sood, R., An, J., Liang, J., Stramm, L., Wek, R.C., 1998. Identification and Characterization of Pancreatic Eukaryotic Initiation Factor 2 α-Subunit Kinase, PEK, Involved in Translational Control. Mol Cell Biol 18, 7499–7509.
Shiang, R., Thompson, L.M., Zhu, Y.Z., Church, D.M., Fielder, T.J., Bocian, M., Winokur, S.T., Wasmuth, J.J., 1994. Mutations in the transmembrane domain of FGFR3 cause the most common genetic form of dwarfism, achondroplasia. Cell 78, 335–342. https://doi.org/10.1016/0092-8674(94)90302-6
Shore, E.M., Xu, M., Feldman, G.J., Fenstermacher, D.A., Cho, T.-J., Choi, I.H., Connor, J.M., Delai, P., Glaser, D.L., LeMerrer, M., Morhart, R., Rogers, J.G., Smith, R., Triffitt, J.T., Urtizberea, J.A., Zasloff, M., Brown, M.A., Kaplan, F.S., 2006. A recurrent mutation in the BMP type I receptor ACVR1 causes inherited and sporadic fibrodysplasia ossificans progressiva. Nat Genet 38, 525–527. https://doi.org/10.1038/ng1783
Shyamasundar, L.G., Loganathan, L., Kumar, A., Selina, A., Madhuri, V., 2020. MATN3 Mutation Causing Spondyloepimetaphyseal Dysplasia. Indian J Pediatr 87, 227–228. https://doi.org/10.1007/s12098-019-03100-5
Siebel, C., Lendahl, U., 2017. Notch Signaling in Development, Tissue Homeostasis, and Disease. Physiol Rev 97, 1235–1294. https://doi.org/10.1152/physrev.00005.2017
Sim Choi, H., Woo Kim, J., Cha, Y., Kim, C., 2006. A Quantitative Nitroblue Tetrazolium Assay for Determining Intracellular Superoxide Anion Production in Phagocytic Cells. Journal of Immunoassay and Immunochemistry 27, 31–44. https://doi.org/10.1080/15321810500403722
Skillington, J., Choy, L., Derynck, R., 2002. Bone morphogenetic protein and retinoic acid signaling cooperate to induce osteoblast differentiation of preadipocytes. Journal of Cell Biology 159, 135–146. https://doi.org/10.1083/jcb.200204060
Smith, R.K.W., Zunino, L., Webbon, P.M., Heinegård, D., 1997. The distribution of Cartilage Oligomeric Matrix Protein (COMP) in tendon and its variation with tendon site, age and load. Matrix Biology 16, 255–271. https://doi.org/10.1016/S0945-053X(97)90014-7
Södersten, F., Ekman, S., Schmitz, M., Paulsson, M., Zaucke, F., 2006. Thrombospondin-4 and cartilage oligomeric matrix protein form heterooligomers in equine tendon. Connect Tissue Res 47, 85–91. https://doi.org/10.1080/03008200600584124
Sood, R., Porter, A.C., Ma, K., Quilliam, L.A., Wek, R.C., 2000. Pancreatic eukaryotic initiation factor-2alpha kinase (PEK) homologues in humans, Drosophila melanogaster and Caenorhabditis elegans that mediate translational control in response to endoplasmic reticulum stress. Biochem. J. 346 Pt 2, 281–293.
Spayde, E.C., Joshi, A.P., Wilcox, W.R., Briggs, M., Cohn, D.H., Olsen, B.R., 2000. Exon skipping mutation in the COL9A2 gene in a family with multiple epiphyseal dysplasia. Matrix Biology 19, 121–128. https://doi.org/10.1016/S0945-053X(00)00055-X
Stange, K., Désir, J., Kakar, N., Mueller, T.D., Budde, B.S., Gordon, C.T., Horn, D., Seemann, P., Borck, G., 2015. A hypomorphic BMPR1B mutation causes du

Pan acromesomelic dysplasia. Orphanet J Rare Dis 10, 84. https://doi.org/10.1186/s13023-015-0299-5
Steenport, M., Khan, K.M.F., Du, B., Barnhard, S.E., Dannenberg, A.J., Falcone, D.J., 2009. Matrix metalloproteinase (MMP)-1 and MMP-3 induce macrophage MMP-9: evidence for the role of TNF-alpha and cyclooxygenase-2. J Immunol 183, 8119–8127. https://doi.org/10.4049/jimmunol.0901925
Stickens, D., Behonick, D.J., Ortega, N., Heyer, B., Hartenstein, B., Yu, Y., Fosang, A.J., Schorpp-Kistner, M., Angel, P., Werb, Z., 2004. Altered endochondral bone development in matrix metalloproteinase 13-deficient mice. Development 131, 5883–5895. https://doi.org/10.1242/dev.01461
St-Jacques, B., Hammerschmidt, M., McMahon, A.P., 1999. Indian hedgehog signaling regulates proliferation and differentiation of chondrocytes and is essential for bone formation. Genes Dev. 13, 2072–2086.
Stricker, S., Fundele, R., Vortkamp, A., Mundlos, S., 2002. Role of Runx genes in chondrocyte differentiation. Dev Biol 245, 95–108. https://doi.org/10.1006/dbio.2002.0640
Su, W., Liu, G., Liu, X., Zhou, Y., Sun, Q., Zhen, G., Wang, X., Hu, Y., Gao, P., Demehri, S., Cao, X., Wan, M., 2020. Angiogenesis stimulated by elevated PDGF-BB in subchondral bone contributes to osteoarthritis development. JCI Insight 5. https://doi.org/10.1172/jci.insight.135446
Suleman, F., Gualeni, B., Gregson, H.J., Leighton, M.P., Piróg, K.A., Edwards, S., Holden, P., Boot-Handford, R.P., Briggs, M.D., 2012. A novel form of chondrocyte stress is triggered by a COMP mutation causing pseudoachondroplasia. Hum. Mutat. 33, 218–231. https://doi.org/10.1002/humu.21631
Sun, X., Liu, J., Crary, J.F., Malagelada, C., Sulzer, D., Greene, L.A., Levy, O.A., 2013. ATF4 Protects Against Neuronal Death in Cellular Parkinson's Disease Models by Maintaining Levels of Parkin. J. Neurosci. 33, 2398–2407. https://doi.org/10.1523/JNEUROSCI.2292-12.2013
Superti-Furga, A., Neumann, L., Riebel, T., Eich, G., Steinmann, B., Spranger, J., Kunze, J., 1999. Recessively inherited multiple epiphyseal dysplasia with normal stature, club foot, and double layered patella caused by a DTDST mutation. J Med Genet 36, 621–624.
Svensson, L., Aszódi, A., Heinegård, D., Hunziker, E.B., Reinholt, F.P., Fässler, R., Oldberg, A., 2002. Cartilage oligomeric matrix protein-deficient mice have normal skeletal development. Mol. Cell. Biol. 22, 4366–4371. https://doi.org/10.1128/mcb.22.12.4366-4371.2002
Tabas, I., Ron, D., 2011. Integrating the mechanisms of apoptosis induced by endoplasmic reticulum stress. Nat Cell Biol 13, 184–190. https://doi.org/10.1038/ncb0311-184
Takahashi, K., Tanabe, K., Ohnuki, M., Narita, M., Ichisaka, T., Tomoda, K., Yamanaka, S., 2007. Induction of Pluripotent Stem Cells from Adult Human Fibroblasts by Defined Factors. Cell 131, 861–872. https://doi.org/10.1016/j.cell.2007.11.019
Takahashi, K., Yamanaka, S., 2006. Induction of Pluripotent Stem Cells from Mouse Embryonic and Adult Fibroblast Cultures by Defined Factors. Cell 126, 663–676. https://doi.org/10.1016/j.cell.2006.07.024
Tan, J.T., Kremer, F., Freddi, S., Bell, K.M., Baker, N.L., Lamandé, S.R., Bateman, J.F., 2008. Competency for Nonsense-Mediated Reduction in Collagen X mRNA Is Specified by the 3′ UTR and Corresponds to the Position of

Mutations in Schmid Metaphyseal Chondrodysplasia. Am J Hum Genet 82, 786–793. https://doi.org/10.1016/j.ajhg.2008.01.006
Thielen, N.G.M., van der Kraan, P.M., van Caam, A.P.M., 2019. TGFβ/BMP Signaling Pathway in Cartilage Homeostasis. Cells 8, E969. https://doi.org/10.3390/cells8090969
Thomas, J.T., Cresswell, C.J., Rash, B., Nicolai, H., Jones, T., Solomon, E., Grant, M.E., Boot-Handford, R.P., 1991. The human collagen X gene. Complete primary translated sequence and chromosomal localization. Biochem. J. 280 (Pt 3), 617–623.
Thomas, S.E., Dalton, L.E., Daly, M.-L., Malzer, E., Marciniak, S.J., 2010. Diabetes as a disease of endoplasmic reticulum stress. Diabetes Metab. Res. Rev. 26, 611–621. https://doi.org/10.1002/dmrr.1132
Thor, H., Smith, M.T., Hartzell, P., Bellomo, G., Jewell, S.A., Orrenius, S., 1982. The metabolism of menadione (2-methyl-1,4-naphthoquinone) by isolated hepatocytes. A study of the implications of oxidative stress in intact cells. J Biol Chem 257, 12419–12425.
Thur, J., Rosenberg, K., Nitsche, D.P., Pihlajamaa, T., Ala-Kokko, L., Heinegård, D., Paulsson, M., Maurer, P., 2001. Mutations in cartilage oligomeric matrix protein causing pseudoachondroplasia and multiple epiphyseal dysplasia affect binding of calcium and collagen I, II, and IX. J Biol Chem 276, 6083–6092. https://doi.org/10.1074/jbc.M009512200
Tohmonda, T., Miyauchi, Y., Ghosh, R., Yoda, M., Uchikawa, S., Takito, J., Morioka, H., Nakamura, M., Iwawaki, T., Chiba, K., Toyama, Y., Urano, F., Horiuchi, K., 2011. The IRE1α–XBP1 pathway is essential for osteoblast differentiation through promoting transcription of Osterix. EMBO Rep 12, 451–457. https://doi.org/10.1038/embor.2011.34
Touleimat, N., Tost, J., 2012. Complete pipeline for Infinium® Human Methylation 450K BeadChip data processing using subset quantile normalization for accurate DNA methylation estimation. Epigenomics 4, 325–341. https://doi.org/10.2217/epi.12.21
Toydemir, R.M., Brassington, A.E., Bayrak-Toydemir, P., Krakowiak, P.A., Jorde, L.B., Whitby, F.G., Longo, N., Viskochil, D.H., Carey, J.C., Bamshad, M.J., 2006. A novel mutation in FGFR3 causes camptodactyly, tall stature, and hearing loss (CATSHL) syndrome. Am J Hum Genet 79, 935–941. https://doi.org/10.1086/508433
Trudel, S., Stewart, A.K., Rom, E., Wei, E., Li, Z.H., Kotzer, S., Chumakov, I., Singer, Y., Chang, H., Liang, S.-B., Yayon, A., 2006. The inhibitory anti-FGFR3 antibody, PRO-001, is cytotoxic to t(4;14) multiple myeloma cells. Blood 107, 4039–4046. https://doi.org/10.1182/blood-2005-10-4179
Tsang, K.Y., Chan, D., Bateman, J.F., Cheah, K.S.E., 2010. In vivo cellular adaptation to ER stress: survival strategies with double-edged consequences. J. Cell. Sci. 123, 2145–2154. https://doi.org/10.1242/jcs.068833
Uehara, Y., Hirose, J., Yamabe, S., Okamoto, N., Okada, T., Oyadomari, S., Mizuta, H., 2014. Endoplasmic reticulum stress-induced apoptosis contributes to articular cartilage degeneration via C/EBP homologous protein. Osteoarthritis and Cartilage 22, 1007–1017. https://doi.org/10.1016/j.joca.2014.04.025
Urano, F., Wang, X., Bertolotti, A., Zhang, Y., Chung, P., Harding, H.P., Ron, D., 2000. Coupling of Stress in the ER to Activation of JNK Protein Kinases by Transmembrane Protein Kinase IRE1. Science 287, 664–666. https://doi.org/10.1126/science.287.5453.664

Usui, M., Yamaguchi, S., Tanji, Y., Tominaga, R., Ishigaki, Y., Fukumoto, M., Katagiri, H., Mori, K., Oka, Y., Ishihara, H., 2012. Atf6α-null mice are glucose intolerant due to pancreatic β-cell failure on a high-fat diet but partially resistant to diet-induced insulin resistance. Metabolism 61, 1118–1128. https://doi.org/10.1016/j.metabol.2012.01.004

Van Camp, G., Snoeckx, R.L., Hilgert, N., van den Ende, J., Fukuoka, H., Wagatsuma, M., Suzuki, H., Smets, R.M.E., Vanhoenacker, F., Declau, F., Van de Heyning, P., Usami, S., 2006. A new autosomal recessive form of Stickler syndrome is caused by a mutation in the COL9A1 gene. Am J Hum Genet 79, 449–457. https://doi.org/10.1086/506478

van Heesbeen, H.J., Smidt, M.P., 2019. Entanglement of Genetics and Epigenetics in Parkinson's Disease. Front Neurosci 13, 277. https://doi.org/10.3389/fnins.2019.00277

van Meurs, J.B., Boer, C.G., Lopez-Delgado, L., Riancho, J.A., 2019. Role of Epigenomics in Bone and Cartilage Disease. J. Bone Miner. Res. 34, 215–230. https://doi.org/10.1002/jbmr.3662

Veal, E.A., Underwood, Z.E., Tomalin, L.E., Morgan, B.A., Pillay, C.S., 2018. Hyperoxidation of Peroxiredoxins: Gain or Loss of Function? Antioxid Redox Signal 28, 574–590. https://doi.org/10.1089/ars.2017.7214

Vidal, R.L., Figueroa, A., Court, F.A., Thielen, P., Molina, C., Wirth, C., Caballero, B., Kiffin, R., Segura-Aguilar, J., Cuervo, A.M., Glimcher, L.H., Hetz, C., 2012. Targeting the UPR transcription factor XBP1 protects against Huntington's disease through the regulation of FoxO1 and autophagy. Hum. Mol. Genet. 21, 2245–2262. https://doi.org/10.1093/hmg/dds040

Vincent, T.L., 2019. IL-1 in osteoarthritis: time for a critical review of the literature. F1000Res 8, F1000 Faculty Rev-934. https://doi.org/10.12688/f1000research.18831.1

Vincenti, M.P., Brinckerhoff, C.E., 2002. Transcriptional regulation of collagenase (MMP-1, MMP-13) genes in arthritis: integration of complex signaling pathways for the recruitment of gene-specific transcription factors. Arthritis Research & Therapy 4, 157. https://doi.org/10.1186/ar401

von Blume, J., Alleaume, A.-M., Kienzle, C., Carreras-Sureda, A., Valverde, M., Malhotra, V., 2012. Cab45 is required for Ca2+-dependent secretory cargo sorting at the trans-Golgi network. J Cell Biol 199, 1057–1066. https://doi.org/10.1083/jcb.201207180

Vortkamp, A., Lee, K., Lanske, B., Segre, G.V., Kronenberg, H.M., Tabin, C.J., 1996. Regulation of rate of cartilage differentiation by Indian hedgehog and PTH-related protein. Science 273, 613–622. https://doi.org/10.1126/science.273.5275.613

Vu, T.H., Shipley, J.M., Bergers, G., Berger, J.E., Helms, J.A., Hanahan, D., Shapiro, S.D., Senior, R.M., Werb, Z., 1998. MMP-9/Gelatinase B Is a Key Regulator of Growth Plate Angiogenesis and Apoptosis of Hypertrophic Chondrocytes. Cell 93, 411–422.

Wagner, T., Wirth, J., Meyer, J., Zabel, B., Held, M., Zimmer, J., Pasantes, J., Bricarelli, F.D., Keutel, J., Hustert, E., Wolf, U., Tommerup, N., Schempp, W., Scherer, G., 1994. Autosomal sex reversal and campomelic dysplasia are caused by mutations in and around the SRY-related gene SOX9. Cell 79, 1111–1120. https://doi.org/10.1016/0092-8674(94)90041-8

Wang, C., Brisson, B.K., Terajima, M., Li, Q., Hoxha, K., Han, B., Goldberg, A.M., Sherry Liu, X., Marcolongo, M.S., Enomoto-Iwamoto, M., Yamauchi, M., Volk,

S.W., Han, L., 2020. Type III collagen is a key regulator of the collagen fibrillar structure and biomechanics of articular cartilage and meniscus. Matrix Biol 85–86, 47–67. https://doi.org/10.1016/j.matbio.2019.10.001
Wang, C., Tan, Z., Niu, B., Tsang, K.Y., Tai, A., Chan, W.C.W., Lo, R.L.K., Leung, K.K.H., Dung, N.W.F., Itoh, N., Zhang, M.Q., Chan, D., Cheah, K.S.E., 2018. Inhibiting the integrated stress response pathway prevents aberrant chondrocyte differentiation thereby alleviating chondrodysplasia. eLife 7, e37673. https://doi.org/10.7554/eLife.37673
Wang, C., Youle, R.J., 2009. The Role of Mitochondria in Apoptosis. Annu Rev Genet 43, 95–118. https://doi.org/10.1146/annurev-genet-102108-134850
Wang, S., Kaufman, R.J., 2012. The impact of the unfolded protein response on human disease. J Cell Biol 197, 857–867. https://doi.org/10.1083/jcb.201110131
Wang, W., Rigueur, D., Lyons, K.M., 2020. TGFβ as a gatekeeper of BMP action in the developing growth plate. Bone 137, 115439. https://doi.org/10.1016/j.bone.2020.115439
Wang, Weiguang, Lian, N., Li, L., Moss, H.E., Wang, Weixi, Perrien, D.S., Elefteriou, F., Yang, X., 2009. Atf4 regulates chondrocyte proliferation and differentiation during endochondral ossification by activating Ihh transcription. Development 136, 4143–4153. https://doi.org/10.1242/dev.043281
Wei, J., Sheng, X., Feng, D., McGrath, B., Cavener, D.R., 2008. PERK is essential for neonatal skeletal development to regulate osteoblast proliferation and differentiation. J. Cell. Physiol. 217, 693–707. https://doi.org/10.1002/jcp.21543
Weir, E.C., Philbrick, W.M., Amling, M., Neff, L.A., Baron, R., Broadus, A.E., 1996. Targeted overexpression of parathyroid hormone-related peptide in chondrocytes causes chondrodysplasia and delayed endochondral bone formation. Proc Natl Acad Sci U S A 93, 10240–10245.
Weirich, C., Keene, D.R., Kirsch, K., Heil, M., Neumann, E., Dinser, R., 2007. Expression of PSACH-associated mutant COMP in tendon fibroblasts leads to increased apoptotic cell death irrespective of the secretory characteristics of mutant COMP. Matrix Biol 26, 314–323. https://doi.org/10.1016/j.matbio.2007.01.004
Weng, Z., Wang, C., Zhang, C., Xu, J., Chai, Y., Jia, Y., Han, P., Wen, G., 2019. All-Trans Retinoic Acid Promotes Osteogenic Differentiation and Bone Consolidation in a Rat Distraction Osteogenesis Model. Calcif Tissue Int 104, 320–330. https://doi.org/10.1007/s00223-018-0501-6
Wiberg, C., Klatt, A.R., Wagener, R., Paulsson, M., Bateman, J.F., Heinegård, D., Mörgelin, M., 2003. Complexes of matrilin-1 and biglycan or decorin connect collagen VI microfibrils to both collagen II and aggrecan. J. Biol. Chem. 278, 37698–37704. https://doi.org/10.1074/jbc.M304638200
Willard, V.P., Diekman, B.O., Sanchez-Adams, J., Christoforou, N., Leong, K.W., Guilak, F., 2014. Use of cartilage derived from murine induced pluripotent stem cells for osteoarthritis drug screening. Arthritis & Rheumatology (Hoboken, N.J.) 66, 3062–3072. https://doi.org/10.1002/art.38780
Willmer, T., Johnson, R., Louw, J., Pheiffer, C., 2018. Blood-Based DNA Methylation Biomarkers for Type 2 Diabetes: Potential for Clinical Applications. Front Endocrinol (Lausanne) 9. https://doi.org/10.3389/fendo.2018.00744
Wilson, R., Freddi, S., Chan, D., Cheah, K.S.E., Bateman, J.F., 2005. Misfolding of Collagen X Chains Harboring Schmid Metaphyseal Chondrodysplasia

Mutations Results in Aberrant Disulfide Bond Formation, Intracellular Retention, and Activation of the Unfolded Protein Response. J. Biol. Chem. 280, 15544–15552. https://doi.org/10.1074/jbc.M410758200
Winterpacht, A., Superti-Furga, A., Schwarze, U., Stöss, H., Steinmann, B., Spranger, J., Zabel, B., 1996. The deletion of six amino acids at the C-terminus of the alpha 1 (II) chain causes overmodification of type II and type XI collagen: further evidence for the association between small deletions in COL2A1 and Kniest dysplasia. J Med Genet 33, 649–654. https://doi.org/10.1136/jmg.33.8.649
Wit, J.M., Oostdijk, W., Losekoot, M., van Duyvenvoorde, H.A., Ruivenkamp, C.A.L., Kant, S.G., 2016. MECHANISMS IN ENDOCRINOLOGY: Novel genetic causes of short stature. Eur J Endocrinol 174, R145-173. https://doi.org/10.1530/EJE-15-0937
Wohl, A.P., Troilo, H., Collins, R.F., Baldock, C., Sengle, G., 2016. Extracellular Regulation of Bone Morphogenetic Protein Activity by the Microfibril Component Fibrillin-1. J Biol Chem 291, 12732–12746. https://doi.org/10.1074/jbc.M115.704734
Wucherpfennig, A.L., Li, Y.P., Stetler-Stevenson, W.G., Rosenberg, A.E., Stashenko, P., 1994. Expression of 92 kD type IV collagenase/gelatinase B in human osteoclasts. J Bone Miner Res 9, 549–556. https://doi.org/10.1002/jbmr.5650090415
Xie, Y., Zhou, S., Chen, H., Du, X., Chen, L., 2014. Recent Research on the growth plate: Advances in fibroblast growth factor signaling in growth plate development and disorders. Journal of Molecular Endocrinology 53, T11–T34. https://doi.org/10.1530/JME-14-0012
Xie, Y., Zinkle, A., Chen, L., Mohammadi, M., 2020. Fibroblast growth factor signalling in osteoarthritis and cartilage repair. Nat Rev Rheumatol 16, 547–564. https://doi.org/10.1038/s41584-020-0469-2
Xie, Z., Singh, M., Singh, K., 2004. Differential regulation of matrix metalloproteinase-2 and -9 expression and activity in adult rat cardiac fibroblasts in response to interleukin-1beta. J Biol Chem 279, 39513–39519. https://doi.org/10.1074/jbc.M405844200
Xu, J., Lawshe, A., MacArthur, C.A., Ornitz, D.M., 1999. Genomic structure, mapping, activity and expression of fibroblast growth factor 17. Mech Dev 83, 165–178. https://doi.org/10.1016/s0925-4773(99)00034-9
Xu, T., Wang, C., Shen, J., Tong, P., O'Keefe, R., 2018. Ablation of Dnmt3b in chondrocytes suppresses cell maturation during embryonic development. J. Cell. Biochem. 119, 5852–5863. https://doi.org/10.1002/jcb.26775
Xue, M., McKelvey, K., Shen, K., Minhas, N., March, L., Park, S.-Y., Jackson, C.J., 2014. Endogenous MMP-9 and not MMP-2 promotes rheumatoid synovial fibroblast survival, inflammation and cartilage degradation. Rheumatology 53, 2270–2279. https://doi.org/10.1093/rheumatology/keu254
Yamamoto, K., Sato, T., Matsui, T., Sato, M., Okada, T., Yoshida, H., Harada, A., Mori, K., 2007. Transcriptional induction of mammalian ER quality control proteins is mediated by single or combined action of ATF6alpha and XBP1. Dev. Cell 13, 365–376. https://doi.org/10.1016/j.devcel.2007.07.018
Yamamoto, K., Yoshida, H., Kokame, K., Kaufman, R.J., Mori, K., 2004. Differential contributions of ATF6 and XBP1 to the activation of endoplasmic reticulum stress-responsive cis-acting elements ERSE, UPRE and ERSE-II. J. Biochem. 136, 343–350. https://doi.org/10.1093/jb/mvh122

Yang, G., Zhu, L., Hou, N., Lan, Y., Wu, X.-M., Zhou, B., Teng, Y., Yang, X., 2014. Osteogenic fate of hypertrophic chondrocytes. Cell Res 24, 1266–1269. https://doi.org/10.1038/cr.2014.111
Yang, L., Tsang, K.Y., Tang, H.C., Chan, D., Cheah, K.S.E., 2014. Hypertrophic chondrocytes can become osteoblasts and osteocytes in endochondral bone formation. PNAS 111, 12097–12102. https://doi.org/10.1073/pnas.1302703111
Yang, X., Trehan, S.K., Guan, Y., Sun, C., Moore, D.C., Jayasuriya, C.T., Chen, Q., 2014. Matrilin-3 inhibits chondrocyte hypertrophy as a bone morphogenetic protein-2 antagonist. J. Biol. Chem. 289, 34768–34779. https://doi.org/10.1074/jbc.M114.583104
Yasoda, A., Kitamura, H., Fujii, T., Kondo, E., Murao, N., Miura, M., Kanamoto, N., Komatsu, Y., Arai, H., Nakao, K., 2009. Systemic administration of C-type natriuretic peptide as a novel therapeutic strategy for skeletal dysplasias. Endocrinology 150, 3138–3144. https://doi.org/10.1210/en.2008-1676
Yasoda, A., Komatsu, Y., Chusho, H., Miyazawa, T., Ozasa, A., Miura, M., Kurihara, T., Rogi, T., Tanaka, S., Suda, M., Tamura, N., Ogawa, Y., Nakao, K., 2004. Overexpression of CNP in chondrocytes rescues achondroplasia through a MAPK-dependent pathway. Nat Med 10, 80–86. https://doi.org/10.1038/nm971
Yin, Y., Ren, X., Smith, C., Guo, Q., Malabunga, M., Guernah, I., Zhang, Y., Shen, J., Sun, H., Chehab, N., Loizos, N., Ludwig, D.L., Ornitz, D.M., 2016. Inhibition of fibroblast growth factor receptor 3-dependent lung adenocarcinoma with a human monoclonal antibody. Disease Models & Mechanisms 9, 563–571. https://doi.org/10.1242/dmm.024760
Yong, J., Bischof, H., Burgstaller, S., Siirin, M., Murphy, A., Malli, R., Kaufman, R.J., 2019. Mitochondria supply ATP to the ER through a mechanism antagonized by cytosolic Ca2. Elife 8, e49682. https://doi.org/10.7554/eLife.49682
Yoon, S.O., Park, D.J., Ryu, J.C., Ozer, H.G., Tep, C., Shin, Y.J., Lim, T.H., Pastorino, L., Kunwar, A.J., Walton, J.C., Nagahara, A.H., Lu, K.P., Nelson, R.J., Tuszynski, M.H., Huang, K., 2012. JNK3 perpetuates metabolic stress induced by Abeta peptides. Neuron 75, 824–837. https://doi.org/10.1016/j.neuron.2012.06.024
Yoshida, H., Haze, K., Yanagi, H., Yura, T., Mori, K., 1998. Identification of the cis-acting endoplasmic reticulum stress response element responsible for transcriptional induction of mammalian glucose-regulated proteins. Involvement of basic leucine zipper transcription factors. J. Biol. Chem. 273, 33741–33749.
Young, D.A., Barter, M.J., Soul, J., 2022. Osteoarthritis year in review: genetics, genomics, epigenetics. Osteoarthritis and Cartilage 30, 216–225. https://doi.org/10.1016/j.joca.2021.11.004
Zaia, J., Boynton, R.E., McIntosh, A., Marshak, D.R., Olsson, H., Heinegård, D., Barry, F.P., 1997. Post-translational Modifications in Cartilage Oligomeric Matrix Protein: Characterization of the N-linked oligosaccharides by matrix-assisted laser desorption ionization time-of-flight mass spectrometry. Journal of Biological Chemistry 272, 14120–14126. https://doi.org/10.1074/jbc.272.22.14120
Zankl, A., Briggs, M., Bateman, J.F., 2018. Chapter 27 - Skeletal Dysplasias, in: Thakker, R.V., Whyte, M.P., Eisman, J.A., Igarashi, T. (Eds.), Genetics of

Bone Biology and Skeletal Disease (Second Edition). Academic Press, pp. 469–480. https://doi.org/10.1016/B978-0-12-804182-6.00027-7
Zelzer, E., Glotzer, D.J., Hartmann, C., Thomas, D., Fukai, N., Soker, S., Olsen, B.R., 2001. Tissue specific regulation of VEGF expression during bone development requires Cbfa1/Runx2. Mech. Dev. 106, 97–106.
Zelzer, E., Mamluk, R., Ferrara, N., Johnson, R.S., Schipani, E., Olsen, B.R., 2004. VEGFA is necessary for chondrocyte survival during bone development. Development 131, 2161–2171. https://doi.org/10.1242/dev.01053
Zhang, P., Jobert, A.S., Couvineau, A., Silve, C., 1998. A homozygous inactivating mutation in the parathyroid hormone/parathyroid hormone-related peptide receptor causing Blomstrand chondrodysplasia. J Clin Endocrinol Metab 83, 3365–3368. https://doi.org/10.1210/jcem.83.9.5243
Zhang, P., McGrath, B., Li, S., Frank, A., Zambito, F., Reinert, J., Gannon, M., Ma, K., McNaughton, K., Cavener, D.R., 2002. The PERK eukaryotic initiation factor 2 alpha kinase is required for the development of the skeletal system, postnatal growth, and the function and viability of the pancreas. Mol. Cell. Biol. 22, 3864–3874.
Zhang, Y.W., Yasui, N., Kakazu, N., Abe, T., Takada, K., Imai, S., Sato, M., Nomura, S., Ochi, T., Okuzumi, S., Nogami, H., Nagai, T., Ohashi, H., Ito, Y., 2000. PEBP2alphaA/CBFA1 mutations in Japanese cleidocranial dysplasia patients. Gene 244, 21–28. https://doi.org/10.1016/s0378-1119(99)00558-2
Zheng, C., Lin, X., Xu, X., Wang, C., Zhou, J., Gao, B., Fan, J., Lu, W., Hu, Y., Jie, Q., Luo, Z., Yang, L., 2019. Suppressing UPR-dependent overactivation of FGFR3 signaling ameliorates SLC26A2-deficient chondrodysplasias. EBioMedicine. https://doi.org/10.1016/j.ebiom.2019.01.010
Zheng, Q., Zhou, G., Morello, R., Chen, Y., Garcia-Rojas, X., Lee, B., 2003. Type X collagen gene regulation by Runx2 contributes directly to its hypertrophic chondrocyte–specific expression in vivo. J Cell Biol 162, 833–842. https://doi.org/10.1083/jcb.200211089
Zhou, X., von der Mark, K., Henry, S., Norton, W., Adams, H., de Crombrugghe, B., 2014. Chondrocytes transdifferentiate into osteoblasts in endochondral bone during development, postnatal growth and fracture healing in mice. PLoS Genet 10, e1004820. https://doi.org/10.1371/journal.pgen.1004820
Zhu, G., Kang, L., Wei, Q., Cui, X., Wang, S., Chen, Y., Jiang, Y., 2014. Expression and Regulation of MMP1, MMP3, and MMP9 in the Chicken Ovary in Response to Gonadotropins, Sex Hormones, and TGFB11. Biology of Reproduction 90. https://doi.org/10.1095/biolreprod.113.114249
Zhu, H., Wang, G., Qian, J., 2016. Transcription factors as readers and effectors of DNA methylation. Nat Rev Genet 17, 551–565. https://doi.org/10.1038/nrg.2016.83
Zhu, Q., Zhong, J.J., Jin, J.F., Yin, X.M., Miao, H., 2013. Tauroursodeoxycholate, a chemical chaperone, prevents palmitate-induced apoptosis in pancreatic β-cells by reducing ER stress. Exp Clin Endocrinol Diabetes 121, 43–47. https://doi.org/10.1055/s-0032-1321787